Study on Assessment and Adaptation to Saltwater Intrusion under the Impacts of Tide, Sea-Level Rise, Flow and Morphological Changes in the Vietnamese Mekong Delta

Nguyen Thi Phuong Mai

Study on Assessment and Adaptation to Saltwater Intrusion under the Impacts of Tide, Sea-Level Rise, Flow and Morphological Changes in the Vietnamese Mekong Delta

NGUYEN THI PHUONG MAI

A Dissertation

Submitted in Partial Fulfillment of the Requirements for the Degree of

Doctor of Philosophy (Ph.D.)

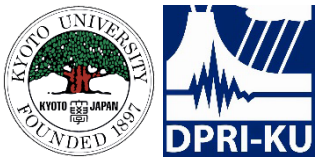

Department of Urban Management

Graduate School of Engineering

Kyoto University

2022

Acknowledgments

I am a delighted person; God gave me three dedicated supervisors to help me do my research and brought many relatives and excellent friends to encourage and support me for four years. This is an opportunity for me to express my deep gratitude to them:

First of all, I wish to express my thanks and great gratitude to Prof. Sumi Tetsuya, my supervisor, for accepting me as his Ph.D. student in his laboratory. His recommended letter gave me a Ph.D. scholarship in Kyoto. Also, his suggestions and corrections through guidance and discussions gained me invaluable knowledge and substantially improved my research. Furthermore, he offered me opportunities to attend international conferences that helped me change my mind and learn many things there, especially in Japan. As a result, I understand developing and protecting the river systems based on sustainable development and a friendly environment.

I want to express my highest gratitude to Assoc. Prof. Dr. Sameh Ahmed Kantoush. He encouraged me to become his Ph.D. student. He always gives me advise instruction, always forgives my mistakes, and supported me with his highest enthusiasm in my study and my short present in Japan. I can finish my research on time with his guide and patient during discussions. Furthermore, he always encouraged me to write papers and apply to international conferences; from that, I learned so many ways to solve my study and helped me have a new see in water resources research.

Also, I would like to express from my heart to one person who always supported, guided, and helped me for four years. He is Prof. Tang Duc Thang working at the Southern Institute of Water Resources Research (SIWRR). His advice helped me plan to go field trip to solve my research and let me connect with people who gave me so much data, which was very useful for my research. In addition, he was always willing to spend so much time answering my question carefully and giving me exciting books to make sure I could clearly understand what I was doing. He is very busy with the meeting and his research, but he always arranges his schedule to go on the field trip with me and explain everything related to my research in the Vietnamese Mekong Delta.

I want to thank Assoc. Prof. Dr. Takemon Yasuhiro, Assist. Prof. Dr. Nohara Daisuke. I had a perfect field trip with Dr. Takemon, and then he took me to go to visit a reservoir with an Arch

dam which I had never seen before and explain how to collect data by fly-cam. Discussions with Dr. Nohara Daisuke helps me know how to set up the optimization of reservoir operations. Thank you so much for helping me during my time in Panama City. I also would like to thank Mrs. Obara Hisae and Mrs. Ibraki Junko. They always set up all things for me when I came to Japan, attended international conferences, and supported me in doing any documents relative to my scholarship. Many thanks to all of the members of Sumi Laboratory for the welcome and the helping me during my short time in Japan. I would like to also thank to Prof. Hori Tomoharu and Prof. Tanaka Kenji for giving me valuable questions to learn and discuss on broad ideas related groundwater management and climate change impacts.

My deep thanks are also extended to Assoc. Prof. Dr. Le Trung Thanh and Dr. Nguyen Thai Quyet from Thuyloi University to teach and check my numerical model and Mr. Do Dac Hai from SIWRR for sharing the research data.

Special thanks to Dr. La Vinh Trung and Dr. Doan Van Binh from Vietnamese-German University for introducing me to Prof. Sumi and Prof. Sameh and encouraging me to study Ph.D. Then they support me so much during the field trip, data analysis, and writing papers. Also, I would like to thank all of my partners in ThuyLoi Univerity – Southern campus for their helping and encouragement when I have a seminar every year between Kyoto Univerity and ThuyLoi University.

Many thanks to the Japan Society for the promotion of Science (JSPS) for giving me the Ph.D. scholarship. Furthermore, my research funding was partly supported by the Japan-ASEAN Science, Technology and Innovation Platform (JASTIP) and the Supporting Program for Interaction-Based Initiative Team Studies SPIRITS 2016 of Kyoto University.

Lastly, I would like to express my special gratitude to my father, NguyenNangPhuong, my mother, NguyenThiLoc, my husband, AnDinhNha, and three of my handsome sons, AnDinhMinh, AnDinhPhuc and AnDinhDuc for their unconditional love, support, sympathy, sacrifice, and encouragement to complete my research.

Table of contents

List of figures

List of tables

List of symbols

A: cross-section areac(m^2)

B: the estuarine channel width (m)

S: salinity concentration (psu)

CA_{max}: maximum salinity measured by CastAway CTD equipment (psu)

CA_{min}: minimum salinity measured by CastAway equipment (psu)

D: dispersion coefficient

ΔH_{tide}: mean tidal range (m)

$\Delta\tau$:time period

Δx:distance between two sections (km)

E: the tidal excursion(km)

E_f: Nash-Sutcliffe number

E_ρ: Internal estuary number

f_{1j}, f_{2j}: mass percentage of the sand and mud fractions, respectively (%)

F_D : the estuarine densimetric Froude number

f_i, i=1, 2, …n: the estimated data which are associated with y_i

g: gravity acceleration (m/s^2)

h: water depth (m)

H: water level (m)

h_o: water depth at the river mouth (m)

HW: High water (m)

HWS: high water slack (m)

i_o: the slope of the river

K: linear decay coefficient

LW: low water (m)

LWS: low water slack (m)

n: Pritchard's number

Q: discharge (m^3/s)

q: in/out side flow of channel section (lateral in/out flow (q = 0))

Q_f : the river flow during the tidal period T (m3/s)

R^2: coefficient of determination

R_{iE}: Richardson's number

S_0: bed slope

S_{bot} : water salinity at the bottom (psu)

S_f: friction slope

S_m : averaged water salinity (psu)

S_{max}: maximum salinity (psu)

$S_{max\ bot}$: maximum salinity at the bottom (psu)

$S_{max\ suf}$: maximum salinity in the surface (psu)

S_{min}: minimum salinity (psu)

S_{surf} : water salinity on the surface (psu)

υ: the tidal amplitude (m)

u_f : the river flow velocity (m/s)

V_{max}: maximum velocity (m/s)

W: the volume of water runoff over the tidal cycle (m3)

W_{total}: total annual flow

W_{dry}: total dry flow

W_{wet}: total wet flow

WL: water level (m)

y_i, i=1, 2, …n: observed data

$\underline{y}$: mean of observed values

α: Simmon's number

ΔS : difference of salinity between bottom and surface (psu)

Δ_ρ: the density difference between sea and river (kg/m^3)

ρs and ρ: density of sea water and fresh water (kg/m^3)

Abbreviations

ADCP: acoustic Doppler current profiler

CMD: Cambodian Mekong Delta

CS: Chaing Saen

DEM: digital elevation map

ENSO: El Niño Southern Oscillation

GPS: a global positioning system

GDP: Gross Domestic Product

IPCC: intergovernmental panel on climate change

JASTIP: Japan-ASEAN Science, Technology and Innovation Platform

LMB: lower Mekong River Basin

MR: Mekong River

MRB: Mekong River Basin

MRC: Mekong River Commission

E_f: Nash-Sutcliffe number

Sce: simulation scenario

SLR: sea-level rise

SI: Salinity intrusion

SIWRR: Southern Institute of Water Resources Research

VMD: Vietnamese Mekong Delta

1D: 1-dimensional

Abstract

The Vietnamese Mekong Delta (VMD) has to face drought and prolonged saltwater intrusion in the dry season every year. Saltwater significantly affects agriculture, people's daily lives, and the environment. In 2015-2016, the most severe drought in the past 90 years was accompanied by severe saltwater intrusion in the VMD. Salinity threshold of 4 psu has intruded 60-73 km into the VMD, which is 20-30 km further than mean annual years. Over 2,297 thousand hectares of the VMD have been affected by saltwater and approximately 976,000 people lack fresh water for daily consumption. Four years later, an extreme drought year again occurred in 2019-2020. The maximum salinity was 0.6 psu to 0.8 psu higher than that in 2016, and intrusion length is deeper from 3 km to 5 km. However, the most important thing is that the salinity appeared 1 - 1.5 months earlier and reached a peak value of 1.5 - 2.0 months sooner than the average of many years.

Salinity intrusion is a typical phenomenon of river mouths where two distinct water masses, riverine and marine, interact. Tides and sea level have significantly influenced salinity concentration and intrusion length, so upstream currents are needed to push the salinity to the sea. However, over 100 large, medium, and small reservoirs were constructed along the Mekong River causing upstream flow and sediment changes in the VMD. As a result, there was a lack of fresh water in the dry season and severe riverbed incision developed in VMD. Combined with the high sea level which also occurs in January and February, the trend of salinity in VMD became more and more serious.

Therefore, this study assesses the situation of salinity intrusion in VMD under the effect of upstream dam's development, tides, sea-level rise, upstream flow, and morphology changes. So a long-term series of water level, discharge and sediment data at Chiang Saen, Kratie, TanChau, and ChauDoc stations were used to analyze the altered flow and sediment in the VMD. In addition, data analysis (estuary water levels, tides, and salinity time series) and numerical simulation model were also used to assess the impact of the four factors mentioned above on the saltwater intrusion mechanism in VMD through six scenarios. Then, seven solutions are proposed to mitigate and adapt to saltwater intrusion.

The upstream dams development changes the upstream flow by transferring water from the wet season to the dry season, so the total wet flow is reduced in the whole basin with a smaller flood peak, and the peak flood occurs a month later than that in the past. The total dry flow increased by

20.96% at Chaing Saen and 34.83% (10.5 km^2) at Kratie; however, the total monthly flow only increases from March to May while the dry season starts from December. So that is the main cause of salinity that started in December and reached its peak value in February. One simulated reservoir scenario released water one month earlier than the baseline scenario in 2016. Salinity concentrations in the VMD were gradually reduced by 11.6% to 15.9% because the discharge increases by 5.1% and 6.9% at DaiNgai and Tra Vinh stations, respectively. The intrusion length would also decrease by about 4 to 7 km on all tributaries.

When the reservoirs are in operation, they store water and trap the sediment flow; the average amount of sediment load in the VMD decreased from 166.4 Mt before the 1993 period to 42.3 Mt since 2012. That is the main reason leading to this problem. The river bed is lowered with an average drop of the main tributary of 0.22 mm/yr and 0.34 mm/yr on the Hau and Tien rivers. Based on simulated scenarios, the impact of river incision on salinity intrusion shows that salinity concentration would be increased by 0.8-0.9 psu, and salinity profile would move 1.8 km and 4.5km further upstream if 1.76m and 2.76 riverbed incisions were in the Hau and Tien rivers.

Global climate change increases sea level by about 5.25 mm/yr at VungTau station. The highest sea level is from October to February. This is one of the main drivers of n salinity intrusion, followed by river flow. For example, the salinity profile would move 4 to 7 km further upstream, and salinity would increase by 1.4 to 1.9 psu if the sea level rises by 47.25 mm in the next five years (2025).

Tides strongly influenced the river's spatial and temporal salinity distribution in the daily, monthly, and seasonal cycles. In the daily tidal cycle, maximum salinity (S_{max}) occurs at the bottom and lags one to three hours after maximum water level. In the spring–neap tidal cycle, S_{max} at the bottom occurs at the transition period from neap to spring tides (3-7 days before spring tide), while S_{min} appears in the transition period from spring to neap tides. Also, in the springtide, the intrusion length of 0.4 psu threshold at the flood tide is longer than 14.3km, 15km, 16.5km than at the ebb tide in TranDe, DinhAn, and CoChien branches, respectively combined with partial mixing and moderate stratification prevails over the 50 km TranDe and DinhAn branches. At the same time, weak mixing and strong stratification appeared during the Neap tide of the Hau and Co Chien Rivers.

The results of my research are an essential reference for the dividing ecological zone (Freshwater–Brackish water–Saltwater) along the main river and the land. Furthermore, seven

mitigation measurements including four non-structural solutions (early warning, long-term adaptation plans, long term water use plan, saving water use) and three structural solutions (improving infrastructure, household water storage, and keeping flood inundation areas) as mentioned earlier. If most of the above-mentioned solutions are applied simultaneously and continuously; the results will be very effective. Particularly for the solution number five (improving infrastructure), it is necessary to have a plan, a roadmap for implementation, funding sources, an assessment of the level of impact on the environment and how to effectively and long-term manage and operate the project.

Chapter 1: Introduction

1.1 Overview of salinity intrusion and the drivers on salinity intrusion

Salinity intrusion is the process of seawater intruding into rivers and land. That is a typical phenomenon of river mouths where two different water masses, riverine and marine, are interacting (Fischer 1979). Salinity intrusion in the estuaries depends on various drivers. These drivers are river flow, morphology, tides, sea-level rise, winds, water use, human activities, and geomorphological factors (topography, bathymetry) (Figure 1.1). The tendency of saltwater intrusion in coastal estuaries worldwide is increasing due to the lack of freshwater sources to push saltwater, subsidence topography, climate change, and especially human impacts on the natural elements of flow.

Water accounts for more than 75% of the earth's surface, but freshwater for life is minimal. The maximum amount is about 1.0% of the total water on earth. However, this amount of fresh water is unevenly distributed. It varies significantly from season to season and depends on the natural cycle and variability of precipitation, runoff, and evaporation (UN-Water 2010b). Therefore, it is not easy for people to access freshwater resources around the world. More seriously, global freshwater resources are in crisis due to population growth, rapid socio-economic development, industrialization, modernization, and severe impacts of climate change. Many regions of the world face depletion and scarcity of freshwater resources, affecting water quality and the sustainable development of socio-economic and ecological systems.

Besides, the demand for electric power supply to the world is also increasing, which leads to the appearance of hydroelectric dams, water-raising works, multi-purpose reservoirs along the main and tributaries of rivers—a river system for power generation. For instance, during the second half of the 20th century, the number of large dams over 15m high, has increased from 5,000 to 45,000 (WCD, 2000) and projected to be grow to 50,000 (Gupta et al., 2012; Kummu et al., 2010) and half of them were built in China (Wu et al., 2018). About 115 of these are mega dams (> 100m high and > 1 km3 storage capacity). The annual production of electricity power was around 3,750 TWh in 2013 (Fan et al., 2015). Reservoirs appearing especially mega-dams, have been warned to have significant impacts on river hydrology, primarily through changes in the timing, magnitude, duration, and frequency of low and high flows (Lauri et al., 2012; Lu et al., 2014; Manh et al., 2015; Räsänen et al., 2017). Dams normally cut the flood peak and reduce the amplitude of annual flood pulses. Besides, the minimum and dry flow will slightly increase, but

the distribution is not uniform for all dry season months (Mai et al., 2018; Räsänen et al., 2017). Therefore, the total downstream flow of the dams is significantly reduced because the reservoir water storage and flow distribution fluctuate according to the power generation demand, not for the downstream water demand. The downstream flow of Three Gorges Dams reduced nearly 8 – 18% at Datong station in 2008 (Bing et al., 2013). This leads to the downstream of the dam and the estuary areas facing the lack of freshwater to push the salinity for domestic use and irrigation.

Besides, dams trap sediment, so this is one of the main factors for decreasing the trend of the world sediment flux, which causes the river bed and estuary erosion, leading to lowering the riverbed, increasing the possibility of saltwater entering the river and causing ecosystem degradation. When the Aswan High Dam in Egypt reservoir was completed, the sediment content in the Nile River decreased by 100 Mt/yr Dam (Milliman and Syvitski, 1992). The completion of the Glen Canyon dam has reduced by 99.5% of the fine sediment reaching the Grand Canyon in the Colorado River, USA (Tena and Batalla, 2013). The sediment budget of the Yangtze River in China had reduced from 164 Mt/yr to 9 Mt/yr (Tena and Batalla, 2013) when the Three Gorges Dams operated in 2003. Similarly, when the Hoa Binh and ThacBa reservoirs were completed, the sediment flux of the Red River in Vietnam was reduced by about 70% (Lu et al., 2015).

In addition, when the demand for agricultural areas increases, the demand for irrigation water increases, but the water source in this basin is not enough, so water is transferred from one basin to another by water diversions, so the lower regions are affected. Due to severe water shortages, the river basins are increasingly facing drought and saltwater intrusion.

Moreover, the coastal zone is the home of more than two billion people around 200km from the coast. (Creel, 2003) These areas are facing a shortage of surface water, so it has to exploit groundwater for use. Many regions exploit excessive amounts of groundwater for domestic, irrigation, and industrial purposes. Extreme groundwater exploitation leads to subsidence and land subsidence, making saline intrusion penetrate deeply and for a long time.

It is impossible not to mention the impact of climate change and sea-level rise on the estuary because that is also a cause of flow change, but the level of influence is smaller than that of the hydropower dams (Arias et al., 2014; Lauri et al., 2012). Combining the impact of sea level rise with the complexity of the tidal mechanism and flow reduction will make the evolution of saltwater intrusion in the estuarine complex and increase in time, salinity concentration and saltwater intrusion length. For example, many studies have concluded that when sea level increases by 20cm,

30cm, 35cm, or 1m, the length of saltwater intrusion will increase from 10km to 27km (Duong et al., 2.18; Toan et al., 2014; Khang et al., 2008).

1.2 Statement problems

Like the world's river basins, the Vietnamese Mekong Delta (VMD) has a flat topography, with most elevations being approximately 0.5 to 1.0 m above mean sea level. Every year in the dry season, when high tidal range combines with 5.6 mm/yr sea level rise, 1.9 – 2.8 cm/yr of subsidence, and more fluctuation upstream flow (Figure 1.1) so 1.7 – 2.1 million ha of VMD area is affected by salinity intrusion (Nguyen, 2008 and Toan, 2015). Most of the sluice gates in the coastal zone have to be closed for a long time during the dry season (1-2 months) to control salinity intrusion.

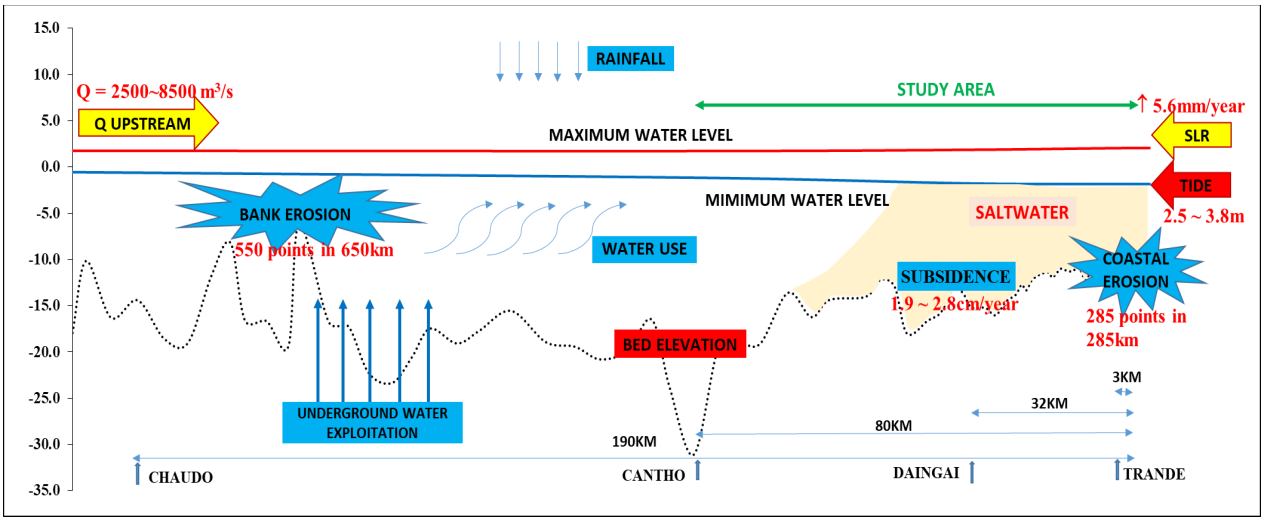

Figure 1.1 The Drivers of Salinity Intrusion

Over the past forty years, many irrigation projects have been built to control salinity, store freshwater, control flooding and water drainage, and improve acidic – saline soils, which have contributed to changing the face of the VMD. As a result, the area of annual rice fields increased from 2.4 million hectares in 1985 to 4.3 million hectares in 2015 (Department of Statistics). As a result, the delta becomes the rice bowl, seafood, and fruit basket of Vietnam, with total food production increased from 6.3 million tons in 1985 to 25.7 million tons in 2015-- more than 50% of the country's food production, 90% of rice exports, more than 70% of seafood exports and about 55% of the fruit export output.

Every year, VMD faces drought and prolonged saline intrusion in the dry season. In 2015-2016, the most severe drought over the past 90 years was accompanied by severe saltwater intrusion in

the VMD. Salinity threshold of 4 psu has intruded 60-73 km into the VMD, which is 20-30 km further than many years average values. This caused severe damage to agriculture and the livelihoods of people in the VMD. By the end of 2015, about 159,000 hectares (ha) of paddy fields were damaged; around 389,831 households with approximately 976,000 people lacked fresh water for daily consumption (SIWRR report, 2016). Four years later, the peak of salinity in 2020 at some stations is even higher than that in 2016, from 0.6 psu to 0.8 psu at DaiNgai and SonDoc stations. The intrusion length of 4 psu in 2020 is 78km, 68km, and 65km on HamLuong, CoChien, and Hau Rivers, 5km, 3km and 5km deeper than 2016 and 35km, 24km and 24km deeper than the average 26 years, also on all three estuaries of HamLuong, CoChien and Hau rivers (Table 1.1, Figure 1.2, Figure 1.3 and Figure 1.4)

Table 1.1 Statistics the intrusion length in VMD of 2020 compare with previous years

Estuary	Maximum intrusion length of 4 psu (km)								
	Dec. 2019	**Jan. 2020**	**Feb. 2020**	**Mar. 2020**	**Apr. 2020**	**May 2020**	**L_{max} (2019-2020)**	**L_{max} (2015-2016)**	**Average many years**
Tieu	45	45	88	90	88	78	**90**	50	38
Dai	45	46							40
HamLuong	**57**	**64**	**78**				**78**	**73**	**43**
CoChien	**57**	**68**	**66**	**51**	**42**	**45**	**68**	**65**	**44**
Hau	**48**	**61**	**65**	**52**	**43**	**41**	**65**	**60**	**41**
CaiLon	41	48	58	59	62	54	**62**	68	53

In recent years, there have some studies, analyses, and forecasts about salinity intrusion in the VMD, mainly focusing on assessing the current situation, changes in salinity concentration, and intrusion length according to scenarios of climate change and sea-level rise (Khang et al., 2008; A.Smajgl et al., 2015; Duong et al., 2017 and Nhan et al., 2019) and of changes in river

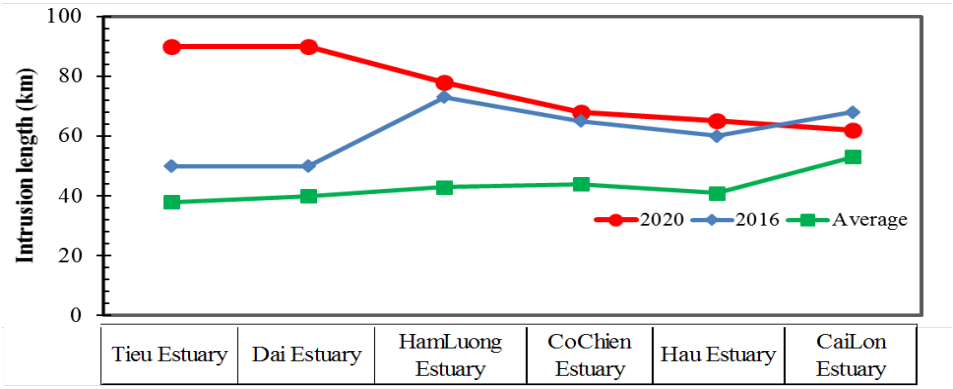

Figure 1.2 The maximum intrusion length at six estuaries of VMD

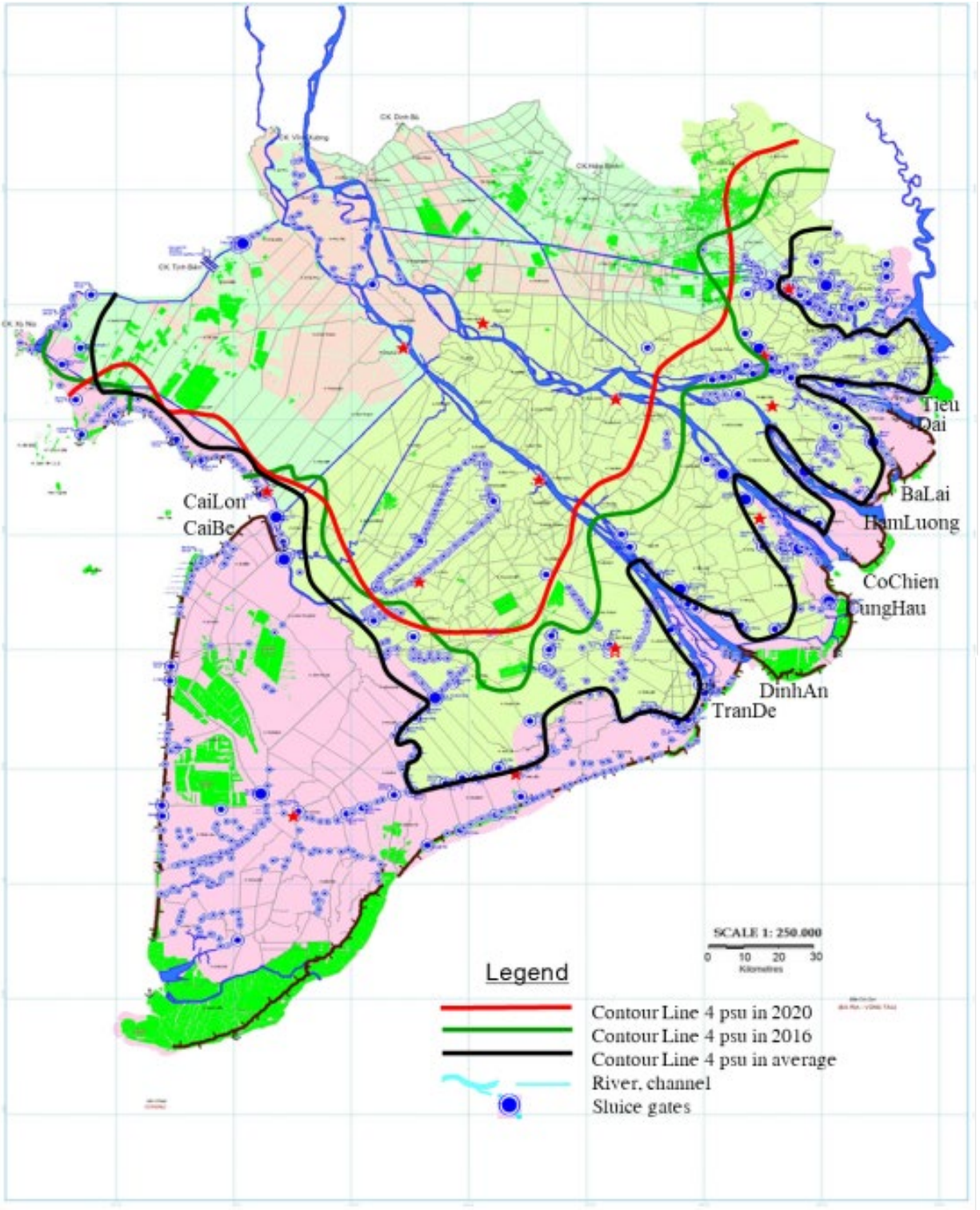

Figure 1.3 Map of salinity intrusion in mean average years, 2016 and 2020 in VMD

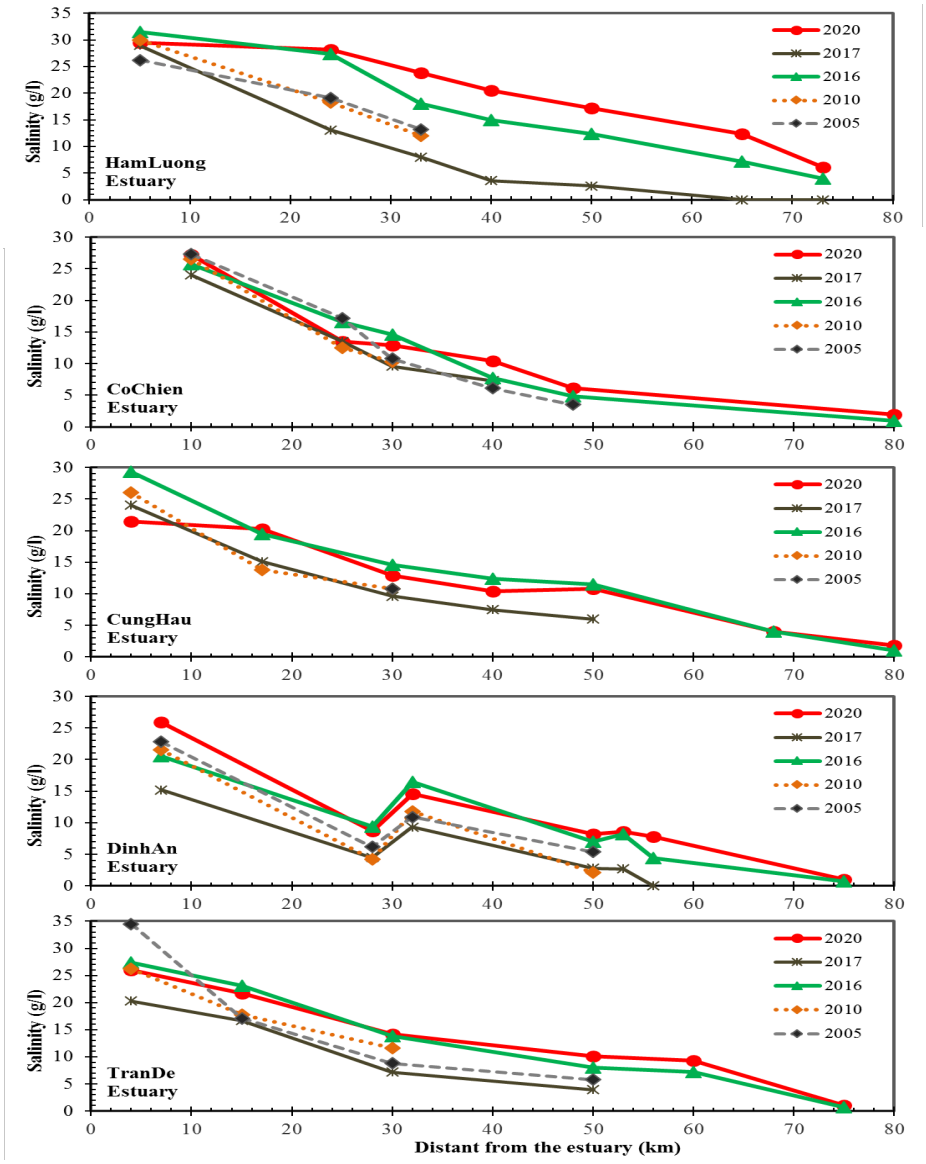

Figure 1.4 The maximum intrusion length along five estuaries of VMD

geomorphology (Viet, 2007). While Nguyen (2008) researched the effect of tides on salinity intrusion in multi-channel estuaries and Toan 2015 studied the impact of upstream development on salinity in the VMD. These studies have made important contributions to the planning and development of irrigation for agricultural production in the delta: saltwater prevention and control, fresh storage, irrigation, and drainage.

However, most studies have considered salinity intrusion under the impact of individual causes or were performed at design frequencies, typical years, and the results mainly show the mean salinity concentration along the river and intrusion length in each scenario. The results are also very useful for the problem of planning projects, design of irrigation systems, and fisheries. The

salinity intrusion reality is influenced by many factors: upstream flow, water demand, river geomorphology, climate, tides, sea level, and wind velocity – direction (figure 1.3). Most of the previous studies considered the influence of one or two factors on mean salinity concentration at one cross-section and intrusion length in a short time, so they could not clarify the salinity intrusion processes. In addition, to account for the different distribution of salinity along the river, at cross-sections and at different river depths, researchers need to find the rule which shows the time to open the sluice gates to intake fresh water. In this study, the author would like to study the effects of four drivers from upstream to delta (in the immediate, short term, or long term) on salinity intrusion by studying the impact of hydropower reservoirs (under normal and abnormal operating conditions) riverbed incision, increasing sea level, and tidal regimes on salinity intrusion processes in the Mekong Delta.

1.3 Research objectives

The main objective of this research is to investigate the impact of upstream discharge, morphology change, and sea-level rise by climate change and tide on salinity intrusion processes in the VMD. After that, adaptive measures should be proposed to mitigate these impacts. To achieve this, the research has specific objectives to pursue:

1. To assess the situation of salinity intrusion in Mekong Delta under the effect of Mekong upstream dams development, sea-level rise, tide, and morphology.
2. To simulate the mechanism of salinity intrusion along the Mekong River under various scenarios due to the influence of upstream reservoir operation, changed morphology, and sea-level rise.
3. Determine spatial and temporal salinity distribution and the river effect due to the tide and flow drivers.
4. To propose the mitigation measures for irrigation and salinity intrusion management.

The main contents of the thesis

This thesis consists of eight chapters which can be divided into four main components: (I) introduction and research methodology (chapter 1), literature review (chapter 2), and methodology (chapter 3), (II) four drivers impact on salinity by upstream flow (chapter 4), morphology change (chapter 5), tidal regime and sea-level rise (chapter 6), (III) adaptive measures to control salinity intrusion (chapter 7) and (IV) conclusions and recommendations (chapter 8).

Chapter 1 is overview of salinity intrusion and a statement of the problems that the MR and the VMD will face due to upstream dams and sea-level rise and tidal regime. It also introduces the research objectives and structures of this thesis.

Chapter 2 is a brief introduction to the research areas, the Mekong River (MR) and Vietnam Mekong Delta (VMD). Then summarizes previous research on the alterations of flow, sediment, morphology, and saltwater by the development of upstream dams. As well as some research results on the effects of tides and climate change on salinity

Chapter 3 presents the approaches and methodologies used in this study to obtain the objectives. Integrated techniques were applied in this study: field surveys, data collection, monitoring, and field measurement, data analysis, and 1D numerical model.

Chapter 4 firstly analyzes long-term alterations of the flow regimes of the lower MR to the VMD under the impact of hydropower dams. First, detailed analyses on extreme (maximum and minimum), daily, monthly, seasonal, and annual discharges and water levels along with the entire lower MR to the VMD are conducted. Secondly, it analyzes the impact of upstream flow alteration on salinity intrusion. Then, two scenarios were diagnosed using the 1D numerical model (Mike 11) was diagnosed the impact of upstream dam operation on salinity concentration and intrusion length.

Chapter 5 analyzes long-term changes in VMD's morphology in the Hau River and Tien River. Using a 1D numerical model, it assesses the impact of morphology change on the salinity intrusion.

Chapter 6 analyzes the impact of sea-level rise and tide on salinity distribution. The results showed the vertical and longitudinal salinity distribution along the Hau and Co Chien River during the high tide and low tide. The spatial and temporal salinity distribution along the 50km river has been conducted in two surveyed cross-sections during one tidal cycle. This chapter gives the results of mixing and stratification in four estuaries.

Chapter 7 assesses the existing hydraulic constructions' ability and proposes mitigation measures for minimization and adapting in VMD.

Chapter 8 summarizes new findings of the research and proposes some directions to guide future studies. It also draws some recommendations to improve the VMD in sustainable water resources management and development.

Chapter 2: Study Areas and Literature Review

2.1 Mekong River Basin

The Mekong River (MR) originates from the Tibetan Plateau in China. It flows through six countries: China, Myanmar, Lao PDR, Thailand, Cambodia, and Vietnam, before discharging into the East Sea of Vietnam. Being 4.900 km long, the MR is the 12th longest river in the world and is the largest river in Southeast Asia. Also, it is the 10th largest river globally in terms of the mean annual discharge of 14,500 m^3/s (MRC, 2016). The Mekong can be divided into the Upper Basin in China, where the river is called the Lancang, and the Lower Mekong Basin from Yunnan downstream to the Sea. The Lancang Basin covers an area of 164,400 km^2, with an annual average volume of 64 billion m^3, accounting for 20.7% of the total Mekong Basin area of 795,000 km^2 and 13.5% of the total Mekong average yearly volume of 475 billion m^3, respectively (MRC, 2005).

Rapid population growth and economic development have increased the demand for water resources and energy in the past few decades (MRC, 2005, 2010b). Many hydropower dams have been constructed in the MR (Fan et al., 2014 and Kuenzer et al., 2012). By 2016, fifty six hydropower dams had been completed along the mainstream and tributaries (Mai, 2018) among 133 proposed dams with over 100 km^3 total storage capacity (Kantoush, 2017), in which six mega-dams (known as Langcang cascade) are in the mainstream. The Gongguoqiao Reservoir started fully operational in 2012, Xiaowan in 2010, Manwan in 2007, Dachaoshan in 2003, Nuozhadu in 2014, and Jinghong in 2009 (Figure 2.1). The total and active storage capacities of these six dams are approximately 41.2 km^3 and 23.1 km^3 (Fan, 2015), accounting for 48.9% and 27.4%, respectively, of the annual mean discharge at Chiang Saen, the nearest hydrological station downstream of the Chinese dams (Figure 2.1). The operations of these dams have altered the flow regime of the Mekong Basin, i.e., increasing the dry season while decreasing the wet season flows (Kuenzer, 2012). Rasenen et al. (2012) concluded that the flow discharges in the dry season at Chiang Saen have significantly increased by 90.0%. Moreover, the operations of all planned dams may lead to increases of 25.0-160.0% and 41.0-108.0% of the dry season discharges at Kratie and ChiangSean, respectively, in comparison between 1982-1992 and 2030-2040 periods (Lauri, 2012). Dams not only have inevitable impacts on the hydrological regime but also impact sediment transport. At Chiang Saen and Vietnam Mekong Delta, the suspended sediment budgets reduced 89.5% and 74.1% respectively after 64 dams completed in MRB while 40.2% was caused by the

six mainstream dams in the Lancang cascade (Binh et al., 2020). Similarly, the annual sediment discharge to the East Sea of Vietnam from the MR has reduced by 74%, from 144 Mt/yr during before 1992 period to 37.7 Mt/yr during 2012-2015 (Binh et al., 2020).

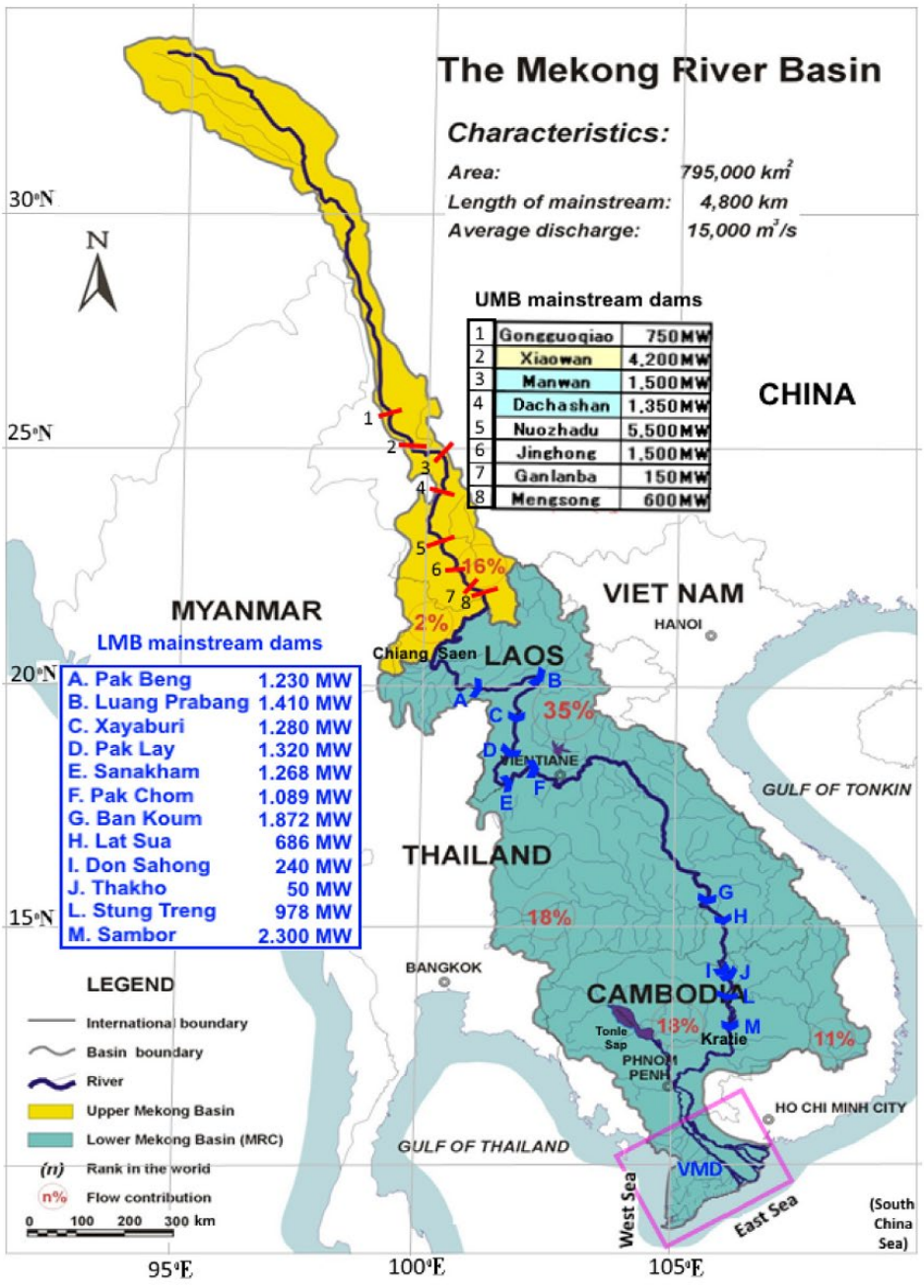

Figure 2.1 Map of the Upper and Lower Mekong River Basin (Sources: Nhan et al., 2019)

Furthermore, eleven hydropower projects have been proposed for the Mekong River mainstream in Lao PDR and Cambodia to tap the available hydropower capacity (Figure 2.1). Construction

and operation of any or all of these projects could potentially have substantial and wide-ranging environmental and socio-economic effects in all four Lower Mekong Basin (LMB) countries. The downstream floodplains of Cambodia and Viet Nam, which make up the Mekong River Delta, in particular could experience the greatest impacts.

2.2 Vietnamese Mekong Delta

The Vietnamese Mekong Delta (VMD) is located at the lowermost branch of MR with a total area of 39,000 km^2 from the Vietnam-Cambodia border to the East Sea (Figure 2.2). The MR is divided into two branches flowing into the Tien River and Hau River in Vietnamese territory. The Tien River is the northern branch of the river system, which separates into five branches (Cua Tieu, Cua Dai, Ba Lai, Ham Luong, Co Chien, Cung Hau) before flowing to the East Sea. The Hau River is the most southern branch of the river system. When the Hau River approaches the sea, it splits into two sub-branches: Dinh An and Tran De at 33km from the estuaries. The Tien and Hau Rivers have a length of approximately 250km and 220km, respectively (Kantoush et al., 2017). Therefore, the discharge distribution between two branches (Tien and Hau River) is unequal. An annual rate of Tan Chau (Tien River)/ Chau Doc (Hau River) in the dry season could be estimated at 84%/16% or 86%/14% (Le, 2006). After the Vam Nao channel, the discharge between the Tien and Hau River is relatively balanced because the Vam Nao channel is a diversion river, shifting water from the Tien River to the Hau River.

The VMD has 21.4 million people (until 2019), accounting for 22% of the national population. This delta is the largest agricultural, fishery and fruit production center in Vietnam. The region's rice production accounts for 50% of the country. The region produces more than 90% of the country's rice export and more than 60% of the country's seafood production. Fruit trees play an important role in the region and in Vietnam in general. The Gross Domestic Product (GDP) of the VMD in June 2019 is 7.8%.

The delta's sustainable development could potentially impacts from climate change (the mean temperature might increase by 0.62ºC during 1958-2014) (IPPC2016), sea-level rise (water level at Vung Tau hydrology station increased with rate of 5.6mm / yr (IPPC, 2016) (or 5.5mm / yr) (Doyle et al., 2010). Maximum amplitudes were 3.2m in 1993 to 3.8m (from Wolanski et al. 1996 and Gugliotta et al. 2017 respectively). In 2016, fifty-six large hydropower dams (> 15m high) were built upstream six of which were mega-dams in the Langcang cascades (Kondolf et al., 2014;

Mai et al., 2018). These cascades reduce the sediment load in the delta from 140Mt / yr (Ta et al., 2002) to 40Mt / yr (Nowacki et al., 2015) and are the leading cause of riverbed incision with the incision rate of 1.24m / yr in The Tien River (Binh et al., 2020) and 0.14m / yr in the Hau River (Alison et al., 2017). In addition, upstream dams have changed the flow in both flood and dry seasons (Li et al., 2008); the total dry season runoff increases, but the flow is in flux (Mai et al., 2018) leading to more and more complicated changes in salinity intrusion in the dry season and changes in water resources, daily life, and agricultural production (affecting seasons, cultivated rice area, reduced productivity and yield of food).

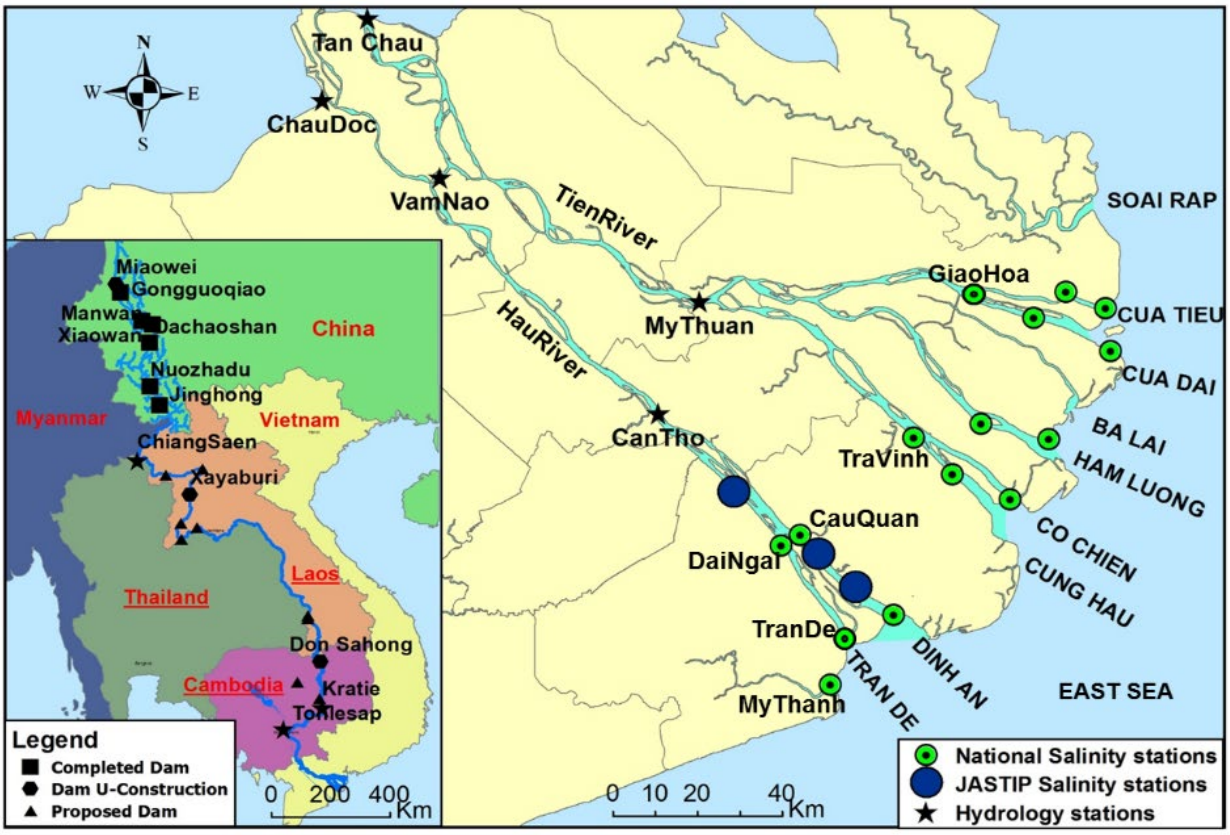

Figure 2.2 Map of the Vietnamese Mekong Delta

The mean annual flow is 15,000 m^3/s, the maximum discharge is about 60,000 m^3/s in the flood season (June – November), and the minimum discharge is around 2,000 m^3/s in the dry season (December – May) (MRC, 2016). The discharges influence the flow at Kratie and Tonle Sap Lake, local rainfall, tidal movement, and the sea level along the East Sea and West Sea (the Gulf of

Thailand). However, when the salinity intrusion problems prevail during the dry season, local rainfall plays a minor role (Le, 2006).

The Tide regime in the East Sea is a semi-diurnal character with 12.25 hours. There are generally two troughs and two peaks during a day, but their relative height varies over a fortnight. When the first trough decreases from day to day, the other trough increases, and vice versa. The tidal range is relatively high, with maximum tidal amplitudes at river mouths of 3.8m (Gugliotta et al., 2017). In general, the tide in the East Sea varies daily, seasonally, and yearly.

2.3 Literature reviews

In recent years, the VMD has been strongly affected by the early onset of salinity intrusion, which is expected to intrude further inland and keep for a longer time. Therefore, many studies on the mechanism of saltwater intrusion have been carried out. However, salinity is affected by many driving factors such as river flow, flow currents, morphology, tides, sea-level rise, winds, water use, human activities, and geomorphological factors (topography, bathymetry). Most of the previous researchers have studied salinity under the influence of one or two driving factors.

For instance, some studies found that the increase in total dry flow from upstream was Eslami et al., 2019b; Li et al., 2017; Lu et al., 2014; Räsänen et al., 2017 or another study which observed the influence of upstream dams development on sediment content by sediment trapping inside the upstream reservoirs by Binh et al., 2020; Gugliotta et al., 2017; Fan et al., 2015, 2018; Manh et al., 2015; Kondolf et al., 2014; MRC, 2010; and intensive downstream sand mining (Eslami et al., 2019b; Brunier et al., 2014). Also, there are some studies on the effects of climate change - one of which is on sea level rise on saltwater intrusion by Duong et al., 2017; Nhan 2016, Toan et al. 2014 and Khang 2008, or on the effects of tide, wind in Figure 2.1 and Table 2.1 summarizes previous studies related to factors affecting salinity, as well as reflections on the salinity mechanism of rivers around the world and the MK River.

Prior studies have been divided into three main groups:

2.3.1 The impact of upstream hydropower dams on the flow and sediment transport

There are many studies on the impact of upstream hydropower dams along the Mekong mainstream, especially the effect of six large lakes on the mainstream in China. Most studies have shown the same trend as damage operation shifting water from the wet season to the dry season, but the amount of water transferred varies greatly. The total wet flows at Chiang Saen station

decreased by 53% (Lauri et al., 2012), or from 32% to 46% between the average of 1960-2014 period with the flow in 2014 (Rasanen et al., 2017). Similarly, at Kratie, the total wet flow reduced by a maximum of 6%, 24%, and 30-40% is the result of Rasanen et al., 2017; Lauri et al., 2012; Kuenzer et al., 2012 respectively. Meanwhile, the total dry flows increased rapidly with a maximum of 90%, 108%, and 187% at Chiang Saen station and 160%, 74% at Kratie station (Table 2.1). Most of the above research results are through numerical models with different scenarios. However, the research results are still biased, and there is a lack of analysis of the flow sequence at the two stations of Chiang Saen and Kratie over a long period.

In addition, many studies on the influence of hydropower reservoirs on the transport of sediment along the river, sediment to the VMD, and the amount of sand extraction at the VMD. When the dams were completed, they trapped sediment which caused the sediment content to fall sharply from 56% to 95% in the report of Arias et al., 2014; Manh et al., 2015; Wolanski et al., 1996. This is also the leading cause of bed incisions along Hau and Tien Rivers. For instance, Brunier et al., 2014 said that the mean depth of both channels would reduce 1-3m by 90Mm^3 to 110 Mm^3 bed sediment loss over a ten year period. Similarly, Allison et al., 2017a concluded that the bed incision rate in Hau River was 0.14mm/yr in the 2008-2018 periods. Both results were similar and lower than the results of Binh et al., 2020. The research was small scale on two tributaries of Tien and Hau rivers, so the results do not fully reflect the extent of influence on VMD.

Both sediments reducing and upstream flow changing had a significant impact on salinity intrusion in VMD (Gugliotta et al., 20174; Nowacki et al., 2015; Zhang et al., 2013, Viet et al., 2007 and Wolanski et al. 1996, 1998) (Table 2.1).

2.3.2 The impact of sea-level rise, tide regime on salinity intrusion and mixing processes

According to the conclusion of IPCC 2016, the sea level rise in Vietnam is likely to be higher than the global average sea level. Especially in the East Sea, the sea level rise is higher than in other areas. The sea-level rise trend is 5.5 - 5.8 mm/yr under RCP4.5 or 6.25 - 8.33 mm/yr under the RCP8.5 scenario. Nhan 2016 analyzed the water level data from 1984 to 2016 of 5 Mekong estuary stations and concluded that the average sea-level rise in the East Sea was 11.8 mm/yr at My Thanh station. Many researchers adopt models to simulate the evolution of salinity concentration and the length of saline intrusion when the sea level increases by 20cm, 45cm, or 1m in the future and

consider the reduction of upstream currents from15% to 29% under different scenarios (Duong et al., 2018; Vu et al., 2018; Toan 2014 and Khang et al. 2008). However, these studies have not considered the tidal factor, except for Nhan 2016.

Tide is one of the critical factors that strongly affect the mechanism of salinity intrusion. However, studies of tidal influence on the salinity mechanism in the VMD are not too prevalent. Nhan 2016 said that the maximum tidal level and tidal amplitude are increasing while the tidal phase at the coast is decreasing. Eslami et al., 2019 calculated the speed at which tidal wave travels are about 35-40km/h, they showed the discharge division in 7 MK estuaries but the result was quite different from the results of Nguyen et al., 2006, 2008 (Figure 2.3). Both researchers analyzed the impact of flow, topography and tide on the salinity intrusion in VMD.

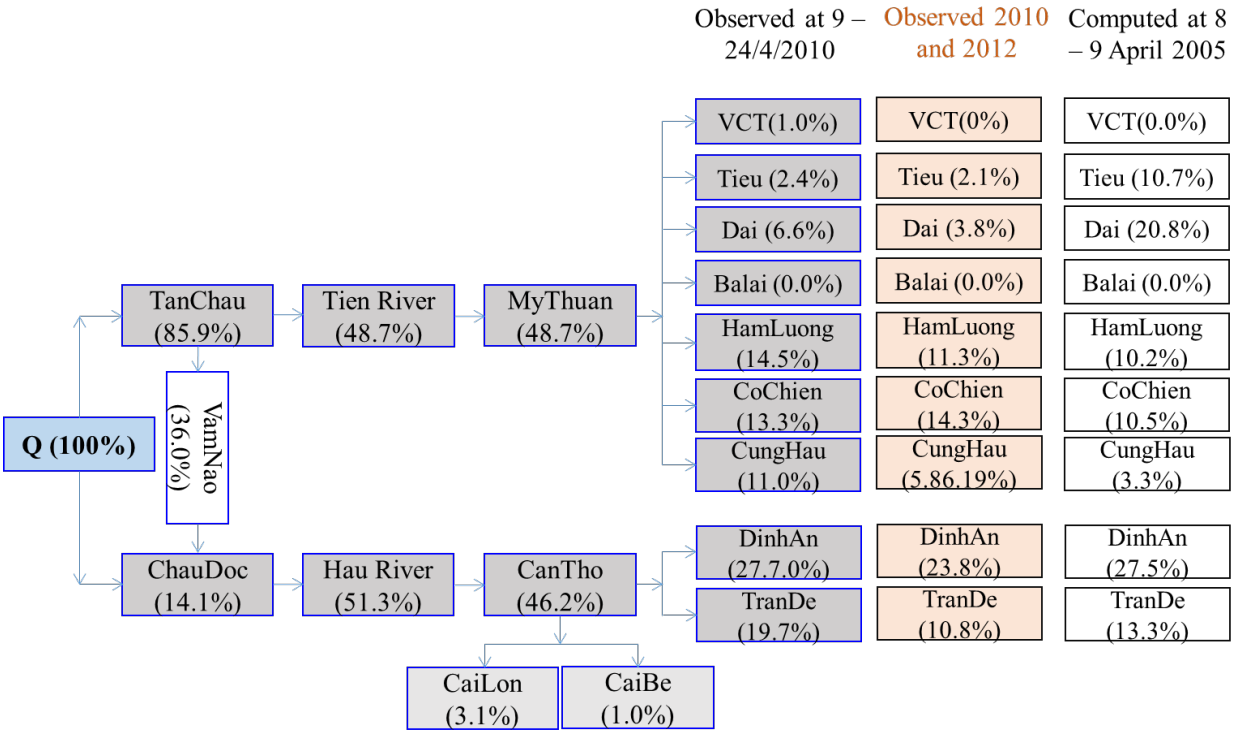

Figure 2.3 Discharge distributions over the branches of the Mekong Delta by Observation and computation**.** (Sources: Nguyen et al., 2008, Report of SIWRP, 2011 and Eslami et al., 2019a)

Prior tidal studies have been divided into three main groups: 1) The tidally-averaged steady-state theories of difference between upstream dispersive versus downstream advective salinity intrusion (Savenije, 2012; Nguyen et al., 2006; 2008; Hansen and Rattray, 1965; Pritchard, 1956), 2). Non-stationary decomposition of salt transport processes such as tidal pumping, tidal straining, gravitational circulation, and residual flow (Simpson et al., 2001; Fischer, 1976; Uncles et al.,

1985) and 3) 3D numerical modeling (Eslami et al., 2021; Bingjun et al., 2017; Wang et al., 2012, Gong et al., 2012). The first group generally provides a primary framework for studying long-term (seasonal or decadal) trends in estuarine systems. A second group is an approach to understanding the physical processes that dominate estuarine salinity dynamics. However, as estuarine systems are often quasi/unsteady and in the transition process, these systems lack detailed high-resolution long-term measurements, so it would be prudent to compare any prognostic evaluation of estuarine dynamics to numerical modeling (the third study group). The difference between upstream dispersive and downstream advective salt flux and the difference between stratification and tidal mixing leads to variations of salinity and its transport mechanisms in multiple temporal and spatial scales. To qualitatively present the effect of freshwater inflow and tides in an estuarine system, a tidally averaged steady-state approach can be adopted. When in-depth quantitative knowledge is required, the Spatio-temporal estuarine variabilities of spring-neap cycles, stratification, transversal variabilities, and their interactions become critical processes (Table 2.2).

2.3.3 The existing mitigation measures on salinity intrusion

Smajgl et al., 2015 described the principle adaptation options to mitigate the effects of salinity intrusion on agricultural production and assess the effective adaptation strategies reliant on land-use change and investments in water infrastructure. As a result, many structural and non-structural measures have been proposed and implemented on a large scale, such as; (1) building a salinity warning system through automatic measuring stations (Apel et al., 2020), (2) changing land use in accordance with water quality such as the conversion of rice mono-culture to rice-shrimp rotational farming as an adaptation strategy, (3) adjustments of rice crop seasons (Dang, 2015), (4) crop system improvement and flow water management programs, (5) SI prevention sluice gate construction projects, (6) seashore protection and improvement project and (7) TraVinh, BenTre fresh water recruitment project (JICA report, 2013) (Table 2.3).

All previous studies related to salinity intrusion processes in river systems worldwide and in the VMD under many different driving factors are summarized on the diagram in Figure 2.4 and Table 2.1, 2.2 and 2.3. The author divided their studies into three groups for instance: group 1 is concerned with the impact of upstream dams on the flow, morphology (sediment) and SI. Group 2 is about the impact of SLR and tide on SI processes while thelast, group 3 focuses on mitigation and adaptive measures with SI processes.

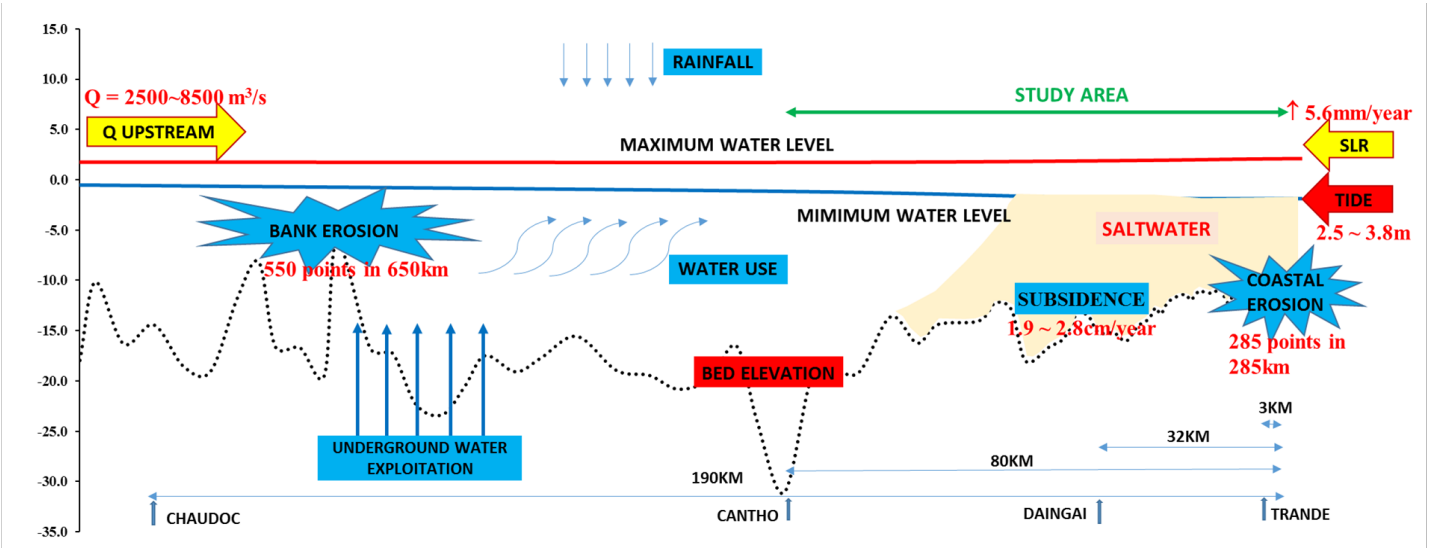

Group 1 : external factors		Group 2: internal factors			Solution
Upstream flow	**Morphorlogy**	**Tide**	**SLR**	**Stratification**	**Mitigation& Adaptation**
Dang et al., 2018	Eslami et al., 2021	Bingjun et al.,	Hong et al., 2020	Mikhailova, 2012	Apel et al., 2020
Räsänen et al.,	Binh et al., 2020	Savenije, 2012	Duong et al., 2018	Kikiaki et al., 2010	Nhan et al., 2019
Allison et al.,	Ha et al., 2018	Zhang et al., 2013	Vu et al., 2018	Geyer, 1999	Chapman et al., 2016
MRC, 2016	Kondolf, et al., 2018	Wang et al., 2012	Vietnam IPCC, 2016	Pritchard, 1995	Smajgi et al., 2015
Hoang et al., 2016	Gugliotta et al., 2017	Gong et al., 2012	CGIAR, 2016	UNESCO, 1991	Dang, 2015
Dang et al., 2016	Allison et al., 2017a	Eslami et al.,	Nhan, 2016	Fischer et al., 1979	JICA Report, 2013
Toan, 2015	Nowacki et al., 2015	Gong et al., 2011	Toan et al, 2014		Orr et al 2012
Fan et al., 2015	Brunier et al., 2014	Kiriaki et al.,	Doyle et al., 2010		
Manh et al., 2015	Kondolf, et al., 2014	Nguyen et al.,	Khang et al., 2008		
Arias et al., 2014	Zhang et al., 2013	Nguyen et al.,			
(Manh et al., 2014)	Viet et al., 2007	Tateishi et al.,			
Kuenzer et al.,	Wolanski et al., 1998		**Wind and Wave**		
Lauri et al., 2012	Wolanski et al., 1996		Gong et al., 2018		
Räsänen et al.,					
Xue et al., 2011					
Lu and Siew, 2006					

Figure 2.4 Summarized the previous studies on the factors impact on the salinity intrusion in VMD

Table 2.1 Summarized the previous studies on the impact of upstream dams on the salinity intrusion (SI) processes in VMD

Factor	Objective	Study area	Method	Significant findings	Authors
River flow and sediment change	Effects of water infrastructures, land subsidence, and SLR on flow regimes	CMD, TSL, and VMD	Numerical model	Dam operations increase and decrease by 20-70% and 0.8-5.9% of floodplain's water level in the wet and dry seasons, respectively, in river-dominated areas. Land subsidence combined with SLR has great impacts on future VMD's inundation.	Dang et al., 2018
	Assess the impacts of dams on flow change	MRB	Data analysis and numerical model	Hydropower operations have considerably modified the river discharge since 2011 and the largest changes were observed in 2014. At Chiang Saen: Q↑ by 121-187% in March-May 2014 and Q↓ in July-August 2014 by 32-46% compared to average $Q_{1960-2014}$. At Kratie: Q↑ 41-74% in March-May 2014 and 0-6% Q↓ in July-August 2014.	Räsänen et al., 2017
	Impacts of dams on the flow, sediment, sand mining, and morphology	VMD	Review	Less sediment arriving VMD from MR is balanced by sediment from the inner shelf. Dams cause channel-bed incision downstream that partly compensates trapped sediment by dams. Sand mining may be reduced due to dams trapping sediment; therefore, sand transporting to the sea may be reduced accordingly.	Allison et al., 2017b
	Impact of climate change on hydrology of MRB	MRB	Reservoir cascade optimization	The Mekong's hydrological cycle intensifies under future climate change Extremely high flow events increase in both magnitude and frequency Extremely low flows occur less often under climate change	Hoang et al., 2016
	The impact of dam on flow regime and Salinity intrusion in VMD	MRB	Three numerical models	Using three numerical models to predict the flow change from the upstream gives a good review for all MRD. Increasing water use upstream leads to a lack of water in VMD.	Toan, 2015

				Abnormal operation of upstream dams has more effect on flow regime, salinity intrusion, and land use. Propose some salinity intrusion mitigation for VMD.	
	The impacts of dams on hydrology, sediment, water quality, ecology and fish	Upper MRB	Review and Data analysis	Dam operations shift water from the wet to dry season. Damming can also produce enormous negative effects on the environment and ecosystems. Flow increases due to climate warming, with the abrupt change in the lower MRB occurring in the mid-1960s and late 1990s	Fan et al., 2015
River flow and sediment change	Assess response of floodplain hydrology and sediment dynamics to dams, climate change, and SLR	CMD, TSL, and VMD	Numerical model	Hydropower dams govern changes in floodplain sediment dynamics of VMD while SLR has the smallest effect. Dams, climate change, and SLR slightly increase inundation in the VMD but decrease floodplain sedimentation by ~40%. The maximum change caused by all these drivers is to reduce 90% of delta sedimentation and 95% of sediment reaching to the sea.	Manh et al., 2015
	The impacts on the flow and climate change	Tonle Sap Lake	Process-based model and Hydrological model	Hydropower dams changes in seasonality by reducing wet season water levels and increasing dry season water levels Combined dams and climate change revealed that areas of open water and rainfed/irrigated rice would expand by 35±3% and 16±5%, respectively, while optimal area for gallery forest would decrease by 40±27%. The estimated annual net sedimentation was projected to decrease by 56±3% from the 3.28±0.93 Mt baseline values	Arias et al., 2014
	Quantify suspended sediment transport and deposition	CMD, TSL, and VMD	Numerical model	River flow, tide, channel system, dikes, and sluice gate operations are the main factors controlling the spatial sediment dynamics Deposited sediment in CMD and VMD are 19-23% and 1-6% of Kratie's sediment, respectively	Manh et al., 2014

River flow and sediment change	Investigate the impact of hydropower dams on the flow and sedimentation	MRB	Review	Assessing the impact of upstream Chinses dams on downstream water level and sedimentation: The W_{dry} ↑ while W_{wet} ↓ (seven previous studies) - During the low flow, the flow in Yunnan contributes about 70% of low flow component at Vientiane and 30-40% at Kratie. - 40 to 50% sediment loss is expected to aggravate coastal erosion and saltwater intrusion in MD, which SLR already threatened. - Hydropower dams can meet the rising energy demand of the upstream countries, but they have severe impacts on the environment and the livelihoods of the rural Mekong population.	Kuenzer et al., 2012
	The cumulative impact of dams and climate change on the hydrology of MR within the next 20-30 years	MRB	Numerical model	The operation of planned dams does not significantly impact the annual water discharge. Still, it causes 25–160% higher dry season (Dec to May) discharges at Kratie, 41–108% higher dry season discharges at Chiang Saen, 5–24% lower wet season discharges at Kratie, and 3–53% lower wet season discharges at Chiang Saen. The discharge decreases by 24% at Kratie and 53% at Chiang Saen during the beginning of the wet season in July. The discharge decreases by 8% at Kratie and 13% at Chiang Saen during September, the wettest month.	Lauri et al., 2012
	Assess the impact on downstream hydrology	MRB from Lancang cascade to Kratie	3D Hydrodynamic model	On average, Q_{dry} ↑ 90% and Q_{wet}↓ 22% at Chiang Saen. Dry season hydrological changes were significant also in all downstream gauging stations, even as far as Kratie The Mekong's hydrological regime has been significantly altered by the Lancang cascade by three scenarios no dams, first three dams completed, and six dams completed.	Räsänen et al., 2012
	Impacts of dams and climate variability on precipitation, flow, and sediment	Middle MRB to VMD	Statistical analysis	No significant change in rainfall and runoff over the past 50 years The runoff will be more sensitive to ENSO if more dams are built	(Xue et al., 2011)

	Impacts of Lancang cascade on alteration of flow and sediment fluxes	Middle MRB	Data analysis	Manwan caused alterations of low, reductions of suspended sediment flux	(Lu and Siew, 2006)
Morphology change	Dynamic of salt intrusion by field observation and integrated coastal-inland modelling	VMD	Field survey and numerical model: 3D	An average near -1.5 m incision in Ham Luong channel during the 2008-2018 period and decrease -3 m along the thalweg, which significantly influences tidal propagation and fresh-saline water dynamics. Stratification increases during the neap tide lead to estuarine circulation dominating upstream salt transport during the neap tide. This study showed that subtidal ocean surges could impact the temporal variation of salinity by up to 20%. A discharge pulse at Kratie (Cambodia) travels to the delta in 3-4 days, and its effect lasts 3-4 days longer than the pulse itself. This study also emphasizes the importance of riverbed levels in controlling salt intrusion.	Eslami et al., 2021
Morphology change	Effects of riverbed incision on the hydrology and SI	VMD – Tien River	Field survey and statistical analysis	Q_{dry} at TanChau increased by up to 23% from the 1980-1992 period to the 1993-2018 period but that the $WL_{dry\text{-}season}$ at My Thuan decreased by up to −46% by the accelerated riverbed incision upstream from My Thuan. *From TC to VamNao, mean incision rate is −0.16 m/yr in 1998–2014 to −0.5 m/year in 2014–2017 by the reduction in the sediment load (from 166.7 Mt/yrr to 57.6 Mt/yr) and sand mining (from 3.9Mm^3 in 2012 to 13.43Mm^3 in 2018).* *From TC to MyThuan, riverbed incision reduces from -0.43 to -14.87m deep (mean value: -5.2m). So, incision rate: -0.03 to -0.93m/yr (mean: -0.33m/yr) in 1998-2014 period. While incision rate is from -0.15 to -3.79m/yr (mean: -1.24m/yr) in 2014-2017 period.*	Binh et al., 2020

				The decreased dry season water level in the Tien River is likely one of the main causes of the enhanced SI by S_{max} and L_{max} much increases in recent drought years.	
	channel morphology and sediment distribution vary along FMTZ and the linking to salinity and process regime	VMD	Field survey and Data analysis	Tien and Hau River have divided two main tracts and four subzones. Tide-induce water level changes affect the entire VMD to Cambodia In low flow, high diluted brackish water reaches ~160km from the river mouth. Salinity intrusion length in the wet – dry season is 15km and 50km. Seaward-deepening trend in the upstream tract and shallowing trend in the downstream tract. Mud content increase seaward, and sand grain size generally decreases seaward.	Gugliotta et al., 2017
	Examine channel bottom morphology link with sediment transport	VMD	Field survey	Channel floor: sand dune (19% of area), soft mud in low-flow (0.25-1m thick) and substratum outcrops of relict facies (80% of area) Mud layer is source of resuspended sediment Dams are main cause of bed incision in Hau River (sand mining has little effect). The incision rate is −0.14 m/yr in 2008−2018 period.	Allison et al., 2017a
Morphology change	Quantify changes in hydrodynamics and sediment transport on temporall-spatially Residual sediment flux Contributors of sediment-transport processes	VMD – Hau River	Field survey	Salt wedge in high-flow and partially mixed estuary in low-flow DinhAn export sediment to sea at rate 1 T/s in high-flow and import from sea at rate 0.3 T/s in low-flow Annual sediment discharge is 40 Mt Fluvial advection control sediment export in high-flow Exchange-flow and tidal process including local resuspension are mainly responsible for low-flow import Coarser sediment in high-flow and finer in low-flow	Nowacki et al., 2015
	Morphological changes of Tien and Hau rivers.	VMD	Statistical analysis	Mean depth of both channel reduces by >1.3m	Brunier et al., 2014

	Finding the controlling factors			Tien and Hau rivers lose bed material of: 90 and 110 Mm^3 over the 10-year period Sand mining is the main cause of bed sediment losses; therefore, will cause bank and shoreline erosion Other contributing factors include: numerous dykes, embankments.	
	Calculation the maximum intrusion length	Modaomen estuary	Field survey and Numerical model -1D	The impact of upstream flow on intrusion length and salinity concentration during a drought is significant. The abrupt change in topography due to intensive dredging campaigns is the most crucial factor leading to the severe saltwater intrusion.	Zhang et al., 2013
	The effect of morphology change on salinity distribution	VMD Dinh An branch	Field survey, numerical model: 3D	The salinity change is influenced by river discharge, tidal level, and estuarine morphology change. The river mouth width directly affects salinity concentration. The influence of morphology changes on salinity distribution should not be ignored when simulating salinity.	Viet and Tanaka, 2007
	Field studies of fine sediment dynamic, salinity and tide current in the low flow	VMD: Hau River	Field survey	The salinity intrusion extended 50km up-river with vertical stratification in salinity occurring around slack tidal currents The suspended sediment was mainly fine silt, with flocculation occurring in the saline region. Saltwater is more turbid than freshwater	Wolanski et al., 1998
	Investigation on sediment dynamic, erosion – deposion, salinity and flow velocity at Hau estuary in high flow.	VMD: Hau River	Field survey	Salt wedge in the high-flow and partially mixed estuary in low-flow with intrusion length about 40km. 95% of annual sediment flux exports to sea and deposits in shallow coastal water (<20 km from river mouths), of which 5% will transport back to rivers by a salt wedge. A maximum turbidity zone was present at the toe of the salt wedge at the flood tide.	Wolanski et al., 1996

Table 2.2 Summarized the previous studies on the impact of SLR, Tide on SI processes and Mixing - Stratification

Factor	Objective	Study area	Method	Significant findings	Authors
Sea Level Rise	Potential physical impacts of SLR on SI	Pearl river estuary -China	Numerical model 3D	We found that, in general, the salinity, stratification, and tidal range will increase as the sea level rises. The rate of increase in stratification in response to the sea-level rise was found to be higher during high-flow conditions	Hong et al, 2020
	Simulation the future flow, water level and SI for 2036 and 2065 period.	VMD- Hau River	Numerical model 1D, 2D	The average discharge in the dry season fluctuates greatly, from 1700 m^3/s to 6000 m^3/s between January and May. Setup 2D model: triangular mesh size: 80-100m to 800-1000 in the river and offshore. Constant salinity boundary in the sea: 35psu. In 2060 with 35cm SLR and reduced 20% in river flow, the L_{max} and S_{max} will increase 3.92km and 1psu. Increasing the saltwater pushing time from 7.27h to 58.95h for maximum discharge of 4500 m^3/s to 400 m^3/s.	Duong et al., 2018
	Assesing the impact of SLR on SI	VMD	Numerical model: 1D	Under 25cm or 30cm SLR, saltwater will intrude up to 50-60 km into the river, and nearly 30.000ha of agriculture area will be affected.	Vu et al., 2018
	Impacts of climate change and SLR on the flood, tidal inundation, salinity intrusion, and irrigation adaptation	VMD	Numerical model: 1D	If the sea level rises 1 m, saline intrusion will be 20 and 27 km further in Tien and Hau River, respectively, compared to average values. Double dikes (low inner dike and outer high dike) are recommended.	Toan, 2014
	The impact of SLR and flow change on SI and rice cropping	VMD	Numerical model: 1D	Under 20cm and 45cm SLR combine with reducing 15% and 29% river flow, respectively. The results show that the salinity concentration increases 2.5 psu and intrusion length increases from 10 to 20km in the main river and 20 to 35km in the paddy field.	Khang et al., 2008
Tide and SLR	Tidal regime deformation by SLR along the coast	VMD	Statistical - analysis and Numerical model	SLR is causing severe negative impacts in many river deltas. The maximum tidal level and tidal amplitude increase while the tidal phase at the coast decreases.	Nhan, 2016

				The average rate of changes of the yearly maximum, average, and minimum sea level in the East Sea are 12.7, 11.8, 8.3 mm/yr (at MyThanh) and 13.8, 7.9, 5.8 mm/yr in West sea (at GanhHao)	
Tide	Dynamic characteristic of saltwater intrustion	Pearl River – China (Modaomen estuary)	Numerical model 1D, 3D	Using regression to build the relationship between **Q~Tidal ~ Intrusion length** The bottom intrusion length increased with the increase in the tidal dynamic during Neap tide to the Spring tide. The length reached a maximum of 3 days before the spring tide. Hourly length of salinity intrusion slows down tidal process at Sanzao station: 0km for approximately 4-5 hours	Bingjun et al., 2017
	Book of Salinity and Tides in Alluvial estuaries	Schelde, Gambia		Classification of alluvial estuaries Relating tide to shape of estuaries Tidal dynamic: effect of river discharge, bottom slope, tidal amplitude, Froude number. Mixing and salinity intrusion by tide in alluvial estuaries in HWS, LWS and TA.	Savenije, 2012 (2nd edition)
	Calculation the maximum intrusion length	Modaomen estuary	Field survey and Numerical model -1D	The impact of upstream flow on intrusion length and salinity concentration during a drought is significant. The abrupt change in topography due to intensive dredging campaigns is the most crucial factor leading to the severe saltwater intrusion.	Zhang et al., 2013
Tide and Wind	The effect of interacting downstream branches on saltwater intrusion dynamic.	Modaomen estuary	Numerical model - 3D	Answer why S_{max} occurs during the neap tide or coming moderate tide instead during the spring tide. Because of the spring-neap tidal variation, wind and current are much stronger during the neap tide than during the spring tide in Hongwan waterway effects on Modaomen estuary.	Wang et al., 2012
	The effect of interacting downstream branches on saltwater intrusion dynamic.	Modaomen estuary	Numerical model - 3D	Hongwan waterway serves as a salt sources for mainstream during the spring tide while Hezhou waterway acts as salt sink for the mainstream.	Gong et al., 2012

				Wind increases the steady shear transport and advection transport so wind alters the saltwater intrusion in the estuary. 20% decrease of saltwater intrusion if closure of the Hongwan and Hezhou waterway. These results **provide scientific basis for water resource management in the region.**	
Tide and river flow	Tidal propagation and flow division dynamics	VMD	Numerical model -1D – 2D	The speed of tidal waves travels, amplifies, and propagates about 35-40km/h through the Tien and Hau branches. Tidal amplitude in Hau and Tien is damping along the estuary by tidal amplitude gradually declines upstream up to 25%. Cumulative discharge division in VMD is presented by percentage of Q TanChau+ChauDoc in each branch: **10.8%, 23.8%, 5.8%, 14.3%, 11.3%, 3.8% and 2.1% at** TranDe, DinhAn, CungHau, CoChien, HamLuong, Dai and Tieu estuary respectively.	Eslami et al., 2019
	Investigate the salt transport mechanism and the response of saltwater intrusion to changes in river discharge and tidal mixing.	Pearl River Delta – China (Modaomen estuary)	Numerical model -1D – EFDC model	The salt transport fluxes were decomposed into three components: steady shear flux, advection flux, and tidal oscillatory salt flux. Steady shear flux reaches a maximum and minimum level during the neap and spring tide, respectively. At the same time, tidal oscillatory flux follows an opposite pattern. Consider the response of an estuary in significant flow – normal flow and high flow. During the normal and high flow, the response of an estuary from neap to spring tide is faster than that in the spring to the neap tide. Intrusion length endured significant fluctuations during spring-neap tidal cycles.	Gong and Shen., 2011
	Salt wedge propagation	Strymon river – Mediterranean	Field survey and Data analysis	Eight factors were controlling the estuarine dynamic. Strong vertical stratification prevails throughout the tidal cycle. Bottom topography plays an interesting role in wedge propagation.	Kiriaki et al., 2010

		estuary - Greece			
	Salinity prediction and calculation discharge distribution in single branch and multi-branches.	VMD – Hau River	Field survey 2005 and 2 numerical model	They are calculated a K Ven Der Burgh's coefficient and the mixing coefficient by observation data. Calculation salinity distribution along the river if topography, tide, and river discharge were known. In a single branch, they were compared with multi-branches. Calculate the discharge distribution in over the branches of VMD by salinity model and compare to the hydraulic model. The results were quite similar. Such as **13.3%, 27.5%, 3.3%, 10.5%, 10.2%, 20.8% and 10,7%** at TranDe, DinhAn, CungHau, CoChien, HamLuong, Dai and Tieu estuary respectively.	Nguyen et al., 2006 and 2008
	Observation SI at the low flow 2005	VMD – CoChien River	Field survey 2005	Completed mixed conditions prevailed at least 36km at spring tide and partly stratified at slack tides. The salinity of upper layer changed regularly between flood-ebb tides: strong mixing saltwater. Turbidity data gradually increases from 18km point upstream to 36km.	Tateishi et al., 2005
Wind and Wave	The effect of winds and waves on SI	Pearl River Delta – China (Modaomen estuary)	Numerical model: 1D	Including wind in the model the L increases by 12km. Local wind increases the SI while remote wind increases the vertical mixing and surface salinity in the estuary but only a slight increase in the bottom. The axial down-estuary wind is most efficient at driving saltwater landward, while cross-estuary wind increases vertical mixing and reduces SI. Wave wind (<1,1m) effect on SI is minor.	Gong et al., 2018
	Stratification and salt-wedge under the idealized tidal influence	Seomjin River - Korea	Numerical model	Depth means straining (DMS) and vertical mixing (VM) seem to play significant roles in stratification. DMS and VM contribute differently to the flow circulation and stratification depending on the location within the estuary.	Hwang et al., 2017

Mixing and stratification				Hydrological and morphological changes shift the stratification patterns. *Rie* and *F*0, have been used to describe the general characteristics of straining and mixing.	
	Processes of seawater intrusion into river mouths	Rhone River, Tiber River, Po River, Frase River, Columbia River, Seine River,	Review and theoretical and empirical approaches	Classification of processes of saltwater vertical mixing by Pritchard number, Simmons parameter, Froude number and Richardson number. Prediction the salinity and intrusion length by empirical equations. Consider the influent on SI processes by some factors: river flow, SLR, tidel range, storm surges and shape of river mouths. Six case studies are used to show the specific features of the process of the SI into the river mouths of different types.	Mikhailova, 2012
	Dynamics of a Partially Mixed Estuary in Spring-neap tidal timescales	Hudson River-NewYork	Field survey	Estuarine circulation was found to depend on the intensity of bottom turbulence: based on the tidal velocity magnitude and tidally averaged near-bottom flow. Estuarine circulation can be modeled by an estimate of the bottom drag coefficient, tidal forcing conditions and the baroclinic pressure gradient. Estuarine circulation inverse depends on the tidal amplitude.	Geyer, 1999
	Guidelines on the study of seawater intrusion into rivers.	Mekong River, Rhin-Meuse estuary, West Dvina, Sulina branch, and the North Dvina	Review and theoretical and empirical approaches	Definition of statement problems and mechanisms of SI. Which shows the classification and stratification of estuaries? Organization of analysis, field survey, and measurement processes then analyze the impacts of changes in river mouth on SI by numerical model and predict the SI by correlation and modeling. Five case studies are used.	UNESCO, 1991

Table 2.3 Solution: Summarized the previous studies about Mitigation and Adaptation

Factor	Objective	Study area	Method	Significant findings	Authors
Solution	Potential physical impacts of SLR on SI	Pearl river estuary - China	Numerical model 3D	We found that in general, the salinity, stratification and tidal range will increase as the sea-level rises. The rate of increase in stratification in response to the sea-level rise was found to be higher during high-flow conditions	Hong et al, 2020
	Simulation the future flow, water level and SI for 2036 and 2065 period.	VMD- Hau River	Numerical model 1D, 2D	The average discharge in the dry season fluctuates greatly, from 1700 m^3/s to 6000 m^3/s between January and May. Setup 2D model: triangular mesh size: 80-100m to 800-1000 in the river and offshore. Constant salinity boundary in sea: 35psu. In 2060 with 35cm SLR and reduce 20% river flow, the L_{max} and S_{max} will increase 3.92km and 1psu. Increasing the saltwater pushing time form 7.27h to 58.95h for maximum discharge of 4500 m^3/s to 400 m^3/s.	Duong et al., 2018
	Assesing the impact of SLR on SI	VMD	Numerical model: 1D	Under 25cm or 30cm SLR, saltwater will intrude up to 50-60 km into the river and nearly 30.000ha of agriculture area will be affected.	Vu et al., 2018
	Impacts of climate change and SLR on the flood, tidal inundation, salinity intrusion, and irrigation adaptation	VMD	Numerical model: 1D	If sea level rises 1 m, saline intrusion will be 20 and 27 km further in Tien and Hau River, respectively, compared to average values. Double dikes (inner low dike and outer high dike) are recommended.	Toan, 2014
	The impact of SLR and flow change on SI and rice cropping	VMD	Numerical model: 1D	Under 20cm and 45cm SLR combine with reducing 15% and 29% river flow respectively. The results show that the salinity concentration increases 2.5 psu and intrusion length increases from 10 to 20km in the main river and from 20 to 35km in the paddy field respectively.	Khang et al., 2008

Chapter 3: Methodologies and Data collection

3.1. Methodologies

Figure 3.1 describes an overview of the thesis's methodology. It comprises a literature review to find knowledge gaps to collect the required data. Firstly, long-term discharge, salinity, and water level data have been collected to analyze the current state of salinity intrusion.

The effects existing hydropower dams on historical upstream flow and sediment budgets which two of main factors drive the salinity intrusion processes. Then, the impact of sea level and tide on the salinity concentration and the intrusion length were analyzed. There was a lack of salinity data during the assessment process due to the lack of the salinity stations and discontinuity of salinity data. Most of the salinity stations collected data 12 times per day with a 2-hour interval and only measured in the dry season. Therefore, two additional monitoring salinity stations were installed in the Hau River with an internal measurement of 30 minutes (February 2017) by the JASTIP project (Figure 3.2). Besides, field surveys have been conducted to evaluate the current status and the efficiency of the existing irrigation works. Most of the sluice gates are closed during the high tide in the dry season (1 to 2 months) to prevent saltwater. However, freshwater still occurs on the surface or in the entire water depth during high tide days. Thus, the sluice gates located 25 to 30km far from the estuaries can be opened to intake freshwater. So longitudinal and vertical salinity distribution were measured along 50km of four river branches and seven cross-sections in the Tien, Hau, and CoChien Rivers to assess salinity distribution and determine the timing and duration of opening the sluice gates during the high tide in the dry season. Furthermore, a numerical model was used to predict/estimate the salinity intrusion length, forecast salinity, design the system planning, and propose mitigation measures.

3.2. Long term data collection

3.2.1 Hydrological and Meteorological data

Table 3.1 shows the summary of data collection. Daily discharges and water levels were collected during 1960-2020 at Chiang Saen and Kratie (Figure 2.1), and daily water levels at two stations along the Lower Mekong River were collected in 2016 at Chiang Saen, Kratie, in the middle MRB (Figure 2.1). Daily discharges and water levels at Tan Chau, Chau Doc, Vam Nao, My Thuan, and Can Tho in the VMD (Fig. 3.2) were available during 1980-2020. Salinity data

were measured 12 times per day, and they were not continuous at 14 salinity stations in VMD (Figure 3.2), in which hourly salinity data were collected at four stations in the Hau and CoChien Rivers from 2016-2020. Daily rain data were collected at 32 stations in the VMD in 1998 and 2015.

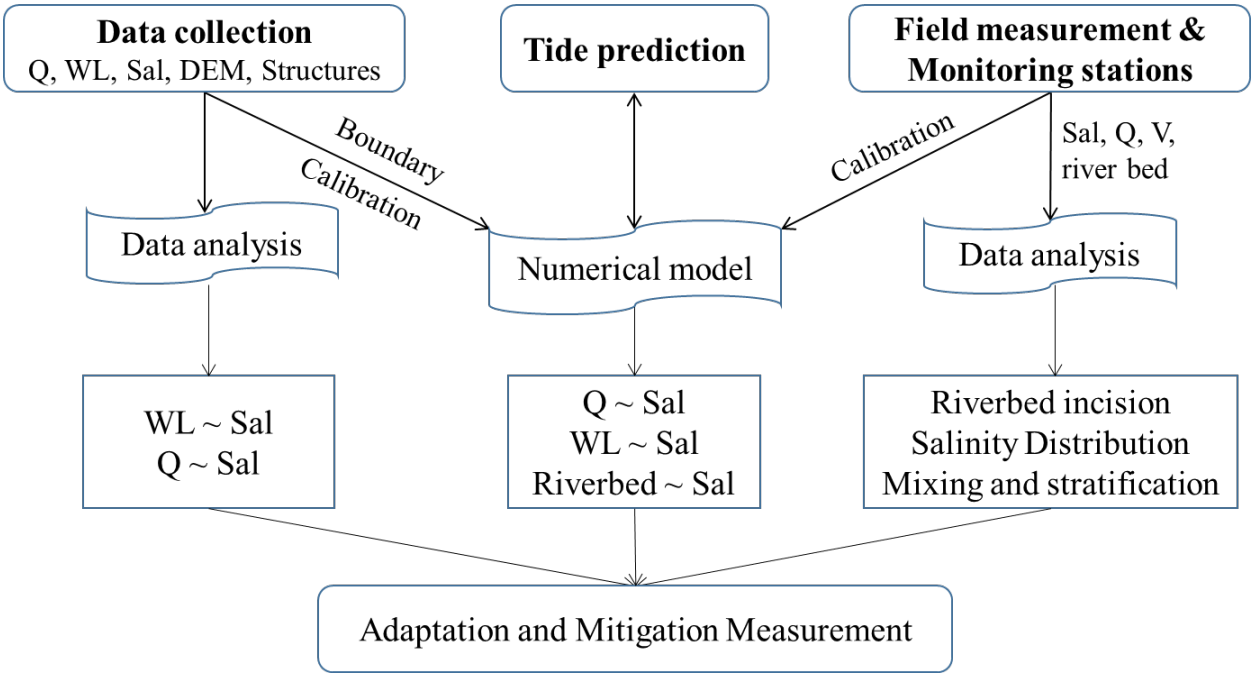

Figure 3.1 Overview of the research methodology and overall objectives.

Discharge and water level data along the Mekong River were collected from the Mekong River Commission (MRC) and the Vietnamese National Center for Hydro-meteorological Data. Hourly water levels at stations in the VMD are monitored using automatic water level recorders, namely Steven A-71 of Steven Water Monitoring System, Inc., USA (e.g., at Tan Chau, Chau Doc, and Can Tho) and ValDai of Valdai Experimental Laboratory, Russia (e.g., at Vam Nao and MyThuan). Hourly discharges were then estimated based on the established stage-discharge rating curves at each station by the Vietnamese National Center for Hydro-meteorological Data.

Daily salinity data have been monitored only in the dry season by the Southern Regional Hydro-meteorological Center (SRHC), but these data were provided by the Southern Institute of Water Resources Research (SIWRR). While hourly salinity data are monitored using automatic equipment and managed by Tra Vinh Irrigation Construction Company Limited.

Table 3.1 Collected hydrological and meteorological data

No	Station Number	Station	River	Data			Time step
				Discharge	Water level	Salinity	
1		Chiang Saen	Mekong	1960-2016	1960-2016		Day
2		Kratie	Mekong	1924-2016	1924-2016		Day
3		Prek Dam	TonleSap		1985 - 2000		Day
4		Tan Chau	Tien River	1980-2020	1996-2015, 1980-2017		Hour
5		Chau Doc	Hau River	1980-2020	1996-2015, 1980-2017		Hour
6		VamNao	Tien - Hau	1980-2020	1996-2015, 1980-2017		Hour
7		Can Tho	Hau River	1980-2020	2000-2015, 1980-2017		Hour
8		My thuan	Tien River	1980-2020	2001-2015, 1980-2017		Hour
9	2	VamKenh	CuaTieu River		2003,2004, 2010 - 2016	1990-2000, 2002-2016	Day
10	8	BinhDai	CuaDai River		2003-2006, 2010 - 2016	1990-2000, 2002-2016	Day
11	10	My Tho	Cua Dai River		2003-2005, 2010 - 2016	1990-2000, 2002-2016	Day
12	11	AnThuan	HamLuong River		2003-2006, 2010 - 2016	1990-2000, 2002-2016	Day
13	12	SonDoc	HamLuong River		2003-2006, 2010 - 2016	1990-2000, 2002-2016	Day
14	16	BenTrai	CoChien River		2003-2006, 2010 - 2016	1990-2000, 2002-2016	Day
15	22	TraVinh	CoChien River		2003-2006, 2010 - 2016	1990-2000, 2002-2016	Day
16	25	TraKha	Hau River		1990-2000, 2002-2018	1990-2000, 2002-2017	Day
17	27	CauQuan	Hau River		1990-2000, 2002-2018	1990-2000, 2002-2017	Day
18	31	TranDe	Hau River		2003,2004, 2010 - 2017	1990-2000, 2002-2017	Day
19	33	DaiNgai	Hau River		1990-2000, 2002-2018	1990-2000, 2002-2017	Day
20	34	An LacTay	Hau River			2016	Day
21	JP1	BacTrang	Hau River			2016-2019	Hour
22	34	CauQuan	Hau River			2016-2019	Hour
23	JP1	TraVinh	Hau River			2016-2019	Hour

3.2.2 Digital map data and satellite images.

All the digital maps, including topography, land used, soil, road, river and canal network, hydraulic works, were collected from the SIWRR. In this study, the canal network in the hydraulic model is combined from all digital maps, Landsat, and Google Earth images.

3.3 Field measurement

Under the JASTIP project, we designed four campaigns of field survey and one campaign to install salinity monitoring stations in the VMD. The schedule and measured reaches of each field survey were summarized in Table 3.2.

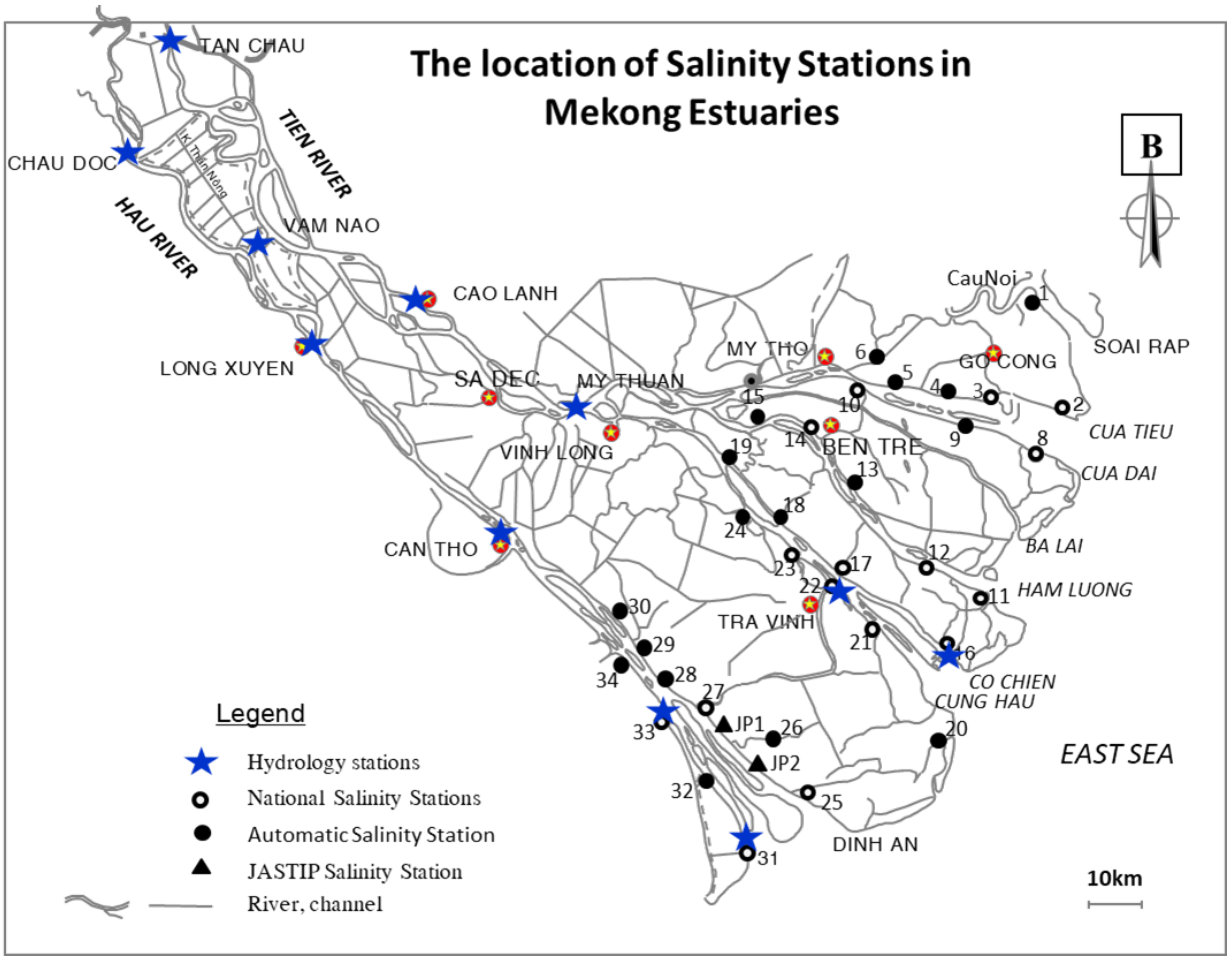

Figure 3.2 The location of salinity stations in VMD.

Table 3.2 Statistics of location measurements in the field

No.	Equipment	Time	Duration	Location	Measurement
1	ADCP, GPS	Aug-17	18 days	570km Tien, Hau and Vam Nao River	Q, V, D and WL
2	Infinity, Pro DSS, Pro 30, CastAway	Mar-18	4 days	60 km Tran De and DinhAn estuaries	S, T, C and D
3	Infinity, Pro DSS, Pro 30, CastAway	Apr-18	2 days	60 km CoChien and CungHau estuaries	S, T, C and D
4	CastAway, ADCP	Apr-19	2 days	Two cross-section (5km and 22km)	Q, V, S, D, C and T
5	Infinity ACTW	monitoring stations Feb-17 to now		Bac Trang (626440.50, 1074415.18) Dinh An (635134.65, 1066339.56)	S, T,C

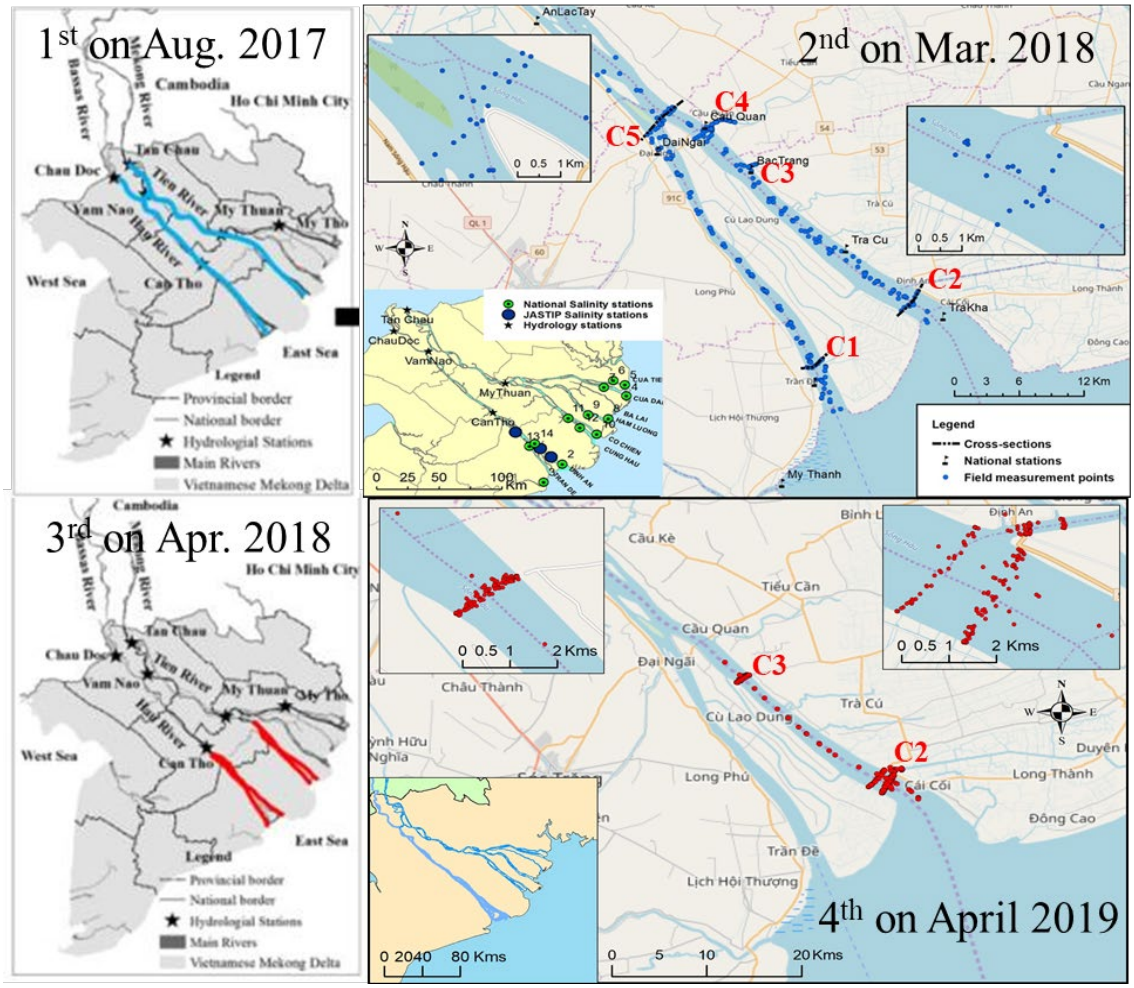

Figure 3.3 The location of four times field survey in VMD

3.3.1 First field survey: Acoustic Doppler Current Profiler (ADCP) measurement

During 18 days in August 2017 (flood flow) various instruments such as Trimble Global Positioning System (GPS), ADCP, handheld Garmin GPS (Figure 3.4) were used to measure the river depths, velocities, and discharges along 570 km in three main rivers including the Hau, Tien and Vam Nao River and measure salinity concentration by Pro30 instrument. The boat moved from Co Chien and Cung Hau estuaries to upstream at Tan Chau station and measured 80 cross-sections between adjacent cross-sections ranging from 1km to 5km. Then we moved to the Vam Nao River to measure 14 cross-sections. Finally, 106 cross-sections from the Chau Doc station to Dinh An and Tran De estuaries in the Hau River were measured at 0.5km to 5km intervals. In

addition, hourly water levels at eleven hydrological stations along with the Tien and Hau Rivers (namely Tan Chau, Vam Nao, Cao Lanh, My Thuan, Tra Vinh, Ben Trai,)

Figure 3.4 The measurement instruments used in the field survey

Chau Doc, Long Xuyen, Can Tho, Dai Ngai, and My Thanh) (Figure 3.2) were collected during the field survey period to derive river bed elevations from river depths measured by the ADCP. These stations are operated by the Southern Regional Hydro-meteorological Center, belonging to the Vietnam National Centre for Hydro-meteorological Forecasting.

The river bathymetry data is available for the main rivers in the VMD, but the data were collected in different years. Therefore, most of the researchers collected segmented topographic and cross-

section data measured at different time scales according to their projects. They are still using bathymetric data measured during 1998-2000 for their simulation, which is quite different from the current situation. Therefore, these will not reflect the To overcome this situation, and research results can reflect the reality, topographic measurements of all main rivers and tributaries in the VMD need to be conducted. Therefore, two hundred cross-sections had been set up into the numerical model to consider the impact of morphology change on salinity intrusion in chapter 5.

3.3.2 Second and third field survey: longitudinal salinity distribution

The second and third field surveys were salinity measurements. Four salinity instruments ((1) Infinity- ACTW – USB-0562, (2) CastAway – CTD version 1.5 made by SonTek/YSI Inc, (3) Pro30, and (4) ProDSS of YSI Professional Series instrument (Figure 3.4) were used to measure salinity concentration, temperature, conductivity distribution along 45km estuaries in Hau and Co Chien Rivers at high tide and low tide during spring tide. The second survey in the Hau River was conducted on 2nd and 3rd March 2018 in the Tran De branch and on 4th and 5th March 2018 in the DinhAn branch. Every day, we measured longitudinal salinity distribution along 45km of the Hau River two times; one during low tide and the other during high tide, and at five cross-sections at low tide and high tide (Figure 3.3). The first observation was done during low tide, starting at 8:11 at a location 45km far from the estuary to head downstream at 13:32. The salinity threshold 0.2 psu was measured at 45km point, the boat stopped 19 times to measure vertical salinity distribution at different profiles. At one-point, quick measurement was done over the full depth at 0.3 m intervals starting from the surface to the bottom with a conductivity meter with a 30 m cable. The high tide appeared at the estuary at 15:00. The measurement started from 0km point to upstream and stopped at a point that got 0.2 psu.

Before going to the field, using the "Tidal prediction" to see the tide at VungTau station this place also effects by the tidal regime of East Sea of Vietnam, to estimate the spring tide in March 2018 and make the schedule for field survey (Figure 3.3). The third field measurements in the Co Chien and Cung Hau estuary branches were carried out on 6th and 7th April 2018, respectively at the moments of high tide and low tide during spring tide.

3.3.3. The fourth field survey: vertical salinity distribution at two cross-sections in DinhAn estuary branch

The fourth field survey was conducted on 21st and 22nd April 2019 to measure salinity distribution, discharge, and velocity at two cross-sections: one is at 5 km (cross-section 2) and the

other is at 22 km (cross-section 3) from the DinhAn river mouth (Figure 3.3). Each cross-section was measured during 12 hours (one tidal cycle) by CastAway – CTD and GPS-equipped Acoustic Doppler Current Profiler (ADCP). The ADCP was mounted securely on the side of the boat, connected to a computer for in-situ measurements. The measurement was headed from the left bank to the right bank at 9 am, it took 20 to 30 minutes at cross-sections 3 and 2, respectively. At one cross-section, the boat stopped 9 to 11 times to measure vertical salinity distribution depending on the width of the cross-section.

3.3.4 Setup two monitoring stations in Hau River

Figure 3.5 Field activities in installing salinity stations

Under the JASTIP project, the first campaign, we conducted to install instruments for salinity measurement in downstream of the Hau River in the VMD. In the first campaign taken on 28th February 2016, one salinity meter was installed at An Lac Tay (station number 34), Soc Trang Province (Figure 3.2). The An Lac Tay station locates in the Hau River right bank, looking downward. It is about 50 km from the East Sea.

The second campaign was conducted from 10th to 11th February 2017. One more salinity meter was installed on the left bank of the Hau River, at the BacTrang station (JP1 - Figure 3.2), which is about 25 km from the river mouth and around 25 km downstream of the An Lac Tay station. However, the salinity concentration at the An Lac Tay station was too small in 2017. Therefore it was shifted downstream to the DinhAn station (JP2), which is also in the Hau River, to be able to measure salinity concentrations continuously. The DinhAn station is about 20 km from the estuary.

3.4 Numerical simulations

3.4.1 MIKE11-HD-AD

The Danish Hydraulic Institute developed MIKE 11 models. MIKE 11 is a modeling package for simulation surface runoff, flow, sediment transport, and water quality in rivers, channels, estuaries, and floodplains. The most commonly applied hydrodynamic (HD) model is a flood management tool simulating the unsteady flows in complex rivers and channel systems. It has been successfully used in different river basins around the world.

The MIKE 11 HD model was built based on the Saint-Venant. Equation (3.1) is a model for one-dimensional unsteady flow computation. The model has been designed to perform detailed modeling of rivers, including special treatment of floodplains, road overtopping, culverts, gate openings, and weirs. The continuity (3.2) and momentum equations (3.3) solution is based on an implicit finite difference scheme. Boundary conditions include water level (h), flow discharge (Q), and Q/h relation. The water level must be specified at either the upstream or the downstream boundary of the model. The flow discharge can be applied to either the upstream or the downstream boundary condition and can also be applied to the side tributary flow (lateral inflow). The lateral inflow is used to describe runoff. The Q/h relation can only be applied to the downstream boundary. The advection-dispersion (AD) module is based on the advection-dispersion equation (3.4). The module requires output from the hydrodynamic module in time and space. This model was used to simulate the salinity intrusion in river and channel networks.

The Saint-Venant. Equation:

$$\frac{\partial Q}{\partial t} + \frac{\partial}{\partial x}\left(\frac{Q^2}{A}\right) + gA\frac{\partial h}{\partial x} = gA\left(S_0 - S_f\right) + qu \quad \textbf{or} \quad \frac{\partial Q}{\partial t} + \frac{\partial}{\partial x}\left(\frac{Q^2}{A}\right) + gA\frac{\partial h}{\partial x} = gA\left(S_0 - S_f\right) \qquad (3.1)$$

The continuity equations:

$$\frac{\partial A}{\partial t} + \frac{\partial Q}{\partial x} = 0 \qquad (3.2)$$

momentum equations

$$F_m = -\rho B h u \frac{du}{dx} \Delta x \quad (3.3)$$

The advection-dispersion equation

$$\frac{\partial AC}{\partial t} + \frac{\partial QC}{\partial x} - \frac{\partial}{\partial x}\left(AD\frac{\partial C}{\partial x}\right) = -AKC + C_2 q \quad \textbf{or} \quad \frac{\partial AC}{\partial t} + \frac{\partial QC}{\partial x} - \frac{\partial}{\partial x}\left(AD\frac{\partial C}{\partial x}\right) = 0 \quad (3.4)$$

In which:

A: cross-section area

S_0: bed slope

S_f: friction slope

q: in/out side flow of channel section (lateral in/out flow (q = 0))

u: flow velocity

Dx: distance between the sections

Dt: time period

C: salinity concentration

C_2: sources/ sink salinity concentration

D: dispersion coefficient

K: linear decay coefficient

3.4.2 Setup model and calibration

3.4.2.1 Setup model

The model was set up for the whole Mekong Delta, including 2089 branches with 20734 points as in **Figure 3.6**. The computational scheme consists of five discharge boundaries in the upstream, including (1) daily discharge in Kratie, (2) daily water level at PrekDam (Tonle Sap), (3) daily discharge at the VamCoDong River, (4) daily discharge at the SaiGon River and (5) daily discharge in the DongNai River. Fifty-nine water level and downstream salinity boundaries were used using hourly water levels and odd hourly salinity concentrations at seven hydrology stations such as BinhDai, VamKenh, BenTrai, MyThanh, SongDoc, GanhHao, and RachGia. Two hundred cross sections describing the geometry from TanChau to the CoChien River and from ChauDoc to the Hau River and VamNao channel were measured in August 2017. Two hundred and ninety-eight control structures, nineteen weirs, and fourteen culverts had been considered in the model.

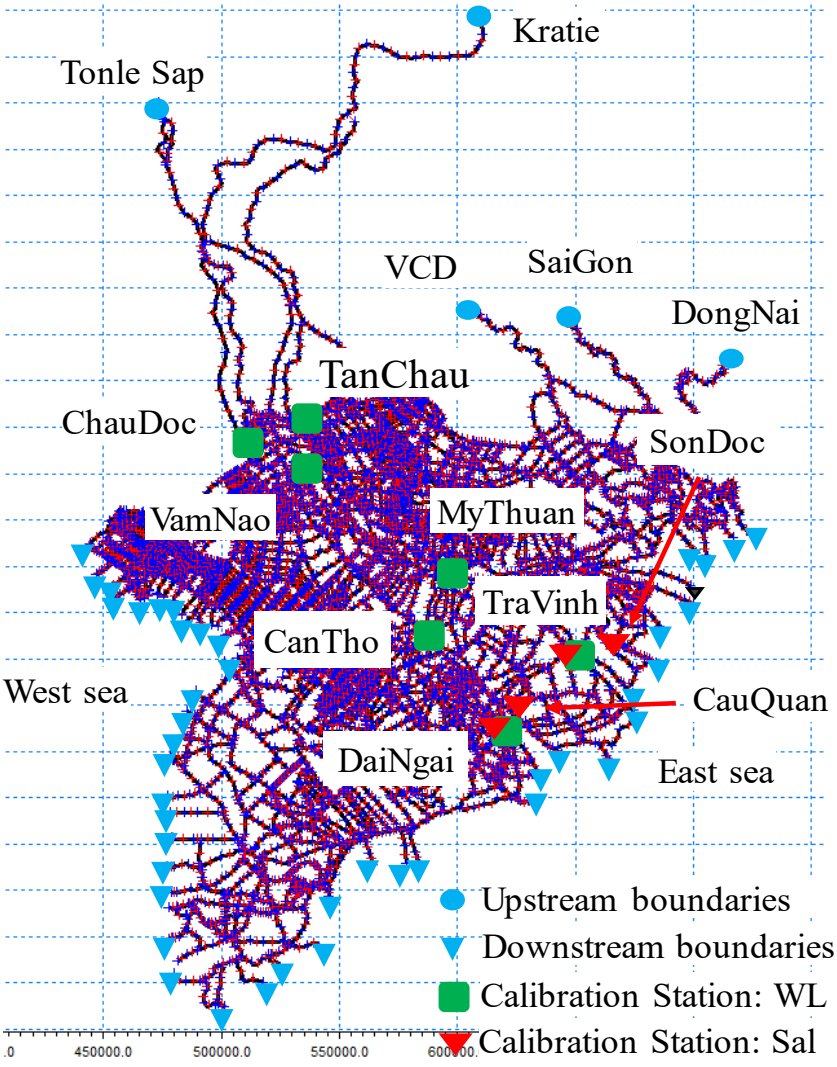

Figure 3.6 1-D Hydrodynamic model setup

3.4.2.2 Evaluation of numerical model performance

To evaluate the performance of the numerical model, coefficient of determination (R^2) and Nash-Sutcliffe number (E_f) is used.

The coefficient of determination is computed as follow:

$$R^2 = \left(\frac{n\sum_{i=1}^{n}(y_i \times f_i) - \sum_{i=1}^{n} y_i \sum_{i=1}^{n} f_i}{\sqrt{n\sum_{i=1}^{n} y_i^2 - \left(\sum_{i=1}^{n} y_i\right)^2}\sqrt{n\sum_{i=1}^{n} f_i^2 - \left(\sum_{i=1}^{n} f_i\right)^2}} \right)^2 \quad (3.5)$$

Where y_i, i=1, 2, …n are the observed data with n values; f_i, i=1, 2, …n is the estimated data associated with y_i. The range of R^2 is between 0 and 1.0. The high the values of R^2, the more reliable the model is developed.

The Nash-Sutcliffe number indicates how well the simulated data matches the corresponding observed values. E_f is computed as follow:

$$E_f = 1 - \frac{\sum_{i=1}^{n}(y_i - f_i)^2}{\sum_{i=1}^{n}(y_i - \bar{y}_i)^2} \tag{3.6}$$

in which $\bar{y}$ is the mean of observed values, computed as follow:

$$\bar{y} = \frac{\sum_{i=1}^{n} f_i}{n} \tag{3.7}$$

3.4.2.3 Calibration and verification model

The model calibration was carried out with the water level and salinity concentration data of 2016 by two steps and verification by data of 2005. In the first step, the Manning coefficients and initial water level in rivers were adjusted to obtain the best fit between simulated and measured water levels at ChauDoc, TanChau, CanTho, MyThuan, DaiNgai, and MyTho stations (Figure 3.7 and 3.8). The accuracy of the numerical results is evaluated by using Nash-Sutcliffe coefficient (E_f) and correlation coefficient (R^2) with E_f and R^2 consistently higher than 0.85 (Table 3.3). Secondly, calibration for the advection-dispersion module was conducted by initial salinity concentrations, and dispersion coefficients for the river reach with observed data at DaiNgai, CauQuan, and TraVinh salinity stations about 30 km from estuary (Figure 3.9).

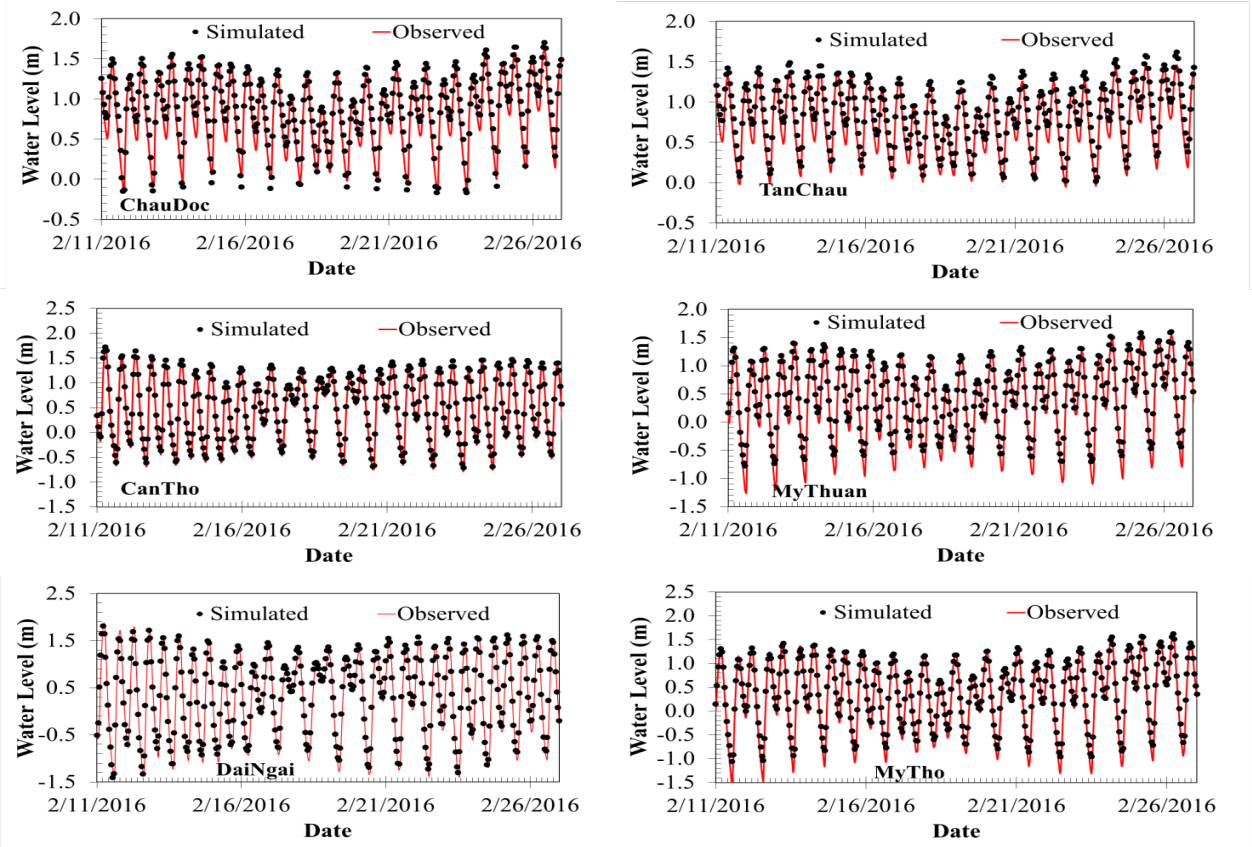

Figure 3.7 Simulated and observed water level for model calibration in 2016

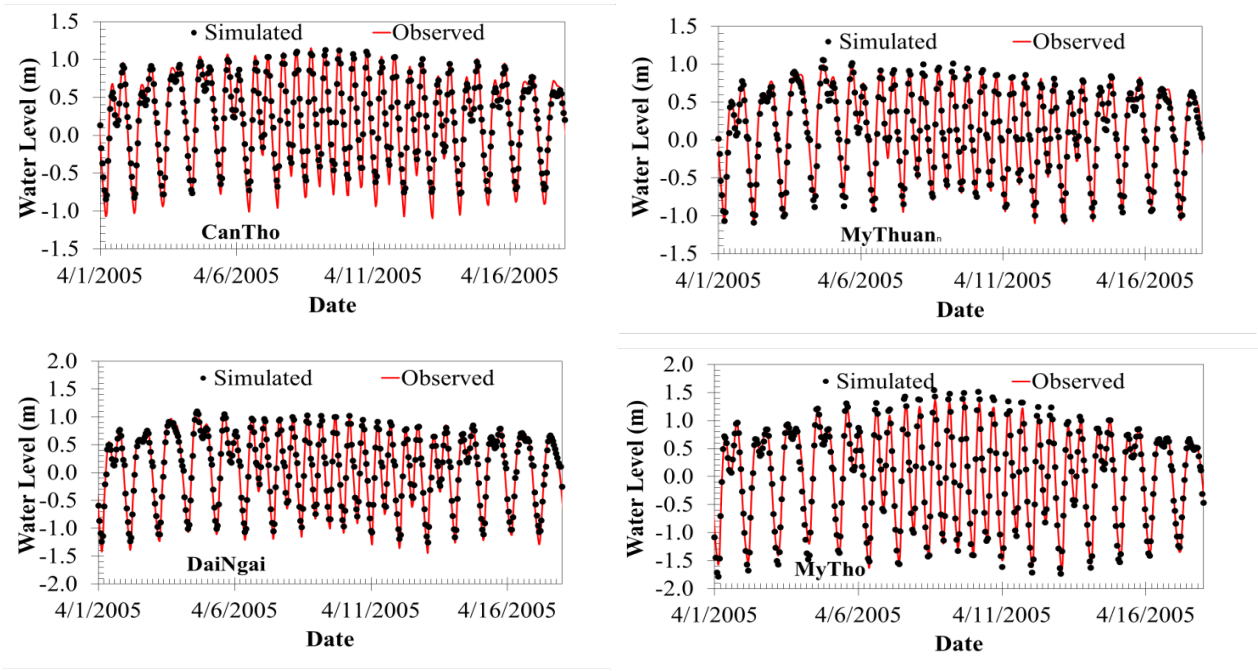

Figure 3.8 Simulated and observed water level for model verification in 2005

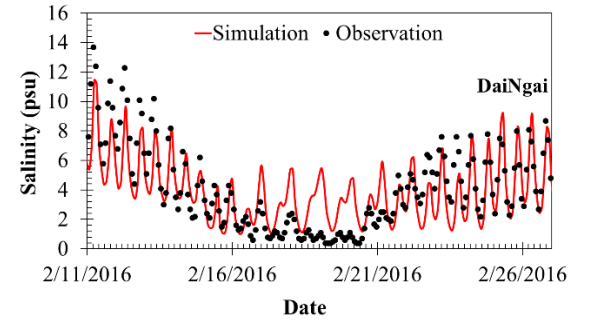

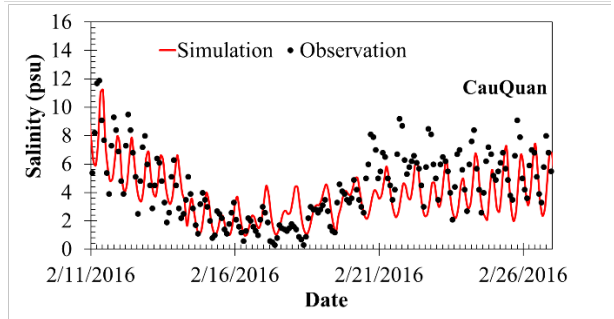

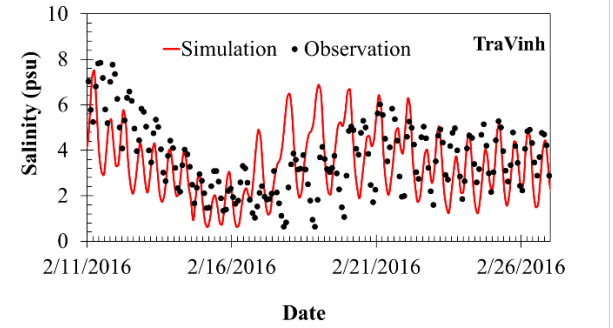

Figure 3.9 Salinity Calibration in 2016

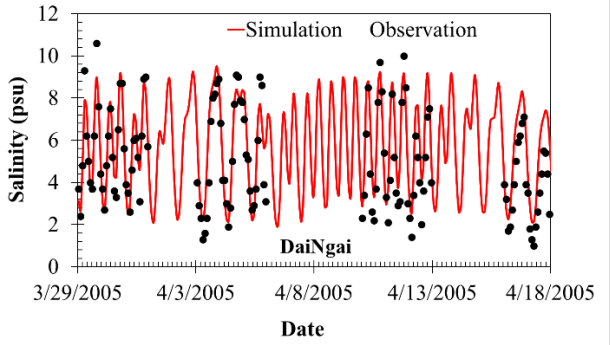

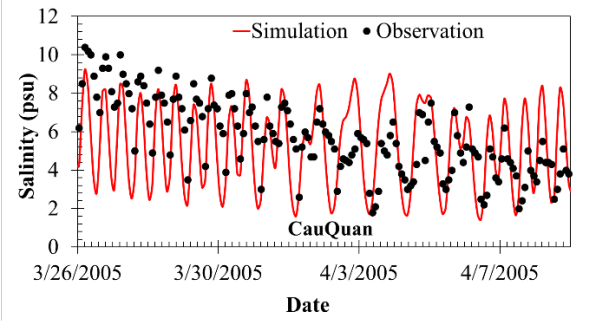

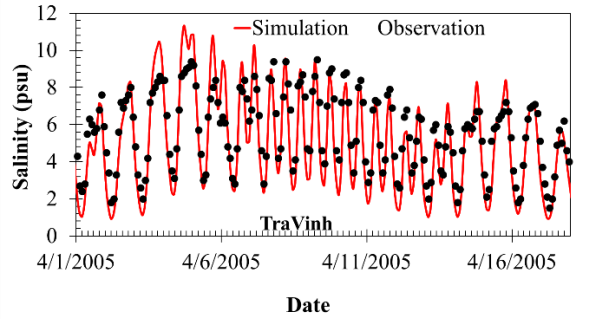

Figure 3.10 Salinity Verification in 2005

Table 3.3 showed the correlation coefficient (R2) for calibration and verification salinity concentration; the value is over 0.62, which is not so high. It can be accepted for salinity simulation because the maximum simulation values usually are higher than the maximum observation. Based on the performance indicators, one can see that a satisfactory model–data agreement is obtained.

Table 3.3 Value of two performance indicators at eight stations

Stations		Tan Chau	Chau Doc	My Thuan	Can Tho	My Tho	Dai Ngai	Cau Quan	TraVinh
Calibration 2016									
Water level	R^2	0.957	0.906	0.962	0.947	0.978	0.913		
	E_f	0.898	0.849	0.931	0.893	0.951	0.900		
Salinity	R^2						0.785	0.731	0.762
	E_f						0.753	0.702	0.748
Verification 2005									
Water level	R^2	0.985	0.891	0.949	0.89	0.947	0.970		
	E_f	0.946	0.840	0.970	0.926	0.962	0.960		
Salinity	R^2						0.830	0.657	0.795
	E_f						0.794	0.638	0.752

Chapter 4: Impacts of upstream dams development on flow and Salinity intrusion

4.1 Introduction

In the Upper Mekong Basin (UMB), China has proposed to build a cascade of eight Mekong mainstream dams inside China, planning to use 828m of water column difference of 772km river section to produce 16.2 GW per year (Fan et al., 2015 and Kuenzer et al., 2013). Before 2016, six of them had been completed. The cascade is often termed the "Lancang cascade" (Kuenzer et al., 2012). Construction started in 1986 and six of eight dams were completed in 1993, 2003, 2008, 2011, and 2014. The dams were named the Manwan, the Dachaoshan, the Xiaowan, the Jinghong, the Gongguoqiao and the Nouzhadu, respectively. The Nuozhadu reservoir was filled with water in November 2011 and power generation started in September 2012 (Mai et al., 2017). So, six of the eight dams were operational by 2012 (Rasanen et al., 2012). The total and active storage capacity of these six dams is approximately 41.18 km^3 and 23.08 km^3 (Table 4.1), accounting for 49.6% and 27.8%, respectively, of the annual mean discharge at Chiang Saen (83km^3), the nearest hydrological station downstream of the Chinese dams (Figure 1.1).

The Lower Mekong Delta (LMB) has 36 completed dams and has approximately 60 to 100 planned dams (Rasanen et al., 2012). Large-scale projects like those mean that the river systems are fragmented, and the ecosystems and the livelihood of rural people are affected. These impacts inevitably lead to the expense of the environment and society, making ambitious hydroelectric plans controversial and highly political (Fu et al., 2010; Rasanen et al., 2012). The flow regimes of the Mekong River (MR) have been significantly altered by hydropower dams, which reduce the total flood flow and increase the total dry flow, interrupting the connectivity between rivers and floodplains (Binh et al. 2019). Hydropower dams also trap sediment, reducing the volume of sediment that can be transported downstream to maintain river channels and coastal zones (Kondolf et al., 2014). Moreover, fish migration paths are blocked by dams built across the rivers. All these factors lead to a degradation of ecosystems in the MRB (Arias et al., 2014).

By 2016, fifty-six hydropower dams had been completed along the mainstream and tributaries (Mai et al. 2018), but the six mega-dams (Langcang cascade) in the mainstream have had more impact on the flow regimes of the MR (Manh et al., 2015). The sea-level rise is still one of the

drivers of the flow regime's change. However, Lauri et al. (2012) found that the impact of sea-level rise on flow regimes in the MR is smaller than the impact of hydropower dams. Several previous researchers expected such dams to increase dry season flows and decrease the wet season flows. Chapman and He (1996) predicted a mean increase in discharge of 17% after the completion of Xiawan and Nuozhadu and substantial increases in dry season flow and a reduction in wet season discharges of nearly 25%. According to the analyses of Lu and Siew (2006), it was found that dry season flow increased by over 60% at Chiang Saen. Räsänen et al., (2012) used the numerical model to predict the flow of Langcang cascade in three scenarios (no dams, the first three dams completed, all six dams constructed). Their modeling results and predictions align with several previous studies and suggest a 20–22% decrease in June–November flows and a 90% increase in December–May flows at Chiang Saen station.

Similarly, MRC (2010) also concludes a significant increase in average discharge of 20–40% in the dry season and a decrease in flood season flow of about 5–15%. All of the results are very different in magnitude but similar in pattern. The flood flow decreases in its duration and amplitude while dry season variability is likely to increase. But the increase of the dry flow is not evenly distributed and fluctuates often, while variability within the wet season remains unchanged (Osborne, 2004).

Furthermore, the flow in the dry season mainly increases in the last months of the dry season, according to the research of Räsänen et al. (2017). This study reported that discharges in March-May 2014 increased by 121-187% while those in July-August 2014 reduced by 32-46% at Chiang Saen, compared to the average discharges of 1960-1990. At Kratie, the degree of the flow change is smaller, with an increase of 41-74% in March-May and a reduction of 0-6% in July-August. This is one of the reasons that salinity intrusion in the VMD appears early and penetrates deeply with high concentration. The maximum salinity (S_{max}) in 2016 was about 1 to 1.5 months earlier than that of previous years, while S_{max} occurred in April 1998 and March 2005 (two historical drought years when S_{max} was shifted to take place in February 2016. The annual peak salinity concentration at 30km from the estuaries was 1.4 times larger than that in 1998, and intrusion length was 7-15km longer than in the same period of 1998 (Mai et al., 2018). The drought event in 2016 affected an area of 52.7% of the VMD with a total economic loss of about US$360 million. It was so difficult for managers and farmers to control salinity intrusion and make a water distribution plan for domestic use, agricultural use, and aquaculture use. These parties lacked

information about upstream flow and had little knowledge about upstream dams operation. The local management authorities and the farmers needed support and information about the flow prediction, the mitigation measures, and adaptation from the scientists and stakeholders. This information can help them plan for agricultural uses, domestic uses, and aquaculture uses in the VMD to mitigate the impact of upstream flow changing and salinity intrusion.

Scientists, management authorities, and stakeholders need to assess and investigate historical changes of the flow regime along the MR to inform sustainable integrated water management strategies and to improve decisions regarding shared benefits from the transboundary MR in the coming decades. Any findings from stakeholders based on a short-term flow analysis may lead to the unsustainable development of MRB. The Vietnamese scientists should assess the current status of hydraulic works such as salinity control sluice gates and existing dike systems to control the salinity intrusion in VMD. High-dike plans may destroy soil properties and wetland ecosystems because nutrient-rich fine sediment cannot access wetlands and agriculture areas. Additionally, salinity control sluice gates may increase the intrusion length land-ward by reducing buffering zones near the estuaries.

The purpose of this chapter is to evaluate the upstream flow changes over a long period to clarify the impact of upstream dams on the flow and assess the impact of dry flow changes on salinity in VMD through the numerical model corresponding to two upstream flow change scenarios. Once properly assessed, appropriate measures to adapt to salinity intrusion in VMD can be proposed.

4.2 Influence of upstream dams development on the flow and water level

Starting in 1950, 24 dams were proposed to be built along the Upper MR. The first dam of Langcang cascade, the Manwam dam, was constructed from 1986 to 1996. Over the three decades, dam construction along the upper MR advanced rapidly (Fan et al., 2015). The Manwan dam began operating in 1993 and came into full operation in 1996, and another five dams began filling water: Dachaoshan dam in 2001, Jinghong dam in Apr. 2008, Xiaowan in Dec. 2008, Gongguoqiao in 2011, and Nuozhadu in Nov.2011 (Table 4.1) (Fan et al., 2015). The six dams have accumulated total storage and active storage capacity of approximately 41.18 km^3 and 23.08 km^3, accounting for 49.6% and 27.8% annual mean volume at Chaing Saen (83.0 km^3) and accounting for 10.36% and 5.81% at Kratie (397.4 km^3) during fifty-six year from 1960 to 2016.

Table 4.1 Key indicators of the six upstream dams of Langcang cascade

Reservoir	Reservoir filling year	Catchment area	Dam Height	Total capacity	Active storage	Annual Inflow	Mean annual runoff	Electric capacity
		(km^2)	(m)	(km^3)	(km^3)	(m^3/s)	(km^3)	(MW)
Manwan	Mar. 1993	114,500	132	1.060	0.257	1230	38.8	807
Dachaoshan	Nov. 2001	121,000	121	0.880	0.367	1340	42.3	712
Jinghong	Apr. 2008	149,100	107	1.230	0.249	1840	58.0	833
Xiaowan	Dec. 2008	113,300	292	15.130	9.895	1220	38.5	1854
Gongguoqiao	Sep. 2011	97,300	130	0.510	0.120	985	31.1	390
Nuozhadu	Nov. 2011	144,700	260	22.370	12.195	1750	55.2	2403
Total				**41.180**	**23.083**	**8365**	**263.9**	**6999**

The next few charts assess the effect of the upstream reservoir development on the flow change through analysis of the long-term raw data of the flow (Q) and the water level (H) at upstream stations in Chiang Saen and Kratie from 1960 to 2016. Water level alteration was analyzed at 4 stations of Chiang Saen, Kratie, Chau Doc, and Can Tho from 1980 to 2016. The time series of Q and H data was analyzed in three periods: (1) before dam construction from 1980-1992 (no dam), (2) after six dams were built in the mainstream, and fifty dams in the tributaries construction period from 1993-2011 (building dams), and (3) the period of dams operating from 2012 to 2016 (completed dams).

4.2.1 Change of the total annual flow (Chiang Saen, Kratie, Tan Chau, and Chau Doc)

At each station, the flow hydrographs are divided into two categories: the wet flow (from June to November) and the dry flow (from December to May). Figure 4.1 shows the flow changes at the hydrological stations downstream of six dams. Total annual runoff (W_{total}) and rain flow (W_{wet}) both strongly decrease at ChaingSaen (CS) station from 22.2% and 27.7%, respectively. The upstream flow in the rainy season accounts for more than 76% of W_{total}, so W_{wet} will decrease from 17.6 km^3 to 32 km^3 per year. This amount of water can be stored in reservoirs for power generation. Similarly, downstream, both W_{total} and W_{wet} at Tan Chau and Chau Doc reduced by about 11% (26.2 km^3 at Tan Chau). While, the total W_{wet} at Kratie station, which was located about 2240 km downstream of CS station, decreased insignificantly by about 3% (10.4 km^3), and W_{total} tend to remain unchanged over the years. Therefore, the reservoirs reduced the flow by accumulating

water storage and shifting water from the rainy season to the dry season after the dams began operation.

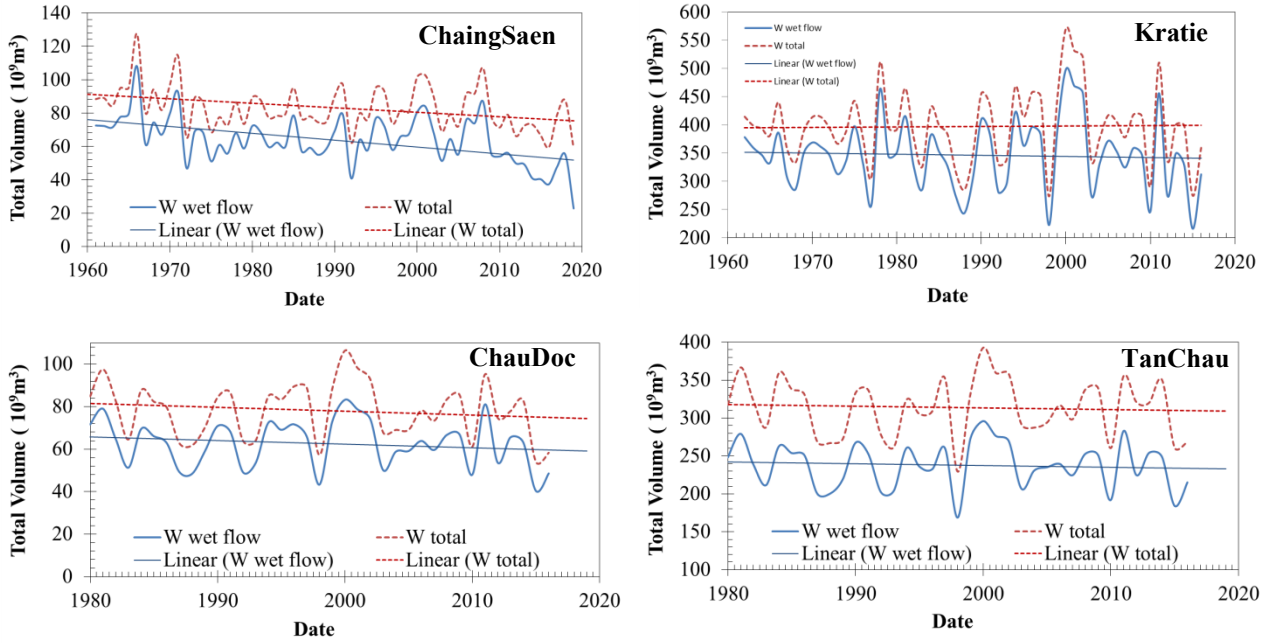

Figure 4.1 Long-term variations of the W_{total} and W_{wet} along the MR.

4.2.2 Change of the total dry flow (Chiang Saen, Kratie, Tan Chau, and Chau Doc)

While the total rain flow at all stations has a decreasing trend, the total dry flow (Wdry) tends to increase strongly at the stations upstream of the MD. The total W_{dry} increases 30.5% and 20.8% at Chaing Saen and Kratie stations, respectively (Figure 4.2). However, W_{dry} only accounts for 23.9% (19.2 km^3) at CS and 13.1% (51 km^3) at Kratie of the total annual flow, so the W_{dry} increases about 5.9 km^3 to 10.8 km^3 at CS and Kratie stations. Figure 4.3 shows the change in total flow in the dry season according to 3 periods: no dam (1), building dams (2), and completed dams (3). The average total dry flow in periods (2) and (3) increases due to the increase of W_{dry} / W_{total} at each station. But the W_{dry} in the third period increases more significantly than in the second period. For instance, at CS station, the ratio of W_{dry}/W_{total} increases from 21.4%, 21.6%, and 35.5% with periods 1, 2, and 3, respectively, and this ratio also increases from 12.3%, 13.5%, and 16.6% at Kratie station. The fluctuation of total dry flow has changed much over the years, with the largest fluctuation of 23.2 km^3 at CS and 36.2 km^3 at Kratie. Consider period (1) and (3), the difference of W_{dry} between periods (1) and (3) is notably high. The W_{dry} increased from 17.8 km^3 to 24 km^3 (20.96%) at CS and from 47.5 km^3 (period 1) to 57.7 km^3 (period 3) (34.83%) at Kratie.

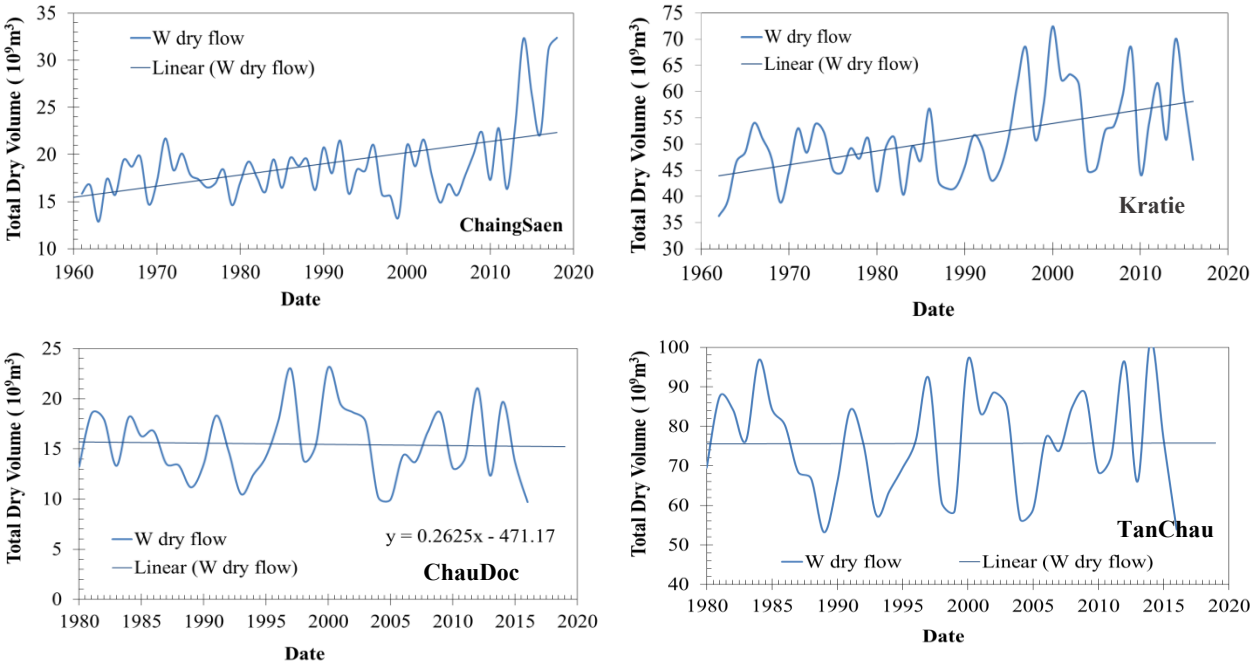

Figure 4.2 Long-term variations of the W_{dry} along with the MR

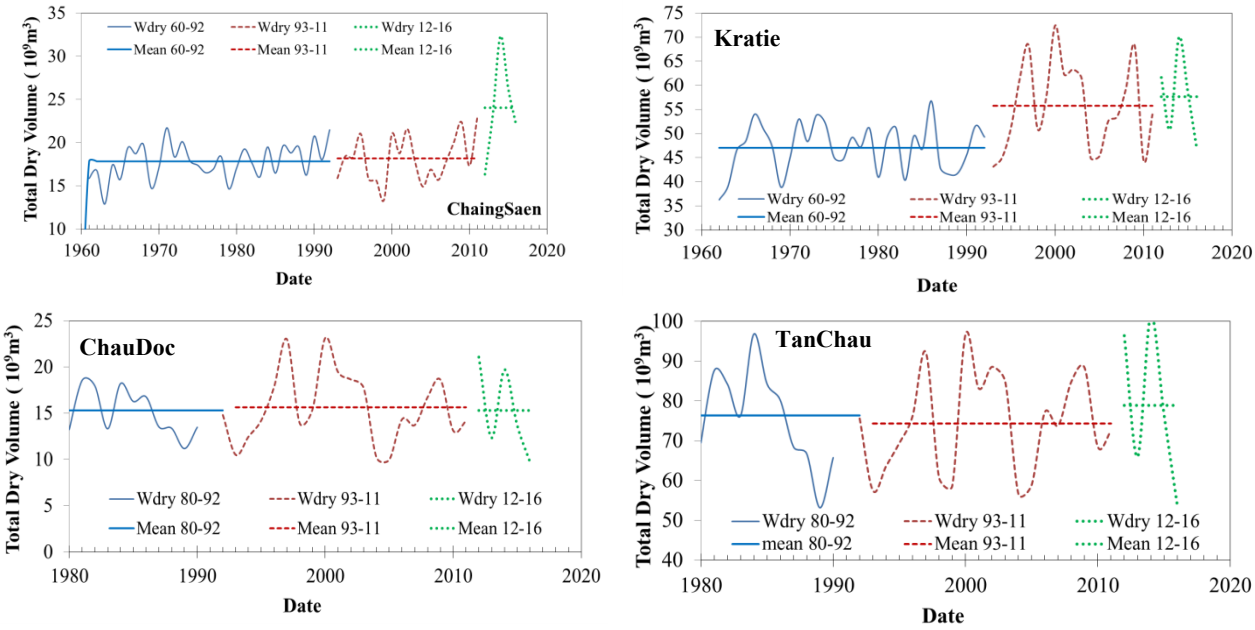

Figure 4.3 Long-term variations of the W_{dry} along with the MR in three stages

While W_{dry} in VMD decrease slightly (4.4%) at Chau Doc and Tan Chau stations, total dry season flow ($W_{dry)}$ at VMD in 2nd period decreased by 2.27% and then increased by 3.7% in 3rd period at Tan Chau (Figure 4.3). The flow at Tan Chau accounts for 84.78% of the total dry flow into the VMD, so in the 3rd period, the increasing flow in Tan Chau means that the flow into the VMD also increased slightly. It can be confirmed that the upstream dams tend to increase the flow in the dry season in the VMD but along the main river some projects to divert water to other basins or to increase water use upstream cause the increasing trend of total dry flow in TanChau and ChauDoc to be minimal.

4.2.3 Change of the annual maximum and minimum discharge (Chiang Saen, Kratie, Tan Chau, and Chau Doc)

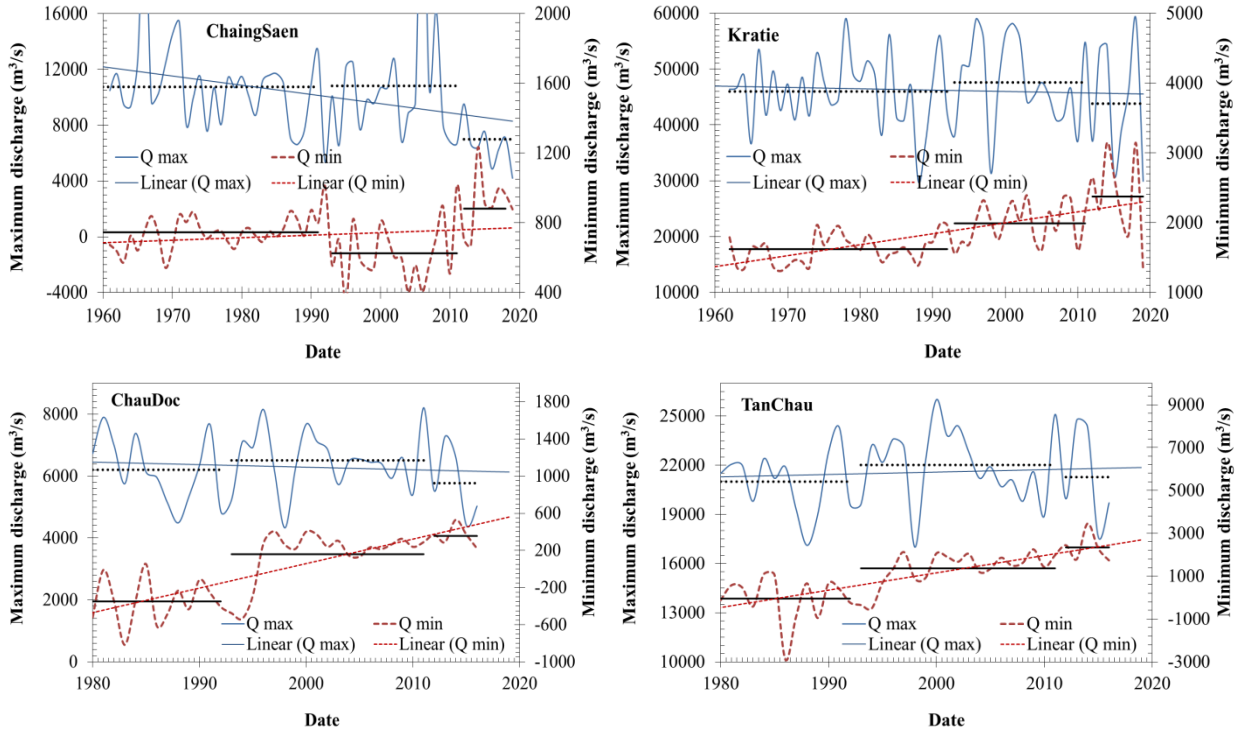

Figure 4.4 Long-term variations of the annual maximum and minimum discharge along the MR

When we consider the variation of the annual maximum discharge, similarly to the W_{total} and W_{wet}, the maximum yearly discharge Q_{max} at Chaing Saen drops drastically from period 1 to 3, with the drop rate reaching 33.3% and the discharge value reduces by 67.76 $m^3/s/yr$. The general trend of all stations is that Q_{max} decreases. However, figure 4.4 shows that during the building dam period

(2), the average Q_{max} increases slightly at all stations. After that, the average Q_{max} value in the 3rd period decreased greatly at all four stations at a rate of 35.4%, 7.89%, 3.36%, and 11.32% at CS, Kratie, TanChau, and Chau Doc stations, respectively. The 3rd period marks the decreasing trend of the stations over fifty-six years.

Meanwhile, Q_{min} tends to increase at all stations. However, in the second period, there is a difference that the average Q_{min} of three stations (Kratie, Tan Chau and Chau Doc) increases significantly compared to the first period (no dam). In contrast, the average Q_{min} at CS decreases significantly (16.2%) for $Q_{min} < 400m^3/s$. But in the 3rd period, Q_{min} increases significantly, reaching $800m^3/s$ to $1200m^3/s$. The remaining three stations also increased by an average Q_{min} rate of 19.35%, 71.38%, and 122.8%, but the value is less than the increase of the 2nd period.

4.2.4 Change of the seasonal and monthly discharge (Chiang Saen, Kratie, Tan Chau, and Chau Doc)

4.2.4.1 In the wet season

Firstly, in comparison between periods 1 and 2, figure 4.5 shows the mean total wet flow W_{wet} in the building dam period is more significant than that of the no-dam period. In addition, flood peak values at four stations were higher than those in period 1. Flood peaks occurred 34 days, ten days, nine days, and 11 days later at CS, Kratie, Chau Doc, and Tan Chau. The peak values also increased from 5% to 10% at Kratie and CS.

Secondly, let's compare period 3 with period 1. In contrast to period 2, the W_{wet} in period 3 is the lowest and decreases from 8.3% to 14.8% at Kratie and CS stations. Reduced rates were high in the upstream stations and then gradually dropped in downstream stations. The flood peak time occurs in August and September, but the values are much smaller. Maximum reduction of peak flow is from 10% to 14.2%. Moreover, the flow in period 3 shows more fluctuation and more flood peaks. The daily wet flow in period 3 reduces during six months of the rainy season leading to a quick reduction of flow in the early dry season.

4.2.4.2 In the dry season.

Figure 4.6 at the CS station clearly shows the change in dry flow when the dams are in operation (period 3). The flow volume increases, and the shape of the flow is highly variable and more fluctuation due to the influence of dams operation (figure 4.7). Distribution of the total dry

flow per total annual flow (W_{dry}/W_{total}) increased from 21.4% in the no dam period (1) to 35.5% in completed dams (3), making W_{dry} increase from 17.8km^3 (1960) to 23.5 km^3 (2016).

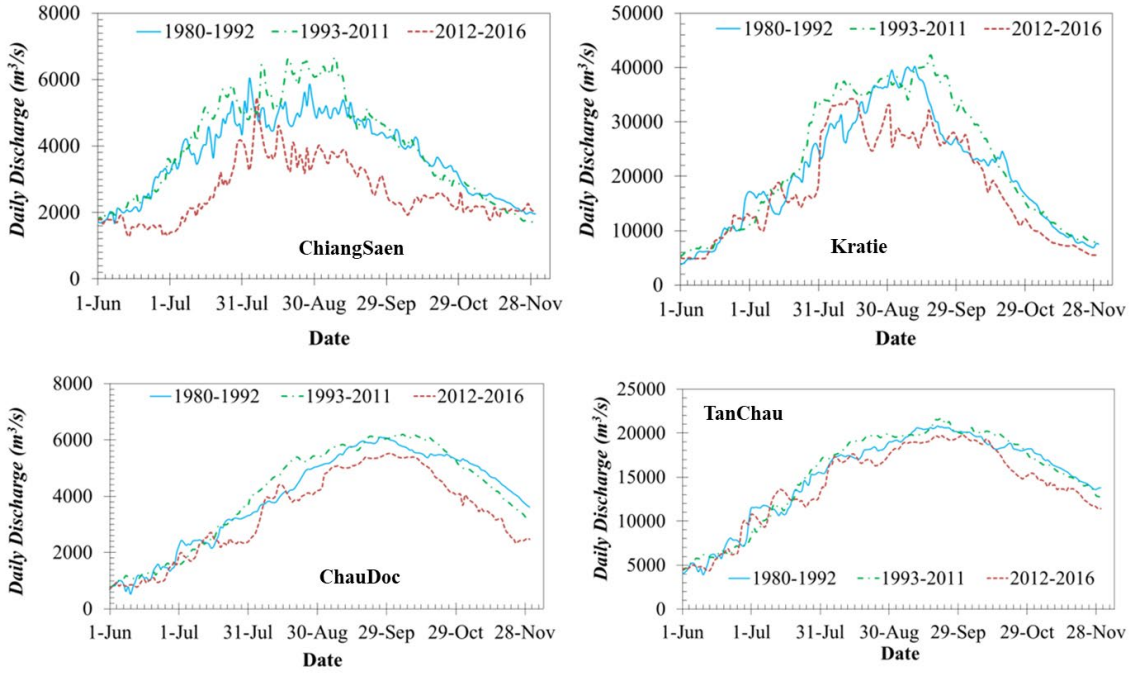

Figure 4.5 Long-term variations of the mean daily discharge in the wet season in three periods: no dam, building dams, and completed dams

Likewise, the W_{dry}/W_{total} at Kratie increased by 12.3%, 13.5%, and 16.6 %, corresponding to 3 periods 1st, 2nd and 3rd. However, this increase is not evenly distributed for all six months of the dry season. Figure 4.7 shows the maximum monthly flow in December and minimum monthly flow in April during the dry season. Compare the month flow between three periods, the flow in the third period in CS increased from January and the monthly flow in Kratie, Tan Chau, and Chau Doc increased from February to May and reduced from Dec. to Jan. Figure 4.6 shows that the flow at Tan Chau and Chau Doc in the beginning of the dry season in period 2nd and 3rd decreased significantly compared to period 1, the largest decrease in period 2 and 3 compared to period 1 is 1700 m^3/s and 2700 m^3/s respectively. This reduction does not only occur at the beginning of the dry season, which is extended from the rainy months of period 3rd because the total monthly flow in the 3rd period at the four stations has dropped very low from July to December (Figure 4.7). The lack of flow at the end of the rainy season and the beginning of dry season, making the salinity intrusion more and more severe due to the increase in salinity concentration and intrusion length.

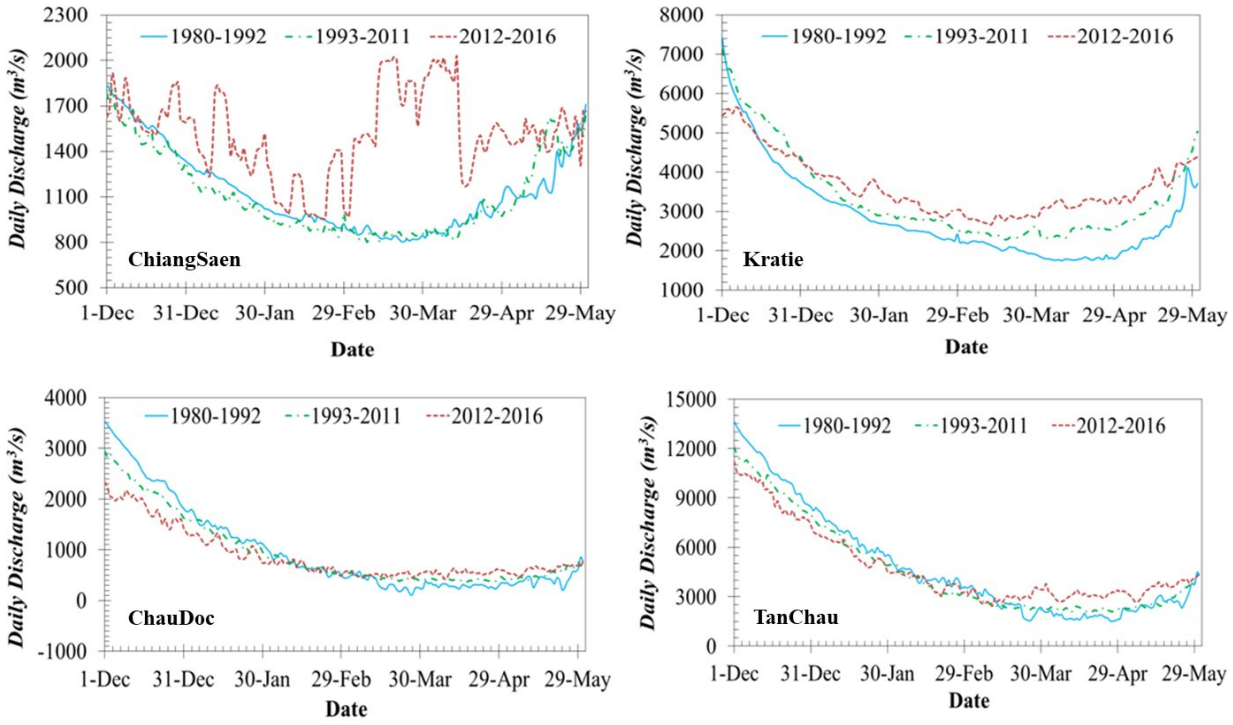

Figure 4.6 Long-term variations of the mean daily discharge in the dry season in three periods: no dam, building dams and completed dams

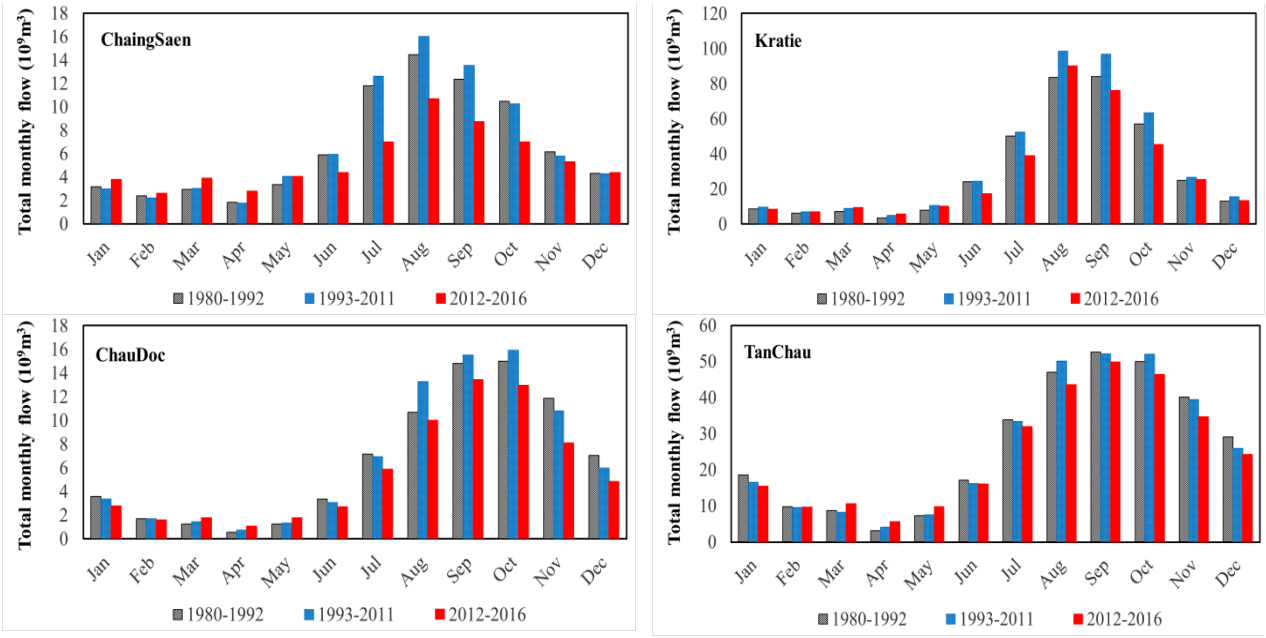

Figure 4.7 Total monthly flow in the dry season in three periods: no dam, building dams, and completed dams

4.3 Moving time along the Mekong mainstream

The daily observed water level and discharge along the Mekong mainstream during the dry season from Chiang Saen to Kratie and TC-CD) - the gateway of VMD have been used to calculate the time moving of the flow from CS to TC-CD. Flow moving time is analyzed by keeping track of the daily observed discharge at Chiang Saen, Kratie, and TC-CD at 5 points in the time series of flow such as two peak points (27th Jan and 28th Feb) and three bottom points (17th Jan, 21st Feb, and 19th Apr 2016).

The flow moving time from Chiang Saen to Kratie stations is different depending on flow values. As shown in Figure 4.8, by tracking the movement of the peak discharge on 27th Jan 2016 in Chiang Saen station, it took 15 days to be at Kratie (11th Feb) and another two days to hit TC-CD (13th Feb). In the case of tracking the movement of low discharge (bottom point), with the same distance, it took 17 days to move from Chiang Saen to Kratie. Table 4.2 shows the moving time of five indicated points in the dry season. The flow moving from CS to Kratie takes about 15 to 17 days and takes 17 to 19 days to go to TC+CD. The result is similar to the conclusion in the MRC report from 2016. The flow travels a total length of 1804 km from Chiang Saen to Kratie and takes 17 days. Thus, this suggested a moving velocity of 1.4 m/s (or 5 km/h). It is assumed that over 1800 km has the same slope. The flow in TC-CD is normally influenced by the flow in Kratie, the outflow of the TonleSap Lake, and the tide from the East Sea. However, the flow volume stored in the TonleSap lake is relatively low (MRC report, 2016) from the mid to the end of the dry season. Therefore, the daily observed water level and discharge variation patterns at Chiang Saen could still be seen at TC-CD.

Table 4.2 Flow moving time from Chiang Saen to TanChau-ChauDoc

Station	Tracking point	Chiang Saen (1) 2364 km		Kratie (2) 560 km	TC_CD (3) 230km	Flow moving time (days)	
		Time	Q (m^3/s)			(1)-(2)	(1)-(3)
1	Bottom 1	17-Jan	960.52	2-Feb	4-Feb	16	18
2	Bottom 2	21-Feb	827.59	8-Mar	10-Mar	16	18
3	Bottom 3	19-Apr	946.00	4-May	6-May	15	17
4	Peak 1	27-Jan	2,406.27	11-Feb	13-Feb	15	17
5	Peak 2	28-Feb	1,409.63	16-Mar	18-Mar	17	19

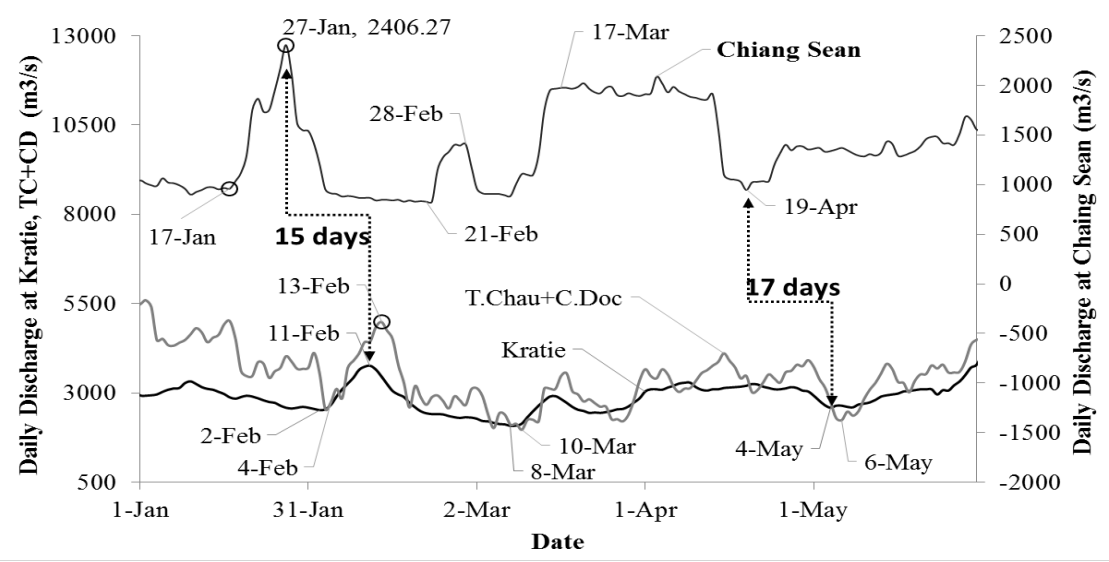

Figure 4.8 Discharge at the ChiangSaen, Kratie and TanChau-ChauDoc Hydrology Station in 2015-2016

4.4 The impact of upstream dams development on the salinity intrusion

4.4.1 Change of salinity in the long-term

Consider the evolution of maximum daily salinity in 3 periods: (1) before 1992 (no dam), (2) building dams from 1993 to 2011, and stage (3) from 2012 to 2020 of completed large dams (completed dam) at CauQuan station in the Hau River and TraVinh station in the CoChien River (Figure 4.9). In the 1st period, the salinity threshold of 4psu appears around March and April and lasts until the end of May or June. Therefore, the maximum salinity seems to be in the last week of April. Whereas, in the 3rd period, 4 psu of saltwater occurs at the end of the first week of January and lasts to mid-April or early May. The duration of 4 psu salinity concentration has been observed during 4 to 4.5 months per 6 months of the dry season (December to May). Therefore, the maximum salinity in the 3rd period appears at the end of January and mid-February, 2.5 to 2.0 months earlier than the 1st & 2nd period because the 2nd period has maximum salinity toward the end of March or the beginning of April.

The total dry flow in Kratie increases 34.83% in the 3rd period but this increase is not evenly distributed for all six months of the dry season: the flow increased from February to May, but decreased significantly from December to January. The cause is that the upstream dams store water

until the end of November and release more water in January, making the flow at the beginning of the dry season in the delta to be the lowest in three periods (Figure 4.6). When the upstream dam releases water at the end of January, so the flow takes at least 19 days to move into the VMD, so the salinity in the delta decreases in March, April, and May.

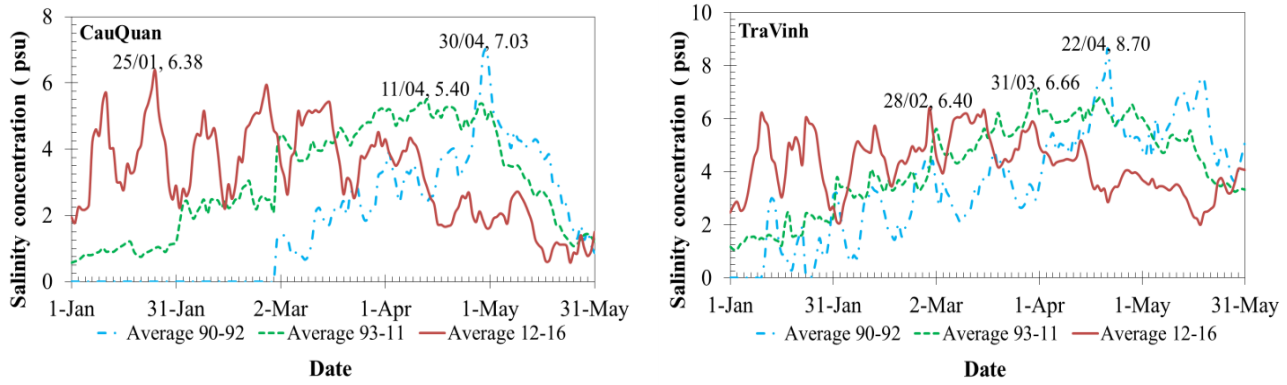

Figure 4.9 Long-term variations of the mean daily salinity in the dry season in three periods: no dam, building dams, and completed dams

On the contrary, the upstream flow got low value at the beginning of the dry season, so salinity appeared as early as December and the salinity threshold of 4psu appeared from January. The maximum salinity concentration occurred at the end of January or mid-February or early March depending on the upstream discharge. The high salinity remained until the end of April or until May. For instance, in 2016, the upstream dams increased the released discharge from the 10th March, so the maximum salinity concentration appeared twice on the Hau River on the 8th February (16.5 psu) and the 8th March (14.6 psu) at the CauQuan station. At TraVinh station on CoChien river, maximum salinity in 2016 appeared on 8th February (14.6psu) and 9th March (12.5psu) (Figure 4.10)

Figure 4.10 shows the maximum monthly salinity of five years with high salinity, which are 1998, 2005, 2010, 2016 and 2020, and the cycle appears to occur earlier from 6 years to 4 years. Before 2005, the maximum salinity usually appeared in April and changed to March in 2005, 2010. In recent years, the salinity peak appeared in February. The salinity concentration in Jan. 2016 and Jan.2020 is nearly 3.5 times higher than in many previous years. This is because saltwater arrives early in 2016 and 2020, with values over 2.3 psu and 9.72 psu in Nov. and Dec., and persists until May and June. The duration time to maintain salinity is about 1.35 times longer than standard years.

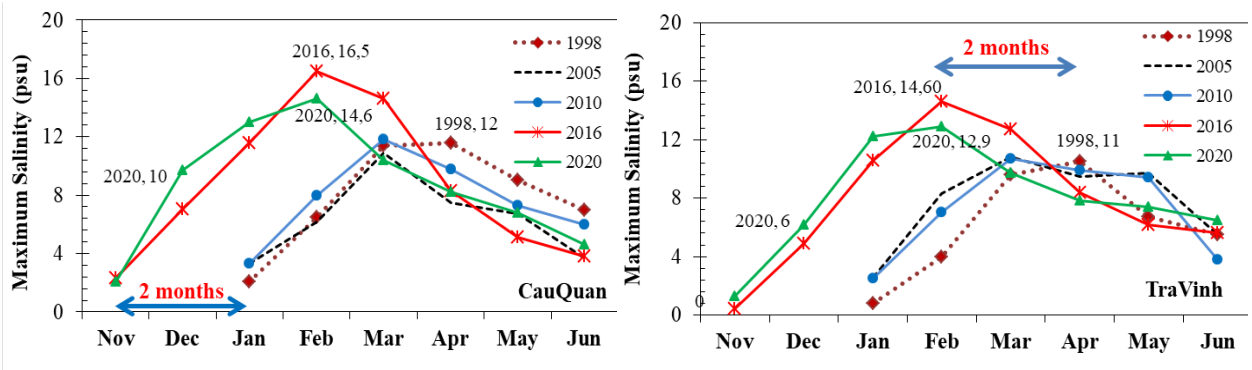

Figure 4.10 Maximum monthly salinity concentrations at CauQuan in the Hau River, TraVinh in the CoChien River

Observing the salinity evolution between 26 to 30 years at four stations: DaiNgai, CauQuan and TraVinh, located around 30km from the sea, and SonDoc, 24km from the sea (Figure 4.11), it is shown that the salinity trend in 2nd period is unstable: increasing trend occurs at CauQuan and SonDoc stations while decreasing trend occurs at DaiNgai and TraVinh stations because the slight increase of the W_{dry} in 2nd period at Kratie, TanChau. The flow is not enough to push salinity on all tributaries (Cau Quan in DinhAn tributary and SonDoc in HamLuong tributary) which are regularly dredged for navigation, so salinity concentration has been high in recent years. While, salinity concentration in the 3rd period increased rapidly from 2012 to 2020, increasing from 20% to 43% in CauQuan and DaiNgai. However, the total dry flow has increased in period 3 (Figure 4.2 and Figure 4.3). But in the last eight years, there were some years with very low W_{dry}, so the highest salinity concentration and most profound intrusion length appeared in the past 90 years (in 2016 and 2020), making the salinity trend of the 3rd period increase sharply. The maximum salinity in 2016 at CauQuan station is 16.5 psu, 1.4 times higher than the previous historical salinity in 1998 (11.6 psu). The peak of salinity in 2020 at some stations is even higher than that in 2016, from 0.6 psu to 0.8 psu at DaiNgai and SonDoc stations. The intrusion length of 4 psu in 2020 is 78km, 68km, and 65km on HamLuong, CoChien, and Hau Rivers, which is 5km, 3km, and 5km deeper than 2016 and 35km, 24km and 24km deeper than the average 26 years. This is similarly reflected on all three estuaries of HamLuong, CoChien and Hau rivers.

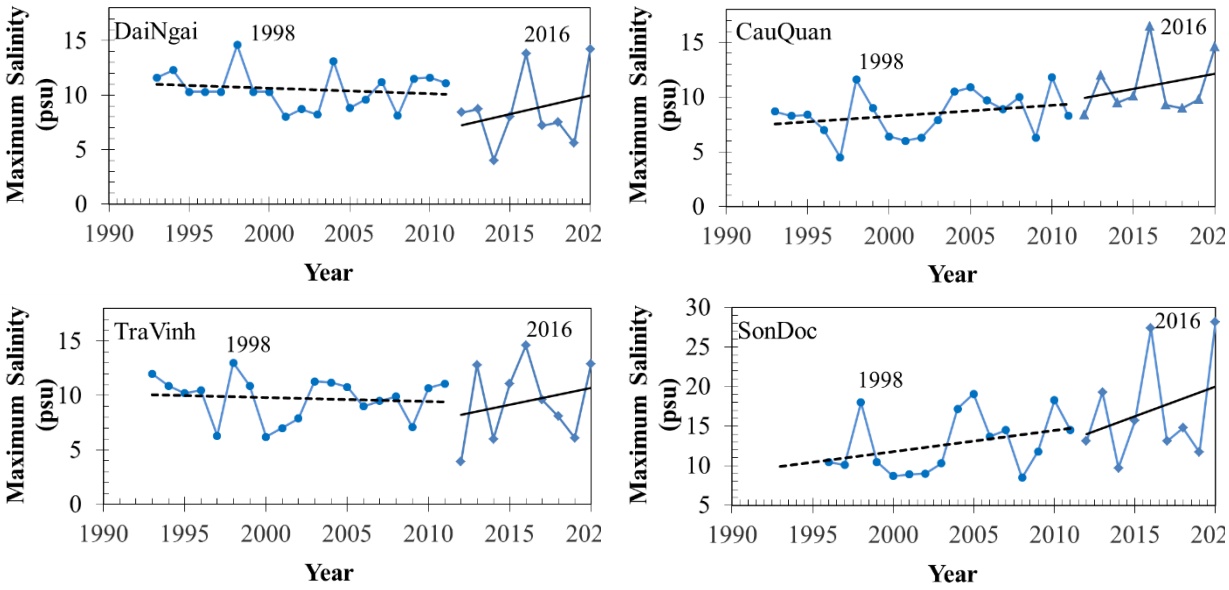

Figure 4.11 Long-term maximum salinity concentrations at DaiNgai, CauQuan in the Hau River, TraVinh in the CoChien River and SonDoc in the HamLuong River

4.4.2 Change of salinity in the short-time

The flow discharge during the dry season into the VMD mainly passes through the Kratie hydrological station and a portion from the TonleSap Lake. Meanwhile, the flow of Chiang Saen station represents 30% to 40% of the total flow of Kratie station (Kuenzer et al., 2013). Therefore, the VMD is affected by the upstream dam operations, which shifts water from the wet season to the middle of the dry season (Fan et al., 2015). For example, the rate of W_{dry}/W_{total} from Dec. to May at Kratie increases from 12.3% in period 1 to 16.6% in period 3. However, the total active storage capacity of Xiaowan and Nuozhadu dams accounts for 22.2 billion m^3, which is 34.69% of the annual mean flow volume at ChiangSaen (64 km^3), so those reservoirs store water for a longer time until the beginning of the dry season (Nov. and Dec.)

Therefore, the total monthly flow from November to January (W_{Nov}, W_{Dec}, W_{Jan}) reduced by 8.0% to 3.0%, during the past 26 years. Significantly, in period 3, W_{Nov}, W_{Dec}, W_{Jan} reduced by 14.0% to 4.0%, which accounts for earlier detection and significant differences in salinity concentration during recent years. Notably, in the dry season of 2016, the flow in Dec. and Jan. at Kratie was lower than in 1998 (a historical drought year) (Figure 4.12). Therefore, China implemented three emergency water supplements to the MR by increasing the released discharge from Jinghong Reservoir (MRC, 2016). During the first one, the flow monitoring on the

mainstream at Chiang Saen started rising from 2.26 m (1,319 m^3/s) on 10th Mar. to 3.25 m on 14th March (2,230 m^3/s) and remained steady at 3.25 m until 12th April. The second emergency supply was from 12th to 22nd April 2016, and the third was from 22nd April to 31st May (Figure 4.13). The flow moving from Chiang Saen to Kratie takes about 15-17 days in the dry season in table 4.2. The flow at Kratie increases from 27th March to 17th June in the first emergency water supplement. However, high saltwater concentration in Hau River appeared two times, from 8th to 10th February and from 8th to 15th March. If the first emergency water supplement had released water in February 2016, VMD would have avoided maximum salinity in March 2016.

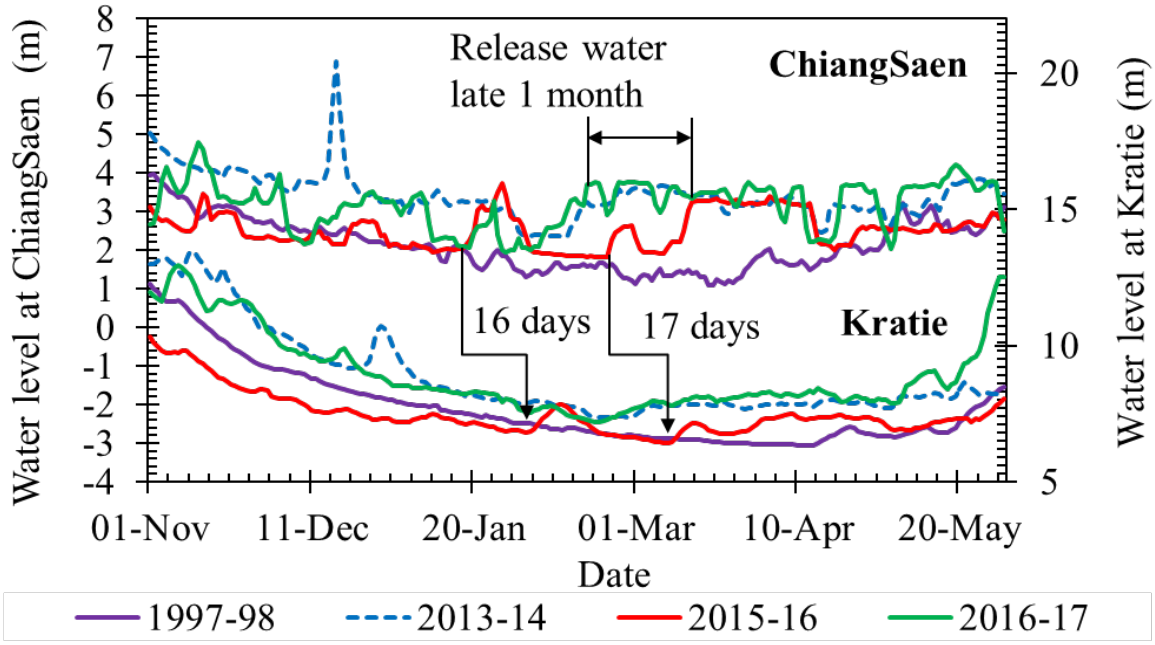

Figure 4.12 The daily water level in Chiang Sean, Kratie stations

4.4.3 Using the numerical model to assess the impact of upstream dams on salinity intrusion

1. Model Scenarios

The baseline (Sc0) considers daily discharges at upstream boundaries and hourly water levels at downstream boundaries (Figure 3.6) of the most severe drought year 2016 (Table 4.3). To assess the impact of upstream dam development, we consider two hypotheses to answer two questions. First, what would have happened if the upstream dams did not release the first emergency water supplement from 10th March to 12th April at Chiang Saen, which means the discharge at Kratie would have been reduced 364 m^3/s from 27th March to 29th April by the flow

of Chiang Saen, representing about 40% of the total flow of Kratie station (Kuenzer et al., 2013). During the first emergency water supplement, the flow monitoring at Chiang Saen started rising from 2.26 m (1,319 m^3/s) on 10th March to 3.25 m (2,230 m^3/s) on 14th March and remained stable at 3.25 m until 12th April.

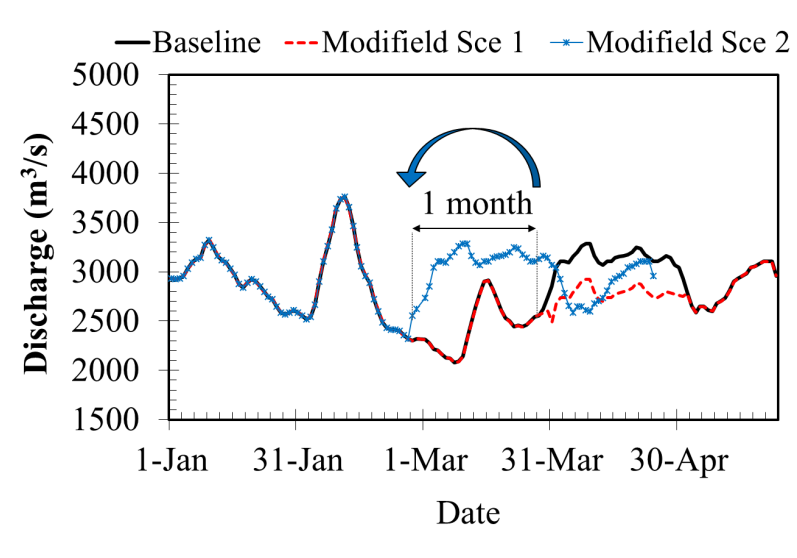

Figure 4.13 The model scenarios

Table 4.3 The scenarios of numerical simulations.

Scenarios	Description of boundary condition	Remark
Baseline (Sc0)	**Upstream**: Discharge hydrographs of 2016 **Downstream**: Water level and salinity of 2016	For calibration
Scenario 1 (Sce1)	Reducing flow discharge boundary by 364 m^3/s [= 0.4(2,230-1,319)] of Kratie from 27th March to 29th April.	**Dams impact**: No increase of flow discharge in the first emergency water supplement (from 10th March to 12th April at ChiangSaen)
Scenario 2 (Sce2)	The first supplement1 month earlier: shifting the discharge from 27th March to 27th February at Kratie Discharge Boundary.	**For mitigation**: dam operation releases water 1 month earlier for the first emergency water supplement to avoid the peak salinity in Mar.

Second question: What is the peak salinity value in March if the first emergency supplement came one month earlier? That means the flow in Kratie will increase from 27th February 2016.

2. Results and discussion

When discharges at Kratie (upstream boundary) were reduced by 364 m^3/s from 27th March to 27th April (**Sce1**), the salinity at each estuary in the VMD would have started to increase from 1st April.

On 10th April, the maximum salinity concentrations of Sce1 at stations located 30 km from the sea increased by 14.0%÷23.2% compared to those of baseline (Table 4.4) because discharge at these stations increased by 2.21% (from -5108.8 m^3/s to -5222 m^3/s) to 2.71% (from -6723 m^3/s to -6905 m^3/s) at DaiNgai and TraVinh stations respectively. The intrusion length would have shifted inward by 4 to 8 km in main streams due to the lack of freshwater to push saltwater back to the sea.

Table 4.4 The results of the numerical model show S_{max} and L_{max} in two scenarios

		Salinity concentration at about 30km from the estuaries.						Intrusion Length of 4g/l		
No.	Scenario	DaiNgai		CauQuan		TraVinh		From TranDe estuary (km)	From Dinh An estuary (km)	From CoChien estuary (km)
		Salinity	(P%)	Salinity	(P%)	Salinity	(P%)			
1	**Baseline on 13 March**	13.8		11.8		8.2		57	57	47
2	Sce 1	13.8		11.8		8.2		57	57	47
3	Sce2	12.2	-11.6	9.8	-17.3	6.9	-15.9	51	51	43
1	**Baseline on 10 April**	7.4		5.4		4.9		41	41	35
2	Sce 1	8.4	14.0	6.4	19.2	6.0	23.2	45	45	40
3	Sce2	6.9	-6.8	5.1	-5.6	4.6	-6.1	39	41	35

In ***Sce2*** (Table 4.4 and Figure 4.14), the modified dam operations under emergency water releases are about one month earlier than the usual (shifting the discharge time series at Kratie from 27th March in the baseline to 27th February in ***Sce2***). Therefore, salinity concentrations in the VMD gradually reduced during March by 11.6% and 15.9% on 13th March because of the discharge increasing by 5.1% (from +2337.6 m^3/s to +2456.1 m^3/s) and 6.9% (from +5226 m^3/s to +5470 m^3/s) at DaiNgai and Tra Vinh stations, respectively. The intrusion length would have also decreased by about 4.0-7.0 km (Table 4.4). Hence, the timing of water release from upstream dams is essential in drought prevention and salinity control in the VMD. Because there are two spring tides a month, which are also the time of high salinity, if the upstream flow comes to the delta at that time, the salt will be pushed back to the sea. It also means that the upstream reservoir increases its discharge in February and March, twice a month before the spring tide, from 17 to 19 days. As a result, the salinity concentration and the intrusion length in the delta will decrease significantly.

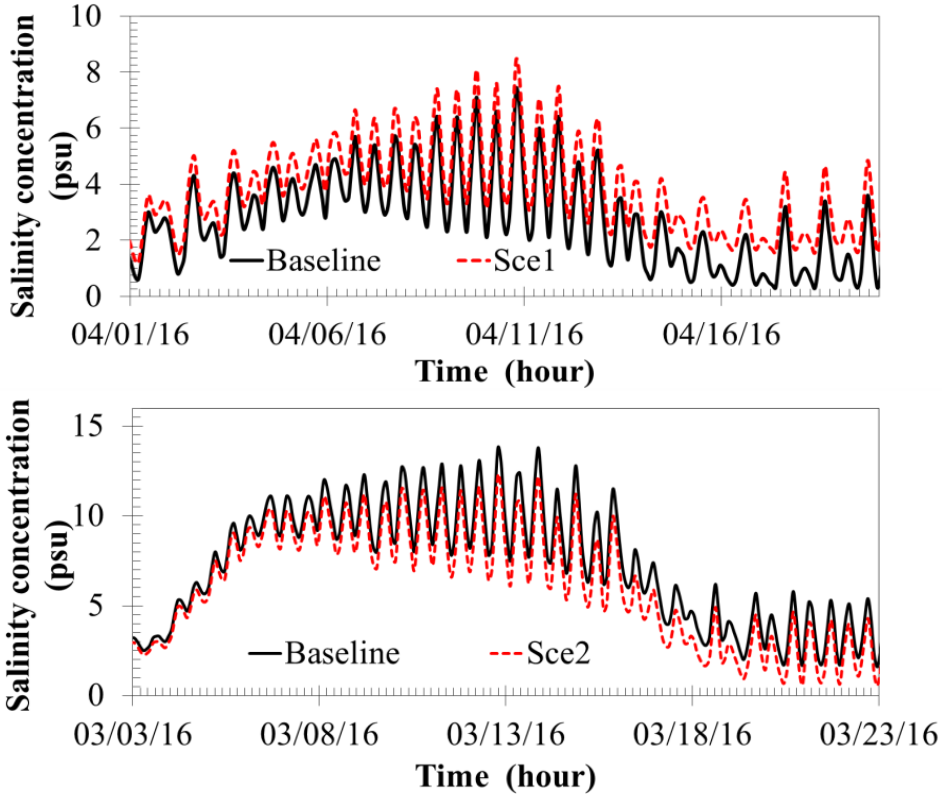

Figure 4.14 Hourly salinity concentrations increasing in Sce1 in April and reducing in Sce2 in March compared to the baseline at DaiNgai station

4.4.4 Conclusion

The flow mechanism will be more complicated when the dams appear across the rivers. For example, when six dams in the Langcang cascade were constructed and then completed, the upstream and downstream flow along the Mekong River have had remarkable alterations.

In the upstream, when six large dams were completed, the total storage accounted for more than 49% of the total flow in Chiang Saen. The total annual and wet season runoff decreased by more than 22% and 27%, respectively. Räsänen et al. (2017) also reported a reduction of 21% in the September discharge at Kratie between two periods, 2010-2014 and 1960-1990 periods, which is in line with our results. Besides, the maximum annual discharge value (Q_{max}) decreased rapidly with a reduced rate of 33.3% from the 1st period to the 3rd period (67.76 m^3/s/yr). But the upstream dams increase the total dry season runoff (20.96%), and the average minimum annual discharge increases by more than 15% to 41% (from 1st and 2nd period to 3rd period). However, the increase

is not uniform in all six months of the dry season. The total monthly volume slightly increases from February to May. The study results are also consistent with Li et al., 2017, Rasanen et al., 2017 and Fan et al., 2015). For instance, in our analysis, the February-April discharges increased by 22.9-39.4%, and the July-October discharges reduced by 12.2-25.6%, similar to 25.9-55.2% increase and 22.3-32.9% decrease respectively as reported by (Li et al., 2017). Rasanen et al. concluded that the discharge in 2014 increased by 121 – 187% in March-May and decreased by 32-46% in July-August compared to average discharges from 1960 – 2014.

In the downstream: at Kratie station, W_{wet} decreased insignificantly by about 3% (10.4 km^3) while the W_{dry} increased 34.83% (10.5 km^3) during the 1960-2016 periods so the W_{total} tended to remain unchanged over the years. That mean the upstream reservoirs reduced the wet flow by accumulating water storage and shifting water from the rainy season to the dry season by reservoir operation. As a result, the ratio of W_{dry}/W_{total} increases from 12.3%, 13.5%, and 16.6% in three periods: no dam, building dams, and completed dams, respectively. Also, at Tan Chau station, which accounts for 84.78% of total dry flow into the VMD, the dry flow slightly increased. That means the upstream dams tend to increase the dry flow at the VMD. But we found that upstream hydropower dams in the VMD have a substantial impact on the dry flow and make it more fluctuate, and the flow increases from March to May and decreases from November to February in the 3rd period. Also, in the 3rd period, the average Q_{min} of the dry season at all downstream stations increase with the rate is 19.35%, 71.38% and 122.8% at Kratie, Chau Doc, and Tan Chau respectively while the average Q_{max} decreases by 7.89%, 3.36% and 11.32% respectively.

The downstream flow change significantly impacts the salinity intrusion in VMD. In the 1st period, the salinity level in the MRD will start to rise by the end of December, reaching its peak in March or April and declining afterward. However, in the 3rd period, the flow reduces at the beginning of the dry season, so salinity concentration starts to rise from November and maintains a high concentration from December to February, and reaches its peak value in February. So its peak appeared two months earlier. Saltwater intruded further inland and remained longer during the dry season.

Using the numerical model to assess the impact of upstream flow change by reducing 364 m^3/s (12%) discharge at Kratie, the maximum salinity concentrations at stations located 30 km from the sea increased by 14.0%÷23.2% compared to those of baseline, and the intrusion length was shifted inward by 4 to 8 km in main streams due to the lack of freshwater to push saltwater back to the

sea. One mitigation scenario that has been considered is to release water from the upstream hydropower dams one month earlier (27th March to 27th February). By doing this, salinity concentrations in the VMD would gradually decrease during March by 11.6% and 15.9% on 13th March because discharge increased by 5.1% and 6.9% at DaiNgai and TraVinh stations, respectively. The intrusion length would also decrease by about 7.0-10.0 km. Hence, the timing of water release from upstream dams is very important in drought prevention and salinity control in the VMD. Because there are twice spring tides a month and it is also the time of high salinity, if the upstream flow comes to the delta, the saltwater will be pushed back to the sea. It also means that if the upstream reservoir increases its discharge in February and March, twice a month before the spring tide from 17 to 19 days, the salinity concentration and the intrusion length in the delta will decrease significantly.

Chapter 5: Impacts of morphology on Salinity intrusion

After the six upstream dams in the Langcang cascade were completed, they have been predicted to trap as much as 83% of the sediment generated from the upper MRB, which is equivalent to 40% of the total sediment budget of the MR (Kondolf et al., 2014). According to Manh et al., 2015, the maximum changes by upstream hydropower development would mean a nearly 90% reduction of delta sedimentation and a 95% reduction of the sediment reaching the sea. Kondolf et al. (2014) also predicted that only 4% of the MR's sediment would reach the Mekong Delta annually if all 133 planned dams were constructed in the future. Before dam construction, the sediment load of the VMD was 160 Mt/yr (Kondolf et al., 2014), but it was significantly reduced to 40 Mt/yr in 2012 –2013 (Nowacki et al., 2015), mainly driven by upstream dams and sand mining. However, the results of Binh et al. 2019 and 2020 concluded the suspended sediment load of the VMD decreased by 74.1% in 2012 –2015 from the pre-dam period (1980), of which 40.2% was caused by the six mainstream dams in the Lancang cascade. The Manwan and Dachaoshan dams alone directly drove 32% of the reduction. Although the sediment loads at all downstream stations of the Lancang cascade were significantly reduced, the sediment load at Jiuzhou, upstream of the Lancang cascade, increased. This indicates that the reduction in the sediment load is not because of a possibly reduced sediment supply from the upper MRB but is because of sediment being trapped by dams. It is confirmed that the upstream dams not only affect the flow change in the MR but also trap a large amount of upstream sediment, leading to a significant reduction of the sediment downstream.

Such a sediment load reduction could cause riverbed incision, riverbank erosion in alluvial rivers and channels, and coastline retreat (Li et al., 2017), which may in turn create difficulties in obtaining intake water for irrigation and may increase salinity intrusion in the VMD. For instance, the riverbed of the Hau River in the VMD measured in 2008 was incised by 1 –5 m more than that measured in 1998, with an average incision of 1.4 m (Allison et al., 2017a). On 1st August 2019, 80m long and 25m wide riverbank of the AnGiang collapsed (Figure 5.1), which was hypothesized to be partly caused by the reduced sediment supply from the MR and sand mining. Approximately 50 – 66% of the current VMD's coastline is experiencing erosion as manifested by a shift from an accretionary phase of 10.6 m/yr during the period of 1973 –1979 to an erosional phase of −2.1 m/yr during the period of 2010 –2015 (Li et al., 2017).

Figure 5.1 On 1st August 2019 at AnGiang, the bank erosion is 80m long and 25 wide.

Figure 5.2 On June 5, 2021, at the bank erosion, is 90m long and 10-15m wide

Sediment reduction is one of the main causes of riverbed incision and riverbank erosion downstream. For example, Kummu et al. (2008) used remote sensing in the Vientiane-Nong Khai area to estimate the MR's bank erosion as 0.8 and 1.0 m/yr (for the main channel) and 2.4 and 4.8 m/yr (for the islands) during the periods of 1961 –1992 and 1992 –2005, respectively. However, the research results do not specify whether the topographic data used for all the analyzed river tributaries are identical. Most of the studies use old topographic data resulting from many research projects in different regions. Therefore, more than two hundred cross-sections were measured along the Tien River from TanChau to CungHau and CoChien estuaries as well as along the Hau river from AnGiang to TranDe and DinhAn estuaries in August 2017 by ADCP, GPS, Handheld Garmin GPS, and Pro30 as described in chapter 3, section 3.3.1. The author uses the measured river cross-sectional data in 2017 compared with the depth data in 2009 to assess the degree of erosion - accretion along the river and paid special attention to the mouth of the Hau river in the last 8 years. Then the author used a model to assess the extent of riverbed erosion on the length of salinity intrusion (SI) and river salinity concentration. According to the research results of Binh et al. (2020b) and Eslami et al. (2019), riverbed incision is an important driver of increasing SI. Eslami et al. (2019) numerically estimated that a 2 m riverbed incision in the Co Chien-Cung Hau channel might increase SI length by 5 km and salinity concentration by approximately 1.5 psu at a station about 20 km from the sea. It is more intense in the Ham Luong channel; a 20% drop in riverbed elevation is likely to increase intrusion length by 10km. At SonDoc station (20km from the estuary), salinity concentration would increase by 2.5 psu.

5.1 A long-term monthly sediment load:

The flow at TanChau in Tien River accounts for 84.78% in the dry season and 95.8% in the wet season of total river flow into VMD. Similarly, over 85% of the sediment load of the VMD from the MR is transported in the Tien River (monitored at Tan Chau); therefore, the suspended sediment behavior at Tan Chau describes the VMD sediment dynamics well. The sediment content at TanChau and ChauDoc is unevenly distributed by season and year (Figure 5.3 and 5.4). In 1 year, the monthly sediment concentration is highest in the flood season with the largest concentration being over 47 Mt. In the dry season, the average content is about 8.07 Mt and the lowest is 0.015Mt. The sediment transport in the VMD is mainly concentrated during July-December (Figure 5.3), accounting for 94.5% of the annual sediment budget with the maximum volume of sediment load usually appearing in September. The maximum annual sediment load into VMD is 1981 (217.27 Mt) and the lowest is 2015 (27.59 Mt).

While the total annual flow (W_{total}) and the total rain flow (W_{wet}) at TanChau decreased by 11% (Figure 4.1), the sediment content in 36 years decreased by 94% (Figure 5.4).

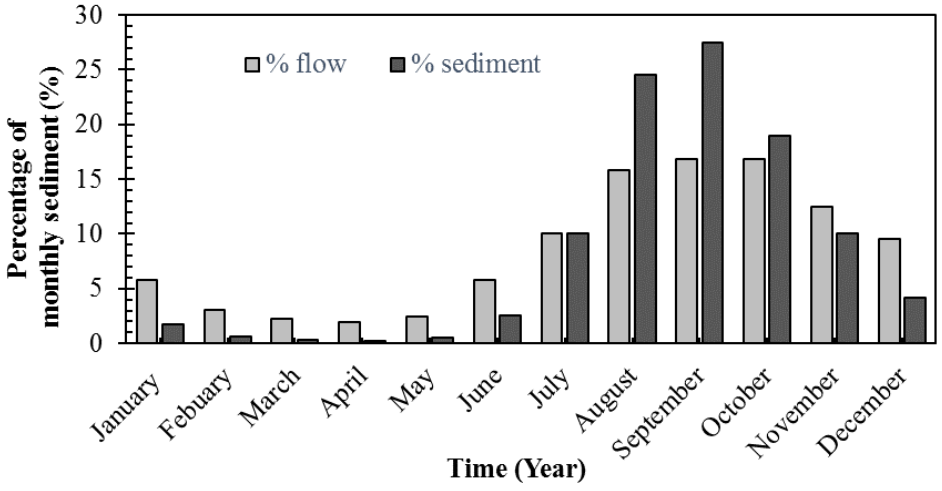

Figure 5.3 The monthly sediment concentration budget at TanChau

Figure 5.3 also shows that in the no-dam period, the sediment load at TanChau is relatively high, with the average value of many years being 166.42 Mt. After 1993 when Manwan dam in the mainstream was completed, the sediment load decreased significantly. In the period 1993-2011 (building dams) the annual sediment load decreased by 64.1% (59.7 Mt) and decreased by more than 74.6% (42.3 Mt) in the period 2012-2016 (completed dams).

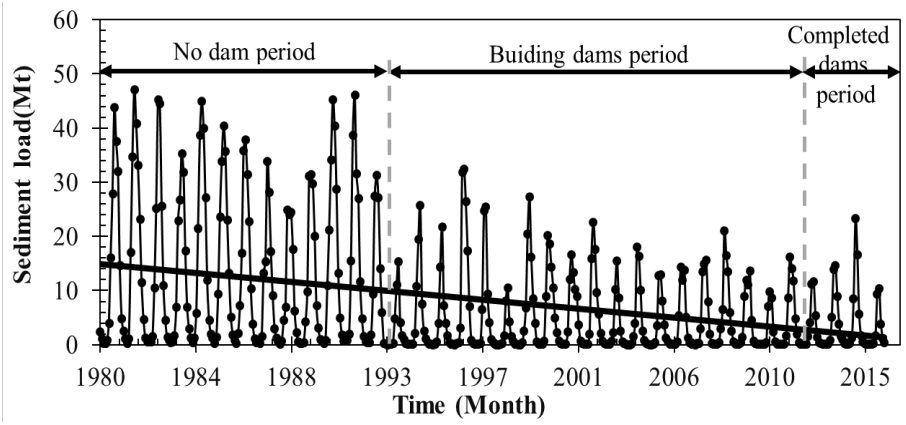

Figure 5.4 The long-term monthly sediment load of the VMD

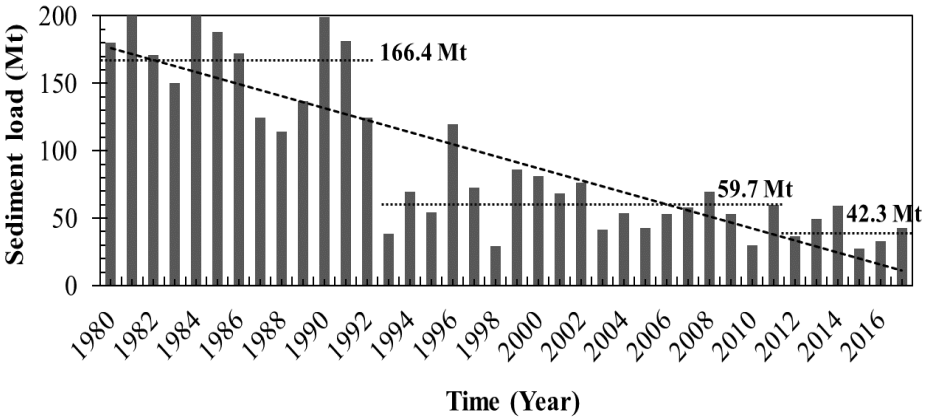

Figure 5.5 The annual sediment load at TanChau and ChauDoc

5.2 Riverbed elevation and cross-sectional shape

5.2.1 Data measurement

The ADCP was used in the first field survey in August 2017 to measure the bed elevation. The boat moved from CoChien and CungHau estuaries upstream at TanChau station and measured 80 cross-sections between adjacent points ranging from 2km to 5km. Then we moved to the Vam Nao River to measure 14 cross-sections. Finally, 106 cross-sections from ChauDoc station in the Hau River to DinhAn and TranDe estuaries were measured at 0.5km to 5km (Figure 3.3). A pole-mounted GPS-equipped Teledyne RD Instruments Workhorse Rio Grande 600 kHz ADCP measured the river depth and 2-dimensional velocities. The ADCP was mounted at 0.3 m under the water surface on the boat side. A Trimble GPS with an antenna was combined with the ADCP (Figure 3.4). These devices were connected to a field computer to control the speed and direction of the boat. The boat moved longitudinally and transversally.

5.2.2 The shape of riverbed elevation and cross-sections along the Hau and Tien River

The riverbed elevation of 220 km the Tien River and 190 km the Hau Rivers is very variable, ranging from several meters deep near the river mouths to more than 30 meters deep in the upper parts (Figure 5.6). The deepest point in the Tien River is at a location of approximately 2 km upstream of the MyThuan station (-46 m deep), while the deepest riverbed in the Hau River is just upstream of the CanTho station (-31 m deep). The riverbeds are shallowest around the last 15 km which is near the river mouths. When reaching the deepest points in both Tien and Hau Rivers, the riverbeds become more superficial as they move seaward.

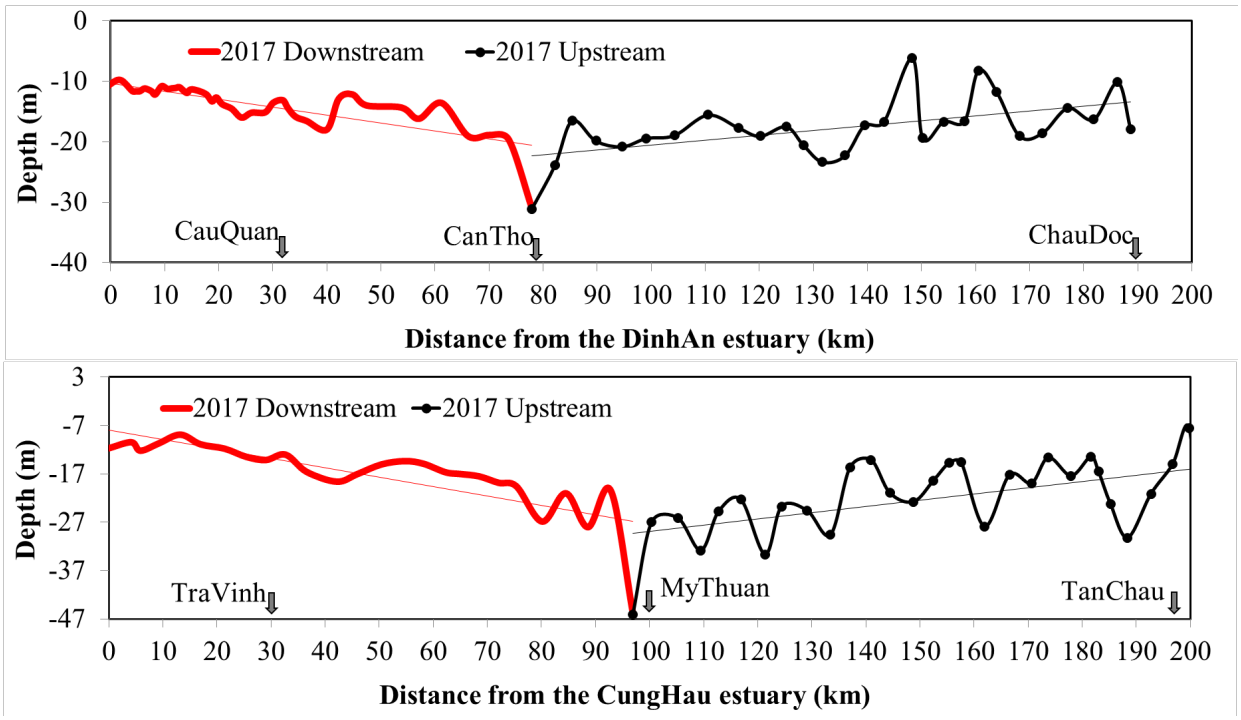

Figure 5.6 Longitudinal variations of riverbed elevation in the Hau and Tien Rivers.

Two clear reaches distinguish the Tien and Hau Rivers regarding riverbed elevation and cross-section shape. The dividing points are at the My Thuan station in the Tien River and at the Can Tho station in the Hau River. The upper reach is deep and narrow (typically less than 1,000 m wide). The riverbed elevation decreases seaward. The cross-section in the upper reach is asymmetric, with the thalweg appearing either on the left or the right bank (Figure 5.7 and 5.8). In the upper reaches, the riverbed elevation decreases seaward, and the slope of the riverbed of the Tien River (i_o = 0.0125%) is steeper than that of the Hau River (i_o = 0.0097%). On the other hand,

the lower reach is shallow and wide (the maximum width can reach 4,000 m at 33 km far from the DinhAn estuary in figure 5.7). The riverbed elevation increases seaward. The cross-section in the lower reach is symmetric. In the last 30 to 33 km from the river mouths of the Tien and Hau Rivers, islands are usually formed in the middle of the river (Figures 5.7 and 5.8). Along 200km of Tien and Hau river, islands appear at regions having cross-sections larger than 1,100 m in the Tien River and larger than 1.700 m in the Hau River. In the lower reaches, the slope of the Tien River (i_o = 0.022%) is still slightly steeper than that in the Hau River (i_o= 0.012%).

5.2.3 The changes of riverbed elevation and cross-sections along the Hau and Tien River

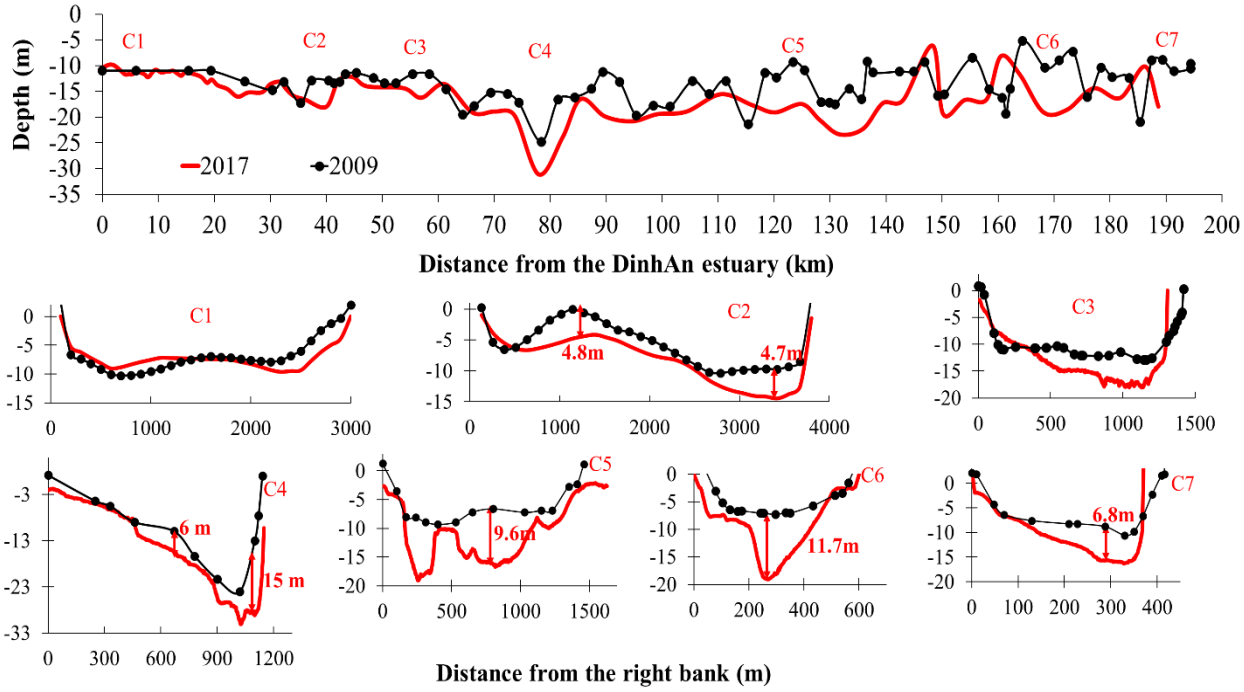

Figure 5.7 Longitudinal and cross-sectional variations of the riverbed in the Hau River

Figure 5.7 and 5.8 shows the riverbed elevation of the Hau and Tien rivers by the historical data (black dot line). The upper reach data were collected in 1998, while the lower reach data were completed in 2009 (in the DinhAn branch) in the Hau River and 2000 (in the CungHau) on the Co Chien river. The depression of riverbed elevation along the deepest points of the Hau and Tien rivers is considered between the historical riverbed elevation data and riverbed elevation data in 2017. Also, seven typical cross-sections along the ChauDoc to DinhAn estuary confirmed a significant riverbed erosion and deposition (Figure 5.7). This figure clarifies in more detail that a

rapid morphological change in the upper part is more extreme than in the lower part, comparing the riverbed elevation data between 2009 and 2017.

Along the Hau River, the riverbed reduces relatively high, ranging from -0.2m to -11.7m in depth with a mean incision rate of the whole section (190 km) of -3.0m. The erosion rate is from -0.01m to -0.7m in one year, so the annual average erosion rate is -0.2 m/yr. In which, the upper section of Hau River from ChauDoc to CanTho (110 km), the degree of riverbed incision is from -0.3m to -11.7m with an average incision value of -4.0 m during 1998-2017. In other words, the incision rates ranged from -0.02 to -0.59 m/yr, with a mean value of -0.22 m/yr. The downstream from CanTho to DinhAn estuary (80km), the incision level is less with erosion range from -0.2m to 4.8m and the average level of erosion -0.8m so that we can calculate the relative ratio. This estuary's maximum and average erosion is 0.22m/yr and 0.07m/yr. Therefore, it was found that the incision rate from ChauDoc to CanTho is more than three from CanTho to the sea.

Along the Tien River, the riverbed erosion significantly incises, ranging from -0.047 m to -16.2 m deep with the mean value of -6.2 m during 1998-2017. In other words, the incision rates range from -0.003 to -0.9 m/yr, with a mean value of -0.34 m/yr. Six typical cross-sections and the Tan Chau to CungHau estuary confirmed a significant riverbed incision (Figure 5.8). This figure also clarifies a rapid morphological change when the river bathymetry measured in August 2017 from the first field survey is compared with the one measured in 1998. When the riverbed elevation changed in the lower part of CungHau branch, the range of riverbed erosion was from -0.003 m to -0.382 m with the mean value of -0.19 m/yr. The incision rates in the upper part were higher than those in the lower part of the Tien river.

The result shows that the mean incision rates in the Hau River are -0.22 m/yr, approximately 1.6 times greater than that of 0.14 m/yr in the 1998-2008 period of Allison et al. 2017. Similarly, the mean annual incision rate in the 1998-2017 period was -0.34 m/yr, 2.12 times as high as that in the 1998-2014 period, being -0.16 m/yr (Binh et al., 2020). This accelerated riverbed incision is likely due to the reduced sediment load of the VMD from 166.4 Mt/yr in the no-dam period to 42.3 Mt/yr in the completed dam period (Figure 5.3) and the increased sand mining from 3.9 Mm^3 in 2012 to 13.43 Mm^3 in 2018 (Binh et al., 2020). However, sand mining causes riverbed incision at the local scale, while upstream dams are responsible for large-scale morphology changes. Allison et al. 2017 also concluded that sand mining was not the leading cause of reducing riverbed elevation in the area between CanTho and the river mouth of the Hau River. Figures 5.7 (C5 and

C6 sections) and 5.8 (C3 sections) show the irregular riverbed geometry at the sections where sand mining takes place, characterized by deep pits while the cross-sections have relatively similar bottom lowering. The rate of river bed erosion in VMD in recent years has been much faster than in periods 1 and 2. Before the construction of the dam, upstream sediment is transported downstream and provides a significant amount of sediment for the river. Then, the sediment is deposited in sand mining sites. However, more than two decades after the completion of the first dam, when the amount of sediment deposited is almost exhausted, and the riverbanks of these areas can reach a new equilibrium condition, the impact of hydroelectric dams on the VMD river bed erosion are drastic. The rate of riverbed incision is predicted to be even faster in the future as more dams are completed.

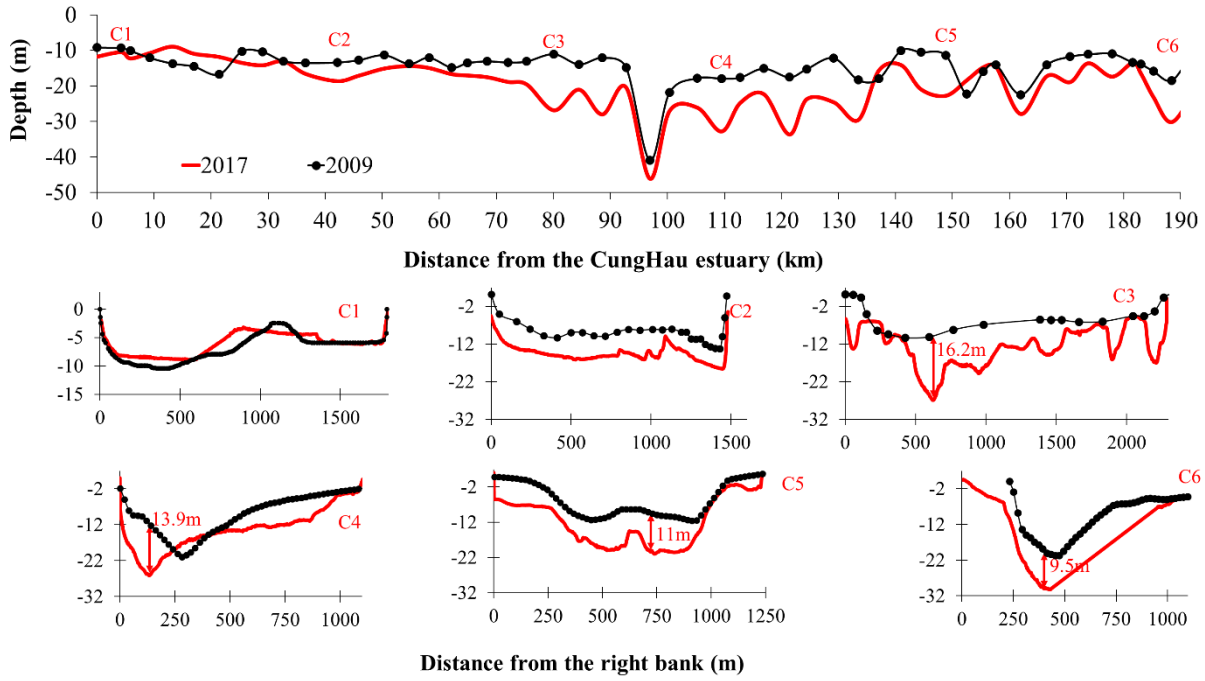

Figure 5.8 Longitudinal and cross-sectional variations of riverbed elevation in the Tien River

5.3 The impact of morphology change on the salinity intrusion by the numerical model

Figures 4.10 and 4.11 show the significant increase in the annual maximum salinity concentration in 30 years at four stations: DaiNgai, CauQuan, TraVinh and SonDoc (in 1990-2020 period) with increasing rate is by 0.16 psu/yr at CauQuan station and 0.3 psu/yr at SonDoc station. Especially in the last 8 years (from 2012 until now, 2020) salinity concentration increased rapidly from 2012 to 2020, from 20% (0.22 psu/yr) to 43% (0.67 psu/yr) in CauQuan and SonDoc stations.

The salinity increased not only in magnitude, but also in the length of intrusion. The intrusion length of the 4 psu contour line in 2020 is 78km, 68km and 65km on HamLuong, CoChien and Hau Rivers, 5km, 3km and 5km deeper than 2016 and 35km, 24km and 24km deeper than the average 26 years on all three estuaries of HamLuong, CoChien and Hau rivers. This study would like to find a linkage between the increased salinity intrusion and accelerated riverbed incision because the former is caused by riverbed incision-induced water level reduction. When the water level reduced in the landward areas, the water surface gradient between sea and land also reduced into the landward, which increases the salinity intrusion.

5.3.1 Simulation scenarios

Table 5.1 The scenarios of numerical simulations.

Scenarios	Description of Boundary condition	Remark
Baseline (Sce0)	**Upstream**: Discharge hydrographs of 2016 + DEM 2017 **Downstream**: Water level and salinity of 2016	For calibration
Scenario 3 (Sce3)	**Upstream**: Discharge hydrographs of 2016 + DEM 2009 **Downstream**: Water level and salinity of 2016	The influence morphology change
Scenario 4 (Sce4)	Riverbed incision from 2017 to 2025: 0.22m/yr x 8 = 1.76m in Hau River and 0.34m/yr x 8 = 2.72m in Tien river.	The influence of river bed incision

The baseline (Sc0) used Q, WL and S in the 2016 severe drought as boundaries. As figure 4.11 mentioned, the repeating cycle of extreme drought years is from 4 to 6 years, so the scenario will consider the influence of riverbed topographic changes on salinity and intrusive length in the drought cycle in the next 5 years from 2020. That is, consider salinity drought in 2025 with the lowering of the riverbed from 2017 with the annual incision rate on the Hau River of 0.22 m/yr and 0.34 m/yr on the Tien River. The level of river bottom decline in 2025 on Hau and Tien rivers is 1.76m and 2.72m respectively.

5.3.2 Results and discussion

Figure 5.9 and Table 5.2 show the results between the Baseline scenario (Sce0) and the third scenario (Sce3). Sce3 was simulated with the upstream discharge boundary, water level and downstream salinity boundaries of 2016 and the topography 1998 for the whole VMD. The results

show that the intrusion length in Sce0 is 5.0 km and 8.2 km longer than that of the Sce3 scenario on the CungHau and DinhAn branches, respectively and this is due to the morphology changes from 1998 to 2017 along 190 km to 210 km length of the Hau and Tien rivers. The mean riverbed incision of the lower part around 80km from the estuary is 0.07m/yr and 0.19m/yr on the Hau and CungHau branches while the mean incision value of the whole Tien (0.34 m/yr) and Hau (0.22 m/yr) river were used for simulation in Sce4 because the numerical model simulated for all Mekong River Delta (VMD) from Kratie to estuaries. However, in figure 5.7 and 5.8, I can see that 30km from the mouth of Cung Hau branch, the bottom topography is increasingly shallow.

In comparison, DinhAn branch has a riverbed lowering from 4km point to the upstream, so the salinity concentration of DinhAn branch in recent years is higher than in CoChien branch in the 30km estuaries. While from 40km upstream, the saltwater value in CoChien branch rises higher and penetrates deeper than that in the Hau River. The largest difference in salinity concentration between the Sce0 and Sce3 scenarios was from 8.7% to 11.2% (from 1.2 psu to 2 psu) during 18 years.

Similarly, comparing the salinity concentrations between the scenarios Sce0 and Sce4 (Sce4: consider saline intrusion in the next 8 years with the average lowering of the Hau and Tien riverbeds of 0.22m/yr and 0.34m/yr), the change was not much with the increase of salinity concentration from 0.8 psu to 0.9 psu and the length of deeper saline intrusion from 1.8 km to 4.5 km (Table 5.2 and Figure 5.9 and 5.10). In Sce4, 1.76 m and 2.72 riverbed incisions in Hau River and Tien River were used to simulate the riverbed incision for next 8 year from 2017 to predict the SI in the next drought year cycle in 2025. That means the topography of all cross-sections in the Hau and Tien River are assumed to drop 1.76m and 2.72m respectively. Therefore, the increase in salinity concentration and intrusion length are the same for any point in one cross-section. While the Sce3 scenario is the actual topographic change between topography in 1998 and 2017, the mean incision rate is considered at the middle point of cross-sections along the Hau and Tien river, while the sections are not symmetrical and the deepest point is not located in the middle of the cross-section but lying on the left or right bank depending on the position of the cross-section. The highest salinity concentration usually occurs at the deepest points of the cross-section, so the increase and decrease in a cross-section is unequal.

Table 5.2 The result of numerical model

No.	Scenario	Salinity concentration at about 30km from the estuaries.						Intrusion Length of 4 psu		
		DaiNgai Station (g/l)		CauQuan Station (g/l)		TraVinh Station (g/l)		From TranDe estuary (km)	From Dinh An estuary (km)	From CoChien estuary (km)
		Salinity	(P%)	Salinity	(P%)	Salinity	(P%)			
1	Baseline on 8 Feb.	13.8		16.4		12.3		58.2	58.2	60
2	Sce 3	12.6	-8.7	14.6	-11.2	11.1	-9.8	50	50	55
3	Sce 4	14.5	5.1	17.2	4.9	13.2	7.3	60	60	64.5

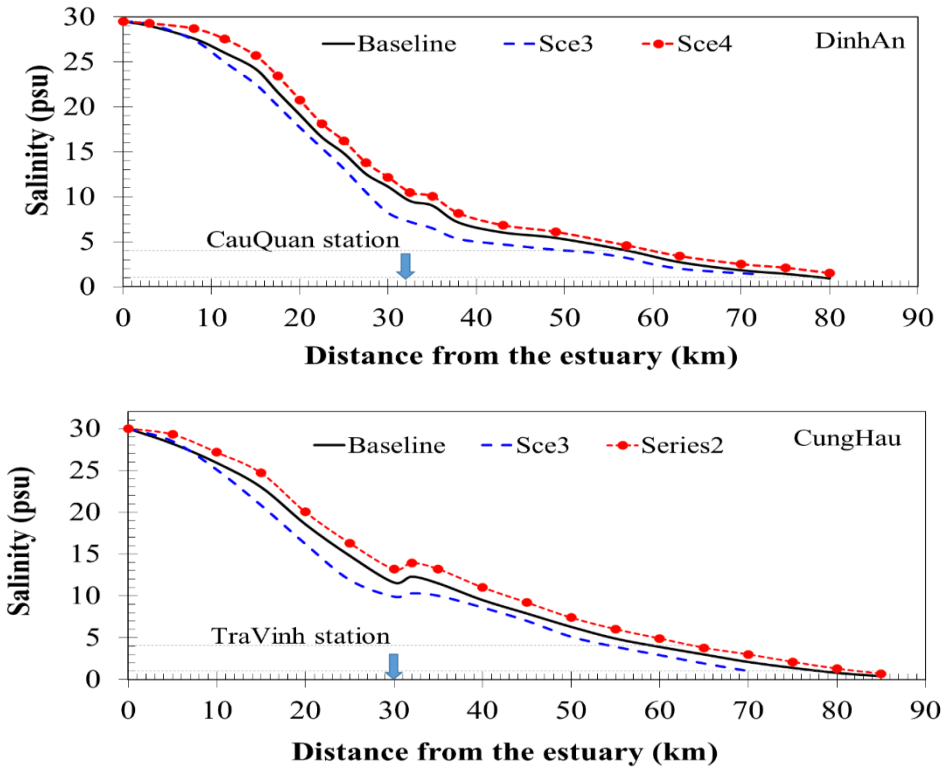

Figure 5.9 Comparison the intrusion length of three scenarios in the DinhAn and CungHau branches

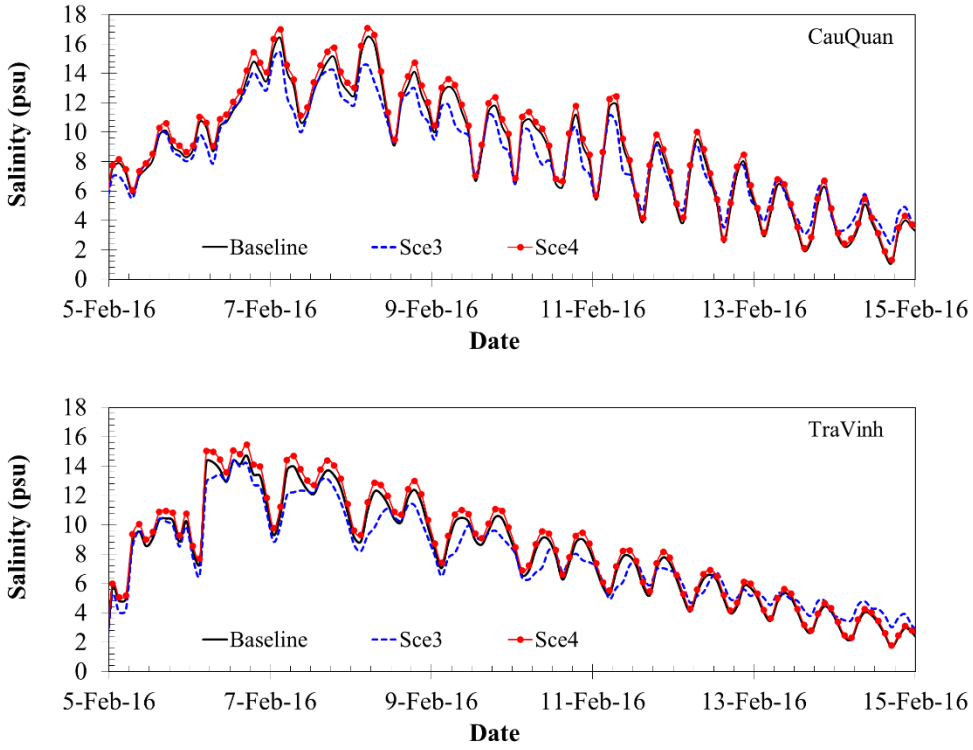

Figure 5.10 Comparison the salinity concentration time series of three scenarios at CauQuan and TraVinh stations.

Table 5.2 summarizes my results. Which are in agreement with the finding of Eslami et al. (2019), who found that riverbed incision strongly affects the salinity intrusion in the VMD, they used numerical model to simulate that 2m riverbed incision in CoChien-CungHau branches may increase intrusion length by 5km and salinity concentration by near 1.5psu at a station 20km far from the sea.

5.4 Conclusions

The transport of sediment plays an important role in the process of erosion and accretion in rivers and estuaries. Moreover, the sediment from the upstream flows to the VMD, accreting alluvium for the river and increasing the fertility, increasing crop productivity, reducing the amount of fertilizers needed for agriculture and preventing environmental pollution caused by less fertilizers. But since 1993, when large upstream dams were built and over 56 hydropower dams have been completed in 2016, Mekong dams have caused large-scale morphology change in VMD by the dams were trapping most of the sediment flow. In the building dam period of 1993-2011,

the annual sediment load decreased by 64.1% (59.7 Mt) and by more than 74.6% (42.3 Mt) in the completed dam period 2012-2016. This is the main cause of erosion or incision of the bottom topography of Hau and Tien rivers in VMD.

Due to the limited data to assess the change of riverbed topography, more than 200 sections of Hau, Tien and Vam Nao rivers were measured in August 2017 with fundings from the JASTIP project provided by Kyoto University. Measurement data helps to divide the Hau and Tien rivers into two parts based on the river slopes and the shape of cross-sections. The upper parts stretch from TanChau to MyThuan in Tien River and from ChauDoc to CanTho in Hau River. The riverbed elevation in each section reduced as it went seaward and the width of cross-section were less than 1500m, while the lower part from CanTho and MyThuan estuaries saw the riverbed elevation increase seaward and the width of cross-sections being 1500m to 4000m.

Comparison of the riverbed elevation data between 2009 and 2017 shows that the mean incision rate from ChauDoc to CanTho (0.22 m/yr) is more than 3 times that of CanTho to the DinhAn estuary (0.07 m/yr). Also, the maximum incision rate in the lower part is 0.22 m/yr so 0.22 m/yr of riverbed incision is used for whole Hau river for simulation, while the mean incision rate in upper and lower part of Tien (CoChien branch) are 0.34 m/yr and 0.19 m/yr respectively.

The erosion of riverbed topography is an increasingly complex and serious cause of saline intrusion in the VMD. The MIKE 11 HD and AD model results show that, when the entire bottom of the Hau River is lowered by 1.76m, the salinity concentration and the intrusion length increase by 0.8 psu and 1.8 km, respectively whilethe salinity value and intrusion length increase to 0.9 psu and 4.5 km when a simulation of 2.76m riverbed incision in CoChien-CungHau river is considered.

Chapter 6: Impacts of tide and Sea Level Rise on Salinity intrusion

6.1 Introduction

6.1.1 Tidal regime of VMD

Tidal regime of along Mekong Coastal zone is different and therefore affect of tide on the coastal regions differently:

Tide in the East Sea: tidal amplitude increases from Vung Tau to Ganh Hao, and the timing of peak and trough at Ganh Hao is about 2 hours slower than that Vung Tau. Therefore, the phases of tidal transmission to the northern tributaries are earlier than those in the southern tributaries.On the other hand, in this sea, the tides have irregular semi-diurnal tides (twice up, twice down in a day), the tidal amplitude can reach nearly 4.0m.

The tidal cycle has the following characteristics:

Daily tidal cycle: There are two oscillations with a tidal period of 24 hours and 50 minutes in a day. The time for the water to rise and fall is equal to a value of 12 hours 25 minutes.

Semi-monthly tidal cycle: There is a spring tide period and a neap tide period in a semi-monthly tidal process. The day of the spring tide (highest peak, lowest trough) occurs during no moon or full moon. The neap-tidal day with the smallest tidal amplitude occurs on the 7^{th} and 23^{rd} lunar days. The difference between the two peaks is small during spring tide, but the difference between the two legs is maximum (Figure 6.1). In contrast, the difference between the two peaks is maximal during the neap tide period, and the difference between the two leg tides is minimized.

- Monthly cycle: in each lunar month, there are two periods of spring tide and two periods of neap tide.

- Multi-year cycle: tides have a long cycle of 18.6 years, but this tidal amplitude is relatively small.

The daily tidal range in the East Sea in Vung Tau is about 3.5 m in hightide and about 1.5 m in lowtide. The amplitude of fluctuation of the tidal peak is 0.5 - 1.0 m. Regarding the trend, the tide level in the East Sea has the following characteristics:

- The peak of maximum water level occurs in the spring tide with 24.5 cycles in the year. During the year, the peak is in November, December and low in June and July with a difference of about 0.5 m.

- The minimum water level according to neap tide in the month. The amplitude of fluctuation of the tidal foot is 0.5 - 2.0 m. During the year, the lowest drop is in June, July and December, January and the highest in March, April, September, October, the difference is about 0.5 - 2 m.

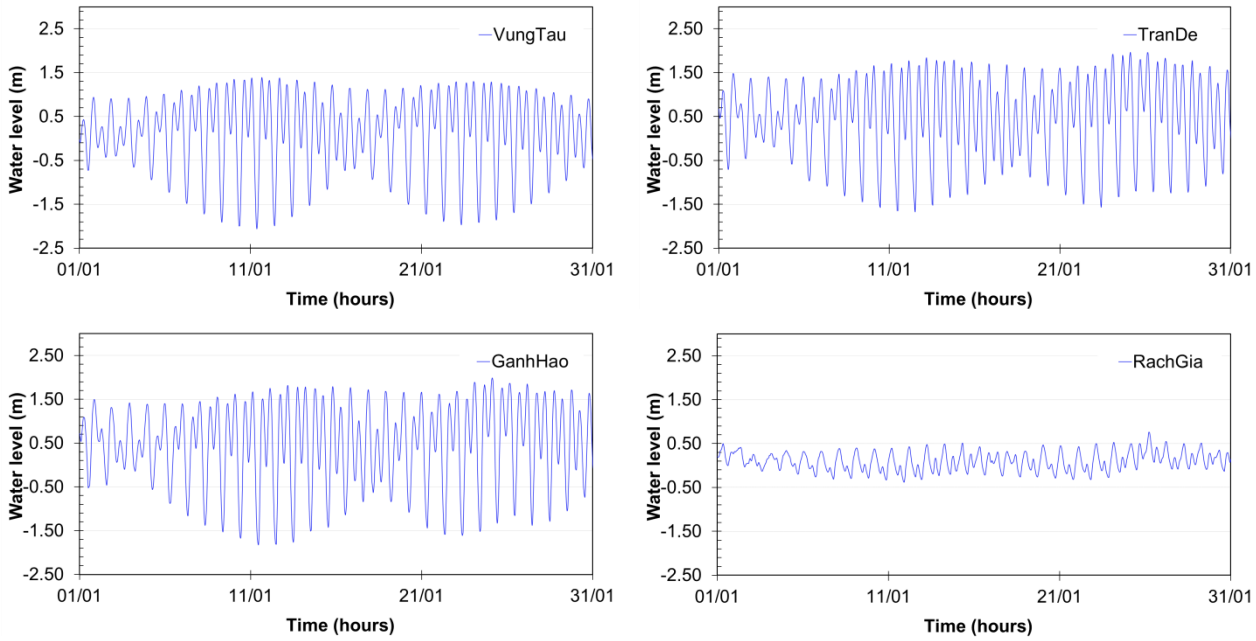

Figure 6.1 The water level along the East sea to Southwest sea of VMD

Tide in the Southwest sea tide belongs to the mixed tide, favors the diurnal tide, and changes in a complicated manner. Although there are two peaks and two troughs during the day, large fluctuations completely dominate, so it has a form similar to a diurnal tide. The tidal shape here is almost opposite to that of the east coast tide: the difference between the two tidal peaks is very large; the difference between the two tides is small. The difference between spring tide and neap tide is the peak tide in the spring tide period is much larger than in the leg tide period while the difference in the peak tide in the high tide period is very large, but it is not significant in the low tide period. During the year, the highest water level drops in the months of March and June and reaches the highest in the months of October and November, with a difference of about 0.2 - 0.25 m. The lowest water level appears in May and June. The tidal amplitude is small, the maximum is only 1.1 ± 0.1 m. This is also the reason why the influence of the West Sea tide on the Mekong Delta is smaller than that of the East Sea tide in general and the VMD in particular. During the month, the maximum water level rises on full moon or new moon day. The lowest water level has no discernible period because of the small two-trough envelope oscillations. The average water level also does not have a clear cycle in the month.

Tide change in the Delta: The tidal influence in the dry season is stronger than that in the flood season. In the dry season, the tide can affect Phnom Penh with tidal amplitude of about 0.5m. The flow tide rises upstream and passes over Tan Chau and Chau Doc. In the flood season, when the flood is high, the affected area is only within the Delta. The East Sea tidal amplitude is very strong due to the large amplitude semi-diurnal tidal regime, so the East Sea currents have a great impact on the estuary and surrounding areas, especially pushing the flow towards the Tien and Hau rivers, not only supplying water to these areas but also increasing salinity intrusion in MK estuaries.

6.1.2 Water level change along Hau Rivers

In the upper part of the Hau rivers, at Chau Doc, seasonal fluctuations in fluvial water discharge cause a change in water level of about 3.06 m (Figure 6.2). Tide-induced water-level changes are significant during the dry season when the spring tidal range is approximately 1.5 m, but they are only a few centimeters to decimeters during the wet season. In the central part of the delta, at Can Tho, tide-induced water-level changes are significant throughout the entire year with the spring tidal range approximately 1.66 m during the wet season and 2.4 m during the dry season (Figure 6.2). The maximum water level at CanTho in the wet and dry season is 2.12m and 1.6m. Near the open coast, at Dinh An, water-level changes are primarily controlled by marine processes, and river-induced, seasonal water-level changes are not as important. The spring tidal range at these stations is almost 3.46 m, and the highest water level occurs in September – October and is driven by the onset of the winter monsoon rather than by high river discharge during the wet season (Figure 6.2).

Figure 6.2 shows that the water level along the Hau River in the wet season has an inflection point, where the gradient of water profile changes abruptly between the CanTho and ChauDoc station at around LongXuyen station which is 130 km from the estuary. The water level in the dry season increases gradually toward upstream in the low tide and decreases gradually in the high tide.

The water level gradients allow us to identify two parts within the VMD. The upstream part is characterized by fluvial dominance, river-induced seasonal water-level changes and significant tidal influence only during the dry season while the downstream part is characterized by marine dominance, tide-induced water-level changes throughout the year, and subordinate fluvial influence. The boundary between these two parts, where fluvial and marine processes are nearly equal, is roughly located near Can Tho.

The riverbed elevation along four branches was measured in the wet season in August 2017 by the ADCP equipment in Chapter 3 and Chapter 5. Salinity concentration was also measured by the Pro30 instrument. Salinity concentration at the river mouth reached 12 psu and dropped to 0.5 psu at around 15km from the river mouth. A Salinity threshold of 0.5 psu extended over 50km in the dry season in March 2018 (Figure 6.2). In the severe drought year 2016, the salinity threshold of 2 psu reached CanTho, which is over 80km from the river mouth. Thus, the study area expanded around 80km from the river mouth.

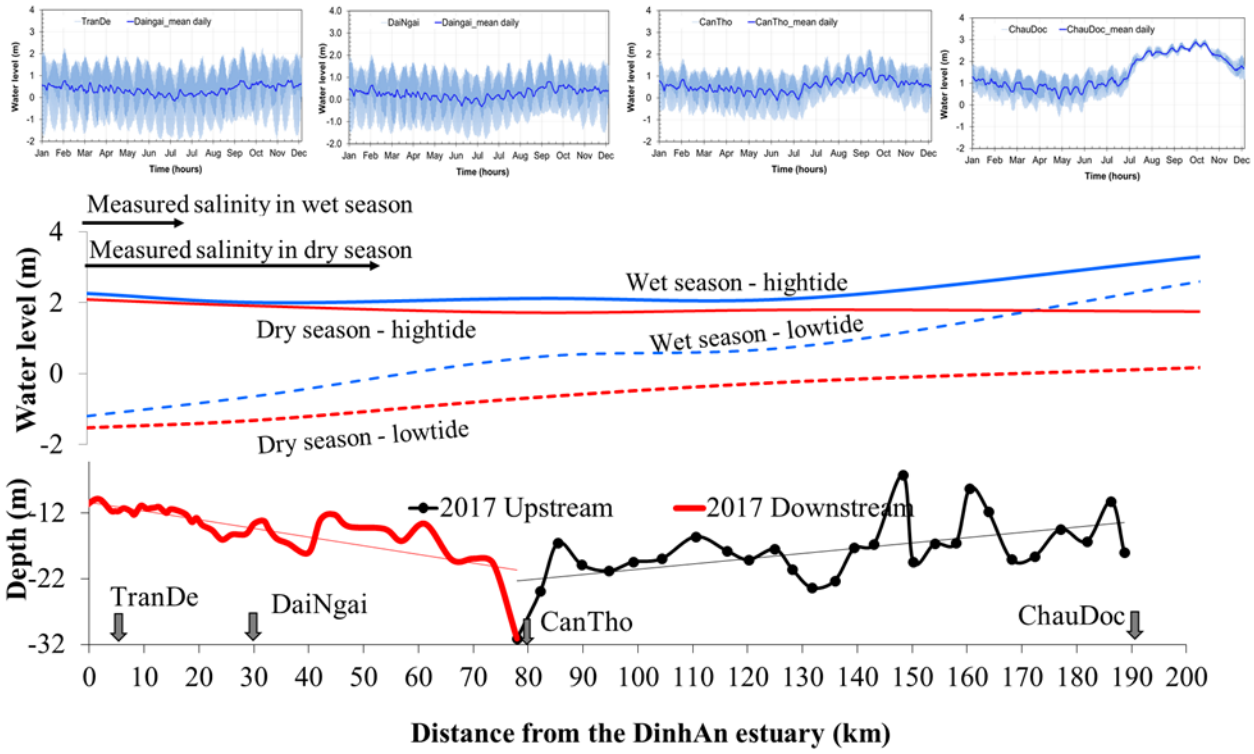

Figure 6.2 Water level changes from January to December 2018 along Hau River

6.2 Impact of Tide on the salinity intrusion

6.2.1 Introduction

Tide is one of the most important factors that strongly affects the mechanism of salinity intrusion. However, the tidal regime entering the river depends on the shape of the estuary, river geomorphology, tidal amplitude, etc. In this chapter, the author concentrates the study on the mechanism of the tides, classification of estuaries, longitudinal – vertical salinity distribution and

mixing –stratification of salinity intrusion in Mekong estuaries. From there, measuring the salinity distribution along the Hau and CoChien rivers together with the measurement of the salinity distribution at the cross-sections to find out the extent of salinity influence during flood – ebb tide in daily tidal cycle as well as the distribution of salinity longitudinally and vertically. Furthermore, this section considers the mechanism of salinity during a monthly tidal cycle (spring – neap tidal cycle) and studies the time lag between the maximum salinity and maximum water level in the daily tidal cycle and in the monthly tidal cycle. Finally, the study analyses the three types of estuary stratification is the mechanism of salt distribution in the two tributaries of Hau and Co Chien Rivers. From there, suitable measures are proposed to collect water or to operate a sluice system to control saltwater along the river and to determine the appropriate timing of fresh water release during the dry season to combat high salinity concentrations during the day.

.*6.2.2 Classification of the estuaries*

The characters and classification of the estuaries are determined by tides, river discharge, waves, density difference, the lateral sediment transport and the climate. Of these drivers, tide and river flows are the two most important in determining estuary shape. However, it is the combination of all these drivers that lead to the wide range of estuary shapes and behaviors, each with a different aquatic environment. Several ways to classify estuaries are described below, according to: a) shape, b) tidal, c) river influence, d) geology and e) salinity.

6.2.2.1 Classification by shape

In estuaries, the following characteristic shapes can be distinguished (by H.H.G. Saveniji, 2012):

- Prismatic: Prismatic: The banks of the estuary are parallel. This is a type of estuary that only exists in a man-made environment where the banks are artificially fixed. Examples are shipping channels that are regularly dredged and where the banks are stabilized. In an estuary where the flood volume is reduced in the upstream direction, the flow velocity amplitude reduces as well so no morphological stability is possible. A constant cross-section can only be maintained through dredging, such as in the Rotterdam Waterway.
- Delta: A near prismatic estuary where the tidal influence is small compared to the amount of river water feeding the delta. Deltas occur in seas with a relatively small tidal range and on rivers with a high sediment load (e.g. the Mississippi, the Nile, and the Mekong).

- Funnel or trumpet shape: The banks converge in the upstream direction. This is the natural shape of an alluvial estuary, where the tidal energy is equally spread along the estuary axis (e.g. the Maputo, the Pungue, and the Schelde).
- Rias, fjords, and sounds: Fjords are the result of glaciers that eroded the underlying rock, after which the valley was submerged by sea level rise. In North America and New Zealand, these fjords are also called sounds. Drowned river valleys (also called by the Portuguese name 'ria') stem from the irregular topography of a watershed drowned by sea level rise, where the feeding rivers carry too little sediment to keep up with the sea level rise. This type of estuary generally has irregular banks with several side channels and embayments.
- Bays: These are semi-enclosed bodies that do not have a significant input from a river. The distinction between a bay and a drowned valley is often not easy to make.
- A good description of several of these estuaries is provided by (Dyer, 1997, pp.7-12).

6.2.2.2 Classification by tide range

Table 6.1 Estuaries Classification based on tidal range

Name	Tidal range (m)	Characteristic	Example
Micro-tidal esruaries	<2	Mostly highly stratified during high flows	Tampa Bay, Apalachicola Bay, Mississippi (USA), Limfjord, Isefjord (Denmark)
Meso-tidal esruaries	2 to 4	Mostly mixed to partially mixed	Mae Klong (Thailand), **Mekong (Vietnam)**, Lalang (Indonesia), Columbia (USA)
Macro-tidal esruaries	4 to 6	Generally well mixed	Thames, Mersey, Tees (UK), Scheldt (Netherlands), Delaware (USA), Pungue (Mozambique)
Hyper-tidal esruaries	>6	Generally well mixed	Seine, Somme (France), Severn (UK), Bay of Fundy (Canada)

Davies (1964) proposed four types of estuaries, including micro-tidal, meso-tidal, macro-tidal, and hyper-tidal estuaries on the basis of their tidal range. Davies assumed that tidal range is a good indicator for the amount of tidal energy dissipated in the estuary, which is responsible for the erosive power of the tide and hence the shape of the estuary. Hayes (1975), who followed the

classification proposed by Davies (1964), suggested the estuaries classification bases on the tidal range which shows in the table 6.1.

6.2.2.3 Classification by tidal influence: following the definition by Langbein (1963)

- **Ideal estuary**: An estuary where, as the tidal wave travels upstream, the amount of energy per unit width lost by friction is exactly equal to the amount of energy gained by the convergence of the banks. In an ideal estuary, the tidal range is constant along the estuary axis.
- **Amplified estuary**: An estuary where the tidal range increases in upstream direction because convergence is stronger than friction. Clearly this process cannot continue indefinitely, implying that at some point along the estuary the friction should become more pronounced, leading to a reduction of tidal amplification and subsequently to tidal damping. The process of damping is enhanced by the river discharge, which increases the friction.
- **Damped estuary**: An estuary where friction outweighs bank convergence. Tidal damping occurs in estuaries with a small convergence length or in drowned river values with a narrow opening.

6.2.2.4 Classification by Geomorphology

Fairbridge (1980) proposed estuary classification in seven types (Table 6.2). This is similar to the classification by Dyer (1997) based on topography and by Savenije (2012) based on geology.

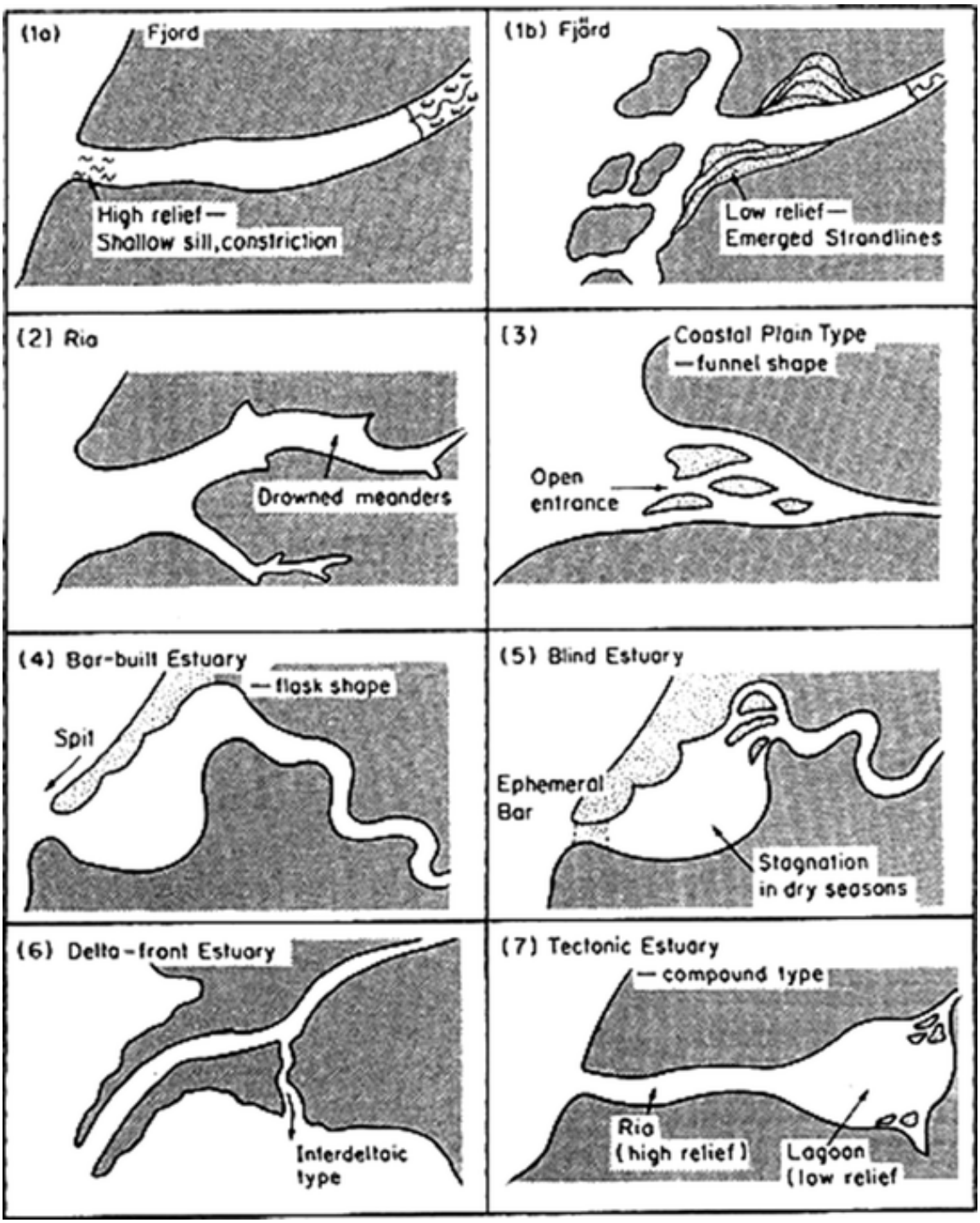

Figure 6.3 The seven types of estuaries base on geomorphology classification (source by Fairbridge, 1980)

Table 6.2 Estuaries Classification base on geomorphology

Type	Name	Remarks	Example
1	1a. Fjord	Low relief – Emerged strandline	Sogne Fjord (Norway), Milford Sound (New Zealand)
	1b. Fjard	Low relief – Emerged strandlines	Solway Firth (England/Scotland)
2	Ria	Drowned meanders in the estuary middle sections	Kingsbridge estuary (UK), Ria de Ribadeo (Portugal), Swan river (Australia)
3	Coastal Plain type – funnel shape	Sea dominant estuary	Chesapeake Bay (USA), Scheldt (Netherlands), Pungue (Mozambique)
4	Bar-built estuary – flask shap	Split bar along coastal lin	Vellar estuary (India), Roanoke river (USA)
5	Blind estuar	Ephemeral bar at inlet. Stagnation in dry season	Balcombe Creek (Australia), Thuan An Inlet (Vietnam)
6	Delta-front estuary	River dominated estuary	**Mekong (Vietnam)**, Nile (Egypt), Mississippi (USA)
7	Tectonic estuary – compound type	Ria (high relief) type at the inlet, Lagoon (low relief) type landward	San Francisco Bay (USA)

6.2.2.5 Classification by river influence (Savenije, 2012)

It can distinguish two extreme cases, the riverine and the marine estuaries:

- Riverine estuary: This estuary is dominated by the riverine flow, both its discharge and sediment supply. The water is fresh and it behaves like a river: parallel banks, regular bank overtopping if they are not protected by dikes, a sandy bottom and sandy banks. The tide propagates as a progressive wave.
- Marine estuary: This estuary is dominated by the sea. The water is completely saline. There is no significant fresh water and sediment input from the landward side. The banks are often muddy. The ecosystem is primarily marine. The tide propagates as a standing wave.

6.2.2.6 Classification by estuarine stratification

Pritchard (1955), Cameron and Pritchard (1963), and later Dyer (1973, 1997) classified estuaries by their stratification and the characteristics of their salinity distributions. This probably is the most common classification for estuaries due to its physical appeal. The advantages of this classification type are show how the circulation of water in the estuaries is maintained and to get quantified, which should enhance and assist in prediction. Four main estuarine types are defined:

(i) highly stratified or salt wedge estuaries; (ii) fjords; (iii) partially mixed estuaries; and (iv) well-mixed estuaries (Table 6.3). Two points should be emphasized that: (i) a given estuary can be well mixed during the dry period but be partially mixed during high discharge periods; and (ii) a given estuary can consist of several classes, for example it can be well mixed in the lower part and partially mixed in the upper part.

Table 6.3 Classification by estuarine stratification

Name	Characteristic	Example
Highly stratified or salt wedge estuaries	Two layers: Upper fresh layer and lower saline layer	Mississippi and Vellar estuary (USA), **Mekong (Vietnam – in flood season)**
Fjords	Two layers: Fresh upperintermediate layer and saline deep lower layer	Silver Bay (USA), Alberni inlet (British Columbia
Partially mixed estuaries	Horizontal and vertical gradually varying density	Rotterdam Waterway (Netherlands), Columbia (USA), Mersey (UK
Well-mixed estuaries	Vertical constant densit	**Mekong (Vietnam – in dry season)**, Scheldt (Netherlands), Pungue, Incomati, Limpopo (Mozambique), Elbe (Germany)

Following the Saveniji 2012, the salinity intrusion mechanism is generally divided into three types:

a) The stratified type, or the saline wedge type,

b) The partially mixed type,

c) The well-mixed type.

These classifications of estuaries show that tide and river discharge are the two dominant drivers for an estuary. Estuary stratification is caused by the density difference between seawater and fresh river water. Kinetic energy supplied by tidal flow reduces the stratification and potential energy supplied by the river discharge enhances stratification. Besides the qualitative classification of estuaries based on their stratification, a number of authors quantitatively classified estuaries on stratification by means of dimensionless numbers, such as Pritchard number n (1955), Simmons number α (1955) and internal estuarine number E_r and Richardson number $R_{iE.}$ All formulas have been used by the book "**Guideline on the study of seawater intrusion into rivers (1991) and** Mikhailova (2013).

Stratification parameter n (Pritchard's number) is used for such classification and is calculated as:

$$n = \frac{\Delta S}{S_m} = \frac{S_{bot} - S_{surf}}{0.5(S_{bot} + S_{surf})} \qquad (1)$$

where ΔS is difference of salinity between bottom and surface, S_m is averaged water salinity, S_{bot} and S_{surf} is water salinity at the bottom and on the surface, respectively.

The second parameter is Simmon's number, which is the flood tidal parameter as the ratio of the volume of river water coming down the river mouth during a tidal cycle per the flood volume and calculated by:

$$\alpha = \frac{W}{P_t} = \frac{Q_f.T}{P_t} = \pi \frac{u_f}{\upsilon} \qquad (2)$$

According to Savenije (1992a): $P_t = E.A$ and $E = \upsilon.T/\pi$ and hence $\alpha = \pi.u_f/\upsilon$

Where: W (L^3) is the volume of water runoff over the tidal cycle, Q_f is the river flow during the tidal period T (the duration of tidal cycle). P_t (L^3) is the volume of tidal prism (is the volume of seawater entering into the river mouth during the flood tide = $\Delta H_{tide}.F_m$ with ΔH_{tide}: mean tidal range within the mouth object, whose area is F_m). u_f (LT^{-1}) is the river flow velocity, υ (LT^{-1}) is the tidal amplitude or is root mean square of the tidal velocity averaged over cross-section and E (L) is the tidal excursion, which is the distance that a water particle travels between slacks.

We can use international: E_ρ number was introduced by M. L. Thatcher and D. R.F. Harleman (1972):

$$E_\rho = \frac{P_t.F_r^2}{Q_f T} = \frac{F_r^2}{\alpha} \qquad (3)$$

The fourth parameter is Richardson's number Ri_E which is computed as (Fischer, 1979):

$$Ri_E = \frac{\Delta\rho}{\rho}\frac{gQ_f}{B\upsilon^3} = \frac{\Delta\rho}{\rho}\frac{gh_o u_f}{\upsilon^3} = \frac{\alpha}{\pi F_r{}^2} \qquad (4)$$

where, B (L) is the estuarine channel width, Δ_ρ (MT^{-3}) is the density difference between sea ρ_s (MT^{-3}) and river ρ (MT^{-3}), h_o (L) is flow depth at the estuary mouth. g (LT^{-2}) is the acceleration due to gravity and F_D (-) is the estuarine densimetric Froude number

$$F_r = \frac{\upsilon}{\sqrt{\frac{\Delta\rho}{\rho}.g.h_o}} \qquad (5)$$

The ranges of n, α, E_ρ and Ri_E show in Table 6.4 gives a comparison on these three stratification parameters.

Table 6.4 Quantitative criteria of different types of salinity stratification

Type of Seawater intrusion	Character of vertical mixing	Character of stratification	Pritchard n	Simmon α	Richardson Ri_E
I	Well mixing	Weak	0 ÷ 0.1	0 ÷ 0.1	< 0.08
II	Partial mixing	Moderate	0.1 ÷ 1.0	0.1 ÷ 1.0	0.08 ÷ 0.8
III	Weak mixing	Salt Wedge	> 1.0	> 1.0	> 0.8

6.2.3 Tidal dynamic

Tides are the rise and fall of sea levels caused by the combined effects of the gravitational forces exerted by the Moon and the Sun and the rotation of the Earth (Dronkers, 2005). Tides are generally classified into four types based on the lunar and solar harmonic components: semidiurnal (e.g., in Vlissingen, the Netherlands; or Immingham, UK); mixed, predominantly semidiurnal (e.g., in Soc Trang, Vietnam; or San Francisco, USA); mixed, predominantly diurnal (e.g., in Manila, Philippines; or Bangkok, Thailand); and diurnal (e.g., in Do Son, Vietnam). As the sun, the earth, and the moon move along their elliptical orbits, they continually change their positions relative to each other. As a result, the total potential height of the astronomical tide changes as a function of geographic location and over time. The most prominent tidal period is the fortnightly spring–neap cycle (a two-week cycle). Due to the 28-day orbital motion of the moon, the moon-earth and sun-earth axes approximately coincide every fortnight. Thus, spring tides occur shortly after the full moon and new moon, whereas neap tides occur at half-moon. There is about a seven-day interval between springs and neaps. The vertical rise and fall of the water surface are generally referred to as the tide, and the accompanying horizontal movement is referred to as the tidal current, with the tidal flow into an estuary called the flood and the outflow of an estuary called the ebb. When a tidal wave reaches the shallower water of an estuary, it is slowed down, amplified, and distorted due to the interaction with the estuarine topography, river discharge, and friction.

There are three types of tidal wave propagating into an estuary: progressive wave, standing wave, and mixed wave.

Progressive wave: The crest and the trough of the wave moves progressively inland. The maximum flood current occurs at the same time as the crest and the maximum ebb current is at the

same time as the trough (Figure 6.4). The phase lag between High Water (HW) and High-Water Slack (HWS) as well as between Low-Water (LW) and Low-Water Slack (LWS) is π/2. The wave celerity is$\sqrt{gh}$. The purely progressive wave only occurs in a frictionless channel with constant cross section and infinite length, which is not the case for real estuaries.

Standing wave: This type of wave usually occurs in a semi-enclosed body (e.g. a bay or a river with a weir). The tidal wave is reflected at the head of the semi-enclosed body and travels back down the waterway toward the ocean. The crest and trough seem to progress at infinite speeds, whereby high water and low water occur instantaneously, with the greatest tidal range at the head of the semi-enclosed body. The tidal range decreases from the head toward the ocean, and, if the body is long enough, reaches a minimum at one location (called a node – at one-fourth of a tidal wavelength from the head) and then starts increasing again to a new maximum (called an antinode). The phase lag between HW-HWS and LW-LWS is zero. The wave celerity is infinitely large (Nguyen, 2008) (Figure 6.4).

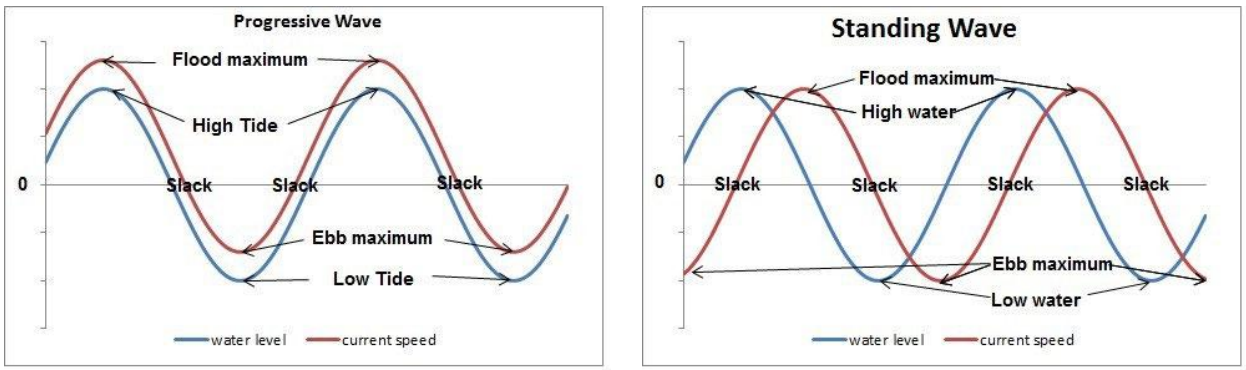

Figure 6.4 Tidal currents in the open ocean and coastal regions (sources from: Marine Science of Australia)

Mixed wave: This type of wave occurs in an alluvial coastal plain estuary, which has a channel with non-constant cross section (e.g. gradually exponential shape). The longitudinal tidal range pattern depends on the relative relation between convergence and friction; therefore, it appears in one of the three forms mentioned above. The phase lag is between 0 and π/2. The wave celerity differs from the progressive wave celerity, depending on the damping or amplifying characteristics. Tidal dynamics in estuaries can be investigated and analyzed numerically or analytically. Equations 3.1 and 3.2 are the Saint-Venant's equations and continuity equation, which can be used to determine the hydrodynamic regimes of estuaries.

6.2.4 Impact of tidal dynamic on the vertical and longitudinal salinity distribution

6.2.4.1 Observations on March 2nd, 2018 in the TranDe branch

a. Longitudinal salinity distribution in TranDe branch

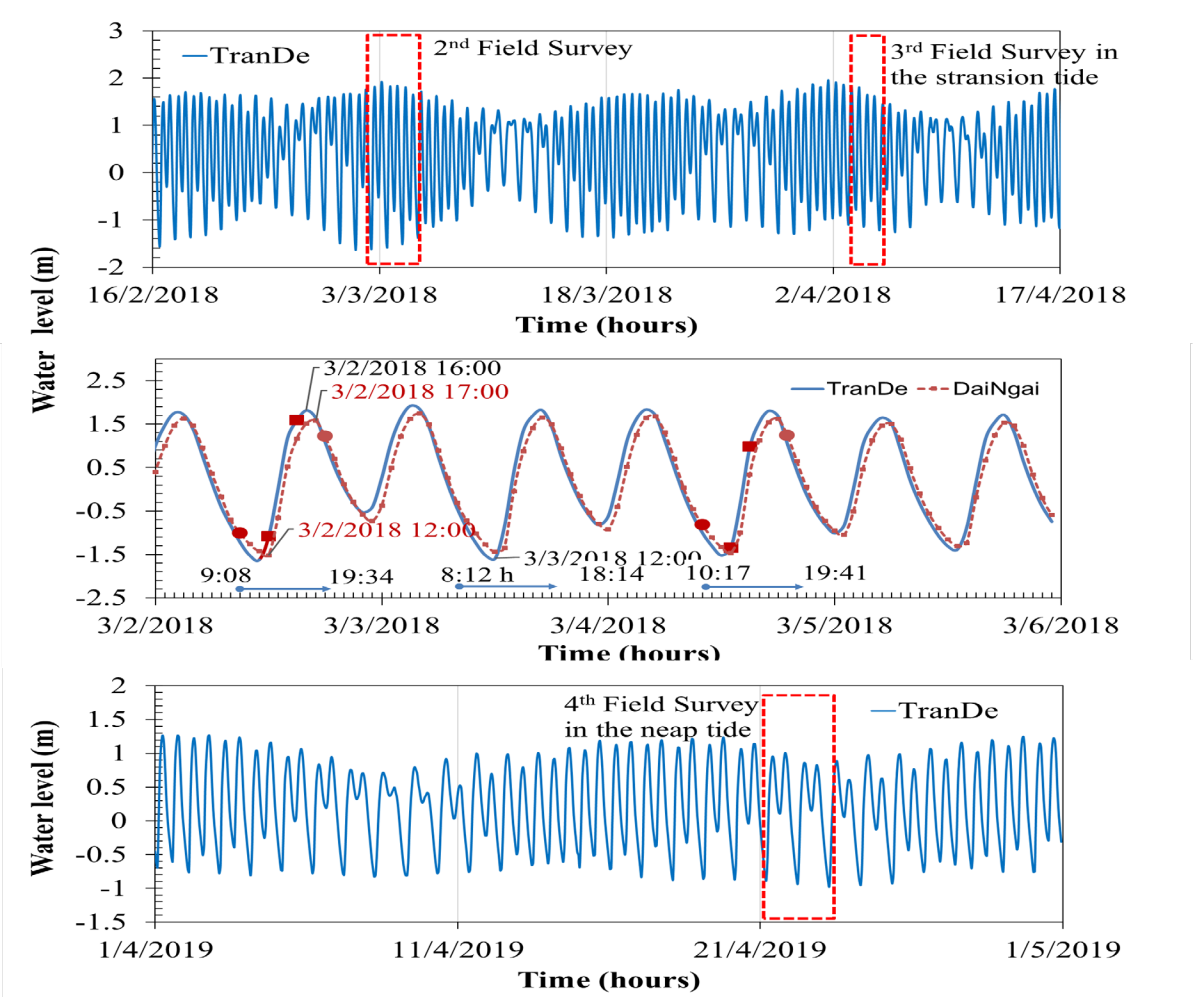

Figure 6.5 The water level at three observation stations during the field survey, salinity measurement time (inside the red rectangular) and positions for cross-section measurement (circle: up station, rectangular: low station)

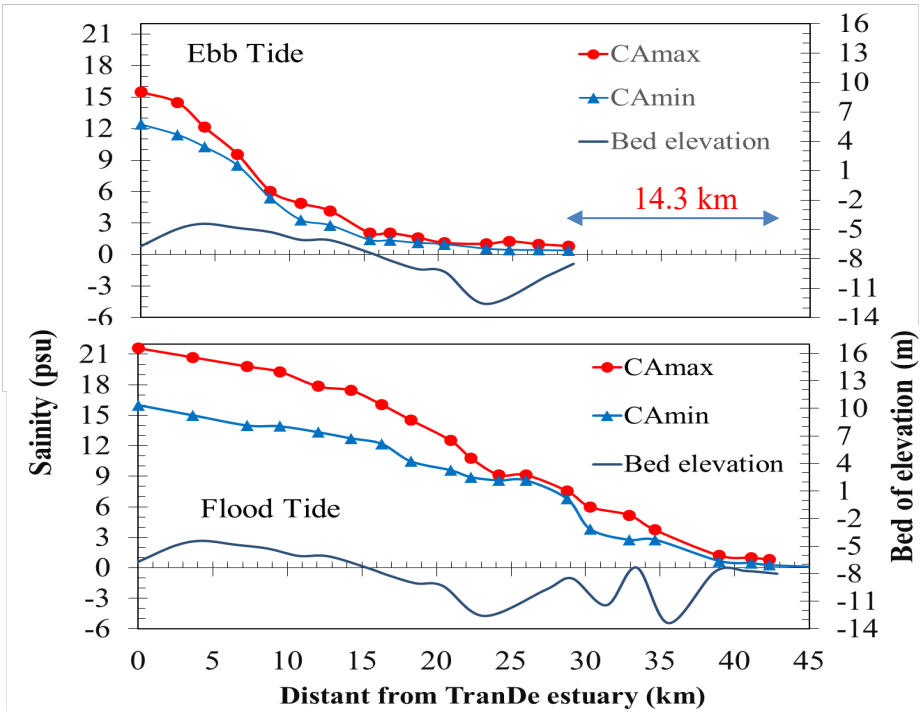

Figure 6.6 Longitudinal distribution of salinity in the TranDe branch on March 2nd, 2018

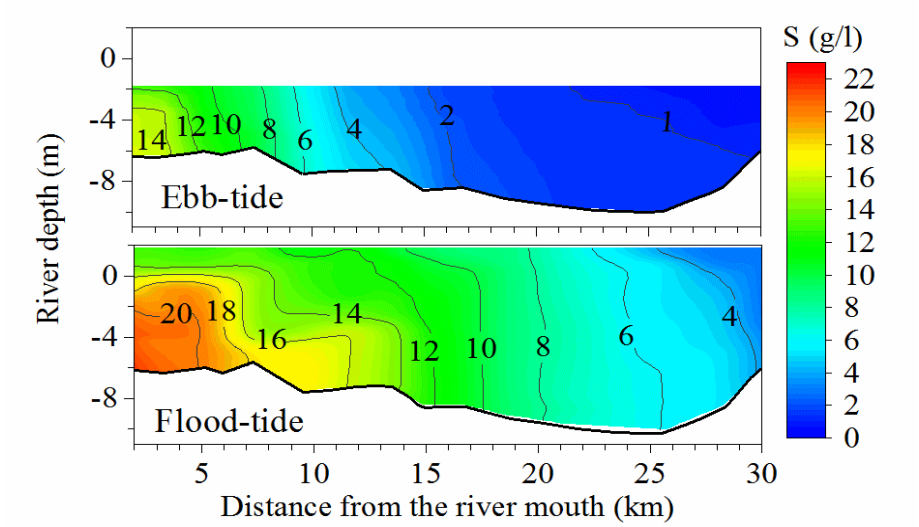

Figure 6.7 Vertical and longitudinal distribution of salinity in the TranDe branch on March 2nd, 2018 in ebb - flood tide

After setting the instruments at the DaiNgai station, which is about 28km from the river mouth, the survey on March 2nd began at 9:08 toward ebb tide down to the river mouth (0 km point) at 13:53 (Figure 6.5). As shown in Figure 6.6, maximum salinity concentration (S_{max}) increased gradually from 0.83 psu to 15.49 psu in the ebb tide, and S_{max} was recorded at the bottom of the

river by CastAway-CTD equipment (CA_{max}). S_{min} was recorded at the surface (CA_{min}) and increased from 0.4 psu to 12.42 psu. Then the boat returned toward flood tide from 16:23 to 19:34 heading upstream from the 0km point to the 42.3km point. S_{max} reduced from 21.5 psu to 0.8 psu.

During the flood and ebb tides, salinity concentration from the river mouth to the 20km point were 8.2 psu to 2.5 psu respectively (Figure 6.7) with the Pritchard number (n) always lower than 1, indicating that partial mixing and moderate stratification prevailed over the TranDe branch. Although salinity at the bottom was usually more than that at the surface, partial mixing of river and seawater was usually observed. Saltwater at the bottom decreased in an upstream direction usually more rapidly than at the surface. Furthermore, the intrusion length of 42.3km at flood tide was 14.3km longer than that at ebb tide.

b. The vertical salinity distribution at cross-sections

The measurements at cross-section 1 (5km far from the river mouth, Figure 3.3) in the Tran De branch were conducted from 11:42 to 12:15 (in the ebb tide) and from 15:34 to 16:03 (in the flood tide).

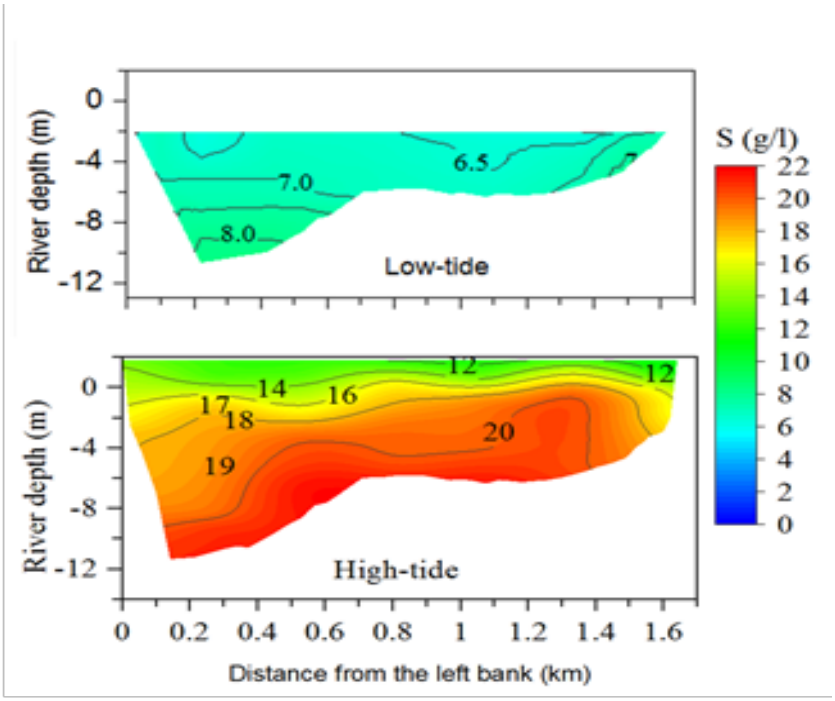

Figure 6.8 Vertical salinity distribution at cross-section 1 at ebb and flood tides in the TranDe branch

During the ebb tide when the river discharge pushes saltwater into the sea, salinity is low. Maximum salinity (S_{max}) was 8.5 psu at the river bottom. In contrast, during high tide saltwater

intruded into the river, and the salinity concentration reached the highest value of 20.7 psu over the river bed. At a cross-section, salinity concentration is distributed unevenly in the vertical and the river width. Vertically, salinity concentration in the surface was 6.2 psu, 11.5 psu and at the bottom is 8.5 psu, 20.7 psu during the ebb-flood tide respectively. S_{max} appeared at the deepest point which was higher than S_{max} on the surface by about 2.3g/l and 8.2g/l at the ebb and flood tides, respectively. Horizontally, at the same water depth, salinity concentration in the ebb tide was small with difference value lower than 1 psu. However, at the same water depth near the water surface in the flood tide, the salinity value on the left bank (towards the sea) was higher than that on the right bank. On the other hand, the salinity value at the bottom on the right bank increased faster than that on the left bank, indicating that the tidal current on the right bank was higher than that on the left bank.

6.2.4.2 Observations on March 4nd, 2018, in the DinhAn branch

a. Longitudinal salinity distribution in DinhAn branch

Figure 6.9 shows longitudinal salinity distribution in the DinhAn branch, conducted from 10:49 at the 30km point at the CauQuan station toward ebb tide, heading downstream. During ebb tide, salinity concentration at the bottom increases from 0.43 psu at the 30km point to 8.92 psu at the 0km point. The boat then returned to the upstream during flood tide from 15:24, two hours before the flood tide reached its peak. Therefore, salinity concentration values at the bottom are not so high and regularly reduce from 20.2 psu at the 0km point to 0.4 psu at the 45km point. The reduction gradient (slope) depends on the riverbed slope. Figure 6.9 also shows that the intrusion length at flood tide is 15km longer than that at ebb tide. Vertical and longitudinal distribution of salinity along the DinhAn branch in Figure 6.10 verifies that partial mixing and moderate stratification prevail over the DinhAn branch with the Pritchard number ranging from 0.1 to 0.7, belonging to type 2 (Table 6.1). Furthermore, a much different salinity concentration between the surface and bottom occurs at the estuary in the flood tide while that appears in between the 10km and 25km points in the ebb tide.

Figures 6.7 and 6.8 show that the salinity concentration collected in the TranDe branch is higher than those in the DinhAn branch. However, this finding might not be completely correct because of the difference of the dates and the time measurement in the two branches. Direct comparison between the two branches may lead to uncertainty in measurements. In fact, the salinity values in the DinhAn branch at the CauQuan station are usually higher than those at the DaiNgai station in

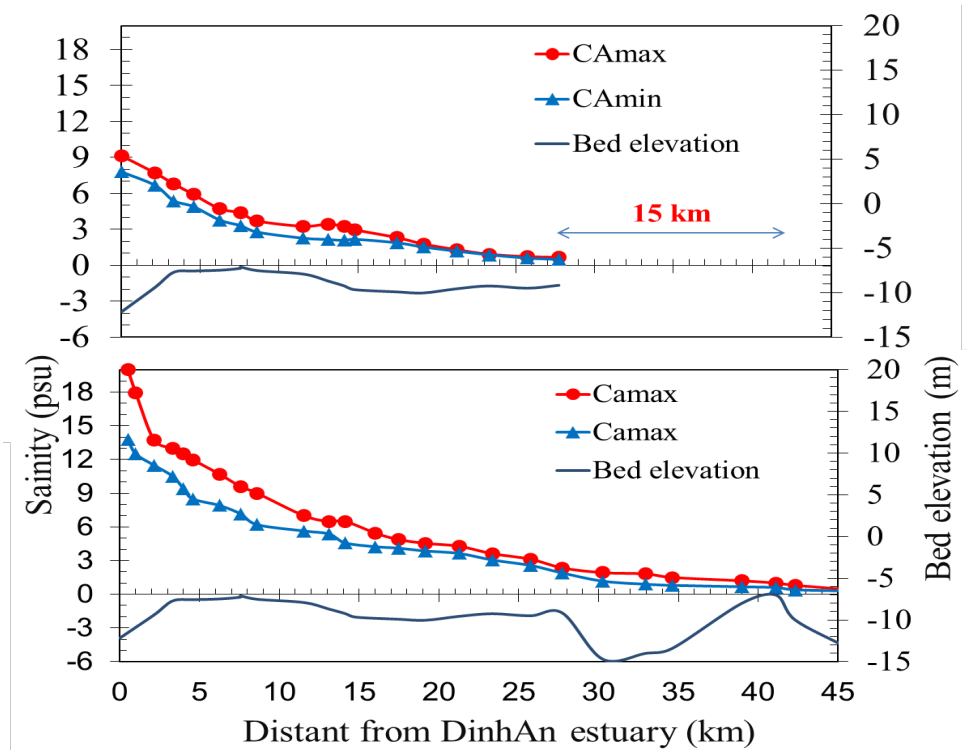

Figure 6.9 Vertical and longitudinal distribution of saltwater in the DinhAn on March 4th, 2018 in ebb - flood tide.

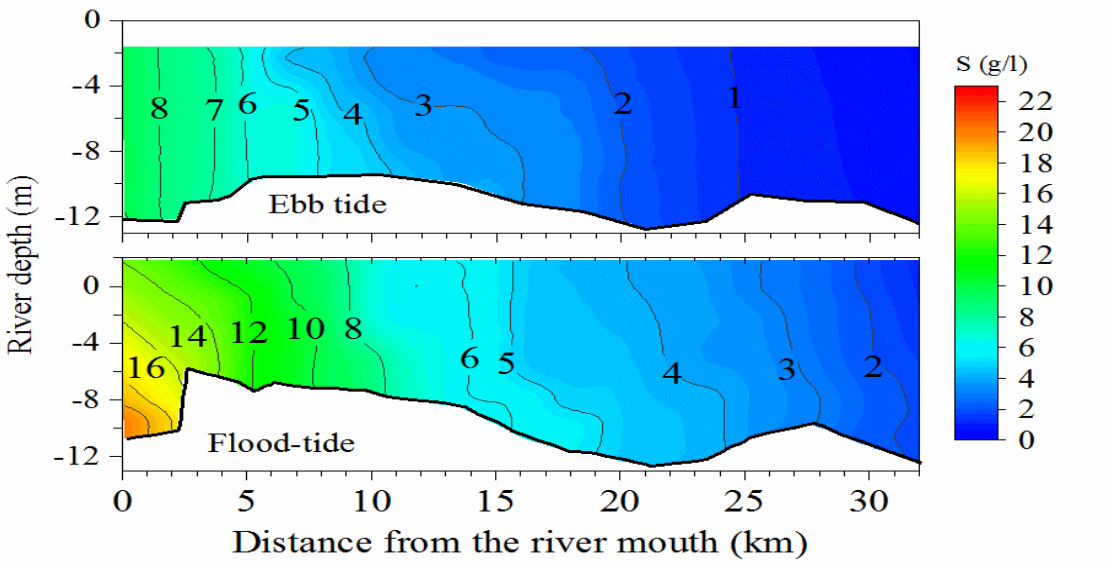

Figure 6.10 Vertical and longitudinal distribution of saltwater in the DinhAn on March 4th, 2018 in ebb - flood tide.

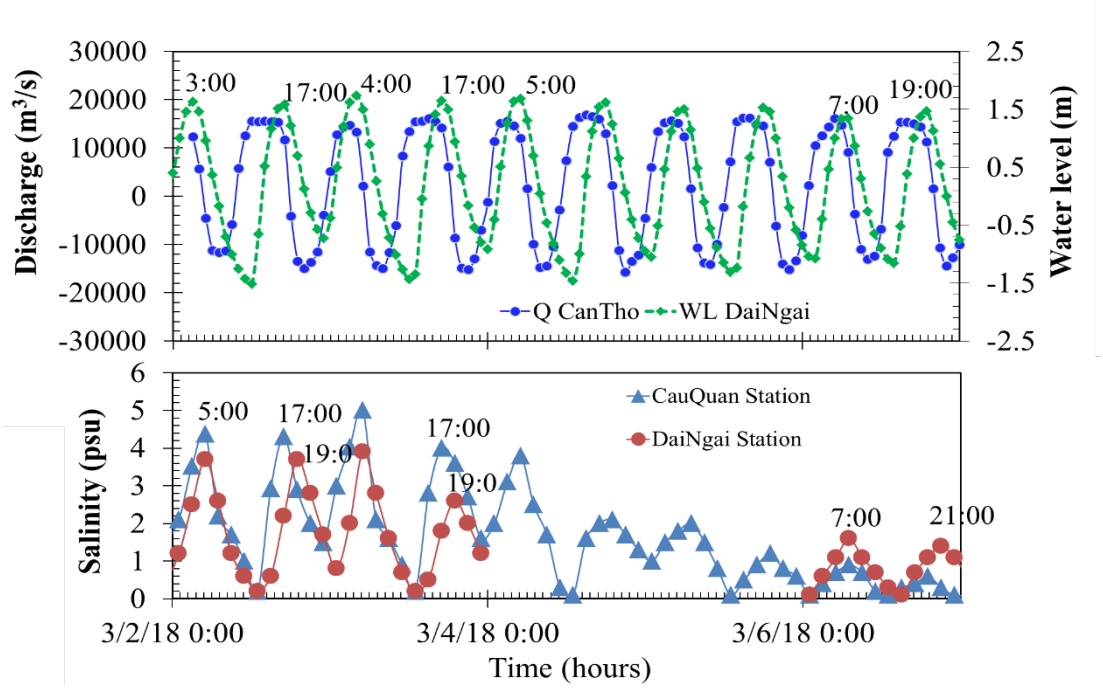

Figure 6.11 Salinity concentrations at the DaiNgai and CauQuan stations, water levels at the DaiNgai station, and discharges at the CanTho station

the TranDe branch (Figure 6.11) but they noted that the distances of the CauQuan and DaiNgai stations from the river mouths are relatively similar. Salinity values at CauQuan and DaiNgai are controlled by the sea water level and river discharge at the CanTho station and sometimes the peak of daily maximum salinity concentration (S_{max}^{d}) at CauQuan appears sooner than that at DaiNgai. That means the speed of tidal propagation in the DinhAn branch is faster than that in the TranDe branch. The peak of S_{max}^{d} at DaiNgai lags two hours after the daily maximum water level (WL_{max}^{d}).

b. The vertical salinity distribution at cross-sections in DinhAn branch

The measurements at cross-section 2 (Figure 3.3) (5km from the DinhAn mouth) were conducted from 14:07 to 14:37 (at the low tide) and from 16:00 to 16:32 (at high tide). Figure 6.12 shows that the right bank is deeper than the left bank. Therefore, S_{max} occurs at the bottom of the right bank. While at the surface the salinity value in the left bank is lower than that in the right, which means the river discharge flows are the surface flow on the left side while the tidal flow is the bottom flow on the right side. The difference of salinity concentrations between the surface and bottom is 3.3 psu and 4.58 psu at the ebb and flood tide, respectively.

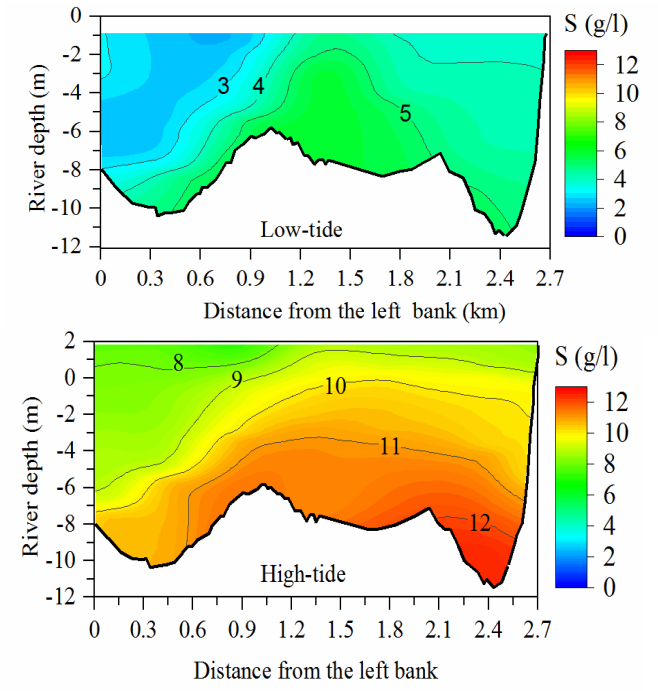

Figure 6.12 Vertical salinity distribution at cross-section 2 at the low and high tides in the DinhAn Branch

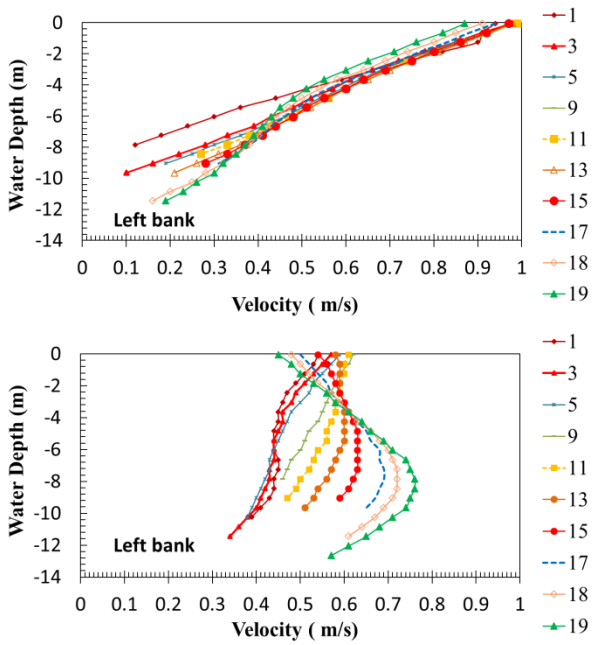

Figure 6.13 a, b: Vertical velocity distribution at low tide and high tide at cross-section 2 in the DinhAn Branch (number 1,3,5, et al is the order of velocity profiles which start from the left bank and distance between each profile is 0.13m)

The vertical salinity distribution is controlled by the value and direction of flow velocity at cross-section 2. Figure 6.13a shows the vertical velocity distribution at low tide. At a cross-section in DinhAn branch, 20 velocity profiles were conducted from the left bank to the right bank. The results indicated that at low tide, the maximum velocity (V_{max} = 1 m/s) is at the surface and minimum velocity is at the bottom with the velocity magnitude being up to 0.1 m/s, which means the low tide velocity shows a decrease from the surface to the bottom. In contrast, at high tide (Figure 6.13b), V_{max} occurs on the right bank and closer to the bottom, which is represented by the triangular green line. This line achieves maximum velocity on the surface during the low tide (Figure 6.12) but reaches maximum velocity near the bottom at profile number 19 during the high tide. This is a typical velocity structure in estuaries (Uncles, 2002) so S_{max} always happens in the bottom and closes to the right bank (Figure 6.12).

6.2.4.3 Observations on Apri 6nd, 2018 in the CoChien branch

After setting the instruments at the LangThe sluice gate, the boat moved to the LangThe canal head which is about 33km from the river mouth. The survey on April 6th began at 7:00 toward ebb tide to the river mouth at 12:30. As shown in Figure 6.14, S_{max} increased gradually from LangThe to the river mouth from 0.4 psu to 17.9 psu in the ebb tide, and S_{max} was recorded at the bottom of the river by CastAway-CTD equipment (CA_{max}). S_{min} was recorded at the surface (CA_{min}) and increased from 0.3 psu to 8.1 psu. Then the boat returned toward flood tide from 15:48 to 19:34 heading upstream from the 0km point to the 51.5 km point to get 0.4 psu. S_{max} reduced from 22.3 psu to 0.4 psu and S_{min} reduced from 8.1 psu to 0.4 psu.

During the ebb and flood tides, salinity concentration between the surface and bottom from the river mouth to the 20km point varied from 3.7 psu to 14.3 psu (Figure 6.14) with the Pritchard number (n) always lower than 1 during the ebb tide, thus partial mixing and moderate stratification prevailed in CoChien river in the ebb tide. But during the flood tide, the value of n was always higher than 1; therefore, weak mixing and strong stratification prevailed in the CoChien branch in the flood tide. However, the mixing and stratification process varied according to the upstream discharge, tidal discharge and flow velocity. Consequently, the type of mixing and stratification is not fixed but changes over time. Furthermore, the intrusion length of 51.5 km in flood tide was 16.5 km longer than that in ebb tide.

6.2.4.4 Spatial temporal salinity distribution in two surveyed cross-sections in the DinhAn branch during 1 tidal cycle (12h25min)

When considering the impact of tides on salinity intrusion, we consider two tidal cycles; ebb-flood tidal cycle in one day and spring-neap tidal cycle in half month. This section discusses salinity intrusion processes during a tidal cycle (12h25min) at two cross-sections. The cross-section 2 is 3km and the cross-section 3 is 22km from the DinhAn estuary (Figure 3.3). At the cross-section 3, vertical and horizontal salinity concentration, discharge and velocity distribution were measured 12 times with a temporal interval of one hour. The cross-section 3 was hourly measured from 9:15 to 21:25 on April 21, 2019. The cross-section 2 was measured from 9:10 to 21:00 on April 22, 2019. Tidal movement from the estuary to the cross-section 2 was approximately 1 hour, and the tide on April 22 came 1 hour later than that on April 21. So, we

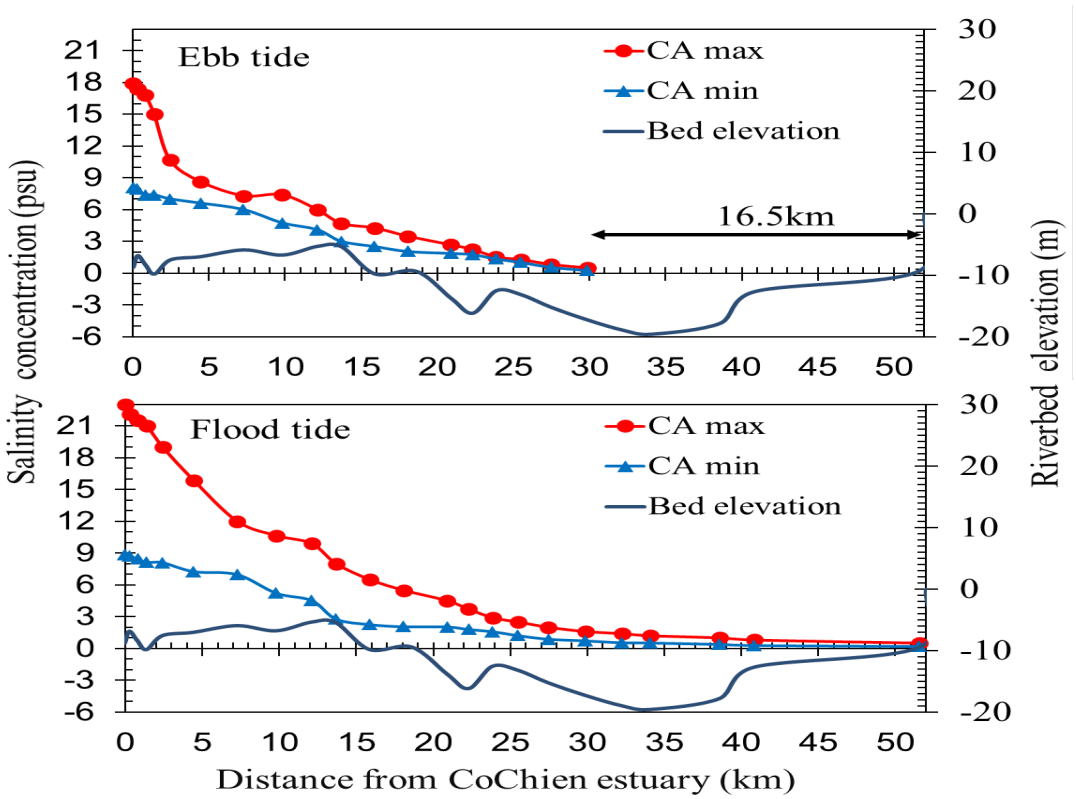

Figure 6.14 Longitudinal distribution of salinity in the CoChien branch on April 6th, 2018

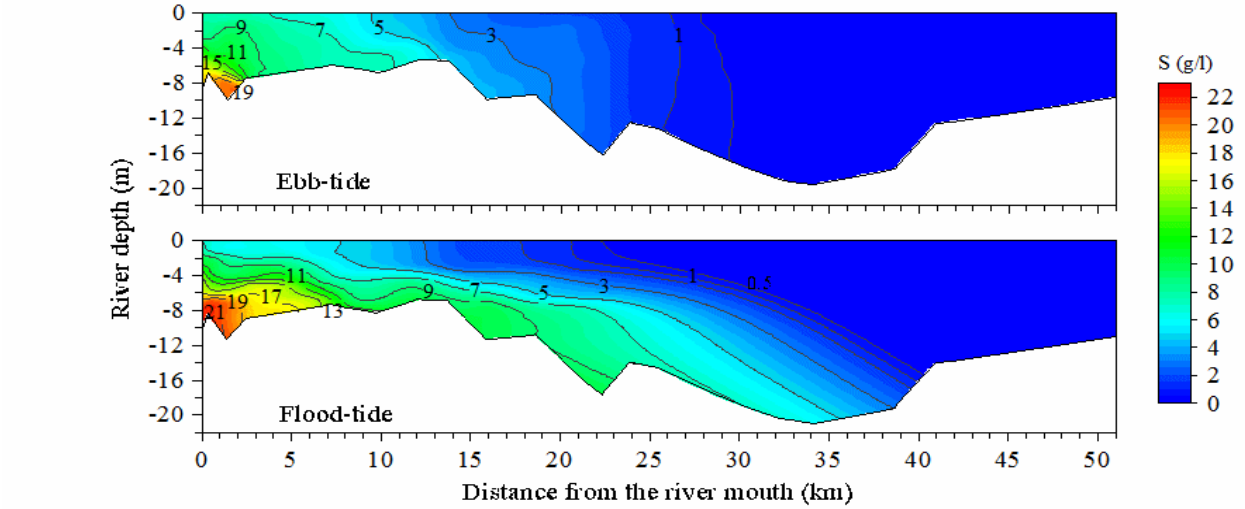

Figure 6.15 Vertical and longitudinal distribution of saltwater in the CoChien on April 6th, 2018 in ebb - flood tide.

started to measure the two cross-sections at the same time around 9:00am. At each cross-section, salinity concentration, discharge and velocity distribution were measured at 8 to 10 vertical profiles; each vertical profile was measured 12 times during 12.25 hours (one tidal cycle) by

CastAway – CTD and GPS-equipped Acoustic Doppler Current Profiler (ADCP). The ADCP was mounted securely on a side boat, being connected to a computer for the in-situ measurement.

At the cross-section 3, Figure 6.16 shows the measurement results every two hours. From 9:15 to 13:00 during the ebb tide, salinity concentration reduced from 0.89 psu to 0.14 psu. The salinity concentration hit its minimum value of 13:00 during the low water level at -0.97m (Figure 6.16). Then the water level rose from -0.97m to its maximum level (WL_{max}) of 1.67m at 18:00, leading to salinity concentration increasing from 0.14 psu to 1.69 psu. S_{max} of 1.04 psu on the surface occurred at 18:00 (Figure 6.16) while Figure 6.17 indicates that S_{max} at the bottom of 1.74 psu was at 19:00 and S_{max} at the bottom was observed when velocity changed from flood tide to ebb tide and close to the high tide. That means that S_{max} at the surface coincided with WL_{max} and S_{max} at the bottom lagged one hour after WL_{max} at the location of 22km from the river mouth (cross-section 1) (Figure 6.16 and 6.17).

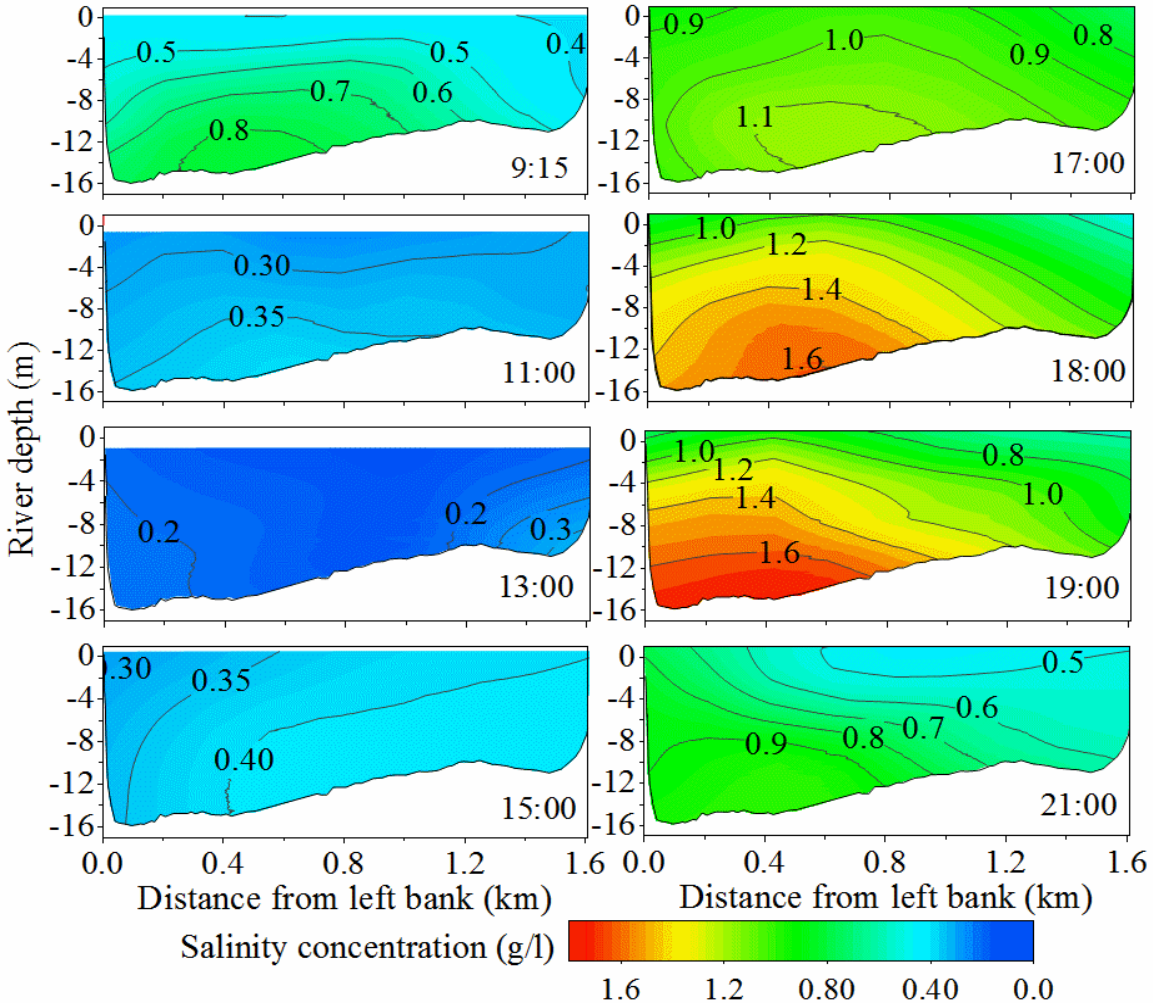

Figure 6.16 The vertical distribution of salinity value at cross-section 3 during one tidal **cycle.**

Figure 6.16 also shows that reduction in the salinity concentration in the left bank was faster than that in the right bank during 9:15-13:00, indicating that the reversal flow velocity (seaward) in the left bank was faster than that in the right bank. On the other hand, the increase in salinity concentration during flood tide from 15:00 to 18:00 in the right bank was faster than that in the left bank as a result of high flow velocity (riverward) in the right bank compared to that in the left bank. Then at 18:00, the flow velocity direction shifted from the middle of the river to the left bank. Thus, the flow ran downstream on the left bank and the S_{max} occurred at the bottom of the left bank.

22km from the estuary there is a sluice gate to control the salinity intrusion. The sill elevation of the gate is -4.5m. Usually in the dry season, which sees high salinity values, the gate is closed. Figure 6.16 reveals that if the local farmer wants to intake water with less than 1 psu concentration, the gate can be opened at least 8 hours during one tidal cycle from 9:00 to 17:00.

At the cross-section 2, the salinity value also depended on the tidal regime, having amplitude of 2.77m at the measurement time. Salinity concentration gradually decreased in the ebb tides and increased in the flood tides. For instance, salinity concentration at the bottom reduced from 12.2 psu to 8.1 psu during low tide (from 9:10 to 12:00) and increased from 8.1psu to 18.3 psu during flood tide (12:00 to 19:00) (Figure 6.19). S_{max} at the bottom appeared at 19:00, two hours later compared to the time of WL_{max} (Figure 6.18). Moreover, S_{max} at the bottom occurred in ebb tide when velocity changed from flood tide to ebb tide and closer to the high water while S_{min} appeared at low water. S_{max} on the surface occurred at the same time with WL_{max} at 17:00 as shown in Figures 6.18 6.19.

The salinity values near the bank and in the middle of the river were quite different. The salinity concentration near the bank was smaller than that in the middle or at the deepest point, and had only a slight change from the surface to the bottom.

On the contrary, when we compare the middle point and the deepest one, the difference in value between the surface and the bottom (ΔS) was high. For instance, at the cross-section 2, ΔS at the deepest point are 7.22 psu and 9.8g psu at the ebb tide and at the flood tide respectively. In practice, salinity measurement stations are located permanently near river banks, thus the data collected cannot represent the entire cross-sections. But we can refer to those data for the operation of the sluice gates located along the river banks.

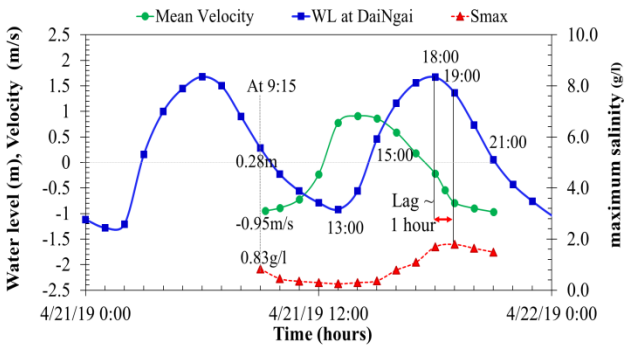

Figure 6.17 The water level and mean velocity at cross-section 3 during 12 hours in 21, April 2019

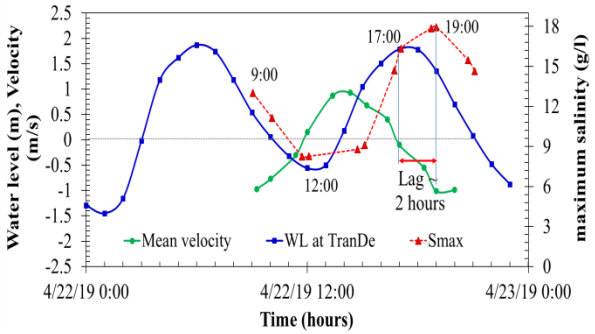

Figure 6.18 The water level and mean velocity at cross-section 2 during 12 hours in 22, April 2019

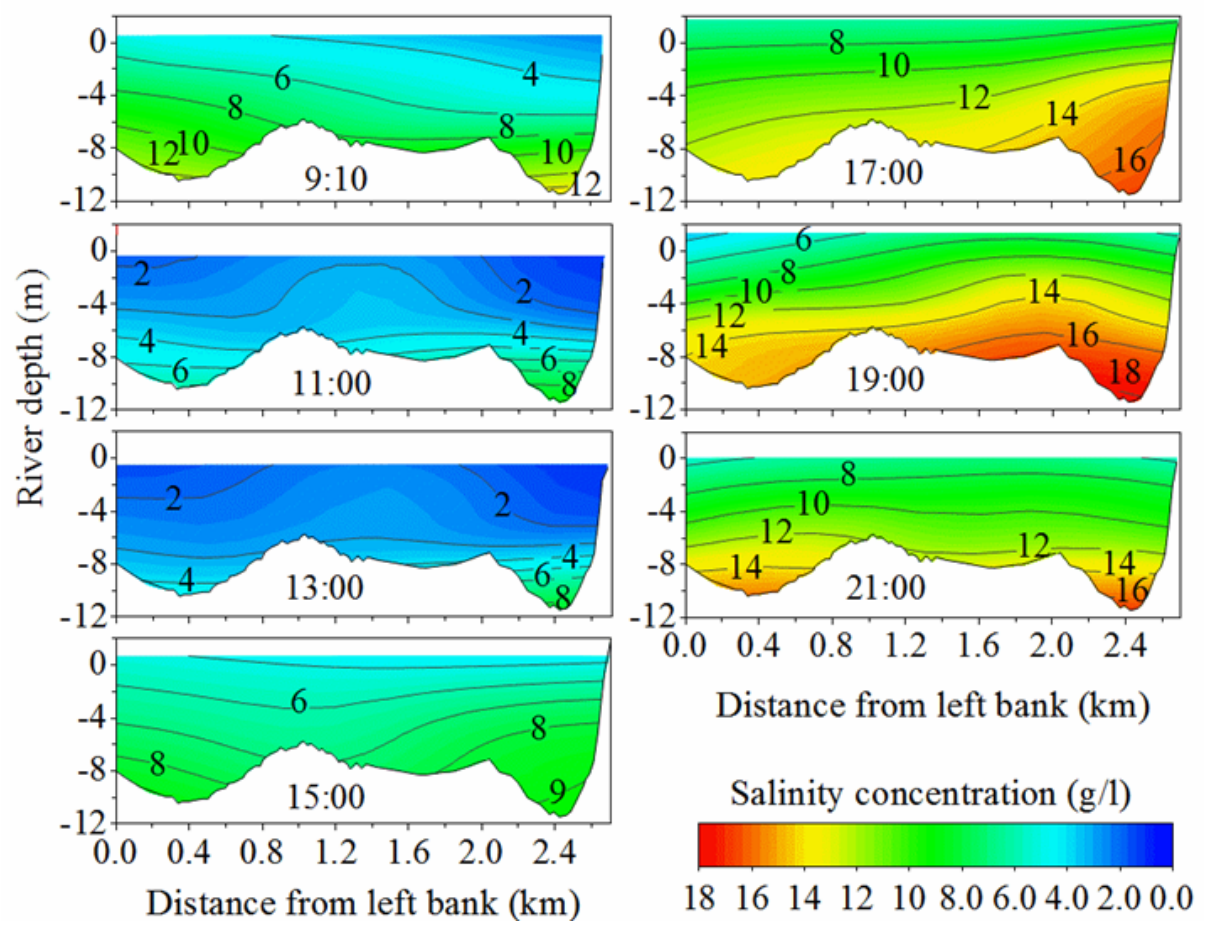

Figure 6.19 The vertical distribution of salinity value at cross-section 2 during one tidal cycle.

A similar observation was revealed by Fischer et al. (1979). Figure 6.17 also indicates that S_{min} occurred when ebb tidal velocity changed from flood tide and closed to low water. The mean velocity during one tidal cycle at the cross-section 3 was used for calculating the stratification

parameters. The processes of saline intrusion are complicated because they are driven by many factors. Among which three main drivers include river discharge, tide and flow velocity which the study analyzed in a half-day tidal cycle. Figure 6.20 represents a schematic that summarizes step-by-step salinity intrusion processes. This figure describes the special features of the dynamics in the river mouth by the relationship between the tide and velocity while illustrating the changing intrusion length during one tidal cycle. Figure 6.20 was drawn from tidal rising time (12:00 at cross-section 2 and 13:00 at cross-section 3) with the lowest water level being -0.97m, tide current of 0.15m/s while the average river flow velocity was 1.1 m/s. At 13:00, salinity concentration on the surface (S_{suf}) and in the bottom (S_{bot}) was 1.5 psu and 8.1 psu at the cross-section 2 and 0.18 psu and 0.21 psu at the cross-section 3, respectively. Then at 15:00, the velocity of saltwater flow was 0.91 m/s was higher than the river flow velocity by 0.63 m/s; so the salinity value increased and the intrusion length intruded deeper in the river. At that time (15:00), S_{suf} and S_{bot} were 4.2 psu and 9 psu, respectively, and at the cross-section 3 they were 0.3 psu and 0.4 psu, respectively. After 2h, salinity concentration and the intrusion length increased slightly. Then 2 hours later, at 17:00, the maximum water level at the mouth of the river was +1.94m while S_{bot} was 16.2 psu and S_{suf} was 7.8 psu. However, the maximum salinity value at the bottom (S_{max_bot}) was 18.1 psu at 19:00 and the value of S_{suf} was 6 psu, meaning that the maximum salinity concentration on the surface (S_{max_suf}) occurs simultaneously with the maximum sea level at that location, while the S_{max_bot} occurred 2 hours earlier than the water level at the cross-section 2. At the cross-section 3, the WL_{max} was recorded at 18:00, but S_{max_bot} appeared at 19:00 after WL_{max} 1 hour. This implies that the S_{max_bot} occurs when the tide has just receded and the water level at the review point is still near the maximum water level because the salinity at the considered point has not receded. Additionally, the salinity has retreated from the upstream, so the salinity concentration increases more and reaches its maximum value then decreases gradually because the river discharge gradually pushes the saltwater back to the estuary. This process repeats over 12 hours and a half, so the salinity may reach the maximum value in the next 12 hours and a half. The S_{max_bot} at each station always occurred after the WL_{max} at this station however, the lag time between the S_{max_bot} and the WL_{max} was different due to the location of each station, the velocity, the flow of riverine-tidal currents, and the topography of each estuary. The results in Figures 6.17 and 6.18 shows that those stations far from the estuary have shorter delays than those near the estuary. Figure 6.20 shows that at the same distance of 30km from the river mouth, the lagged time between $S_{max\ bot}$

and WL_{max} at Cau Quan and DaiNgai stations on the Hau river was 1h and 1.5h, respectively, but at the TraVinh station on the CoChien river it ranged from 2.5h to 3.0h (Figures 6.21 and 6.22).

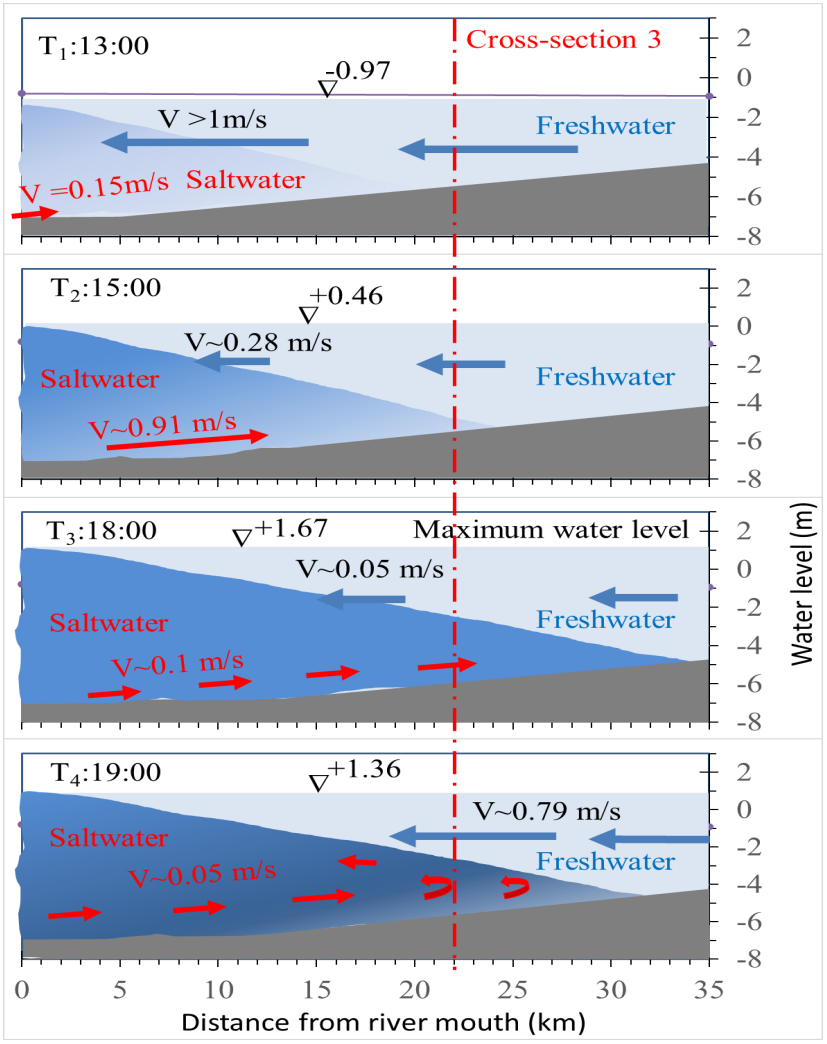

Figure 6.20 The salinity intrusion processes along the river during the half of a tidal cycle on 21, April 2019

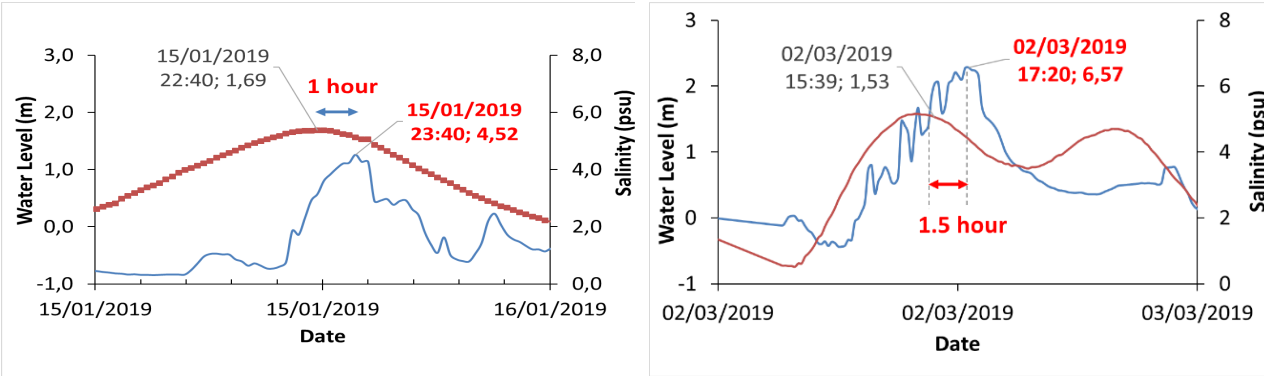

Figure 6.21 The relationship between Sal ~ water level at CauQuan and DaiNgai stations in the Hau River

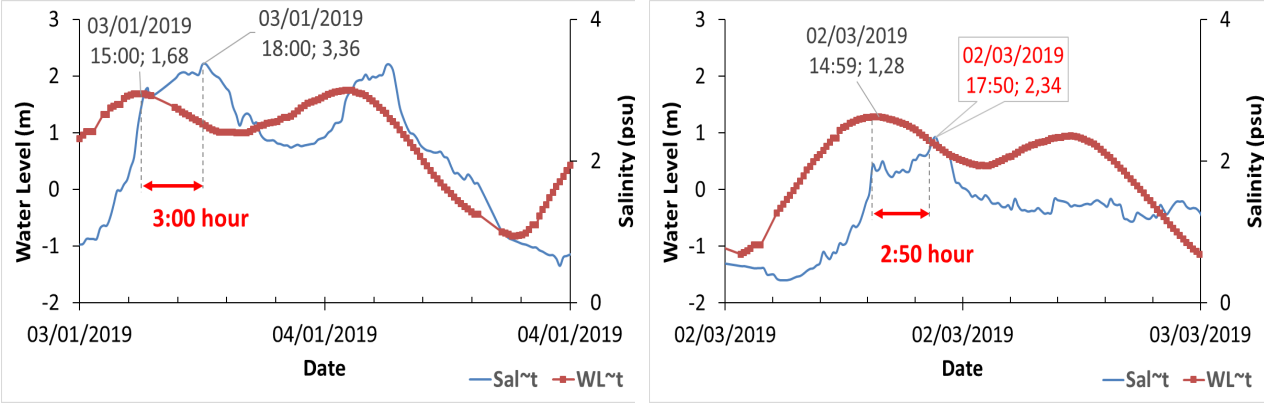

Figure 6.22 The relationship between Sal ~ water level at TraVinh station in the CoChien River

The result of studying the impact of tides on the salinity mechanism in a tidal cycle is that the distribution of salinity changes over a tidal cycle time. During the flood tide, the salinity concentration and length of saline intrusion also increase. However, the maximum salinity value on the surface occurs simultaneously with the maximum water level at that point. While the bottom maximum salinity occurs after the WL_{max}, the time lag difference between S_{maxbot} and WL_{max} depends on the location of those stations relative to the estuary. The station far away from the estuary will have a small-time lag compared to the station near the mouth. The time lag between S_{maxbot} and WL_{max} is from 1h to 3h.

This finding is consistent with the study of Bao et al., (2008) and Gong et al., (2011) but both of them studied salinity intrusion in the Modaomen estuary, China. Gong et al., 2011 reported that the highest bottom salinity occurs at the end of flood current or delays to the onset of the ebb tide and corresponds to a 2–3 h time lag relative to the daily maximum water level, resulting in higher vertically averaged salinities at ebb tide than at flood tide. Also, Bao et al., 2008 notice that the salinity intrusion limit varies with the tidal phase at Sanzhao station with approximately a 5h lag relative to the high slack water in a tidal cycle. They also concluded that maximum salinity intrusion occurs at the transition period from neap to spring tides while minimum salinity intrusion appears at the transition period from spring to neap tides. So how do the salinity intrusion processes in VMD occur two-week cycles? This is the content of part 5 below.

6.2.4.5 The response of salinity intrusion in a month (fortnightly)

Analysis of hourly salinity data and hourly water level at two salinity measurement stations Cau Quan on the Hau River and TraVinh station on the CoChien River. Those stations are two of

five automatic stations of TraVinh province installed along the left bank of Hau River and the right bank of Co Chien River towards the sea. The measuring device is installed from 2017 to the present.

Figure 6.23 and 6.24 shows the relationship between water level and hourly salinity at CauQuan station on Hau River and at TraVinh station on CoChien River, the distance from each station to the sea mouth is about 30km. The maximum daily salinity at CauQuan and TraVinh always occurs after 1h to 3h time lag relative to the maximum daily water level depending on the station. According to the spring-neap tide cycle, we see that when the tide changes from neap tide to spring tide, saltwater has appeared and quickly increased. The S_{max} did not appear at the maximum water level, but S_{max} occurred 3-7 days earlier than the maximum water level in the spring tide, depending on the location of the measuring station and depending on the river branch. That means S_{max} in the fortnight cycle also occurs during the transition period from neap tide to spring tide. For instance, Figures 6.23 and 6.24 show that the S_{max} value appears earlier than the WL_{max} from 5 to 7 days at CauQuan station and from 3 to 4 days at TraVinh station in the neap - spring tide cycle. Then, the salinity values gradually decrease and the minimum salinity concentration in the fortnight cycle occurs during the transition period from spring tide to neap tide, not at the time of the lowest water level in two weeks. This result is similar to the conclusion in the article of Gong et al., 2011. They also conclude that maximum salinity intrusion occurs at the transition period from neap to spring tides while minimum salinity intrusion appears at the transition period from spring to neap tides.

The tide changed in the different time scales such as from year to year, within the year from the season to the season, over a month (spring-neap tidal cycle) and a tidal cycle (ebb-flood tidal cycle) and at a special event (sea level rise, wind, tsunami, etc.). We need to consider the impact of the tide in different time scales on salinity intrusion because tide plays the most important role in regulating salinity intrusion in the estuary, followed by river discharge, morphology change and sea-level rise.

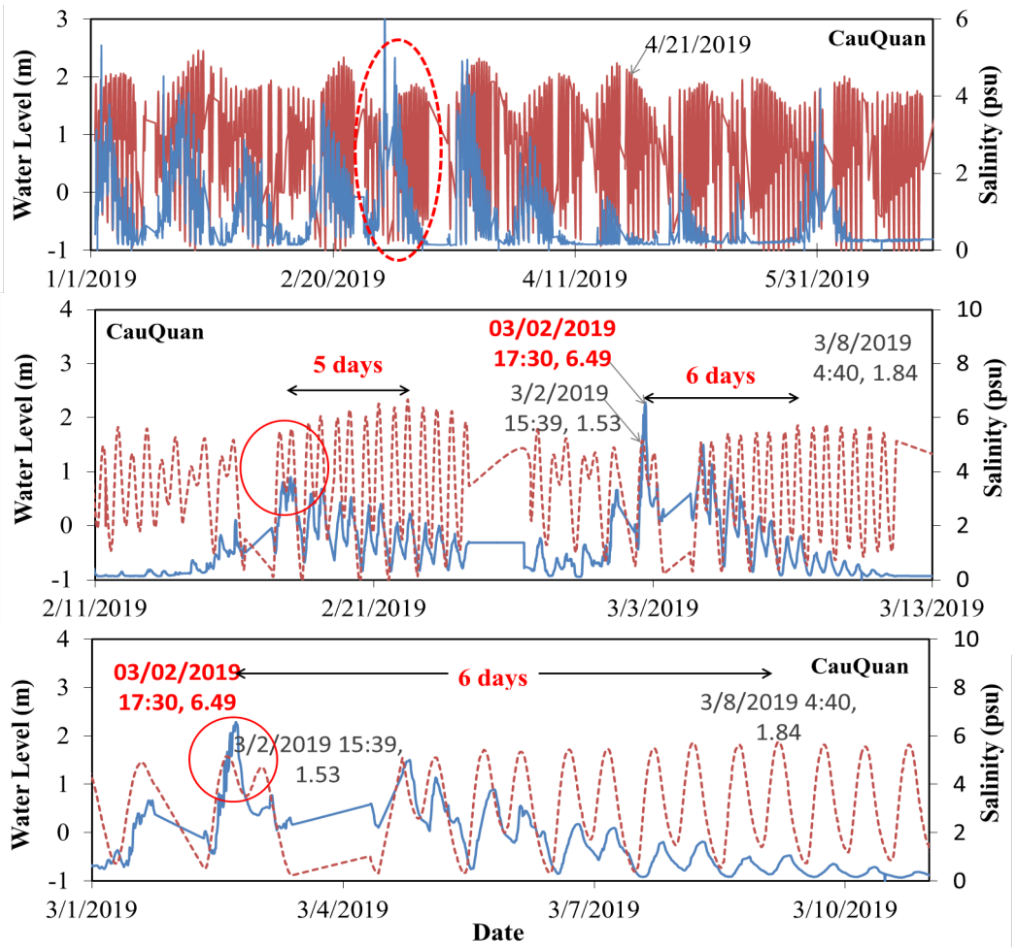

Figure 6. 23 The relationship between Sal ~ WL at CauQuan Station in DinhAn Estuary

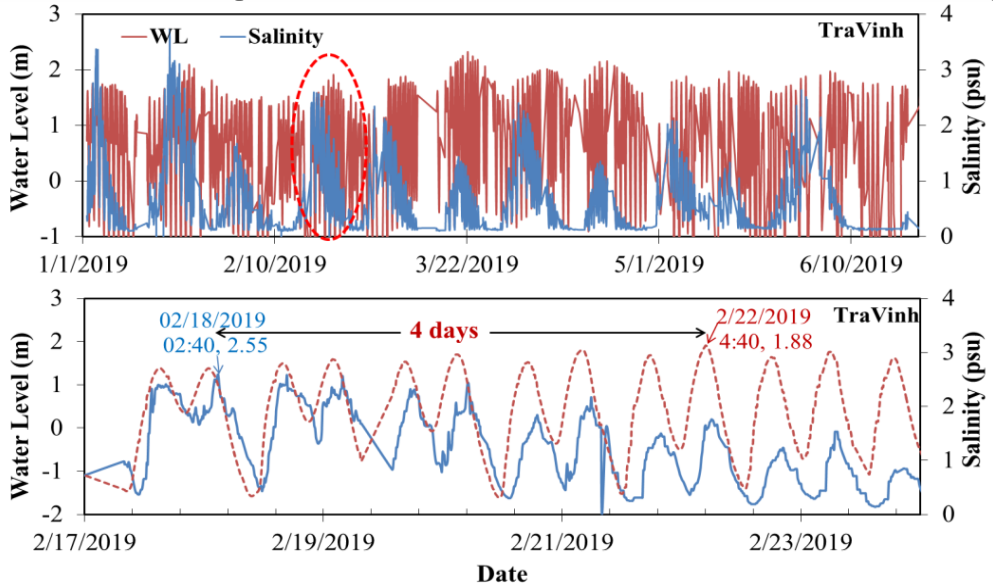

Figure 6.24 The relationship between Sal ~ WL at TraVinh Station in CoChien Estuary

6.2.5 The mixing and stratification in the Hau River

The mixing and stratification are the result of the difference of water density, which means the body of water near the bottom under consideration is heavier water with a greater density than near the water surface. Energy is needed to overcome the stratification by mixing the heavier bottom water with the lighter surface water. This mixing is effectuated by turbulence, with the required energy being supplied by the tidal flow. Beyond that, it is a complicated process completely controlled by the tide, the wind and the river flow. In this research, only the effect of the tide and the river flow are considered. The mixing changes over the daily time scales ranging from days (flood – ebb tide) to weeks (spring-neap tide) and months (seasonal river discharge variations). Residual ebb-flood channel circulation, an important large-scale mixing mechanism for salinity in the Hau River, was also considered in this research.

The salinity data measured along 50km of Hau River from March 2-5, 2018 and 50km of Co Chien River from April 6-7, 2018 in one tidal cycle at Spring tide, combined with Pritchard's number (n) in Table 6.7 are used to evaluate the type of mixing in the river. A longitudinal and vertical salinity distribution along the TranDe tributary in Figure 6.9, the results of n number are in the range from 0.06 to 0.93 in both flood-ebb tides. Similarly, on DinhAn branch in Figure 6.12, it also gives the range of n number from 0.11 to 0.68 during flood-ebb tides. Both tributaries on the Hau River have the Pritchard's number, n between 0.1 and 1, so the vertical salinity distribution indicates partial mixing and moderate stratification.

However, in Figure 6.16, the Pritchard index changes from 0.02 to 0.76 during the ebb tide, but at the flood tide it is greater than 1 from 1.06 to 1.59. That result shows that partial mixing and moderate stratification is typical on the Co Chien branch at ebb tide. When the tide rises (flood tide) on the Co Chien branch, there is a very clear salt stratification and formation of salt wedges within 40km from the mouth of the river depending on the salinity concentration. This is a very important and meaningful result for the operation of saline control sluices along the CoChien river to obtain freshwater during the flood tide in the dry season but note that freshwater is only on the surface and saltwater in the bottom.

Using the value of vertical salinity distribution, water level, mean velocity and mean discharge at two cross-sections conducted at two cross-sections 2 and 3 (Figure 3.3) during 1 tidal cycle on April 21-22, 2019 in part 6.2.4.4 to calculate five mixing and stratification numbers in Table 6.4 such as Pritchard's number (n), Simmom's number (α), Froude number (F_r),

international estuary number E_ρ and Richardson's number (Ri_E). At each cross-section, salinity concentration, discharge and velocity distribution were measured at 8 to 10 vertical profiles; each vertical profile measured 12 times during 12.25 hours (one tidal cycle) by CastAway – CTD and GPS-equipped Acoustic Doppler Current Profiler (ADCP). While hourly water level collected at TranDe, BacTrang and CauQuan station.

The difference of salinity concentration at one cross-section at the same datum in the ebb tide (9:00 to 13:00) as shown in Figure 6.16. Salinity concentration difference between two river banks at the same depth (at -4m elevation) is less than 0.1psu while at flood tide (15:00 to 18:00) it is from 0.1 to 0.4psu. That means at cross-section 3, the advection is more influenced by tide than river flow. Whereas, the changes in river flow at ebb tide (from 9:00 to 13:00) have more effect on the advection at cross-section 2 as shown in Figure 6.19 with salinity value in the middle river higher than that in the banks. Difference in salinity values between middle and banks was approximately 2 psu indicating that at -4m elevation. While during the flood time from 15:00 to 21:00, the salinity concentration was quite similar at the same depth. That means the cross-section 2 is more affected by river flow during the flood tide.

Five stratification parameters in Table 6.4 are used to classify the mixing and stratification during one tidal cycle (12 hours) at DinhAn branch in the Hau River. The results in Table 6.5, 6.6, 6.7, and Table 6.8 indicates that the mixing and stratification in cross-section 1 and 2 so complicated. When we consider only the Pridchard's number, partial mixing and moderate stratification prevailed at cross-section 3 and at the middle point of cross-section 2 (Table 6.5, 6.6 and 6.7) while weak mixing and strong stratification occurred at deepest point of cross-section2 (Table 6.8). The Pritchard number can prevail mixing and stratification at one water column. While three numbers α, E_ρ and R_{iE} parameters can show the stratification during one tidal cycle for one part of river. Table 6.5, 6.6 and 6.9 show that with the value of α, E_ρ and R_{iE} parameters being always in the range of type III of salinity intrusion in Table 6.4. That means along 22km from the DinhAn estuary on April 21, 2019, the salt wedge appeared during one tidal cycle. Because mean river discharge Q^+, mean saltwater flow Q^-, mean flood tidal velocity υ, mean water depth h_o, ρ_s, ρ and tidal range ΔH of one tidal cycle were conducted during this tidal cycle. Combined with 23 cross-sections along 22km of DinhAn branch measured on August 2017 used to calculate the tidal prism then gave the value of α, E_ρ and R_{iE} parameters**. W**eak mixing and strong stratification will prevail stratification of salinity intrusion in DinhAn branch in the transition from spring tide to

neap tide on April 21, 2019 (Figure 6.23). At that time the river flow was high, so fresh water dominated the surface and saltwater dominated the bottom of the river. The same results also appeared in section 2 located 5km from the sea mouth with the value of α, E_ρ and R_{iE} higher than that in cross-section 1 and also belonging to the range of type III (Table 6.4). So, the salinity intrusion processes in DinhAn branch in the transition from spring tide to neap tide were overcome by salt wedge stratification.

This finding shares phenomena with the finding of Nowacki et al. 2015, who gave the conclusion that salt wedge conditions were observed only in the lowermost DinhAn channel at high discharge, while in low discharge both sub-distributary (DinhAn and TranDe) channels are partially mixed estuarine.

Table 6.5 Vertical mixing and stratification in the middle point of Cross-section 3

Time	Q	V	Abs(V)	Depth	S min	Smax	n	α	Fr_ρ	Eρ	Ri_E
4/21/19 9:27	16075.81	0.95	0.95	11.07	0.37	0.73	0.65	4.86	0.53	0.06	3.79
4/21/19 10:08	14513.30	0.89	0.89	10.4	0.47	0.57	0.19				
4/21/19 11:32	11535.47	0.72	0.72	10.99	0.25	0.31	0.21				
4/21/19 12:13	-3669.59	-0.23	0.23	11.87	0.17	0.19	0.11				
4/21/19 13:13	-14681.60	-0.78	0.78	12.99	0.14	0.17	0.19				
4/21/19 14:33	-17493.77	-0.91	0.91	12.12	0.16	0.19	0.17				
4/21/19 15:25	-17156.20	-0.86	0.86	12.96	0.35	0.40	0.13				
4/21/19 16:32	-12091.63	-0.59	0.59	13.06	0.52	0.86	0.49				
4/21/19 17:13	-3900.00	-0.15	0.15	13.28	0.8	1.04	0.26				
4/21/19 18:29	4449.02	0.3	0.3	12.54	1.04	1.69	0.48				
4/21/19 19:30	14636.40	0.79	0.79	12.5	0.93	1.52	0.48				
4/21/19 20:48	16422.86	0.88	0.88	12.17	0.64	1.20	0.61				

Table 6.6 Vertical mixing and stratification in the deepest point of Cross-section 3

Time	Q	V	Abs(V)	Depth	S min	Smax	n	α	Fr_r	Eρ	Ri_E
4/21/19 9:00	16075.81	0.95	0.95	12.62	0.37	0.89	0.83	4.86	0.48	0.05	5.81
4/21/19 10:00	14513.30	0.89	0.89	13.54	0.38	0.54	0.35				
4/21/19 11:00	11535.47	0.72	0.72	14.18	0.27	0.36	0.29				
4/21/19 12:00	-3669.59	-0.23	0.23	14.40	0.2	0.32	0.46				
4/21/19 13:00	-14681.60	-0.78	0.78	14.50	0.16	0.2	0.22				
4/21/19 14:00	-17493.77	-0.91	0.91	15.44	0.21	0.3	0.35				
4/21/19 15:00	-17156.20	-0.86	0.86	16.07	0.31	0.41	0.28				
4/21/19 16:00	-12091.63	-0.59	0.59	16.11	0.55	0.81	0.38				
4/21/19 17:00	-3900.00	-0.15	0.15	15.71	0.94	1.13	0.18				
4/21/19 18:00	4449.02	0.3	0.3	15.25	0.98	1.7	0.54				
4/21/19 19:00	14636.40	0.79	0.79	15.13	0.96	1.4	0.37				
4/21/19 20:00	16422.86	0.88	0.88	14.42	0.75	1.49	0.66				
4/21/19 21:00	16580.27	0.9	0.9	14.23	0.7	1.02	0.6				

Table 6.7 Vertical mixing and stratification in the middle point of Cross-section2

Time	Q	V	Abs(V)	Depth	S min	Smax	n	α	Fr_r	Eρ	Ri_E
4/22/19 9:18	8571.9	0.93	0.93	6.93	4.41	7.39	0.51				
4/22/19 10:19	18506.6	0.97	0.97	7.02	2.93	7.61	0.89				
4/22/19 11:24	14452.1	0.77	0.77	6.76	3.11	3.8	0.20				
4/22/19 12:22	8705.1	0.42	0.42	6.96	2.59	3.05	0.16				
4/22/19 13:22	-60000.0	-0.15	0.15	7.2	2.64	4.3	0.48				
4/22/19 14:22	-19761.0	-0.87	0.87	8.7	2.96	6.86	0.79				
4/22/19 15:34	-22193.0	-0.93	0.93	8.87	4.87	6.41	0.27	14.15	0.68	0.03	4.67
4/22/19 16:22	-16313.7	-0.68	0.68	8.13	5.14	11.79	0.79				
4/22/19 17:20	-10894.1	-0.46	0.46	9.14	6.25	14.55	0.80				
4/22/19 18:22	6542.0	0.3	0.3	8.36	9.83	16.63	0.51				
4/22/19 19:00	10923.9	0.55	0.55	8.17	8.86	16.58	0.61				
4/22/19 20:25	17427.6	1.01	1.01	7.41	6.98	11.81	0.51				
4/22/19 21:18	16650.5	0.99	0.99	6.88	5.81	8.91	0.42				

Table 6.8 Vertical mixing and stratification in the deepest point of Cross-section 2

Time	Q	V	Abs(V)	Depth	S min	Smax	n	α	Fr_r	Eρ	Ri_E
4/22/19 9:18	8571.86	0.93	0.93	9.85	4.47	11.64	0.89				
4/22/19 10:19	18506.61	0.97	0.97	9.62	2.24	8.67	1.18				
4/22/19 11:24	14452.10	0.77	0.77	9.71	1.32	5.24	1.20				
4/22/19 12:22	8705.13	0.42	0.42	9.86	1.32	4.72	1.13				
4/22/19 13:22	-10000.00	-0.4	0.4	10.70	1.80	5.40	1.00				
4/22/19 14:22	-19761.04	-0.87	0.87	11.87	2.29	6.06	0.90				
4/22/19 15:34	-22193.04	-0.93	0.93	12.57	5.43	9.35	0.53	14.80	0.59	0.04	3.87
4/22/19 16:22	-16313.74	-0.68	0.68	11.32	6.14	11.11	0.58				
4/22/19 17:20	-10894.12	-0.46	0.46	10.78	6.67	14.16	0.72				
4/22/19 18:22	6542.00	0.3	0.3	10.59	6.72	15.14	0.77				
4/22/19 19:00	10923.91	0.55	0.55	10.35	5.88	14.78	0.86				
4/22/19 19:25	17427.62	1.01	1.01	10.05	5.57	14.76	0.90				
4/22/19 20:00	16650.48	0.99	0.99	8.19	6.94	14.19	0.69				

Table 6.9 The summary of the stratification parameters for Hau River (S = Strong stratification, M = Partially mixing or Moderate stratification, W= Weak stratification)

Approach method	Cross-section3		Cross-section2	
	Middle point	Deepest point	Middle point	Deepest point
Pritchard: n	0.11 to 0.65	0.18 to 0.83	0.16 to 0.89	0.53 to 1.2
Simmom's number: α	4.86	4.86	14.15	14.80
Internal estuary number E_ρ	0.06	0.05	0.03	0.04
Richardson's number: Ri_E	3.8	5.8	4.7	3.9
Classification (n, a, E_ρ, Ri_E)	(M, S, S, S)	(M, S, S, S)	(M, S, S, S)	(S, S, S, S)

All the results are useful for integrated water resources management and salinity control measurements. Along the left bank of Hau River 50km r from the estuary, there are six completed and two under construction sluice gates, whose threshold elevation varies from -3m to -4.5m. Most

of the gates are used to take in freshwater and control salinity, therefore the gates are usually closed during times of high salinity concentration in the dry season. However, during the period between the high slack water and the low slack water, the gates can open to take freshwater for irrigation. For instance, the Can Chong gate, located at the 29km point on the left side far from the DinhAn estuary, has been opened to take water when S_{max} is less than 1g/l. The threshold of this gate is -4.5m. Figure 6.16 collectively suggests that the Can Chong gate should be opened from 9:00 to 16:00 (eight hours) to take water when maximum salinity concentration is less than 1g/l.

Furthermore, the annual mean sea level along the Eastern coastal areas would increase in the average amplitude of 3.2 mm/year (Nhan 2016). Therefore, the projected intrusion length should be predicted to propose locations of new gates and the threshold of gates to control salinity in the future.

6.3 Impact of Sea level rise

6.3.1 Introduction

Sea level rise poses critical ecological and economical consequences for the low-lying mega-deltas of the world where dependent populations and agriculture are at risk. The world's coastal areas and in particular its mega-deltas are increasingly being inundated and eroded by rising sea levels (Ericson et al., 2006 and Syvitski et al., 2009). The warming of our global environment threatens to speed up the rate of current sea-level rise and perhaps further amplify the detrimental effects of tropical storms, droughts, and record rainfall. Potential effects of sea-level rise include coastal erosion, saltwater intrusion, and submergence of cultural and natural resources. Mega-deltas are at greater risk by human activities for instance: land-use change for agriculture and aquaculture, damming of rivers and groundwater extraction are causing accelerated subsidence and flooding of the land surface.

The Vietnamese Mekong Delta (VMD), one of many mega-deltas worldwide, is at serious risk because of rising sea levels, which may accelerate under climate change (Syvitski et al., 2009) because most of the land surface is below mean sea level and there is a lack of coastal barrier protection. Food security related to rice and shrimp farming in the VMD is currently under threat from saltwater intrusion, relative sea-level rise, and storm surge potential. So, by understanding the degree of potential change in sea level under climate change we can undertake regional assessments of potential impacts and formulate adaptation strategies (Thomas et al, 2010).

6.3.2 Sea level rise trend for the Vietnamese East coastal (Vung Tau station)

Sea level rise is affected by climate change, land subsidence and a decrease in sedimentation deposition rate. Climate change is reflected in the increase in the national average temperature at the beginning of the 21st century with an increase of 0.6 - 0.8ºC. By the middle of the century, the increase is projected to range 1.3 - 1.7ºC. In particular, the Mekong Delta region has an increase of 1.3 - 1.4ºC under the RCP4.5 scenario or from 3.0 - 3.5ºC under the RCP8.5 scenario (IPCC, 2016). The subsidence rate in the Mekong Delta is 3-9 mm/yr, accounting for about 67% of the delta's area in which subsidence due to Holocene sediment consolidation is 0-4 mm/yr, groundwater extraction lowers geology 0-3.5 mm/yr and tectonic movement lowers 0-1.5 mm/yr. The change in land surface elevation due to geological factors is a continuous process in the delta plains. A number of processes can raise or lower land surface elevation such as sediment accumulation, compaction, dehydration, erosion, and organic deposition. The change in land surface elevation can occur due to rising/lowering in the tectonic active area or alluvial deposition in the delta area. In fact, the Mekong Delta has been lowered instead of being raised due to alluvial deposition. This is due to the lack of sediment reaching the delta because of upstream hydropower reservoirs and flood control works. Natural subsidence due to sediment compaction can be up to over 10 mm/year (IPCC, 2016). Over-exploitation of groundwater is also a cause of geological subsidence In Ca Mau, the subsidence level due to groundwater extraction is 1.9-2.8 mm/yr (IPCC, 2016).

According to the conclusion of IPCC 2016, the sea level rise in Vietnam is likely to be higher than the global average sea level. Especially in the East Sea, the sea level rise is higher than in other sea areas. Therefore, the scenarios for sea-level rise to 2050 and 2100 in the East Sea are 22cm (5.5 mm/yr) and 53cm (5.8 mm/yr) under the scenario RCP4.5 and 25cm (6.25 mm/yr) and 75cm (8.33 mm/yr) under the RCP8.5 scenario. With such an increase, the risk of flooding in the Mekong delta is 38.9% if the sea level rises by 100cm. In which, the RCP 4.5 is a medium scenario with stabilization of radiated forcing and the RCP8.5 is a high scenario with a radiated forcing (IPCC, 2016).

Vietnam has a total of 21 sea level measurement stations but only 7 hourly sea level measurement stations (Hanh and Furukawa, 2007). The most reliable data series is at Hon Dau station in northern Vietnam. The series of known water levels at Hon Dau from 1960 to 2000 show a sea-level rise of 1.9 mm/yr, corresponding to the average of global estuaries. Syvitski et al., (2009) also calculated

a 6 mm/yr increase in sea level trend in the Mekong estuary at VungTau station in southern Vietnam, which is the closest to the Mekong Delta, so the data is quite reliable.

Analyzing the rising trend of sea level, the author also used data series from Vung Tau station from 1980 to 2020. The data is collected from the Vietnamese National Center for Hydrometeorological Data. Figure 6.25 shows the maximum daily water level during 40 years and divides it into 3 periods: no dam, building dams and completed dams. Linear regressions of sea-level rise trend in 1980 to 1992 periods demonstrate a 4.16 mm/yr slope and -0.79 mm/yr slope from 1993 to 2011 and a 7.50 mm/yr slope from 2012 to 2020. When analyzing the general trend over time during the 40-year period from 1980 to 2020, the linear regression demonstrates a 5.25 mm/yr slope (Figure 6.27). This latter value is more consistent with the result of Syvitski et al., (2009) and the increase rate in RCP4.5 (5.5 mm/yr). Using data from 1980 to 2020 for analyzing sea level trends in two periods (1980-1989 and 1992-2001) by Doyle et al., (2010) (Figure 6.26), the obtained results are -0.58 mm/yr and 2.01 mm/yr respectively. These results are similar to Doyle's conclusion as linear regressions of sea level trend from 1979 to 1989 at the VungTau station recorded -0.62 mm/yr slope and a 1.77 mm/yr slope from 1992 to 2001 (Doyle et al., 2010). Therefore, the evaluation data series has high reliability and the sea level rise trend of 5.25 mm/yr will be calculated for future sea-level rise scenarios.

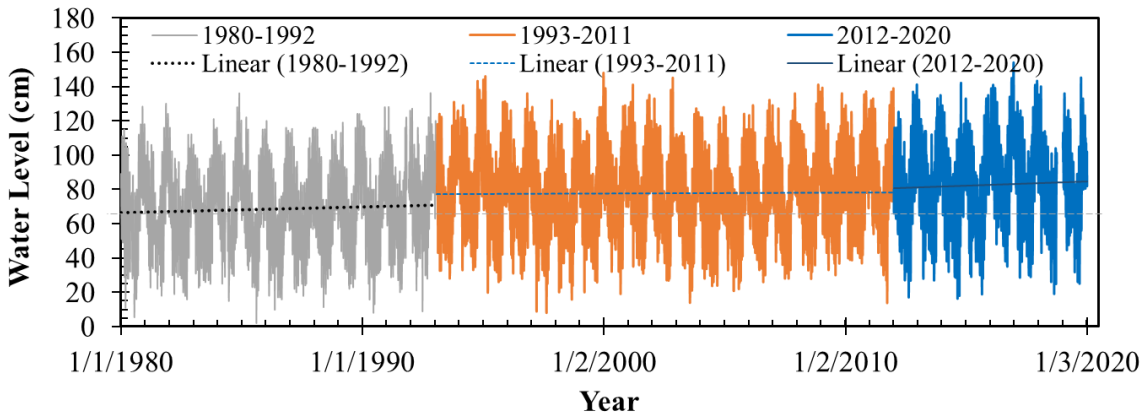

Figure 6.25 Maximum daily water level at Vung Tau during three periods

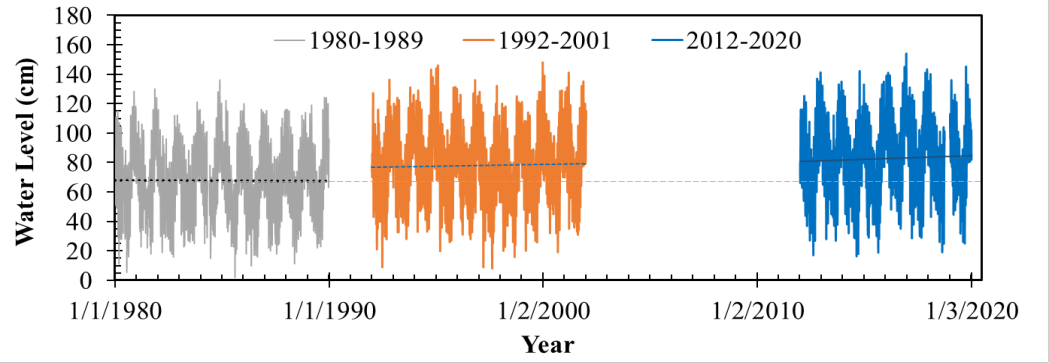

Figure 6.26 Maximum daily water level at Vung Tau with two first periods is the periods in the analysis of Doyle et al., 2010

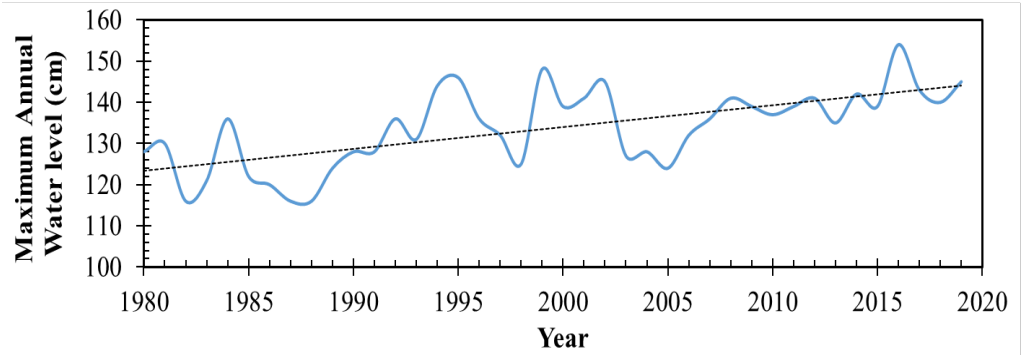

Figure 6.27 Annual water levels at Vung Tau

6.3.3 The impact of sea level rise into salinity intrusion in Mekong Delta by numerical model

Sea level rise is expected to cause negative consequences in erosion, submergence, salinity intrusion, agriculture, and aquaculture in the absence of mitigation or adaptation strategies. In this section, the author focuses on analyzing the effects of sea-level rise on saline intrusion. As analyzed in chapter 4.4.1, the impact of upstream flow changes on salinity intrusion increased in the concentration and duration in recent years. Normally, the salinity level in the MRD will start to rise by the end of December and reach its peak in March or April and decline afterwards. However, in the 3rd period (that of completed dams), salinity started to rise from November and maintained a high concentration from December to February this means that the maximum salinity appeared two months earlier and saltwater intruded further inland and remained longer during the dry season. High salinity concentrations appear and are maintained from November to the end of February. It occurred during times of high sea-level from October to February over 40 years (Figure 6.27). So, sea level also is one of the main drivers which has more effects on salinity intrusion. Two scenarios should be simulated by combining Sce 1 and Sce 2 in table 4.3 of part 4.4.3 with 47.25 mm SLR.

As analyzed in section 4.4.1, the repeating cycle of extreme drought years is from 4 to 6 years. So, in this scenario, the next 5 years of extreme drought is calculated after 2020. The sea-level rise is analyzed at 5.25 mm/yr, so the next two cycles from the 2016 baseline scenario (Sce0) will see an additional water level increase by 47.25 mm (5.25mm/yr x 9 years) for all 69 water levels downstream boundary points at the mouths of the Mekong Delta.

.

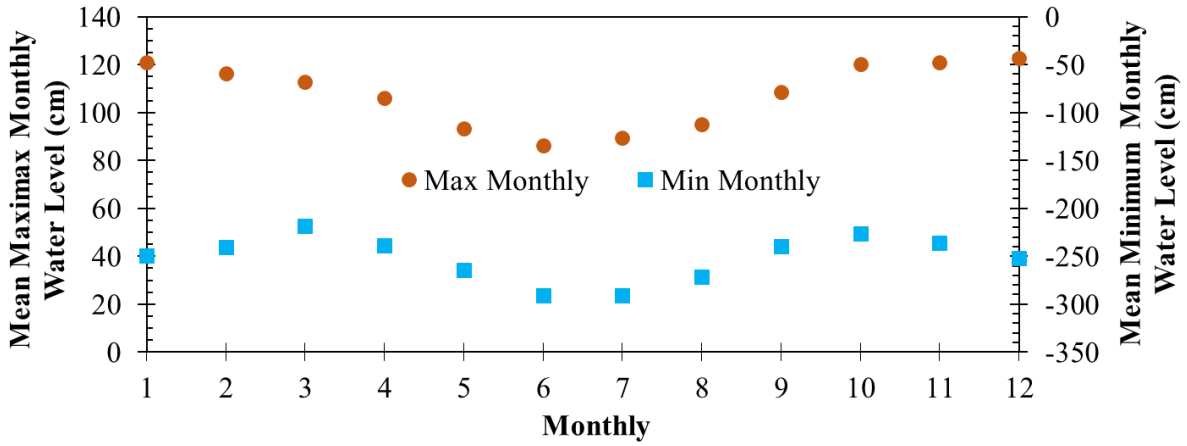

Figure 6.27 Seasonal variation of mean monthly water levels

6.3.3.1 Model Scenarios

Table 6.10 The scenarios of sea level rise in numerical model

Scenarios	Description of boundary condition	Remark
Baseline (Sc0)	**Upstream**: Discharge hydrographs of 2016 **Downstream**: Water level and salinity of 2016	For calibration
Scenario5 (Sce3)	Scenario 1 + Sea level rise by 4.725 cm (= 5.25mm x 9 years)	Dams impact + See level rise (Scenario 1 and scenario 2 were considered in 4.4.3)
Scenario 6 (Sce4)	Scenario 2 + Sea level rise by 4.725 cm	**For mitigation** + See level rise

6.3.3.2 The results

In the Sce1, In the Sce1, we consider if there was no first emergency water supplement from 10th March to 12th April at Chiang Saen, that means the discharge at Kratie reduced 364 m^3/s from 27th March to 27th April in 2016. The maximum salinity at stations located 30 km from the sea would have increased by 14% to 23.2% and intrusion length shifted inward by 16-24 km compared to the baseline.

Table 6.11 The results of the numerical model show S_{max} and L_{max} in four scenarios.

Salinity concentration at about 30km from the estuaries.								Intrusion Length of 4g/l		
		DaiNgai		CauQuan		TraVinh		TranDe	Dinh An	CoChien
No.	Scenario	Salinity (psu)	(P%)	Salinity (psu)	(P%)	Salinity (psu)	(P%)	estuary (km)	estuary (km)	estuary (km)
1	**Baseline on 13 March**	13.8		11.8		8.2		57	57	47
2	Sce 1	13.8		11.8		8.2		57	57	47
3	Sce 2	12.2	-11.6	9.8	-17.3	6.9	-15.9	51	51	43
4	Sce 5	15.9	15.2	13.7	16.10	10.1	23.2	64	64	52
5	Sce 6	14.1	2.2	11.9	0.8	9.2	12.2	57	57	48
1	**Baseline on 10 April**	7.4		5.4		4.9		41	41	35
2	Sce 1	8.4	14.0	6.4	19.2	6.0	23.2	45	45	40
3	Sce 2	6.9	-6.8	5.1	-5.6	4.6	-6.1	39	39	35
4	Sce 5	8.9	20.3	6.9	27.8	6.4	29.9	47.7	47.7	43
5	Sce 6	7.9	6.3	5.9	8.6	5.2	6.6	44	44	41

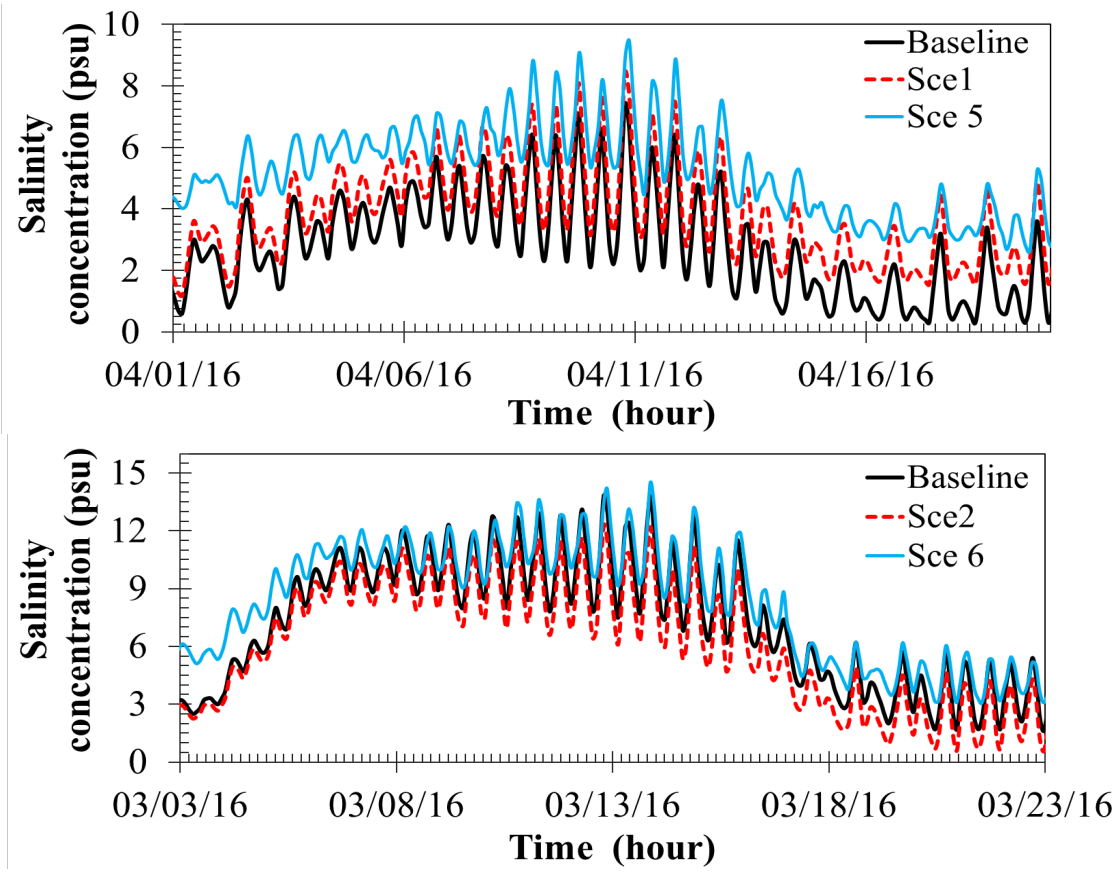

Figure 6.28 Hourly salinity concentrations of Sce1, Sce5 in April and of Sce2, Sce6 in March compared to the baseline at DaiNgai station

Scenarios 5 combine Sce1 with 4.725 cm sea-level rise (Table 6.10) to assess the impact of both upstream dams and sea-level rise on salinity intrusion. The salinity concentrations at DaiNgai and TraVinh stations increased by 20.3% and 29.8%, respectively (Table 6.11) as a result of discharge changes of 4.9% and 5.9%, respectively. Moreover, the length of the salinity intrusion shifted inward by 6.0-7.0 km in main streams due to the lack of fresh water to push saltwater back to the sea. Notice that saltwater intruded over the city of CanTho with a salinity concentration of over 2 psu, which has never happened before. The people in this region, therefore, need to take measures to control or adapt to the saltwater.

Moving on to the mitigation scenario combined with sea-level rise in scenarios 6. When the reservoir was released 1 month earlier than Sce0, the freshwater discharge in the VMD rose 13th March (from 5.15% to 6.9% at all stations 30km from the mouths) so the salinity concentration at these stations was reduced from 11.6% to 15.9%. If we combine Sce 2 with sea-level rise by 4.725 cm at all 59 downstream water level boundaries, the salinity value would increase 0.3-1.0 psu and saltwater would extend 3 to 6 km further inland compared to the results of the baseline. So, the sea level also has significant impact on the salinity concentrations.

6.4 Conclusions

The rising trend of sea level at Vung Tau station was analyzed from 1980 to 2020. The maximum daily water level during 40 years is divided into 3 periods: no dam, building dams and completed dams. The trend of sea-level rise in 1980 to 1992 periods demonstrates a 4.16 mm/yr slope; -0.79 mm/yr slope from 1993 to 2011; and 7.50 mm/yr slope from 2012 to 2020. Analyzing the general trend over 40 years from 1980 to 2020 period, the linear regression of this period demonstrates a 5.25 mm/yr slope. The results were more consistent with the conclusion of Syvitski et al., (2009), Doyle et al., (2010) and the increase rate in RCP4.5 (5.5mm/yr).

High salinity appears and is maintained at the same time as maximum sea level from October to February so sea level also is one of the main drivers of salinity intrusion, followed by river discharge. Two scenarios of sea level rise were simulated in a numerical model. One is combined with the impact of upstream dams with sea level rise considered over the next 5 years (from 2020) extreme drought years plus a sea level rise of 4.725 cm (Sce5) and the other is a mitigation scenario (Sce6).

The results of scenario 5 shows that when there is a sea level rise of 47.25 mm in the next drought years, the maximum salinity would increase by 6.3 % at DaiNgai (20.3% - 14%) and 6.6% at TraVinh (29.9% - 23.2%), intrusion length would shift inland by 6.6 km to 7.0 km in the mainstream compared to the results of Sce0.

Before considering the impact of tides on salinity intrusion, estuaries are defined and classified by shape, tidal range, geomorphology, river influence and stratification. The author concentrated more on the mixing and stratification of salinity intrusion mechanism by four parameters such as Pritchard number n (1955), Simmons number α (1955) and internal estuarine number E_ρ and Richardson number R_{iE}

Longitudinal and vertical salinity distribution research was conducted along 50km of four branches: TranDe, DinhAn, CungHau and CoChien. The results show that the bottom salinity is usually more concentrated than at the surface. Saltwater at the bottom decreases in an upstream direction usually more rapidly than at the surface. The intrusion length at the flood tide is longer than 14.3km, 15km, 16.5km than at the ebb tide at TranDe, DinhAn and CoChien branches, respectively.

Vertical salinity and velocity distribution were measured in 6 cross-sections in TranDe, DinhAn and CoChien branches. Each branch has two cross-sections at 5km and 30km far from the estuaries and the vertical salinity distribution was controlled by the value and direction of the flow velocity at these sections. Maximum velocity V_{max} in the surface appears during the ebb tide and the opposite occurs in the flood tide while V_{max} appears closest to the bottom of the river. Thus, maximum salinity S_{max} always happens in the bottom or the deepest point of the river.

On April 21 and 22, 2019, vertical salinity, vertical velocity, water level, and discharge at two cross-sections at 5km and 22km far from the DinhAn estuary were conducted during one tidal cycle (12h) from 9:00 to 21:00. The tidal wave propagating into the DinhAn estuary is a standing wave with the phase lag between HW-HWS and LW-LWS at approximately 0 (Figure 6.18 and 19). S_{max} at the surface coincided with WL_{max} and S_{min} comes simultaneously with low water while S_{max} at the bottom lagged one and two hours after WL_{max} 22 km and 5km from the DinhAn estuary respectively and also lagged two to three hours at TraVinh station in the CoChien River. That means S_{max} at the bottom occurs during the transition period from flood to ebb tides during the daily cycle.

During the spring – neap tidal cycle, the S_{max} occurred 3-7 days earlier than the highest water-level in the spring tide: 5 to 7 days at CauQuan station and 3 to 4 days at TraVinh station. Also, S_{min} comes 3 to 7 days later than the highest tidal level in the spring tide. Therefore, we can conclude that S_{max} at the bottom occurs at the transition period from neap to spring tides while S_{min} appears at the transition period from spring to neap tides whichcan provide the important information for the pumping stations and sluice gates operations along the Hau and CoChien Rivers to store freshwater need to begin storing water at least 3 to 7 days ahead of the spring tide so as to avoid serious impact from saltwater intrusion.

During the spring tide on March 2 to 5, 2018, vertical and longitudinal salinity distribution along 50km of the DinhAn and TranDe branch verifies that partial mixing and moderate stratification overcome the TranDe and DinhAn branch since the Pritchard number n are always less than 1. While in the spring tide, partial mixing and moderate stratification appears along 50km of the CoChien River in the ebb tide and weak mixing and strong stratification prevail in the CoChien branch in the flood tide.

In the transition period from spring tide to the neap tide on April 21 to 22, 2019, weak mixing and strong stratification will overcome stratification of salinity intrusion in DinhAn branch because the value of α, E_ρ and R_{iE} parameters being in the range of type III of salinity intrusion as shown in Table 6.4.

Chapter 7: Perspectives for Mitigation and Adaptation Measures on Salinity Intrusion

7.1 Introduction

This study investigated characteristics of salinity intrusion concerning the main influencing factors (upstream flow, morphology change, tides, and sea-level rise) in the Vietnamese Mekong Delta. It was shown that the upstream flow regime has the most significant effect on salinity concentration and intrusion length in the VMD.

In addition, the study identified that operation of upstream reservoirs has a strong influence on water discharge and riverbed elevation. Especially, flow regime into the VMD has changed annually after completion of construction of six large dams in China and several reservoirs on the tributaries of the MK River. For instance, the total dry season flow in the VMD has increased by 34.83% at Kratie and 3.7% at TanChau in the 3rd period (completed dam) compared to the 1st period (no dam). An increase of total discharge in the dry season is because most reservoirs store water during the rainy season and release it in the dry season. In addition to total discharge, the ratio of W_{dry}/W_{total} has increased from 21.4%, 21.6%, and 35.5% at CS and 12.3%, 13.5% and 16.6% at Kratie station in the period 1, 2, and 3 respectively. However, the amount of total dry flow distributes differently in the six dry months. For example, the total flow at Kratie, Tan Chau, and Chau Doc stations between 1980 and 2016 showed a decreasing trend in December and January and ing in March, April and May while it remained stable in February. This is a main cause of salinity which occured earlier and more severely due to the increase in salinity concentration and intrusion length (Table 7.1). Besides, the reservoirs do not only store water but also trap the sediment inside the reservoir, causing the flood peak, the frequency of floods, and the amount of sediment to be significantly reduced downstream, especially in the VMD area. The reduction of inflow and sediment from upstream may cause many related environmental issues, such as riverbank erosion and the lowering of riverbed elevation, a reduction in nutrient-rich sediment transference into floodplains, and increased seawater intrusion. In addition to human induced factors, sea-level rise and tides are also threats to the VMD.

As a result, these issues have changed farming practices by intensifying use of agrochemicals and affecting the livelihoods of people in the VMD. These issues may lead to serious challenges to the Vietnamese government in terms of food security and environmental

sustainability. Therefore, setting up operation rules for the upstream reservoir and proposing suitable water resources management solutions in order to ensure sustainable socio-economic development downstream are needed.

Table 7.1 Difference in salinity intrusion between before and after 2011

No.	Contents	Period 1,2	Period 3	Notes
1	Starting time	February	Middle Dec. to January	1 to 1.5 month earlier
2	Maximum Salinity time	April or May	February or March	1.5 to 2 months earlier
3	Finishing time	The end of May	The end of May	Salinity concentration in period 3rd is usually lower than in period 1st or 2nd.

7.2 Mitigation and adaptation measures

7.2.1 Mitigation measures for MRB

Based on analyzing the changes of upstream flow regime into the downstream region, especially in the VMD and its related environmental issues, this study proposed some measures to enhance sustainable socio-economic development in the downstream, especially in the VMD by reducing adverse impacts of upstream dam development (Figure 7.1). It is needed to maintain environmental flow, sediment flow and to ensure a water demand in the downstream region which could support people's livelihoods, farming practices, and ecosystem services.

In extreme cases, reservoir operation rules should be appropriately adjusted to mitigate extreme drought events in the downstream regions, which may minimize transboundary impacts. For example, if the upstream reservoirs have suitable operation rules (such as releasing water one or two months earlier than usual) during extreme drought events in dry seasons of 2016 and 2020, the VMD would have avoided severe socio-economic losses. So, it is very necessary to set up and improve the monitoring system and sharing hydrology data and operation rules among countries for proactive preparedness to face extreme events and make future plans. Moreover, strategic collaboration among riparian countries and different geographical regions is crucial to share the benefits from the Mekong

7.2.2 Mitigation and adaptation measures for VMD

It was noted that saltwater intrusion (SI) processes in the VMD in recent years have been very complicated, especially in 2016 and 2020 (Table 7.1). SI has caused 389.831 households to lack fresh water and over 405.139 hectares of rice crops were affected so short-term and long-term solutions need to be considered. Therefore, both structural and non-structural measures are needed for mitigating the risks of saltwater intrusion.

The comprehensive solutions were proposed in Figure 7.2 to prevent and mitigate the impact of drought and salinity intrusion in short (such as days, weeks, months, seasons, or years) and long-time frames (many years). This diagram includes seven solutions, including four non-structural solutions and three structural solutions.

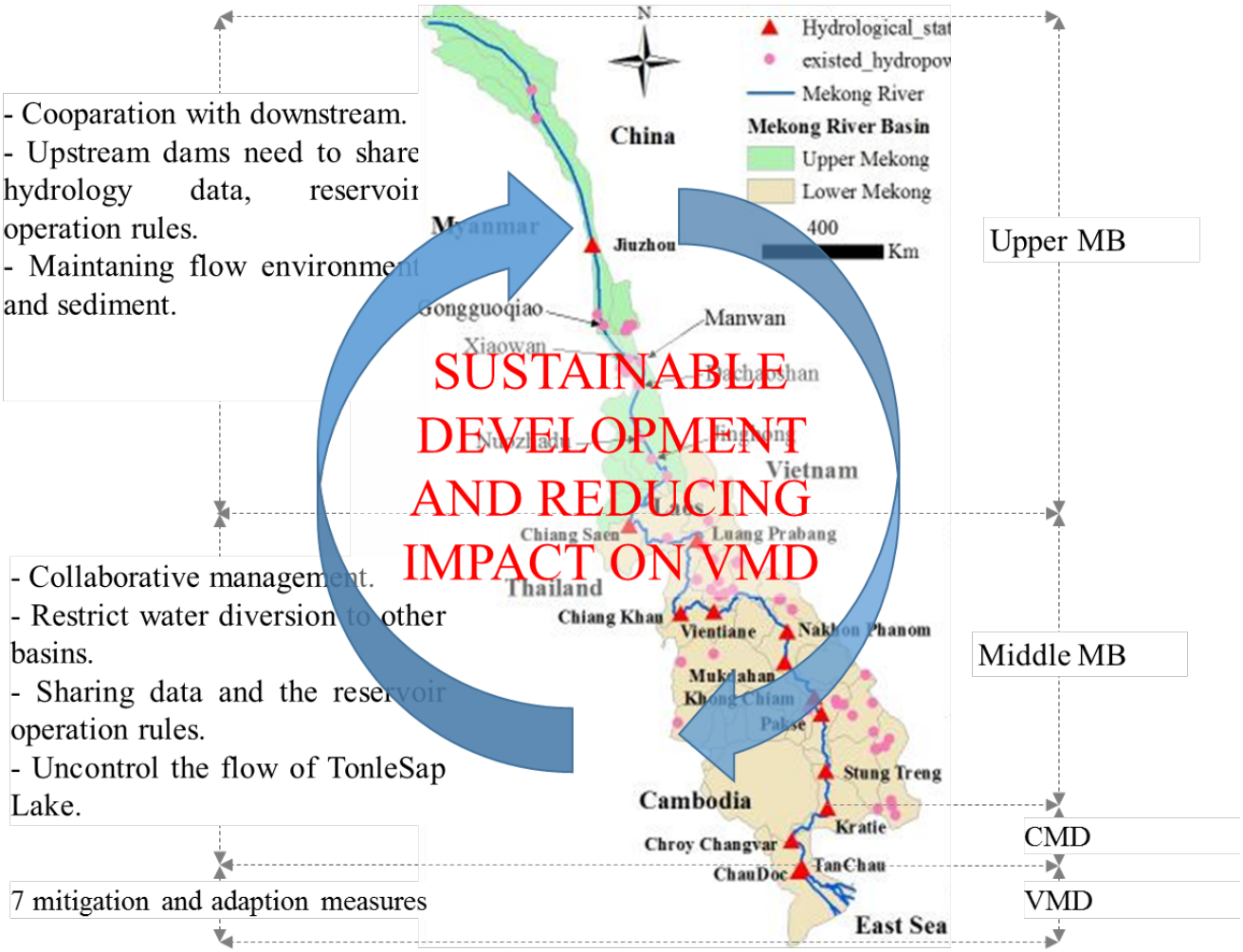

Figure 7.1 Proposed mitigation measures for sustainable development of the Mekong Basin (MB) and reducing SI in VMD

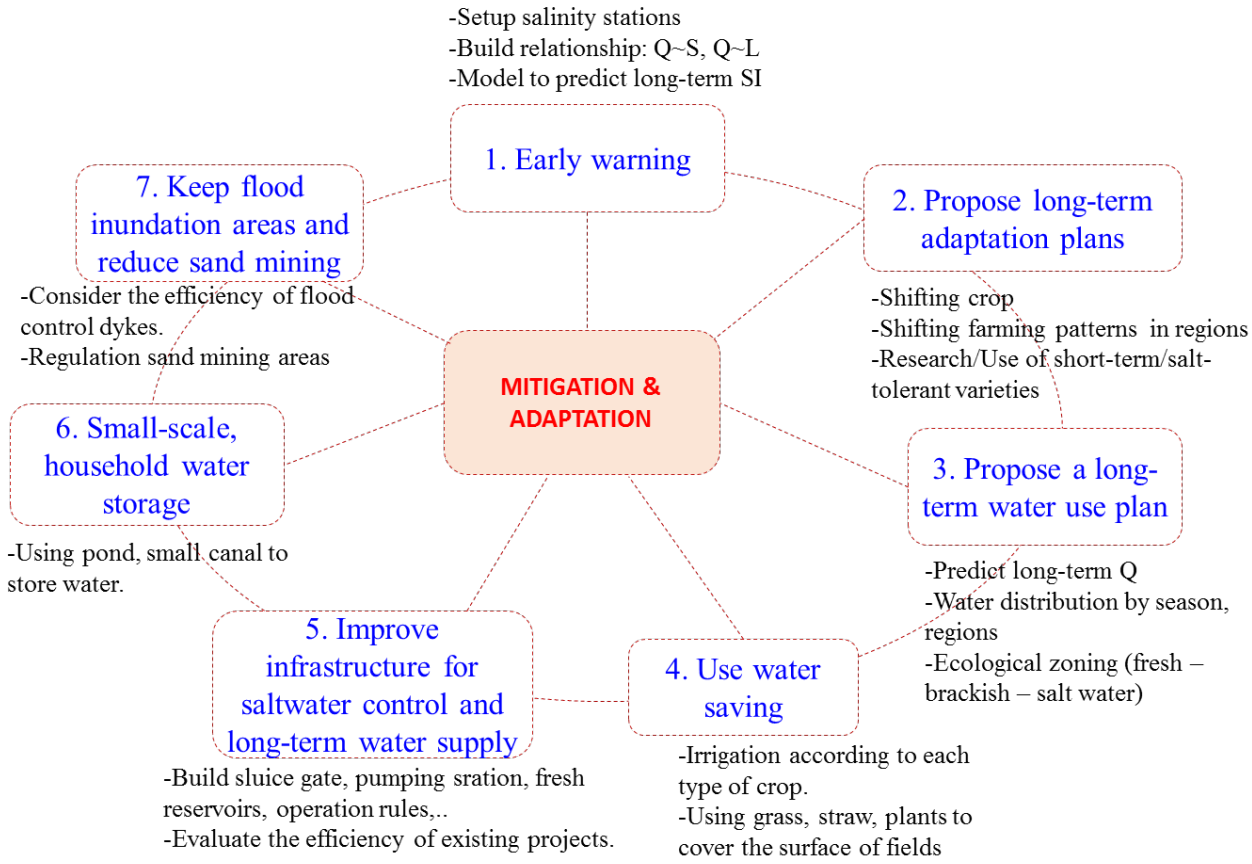

Figure 7.2 Long and short-term measures for mitigation and adaptation with SI in VMD

7.2.2.1 Early warning

1. Install salinity monitoring to determine the open time of sluice gates or water pumping

Up *1. Install salinity monitoring to determine the opening time of sluice gates or water pumping*

Until 2020, there have been about 81 salinity monitoring stations located along 13 main tributaries of the VMD--39 of them in the seven estuaries of the Mekong River. However, salinity data from these stations is sparse and each station has different data collection methods, which are automatic and manual measurements. For example, the automatic stations (< 15 stations) often collect data continuously with an interval time of 20 minutes. While the manual stations only monitor from January to May with an interval time of 2 hours. In addition, 39 monitoring stations have been installed to service the operation of sluices controlling seawater intrusion into the fresh river and canals. However, the number of these monitoring systems is very small compared to 252 salinity control sluices in the delta, about 130 of which are in the MK estuary area. Therefore, more monitoring stations should be placed above the inlets to small rivers or grade 1 canals with

sluices to prevent salinity. It is necessary to automate the manual monitoring stations and share salinity data to be more proactive with the intake of fresh water and prevent seawater intrusion to reduce the damage of the latter.

The salt concentration in the main rivers and canals is quite different due to the riverbed elevation of the tributary and the main canal. This is due to the retention of saltwater along the river bottom as shown in Figure 7.3. Therefore, at the intersection of the river and the canal, it is advisable to incorporate monitoring stations on the main river upstream of these tributaries which have saltwater control sluices and a single station in front of the sluice gates if those sluices are located far from the main river because of the variation in salinity.

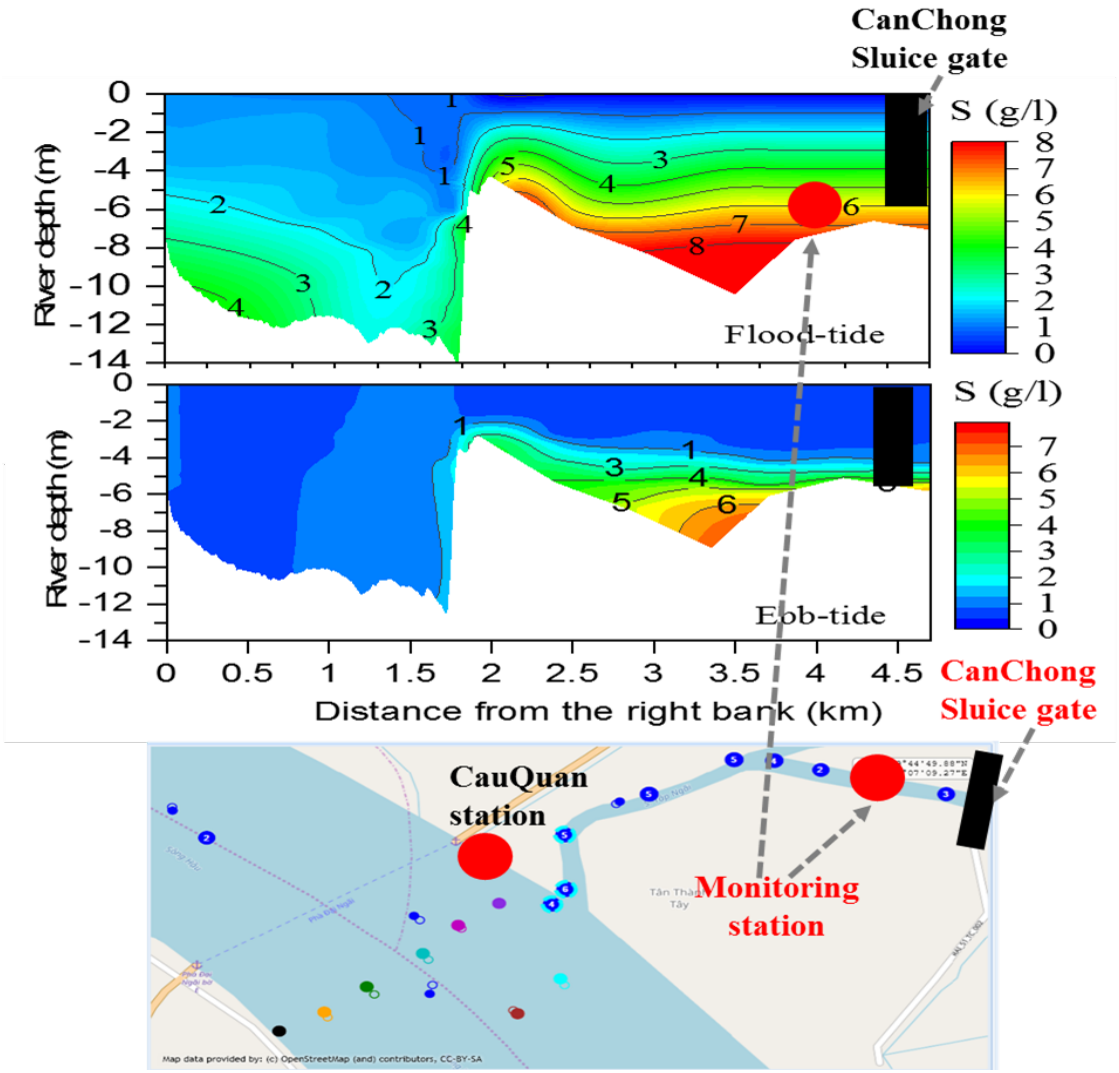

Figure 7.3 The vertical distribution of salinity at one cross-section of the Hau River and 2.5 km long of CauQuan river in front of the CanChong sluice gate.

The maximum salinity value in the Hau River is 4psu while S_{max} at the front of the sluice gate is 6psu during high tide and 1 psu less at low tide. Salinity at CauQuan station while in front of the sluice is still 3-4 psu. If we only put a measuring station in front of the sluice gate (200 m to 300 m), we only see high salinity and dismiss the opening times of the sluice gates or the water-pumping times to collect fresh water in the Hau River when the salinity in the main river is low.

2. Build the relationship between Q ~ sal

In addition to automatic salinity monitoring, it is easy to estimate salinity concentration in the VMD by using the relationship curve between Q and Salinity. Since the moving time of the flow from CS station to Kratie is 15 to 17 days, 17 to 19 days from CS to TanChau_Chau Doc as in section 4.3. So, to forecast salinity on VMD in a short timeframe (such as daily, weekly and monthly timescales), it is necessary to build a correlation between the flow into VMD which is discharged at TanChau and ChauDoc (Q_{TC+CD}) and the salinity at salinity stations in the main estuaries. Figure 7.4 shows the correlation between the average daily discharge at TanChau and ChauDoc station with the mean maximum daily salinity at 4 stations (DaiNgai, CauQuan, TraVinh and SonDoc) over 26 years (1990-2016 period). Using daily flow data at CS station, we can forecast the flow to Kratie and TanChau after 17 to 19 days, which means we can forecast salinity on VMD for at least 19 days.

Correlation results are acceptable with R^2 = 0.55 to 0.7. The relationship shows that the correlation between Q and salinity is inversely proportional. When the total flow into VMD is less than 3.500 m^3/s, the salinity value at all stations about 30 km from the sea is over 4 psu. For instance, the dry flows in 2015-2016 and 2019-2020 had the lowest salinity values during 90 years with the Q_{TC+CD} of 2681 m^3/s and 2265 m^3/s, but the concentrations at all salinity stations reached the highest value during 90 years with values over 14 psu. In particular, SonDoc station had the highest salinity, up to 27.4 psu and 28.2 psu in 2016 and 2020.

3. Prediction of long-term salinity by numerical model

In terms of water resources planning and management, it is crucial to predict seawater intrusion into freshwater systems of the VMD. Hence, this study develops different scenarios for the future according to the following adverse trends, (1) flow change due to abnormal upstream reservoir operation scenarios, (2) upstream flow decreasing due to the diversion of water out of the MRB, (3) increased agricultural development in the upstream countries, combined with

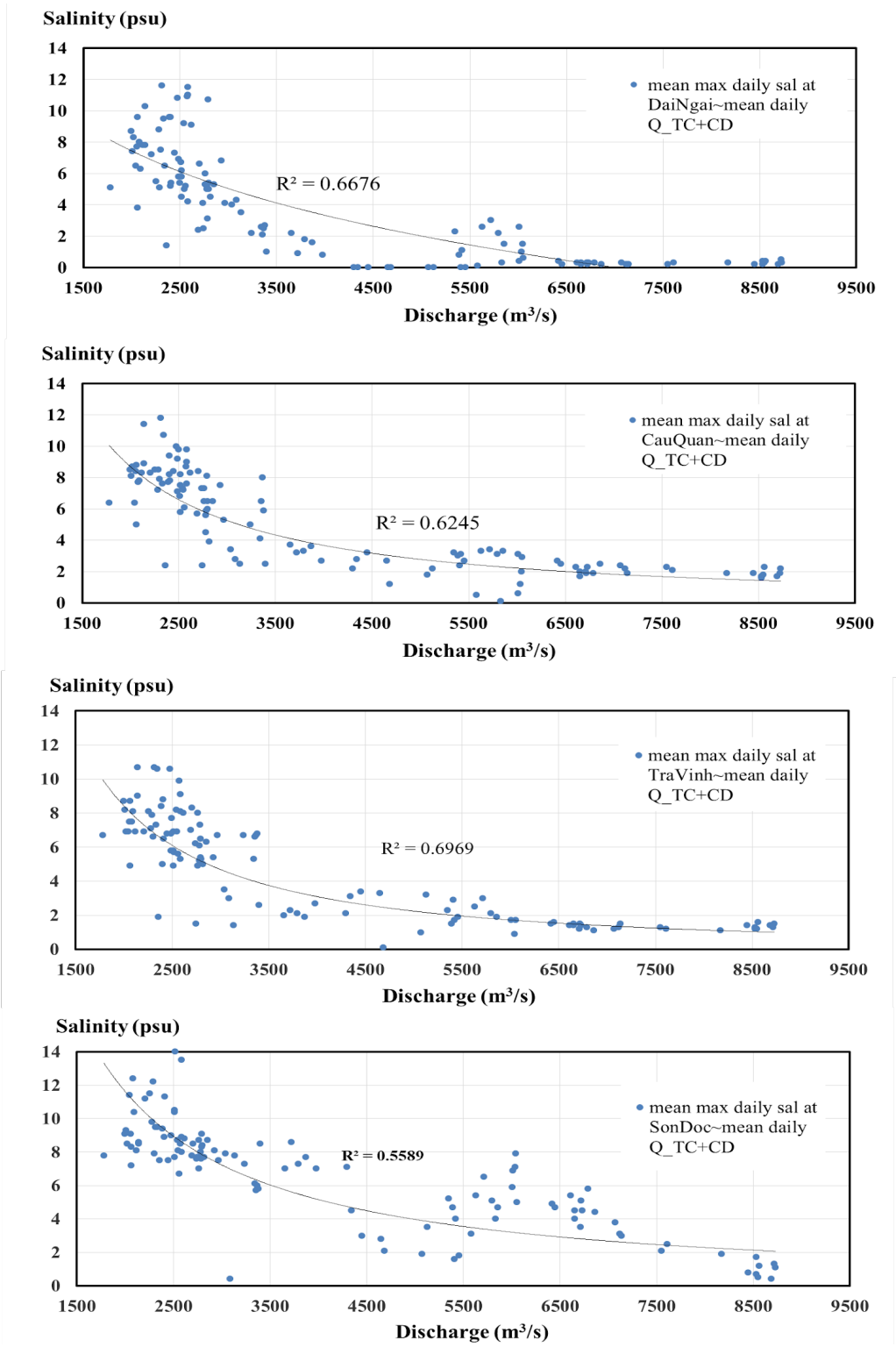

Figure 7.4 Relationship between mean daily Q at TanChau+ChauDoc and mean maximum daily Salinity at 4 stations: DaiNgai**,** CauQuan, TraVinh and SonDoc stations in the Hau, CoChien and HamLuong River

(4) a trend of sea level rise by 5.25 mm/yr or (5) riverbed incision rate by 0.22 m/yr and 0.34 m/yr on the Hau and Tien rivers or (6) simulated salinity processes when 11 hydropower dams on main MR in the territory of Laos, Thailand and Cambodia are completed. Different models should be used to predict the change of SI in the future for researchers and managers to propose solutions to adapt or mitigate the impact of SI on people, agriculture, food security, and the regional economy. In this thesis, the MIKE11 model was used to simulate 6 scenarios: two scenarios for upstream flow change, two scenarios combining flow change with sea level rise, and two scenarios for morphology change. All six scenarios are interested in the change of salinity concentration and intrusion length in the main river according to tables 4.4, 5.2 and 6.2.

7.2.2.2 Proposed long-term adaptation plans

To prevent serious impacts of salinity drought in the VMD, it is very important to develop an adaptation plan which considers the changes of water sources from upstream regions. For instance, early forecasting discharge from upstream of the VMD might have helped authorities to take effective adaptation actions and reduce socio-economic losses due to extreme drought events in the dry season between 2019 and 2020. Hence, this study proposes several details adaptation solutions as follows:

1. Make the production calendar according to river flow

In the years of severe drought and salinity, it is necessary to adjust the production calendar towards:

- Shifting the winter-spring crop to be sowed at least 1 month earlier (in October) for coastal areas affected by salinity (within 40-50 km of from estuaries);
- Need to also consider drainage support solutions for wetlands in order to prepare for heavy rains which can come in October

2. Shifting the farming patterns in some regions

In years of drought and salinity, many regions will have to change production towards:

- Use less water with economical irrigation systems.

- Use crops that require little water or short-term crops (such as converting from rice to cash crops).
- Use salt-tolerant crops like coconut trees, soursop trees, grape trees (5-6 psu), jackfruit trees and mango trees (3-4 psu), guava, pineapple and milkweed trees (1-2 psu) while avocado trees, banana trees, starfruit trees, longan trees, papaya trees, passion fruit trees, durian trees, rambutan trees and mangosteen trees (0.5-1 psu) should be avoided.

7.2.2.3 Propose long-term water use plans

- Predict the upstream flow and the ability for water supply.
- Then make a plan to distribute water according to the production calendar of each region.
- Divide the ecological zoning according to the saltwater value, such as freshwater (< 1 psu: saltwater tolerance of plants), brackish (1-16 psu), and saltwater (>16 psu: saltwater threshold which is suitable shrimp farming). To have a basis for dividing water use and corresponding production zoning, the author uses the model results for the Baseline scale to partition the VMD into 3 parts according to the above saline boundary as shown in Figure 7.5.

7.2.2.4 Saving water use:

In In the situation of more freshwater scarcity in the VMD, farmers need to save water by using an irrigation system. For example, many farming's use drip irrigation systems to deliver water directly to a plant's roots, reducing the evaporation that happens with spray watering systems. Setting the timers to schedule watering for the cooler part of the day will further reduce water loss.

The farmers should cover the crop surface to protect soil that would otherwise be left bare. Covering crops reduce weeds, increase soil fertility and organic matter, and help prevent erosion and compaction. This allows water to more easily penetrate the soil and improves its water-holding capacity. The cover is a material spread on top of the soil to conserve moisture. Mulch made from organic materials such as straw or wood chips will break down into compost, further increasing the soil's ability to retain water.

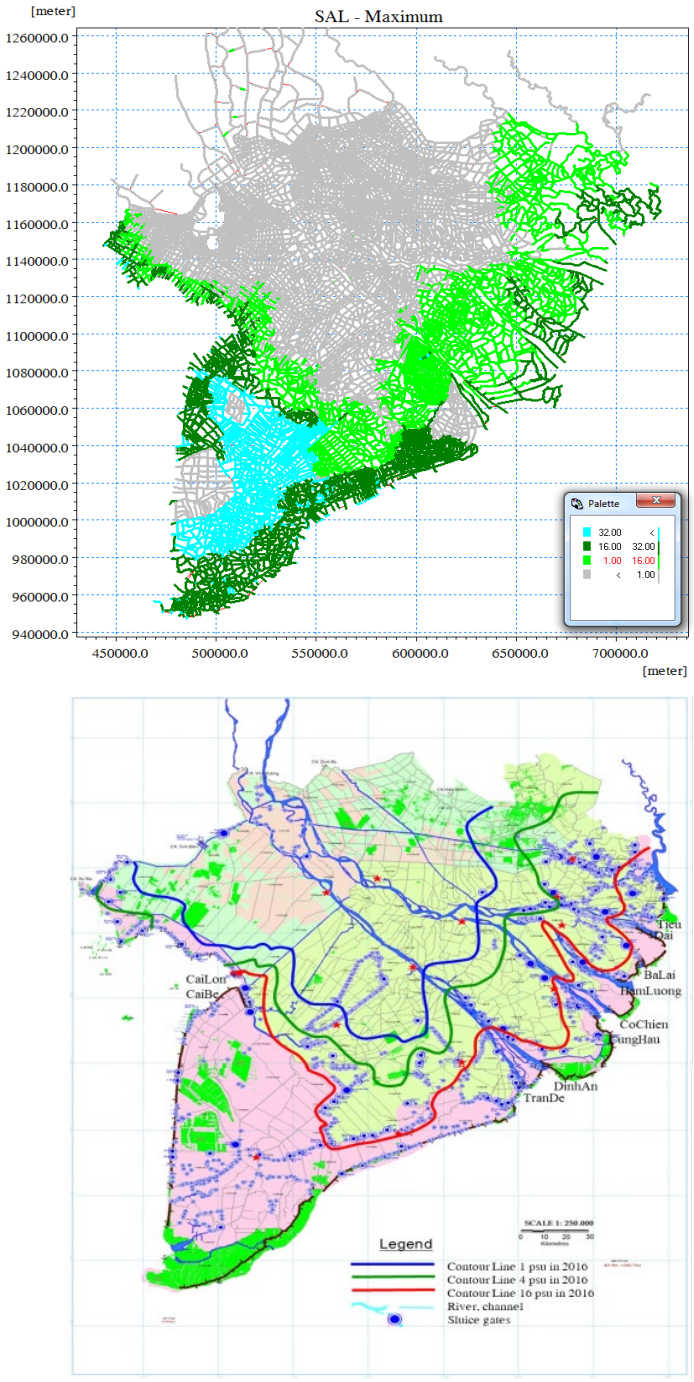

Figure 7.5 Saltwater results by three partitions as above (freshwater < 1psu, brackish water: 1-16 psu) (a) by the numerical model, (b) map of the contour lines

7.2.2.5. Improve infrastructure systems for saltwater control and long-term water supply

1. The status of hydraulic works in the VMD (statistics on 2012)

- For irrigation and water supply: the VMD has more than 15,000 km of main canals and level 1 canals, nearly 27,000 km of level 2 canals, about 50,000 level 3 canals and infield canals, 80 sluice gates over 5 m wide (the largest sluice gates are the Lang The sluices at 100 m and the Ba Lai sluices at 84 m), over 800 sluice gates that are 2-4 m wide and tens of thousands of sluices and small pipes, over 1,000 large and medium-sized electric pumping stations, and tens of thousands of small pumps for active irrigation and drainage (Table 7.2).
- For flood control: the Mekong Delta flooded area has formed a system of river dikes and low ring dikes with a total length of about 13,000 km, including 7,000 km of low dike rings to prevent August floods and protect the Summer-Autumn rice crop. In addition, there are more than 200 km of ring dikes to store fire-proof water for National Parks and Melaleuca forests.
- For controlling salinity and tides: the coastal area of the MD has built 450 km of sea dikes, 1,290 km of river dikes and about 7,000 km of ring dikes along inland canals to prevent saltwater, high tides, and storm surges from the coastal area.
- Water supply for urban areas: most of the residents in towns and cities in the MD are provided with clean water (though there is not enough water in some places). Meanwhile, people in rural areas are only provided with hygienic water at the rate of about 40%.

Table 7.2 Statistics of major hydraulic works in the Vietnam Mekong Delta

No.	Hydraulic works	VMD		The right of Tien River		Between the Tien - Hau River		Long xuyên quadrangle		CaMau Peninsula	
		No.	L(km)	No.	L(km)	No.	L(km)	No.	L(km)	No.	L(km)
1	Main canal	133	3.190	45	1.068	32	1.039	64	1.056	36	633
2	Canal level 1	1015	10.961	343	3.116	200	1.945			428	5.294
3	Canal level 2	7656	26.894	2.187	6.742	1.072	3.363	2.313	7.374	3.297	13.689
4	Canal level 3	36.853	50.019	3.400	7.200	24.773	21.853			7.467	16.692
5	Sluices (B>5m)	984		169		455		38		322	
6	Sluices (B<5m)	20.517		2.491		10.111		1.915		6.000	
7	Low ring dikes		13.332		7.099		1.748		4.485		
8	River dykes		281				281				
9	Sea dykes		523		21		133		63		306
10	Pumping	1.151		338		494		319			

Among the above, the systems of sluices, river dikes, and ring dikes in high salinity areas have received investment but have not yet been completed (closed), so there is still pollution of water sources. Also, the environment and construction work efficiency are not high. The sea dike, river dike, and sluices at TranDe, DinhAn, Cung Hau estuaries have been closed, but the height of dikes is still low and needs to be upgraded. Along the left bank of the CoChien and HamLuong rivers,

the dikes system has been completed, but the sluice system has not been closed, so the whole province of BenTre is affected by the 4 psu salinity line. Besides, the operation process of the sluice systems has many shortcomings due to conflicts in water use purposes, so the efficiency of the works is limited. Large electric pumping stations are degraded because they were built before 1990 and many small electric and gasoline pumping stations work to cover 70-80% of the cultivated area.

2. Some mitigation measures:

● It is necessary to create a new land use plan in coastal areas, scheduled seasonally to develop effective operating procedures for sluices and pumping stations. Shifting the land use from agriculture to aquaculture in areas intruded by saltwater may be an effective alternative to increase income and to adapt to new flow regime conditions. Ca Mau Province is a good model of such land use change. However, aquaculture farming practices must be friendly to the environment and systems. When the estuary is aquatic, the sluices to prevent saltwater from intruding into the estuary about 15-20 km do not need to be closed in the dry season, so saltwater will not intrude deeper upstream. However, it is necessary to build small sluice systems at the boundary of aquaculture and rice cultivation so that saltwater does not penetrate deep upstream of the tributary canal.

● Critical concerns of salinity intrusion management in the VMD determine the quantity and location of salinity control sluice gates, which have been increasingly built and planned along the Tien and Hau rivers over the last decade. Along the left side of the Hau river (DinhAn branch), for example, in response to increasing salinity intrusion, the Vietnamese government built 7 sluice gates in 1998–2005 and an additional three in 2005–2016 from a limited number before 1998; the salinity intrusion length in 2016 increased by 21 km from that of 1998 (Figure 7.6). An additional five sluice gates are under construction, and many are planned in the Hau River (locations are shown in Figure 7.6).

● When sluice gates are completed and closed, the salinity intrusion length in the Hau river may increase more significantly. The situation is the same in other branches of the Tien river. Therefore, we propose to construct new sluice gates along the main rivers in the VMD after a comprehensive assessment of the location and operation routines. Re-evaluation of existing structures is needed, which should pay special attention to clarify the relation between recently

increased sluice gate construction and the increased salinity intrusion length. In this regard, early emergency water release from upstream dams may partly reduce salinity intrusion in the VMD.

● The result of vertical salinity distribution shows the maximum salinity at the bottom and minimum salinity on the surface (Part 6.2.3). Therefore, to extend the time to intake fresh water, the gate should be installed to take water from the surface to the bottom. That means the vertical gate or flap gate type should be replaced with the swing gates, vertical gates which are very popular at VMD. If sluice gate combines with navigation, both swing gates and double vertical gates should be installed for different numbers of gates at one location.

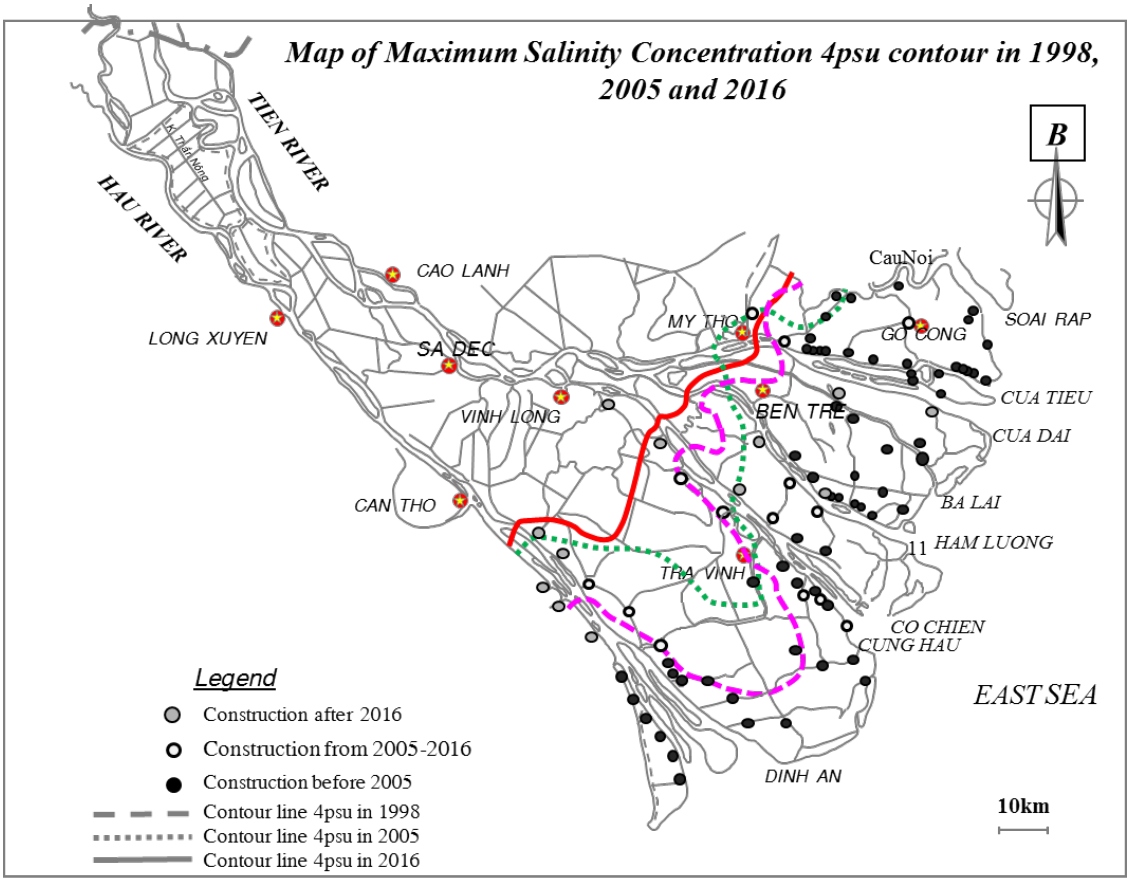

Figure 7.6: The location of sluice gates and contour map of salinity concentration of 4psu of severe drought years in 1998, 2005, and 2016 in the VMD showing increasing intrusion length in recent year

● We can use the flap gate to take the surface water with low salinity concentration but the smooth and steady operation of the flap gate will be prevented due to sedimentation. Moreover,

maintenance is difficult since almost all of this gate will be submerged. This paper recommends that vertical gates with double-leaf type be used for next new salinity control sluice gates.

- Building supplementary fresh water sources systems from upstream in the dry season for the following two areas (Figure 7.7):

+ GiongTrom - BaTri area: at the beginning of the dry season, water is collected from the Ben Tre river and the HamLuong river. If the saltwater is high, use the TanPhu pumping station to get water from the Tien River and pump it to the Ben Tre River.

+ Nam Mang Thit area in TraVinh province. Due to the high saltwater intrusion in the early dry season in recent years, the sluices along the CoChien and Hau rivers have to be closed early, which means a lack of fresh water supply into the lower districts (CauKe, CauQuan, TraCu,). When the intrusion length is below 45km, fresh water from TanDinh and BongBot sluices on the Hau River and from VungLiem and CaiHop sluices on the CoChien river take water to the TraNgoa - LaBan canal as the main shaft to transfer water downwards through 2 combined sluice-pump stations.

- The river bed and estuaries are lowered by 74.6% reduction in sediment erosion to the VMD (in section 5.1), due to sand mining or dredging. It is also the cause of increasingly serious saltwater intrusion. A solution is to increase the estuarine sediment content to form natural dunes to prevent salinity. Figure 7.8 illustrates the evolution of saltwater intrusion length when the estuary forms a Dune with the length equal to the river width and 3m of the height which locates at 5km from DinhAn estuary. Compared with the baseline scenario Sce0, the salinity concentration decreased only slightly, the maximum value reduction of S_{max} was 0.41 psu. However, the intrusion length was reduced by 5km.

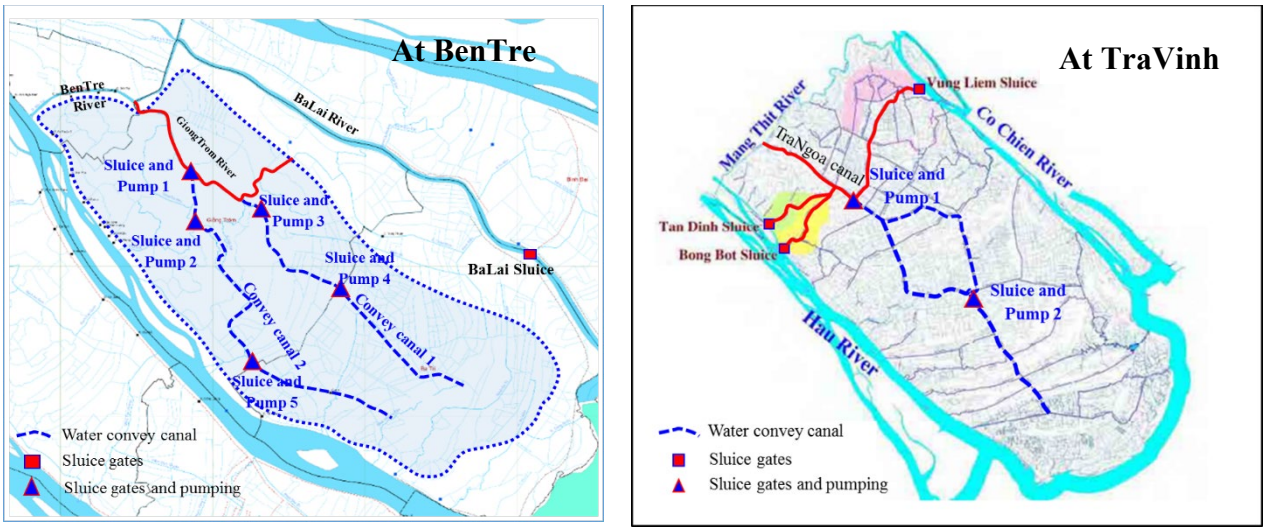

Figure 7.7: The water convey canal project in BenTre and TraVinh provinces

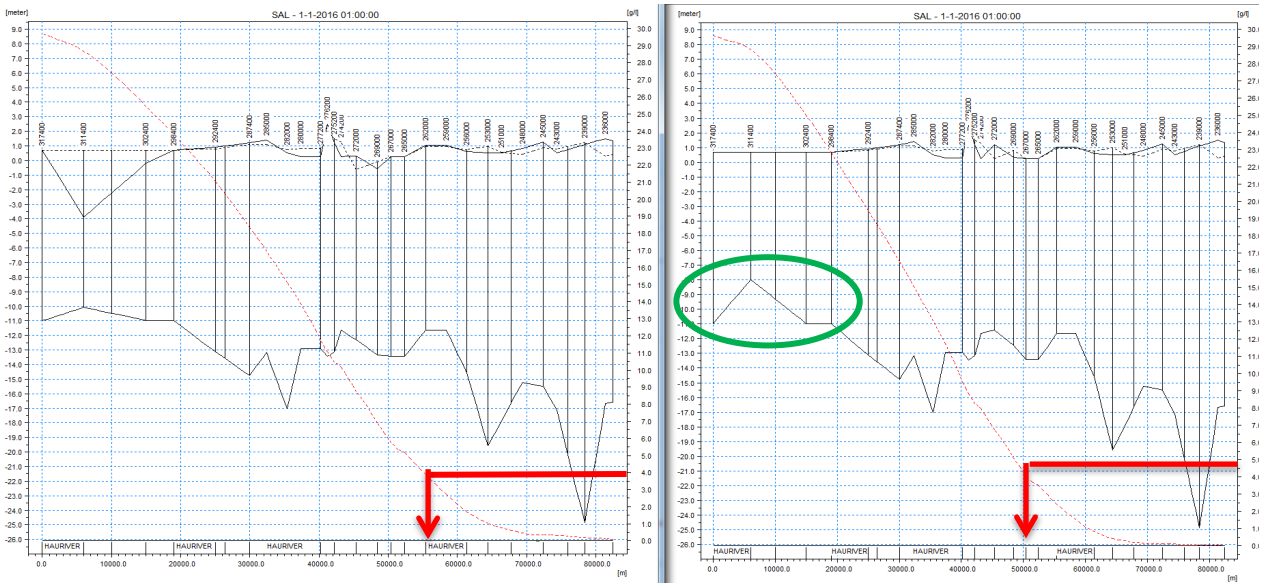

Figure 7.8: The intrusion length of baseline scenario (a) and mitigation scenario by Dune at 5km far from the estuary(b)

7.2.2.6 Small-scale, household water storage

1. Small-scale water storage: Using the lowland zones or canals without navigation to store water from the rainy season, or pump fresh water at low tide (Figure 7.9 and 7.10)

2. The farmers should build their ponds, ditches to capture and store rainfall water or fresh water for domestic use and watering fruit trees. Areas with ponds and ditches account for about 5-10% of fields and gardens areas (Figure 7.11)

3. For domestic use, the farmers can store water in jars, underground rainwater tanks, or large-sized water storage bags.

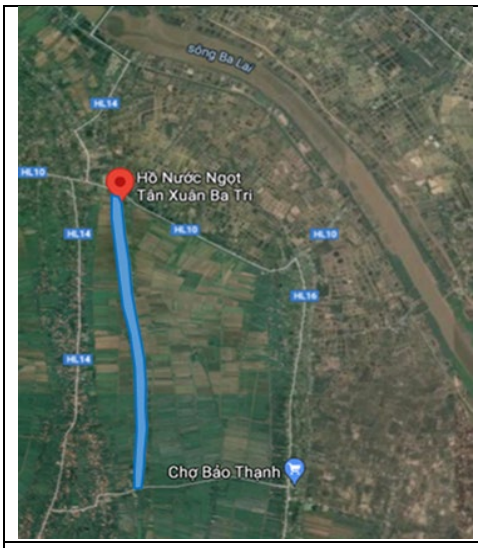

Figure 7.9 Freshwater reservoir in BaTri – ***BenTre with capacity 800.000m3 to supply*** for about 200.000 people. (Existing in 2017)

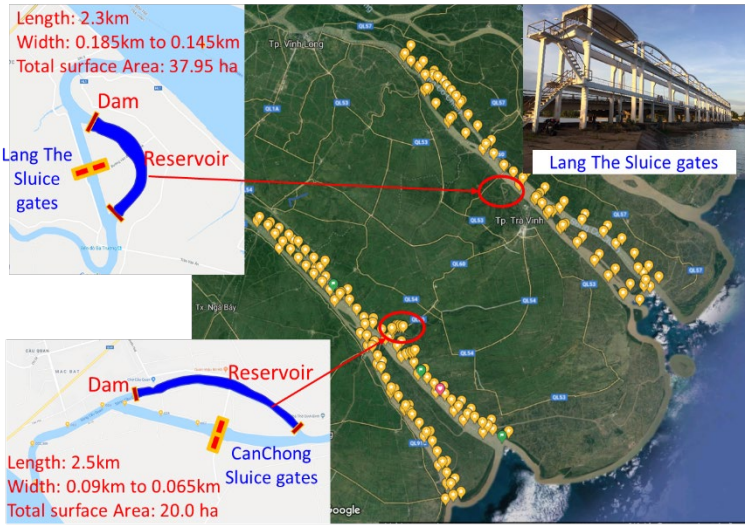

Figure 7.10 Using the old branches after construction the sluice gates to conduct the freshwater reservoirs in TraVinh province.

Figure 7.11 Some kind of storing freshwater of the famers in TraVinh province.

7.3 Conclusion

The results of analysis of the influence of upstream flows, lowering of the riverbed, climate change, and tides on salinity intrusion presented in chapters 4, 5 and 6 have shown the challenges facing VMD during this period and future. It was found that salinity appears early, penetrates deeply, and lasts longer due to the change of flow, the reduction of sediment in the VMD caused by the upstream dam development, sea-level rise, and an increase of tidal amplitudes. The changes of inflow and sediment in the river and canals of the VMD are difficult to control. Therefore, the adaptation solutions would be suitable for reducing the impacts of SI on VMD. There are seven mitigation solutions that could be considered, which consist of four non-structural solutions (early warning, long-term adaptation plans, long term water use plan, saving water use) and three structural solutions (improve infrastructures, household water storage, and keeping flood inundation areas) as mentioned earlier. If most of the above-mentioned solutions are applied simultaneously and continuously; the results will be very effective. Particularly for the solution number 5: improve infrastructure, it is necessary to have a plan, a roadmap for implementation, funding sources, an assessment of the level of impact on the environment and how to effectively manage the project in the long term.

Chapter 8: Conclusions and Recommendation

The main objectives of this study are to investigate the influences of the upstream dams development, morphological changes, sea-level rise and tidal regime on salinity intrusion in the VMD. The hypothesis of this study is that the development and operation of large upstream dams are the main cause of the change in the flow and reduction of sediment downstream. Therefore, this study used the long-term series of water level, discharge and sediment data at Chiang Saen, Kratie and TanChau, and ChauDoc stations to analyze the altered flow and sediment in the VMD. In addition, data analysis (water levels, tides, and salinity time series) and numerical simulation models were also used to assess the impact of those changes on the saltwater intrusion mechanism in VMD through four scenarios, two scenarios for flow, and the other two for morphology changes. More specially, to show the impact of the tide on the salinity intrusion mechanism and salt distribution along the river, three salinity measurements were carried out along more than 50km from the estuary of four tributaries of TranDe, DinhAn, CungHau and CoChien rivers. Based on characteristics of seawater intrusion and its related environmental issues, the study proposed adaptation solutions to sustainable water resources development

8.1 The impact of upstream dams

- It was identified that capacity storage of six large dams in the upper Mekong River basin accounts for more than 49% of the total flow in Chiang Saen (CS). Therefore, those reservoirs cause changes of flow regime by shifting more discharge from the wet season to the dry season. More specially, the total wet season water volume has decreased by more than 27% and 3% (10.4 km^2) at CS and Kratie respectively. In addition, the maximum annual discharge value (Q_{max}) also decreased rapidly with a reduced rate of 33.3% from the 1^{st} period to the 3^{rd} period (67.76 $m^3/s/yr$) at CS and 3.1% at Kratie. Meanwhile, the total dry flow increased 20.96% at CS and 34.83% (10.5 km^2) at Kratie. As a result, the ratio of W_{dry}/W_{total} at Kratie changed from 12.3% in the no dam period to 16.6% in the completed dam period.
- It was also found that upstream hydropower dams have a strong impact on the dry flow, creating more fluctuations which the flow has increased from March to May while it has decreased from November to February in the 3rd period. Hence, salinity concentration rises from November

and maintains a high concentration from December to February and reaches its peak value in February. Eventually, the highest salinity concentration appeared nearly two months earlier, saltwater intruded further inland and remained longer during the dry season.

- The simulation results show that reduction of 346 m^3/s (12.2%) discharges at Kratie, the S_{max}, at stations located 30 km from the sea may increase by 14.0%÷23.2% compared to those of the baseline and the intrusion length intruded four to eight km further upstream. This fact reveals that salinity concentration in the VMD will be extremely high in the short-term if the upstream reservoirs have abnormal operating procedures.
- One mitigation scenario considered is to release water from the upstream hydropower dams one month earlier (27th March to 27th February). By doing this, salinity concentrations gradually reduce during March; particularly, the concentrations were reduced by 11.6% and 15.9% on 13th March because of increasing the discharge by 5.1% and 6.9% at DaiNgai and TraVinh stations, respectively. The intrusion length would also decrease by about 7.0-10.0 km.
- Furthermore, the upstream reservoirs trapped most of the sediment flow. The annual sediment load was reduced from 166.4 Mt in the no dam period to 59.7 Mt (64.1%) in the building dam period and 42.3 Mt (74.6%) in the completed dam period. This is the main cause of erosion or incision of the bottom topography of the Hau and Tien rivers in the VMD.
- I have noted that the mean incision rate from ChauDoc to CanTho (0.22 m/yr) is more than three times the incision rate from CanTho to the DinhAn estuary (0.07 m/yr). While the mean incision rate in the upper and lower part of Tien (CoChien branch) is 0.34 m/yr and 0.19 m/yr respectively.
- The numerical simulation for Sce4, if 1.76m and 2.76 riverbed incisions were simulated in the Hau and Tien rivers, would see salinity concentration increase by 0.8-0.9 psu and the salinity intrusion would extend to 1.8 km and 4.5km further upstream.
-

8.2 The impact of tide and sea level rise

The observed data between 1980 and 2020 shows that the sea level at VungTau station has an increasing trend with a rate of 5.25 mm/yr. Likewise, observation data also showed that sea-level fluctuations had a significant influence on the salinity concentration from October to February.

It is predicted that if the sea-level rises by 47.25 mm in next five years, it will lead to the expansion of the salinity profile from four to seven km further upstream and the concentration of salinity increased by 1.4 to 1.9 psu.

- The field survey results showed that salinity concentration is usually higher at the deeper level and tends to decrease at the near surface level while it has also decreased about 50km from the coast to inland.

- The intrusion length of 0.4 psu at the flood tide is 42.3 km, 45km, and 51.5 km longer than 14.3km, 15km, 16.5km that of the ebb tide in the TranDe, DinhAn and CoChien branches respectively. These distances are meaningful for dividing ecological zones between fresh water, brackish water, and salt water areas. .

- The tidal wave propagation into the DinhAn estuary is a standing wave with the phase lag between High water-high water slack and Low water – low water slack is approximately 0.

- During one daily tidal cycle, S_{max} at the surface coincided with WL_{max} and S_{min} is simultaneous with low water. Meanwhile, S_{max} at the bottom lagged one to three hours after WL_{max} depend on the location, and S_{max} at the bottom occurs at the transition period from flood to ebb tides during the daily cycle while the opposite happens with S_{min} at the bottom occurs at the transition period from ebb to flood tides.

- During the spring-neap tidal cycle, S_{max} at the bottom occurs at the transition period from neap to spring tides (3-7 days before spring tide) while S_{min} appears at the transition period from spring to neap tides.

- The mixing and stratification processes are influenced by dam discharges, sea level, tidal range, and seaward and riverward flow velocity. During the spring tide from 2nd to 5th March 2018, vertical and longitudinal distribution of salinity along 50km of the DinhAn and TranDe branch verifies that partial mixing and moderate stratification prevail over the TranDe and DinhAn branch because the Pritchard number (n) is less than 1. In the neap tide period from 21st to 22nd April 2019, weak mixing and strong stratification appeared in DinhAn and TranDe branches because the value of α, E_ρ and R_{iE} parameters were in the range of type III of salinity intrusion. Similarly, partial mixing and moderate stratification appears along 50km of the CoChien River in the ebb tide and weak mixing and strong stratification prevails in the CoChien branch in the flood tide during the neap tide on 6th to 7th April 2018.

- The results of mixing and stratification are a basic reference for the operation of salinity control sluice gates and understanding these helps to find the appropriate time of opening gates to take in freshwater.

Three scenarios Sce1, Sce4 and Sce5 have considered the impacts of upstream flow changing scenario, morphology changing scenario and sea-level rise scenario on salinity intrusion in 2025. Table 8.1 shows the maximum salinity values of three scenarios occurring on April 10th, then the S_{max} results that changed from the baseline scenario Sce0 to Sce1, Sce4, and Sce5 at DaiNgai were 7.4 psu, 8.4 psu, 8.1 psu and 8.9 psu respectively. The longest salinity intrusion length in April on the Hau River, corresponding to four scenarios Sce0 to Sce1, Sce4, and Sce5 is 41km, 45km, 42.8km and 47.7km. While, Sce5 is a combination of Sce1 plus 47.25 mm SLR, so the actual effect of SLR on salinity is 6.8% to 8.2%. Therefore, the flow factor has the main factor in SI. Tide also has a great influence on salinity, especially in salinity transmission, diffusion and distribution in rivers. The influence of tide always occurs simultaneously with the scenarios mentioned above.

Table 8.1 Compare the impacts of three driven factors on Salinity intrusion on 10th April 2016

Salinity concentration at about 30km from the estuaries.								**L_{max} of 4 psu**	
No.	Scenario	DaiNgai Station (psu)		CauQuan Station (psu)		TraVinh Station (psu)		In Hau River	In CoChien River
		Salinity	(P%)	Salinity	(P%)	Salinity	(P%)	(km)	(km)
1	Sce0	7.4		5.4		4.9		41	35
2	Sce 1	8.4	13.5	6.4	18.5	6.0	22.4	45	40
3	Sce 4	7.9	6.8	6.05	12.0	5.6	14.3	42.5	39.5
4	Sce 5	8.9	20.3	6.9	27.8	6.4	30.6	47.7	43

8.3 Recommendation

- In addition to four factors affecting saltwater intrusion as mentioned above, human activities are also an important factor which has great impacts on saline intrusion. Therefore, managers and scientists should make their decisions after evaluating the effectiveness of projects in the long-term and analyzing environmental impact assessments.

- It is necessary to develop a detailed map of salinity zoning according to salinity concentration and salinity retention time as a basis for building a map of agro-ecological zoning between fresh, brackish, and salt water. Land use planning is highly recommended to follow these ecological zones in order to avoid conflicts of water uses. Also, it is important to set up appropriate operation rules for sluice gates and pumping stations.

- Constructing more sluice gates and small pumping stations at ecological zoning boundaries between fresh-brackish regions would help protect the freshwater areas from saltwater intrusion.

- New farming models would be a suitable option to consider, with options that differ in freshwater ecology (cultivation), brackish water ecology (salt- brackish aquaculture, or a combination of shrimp and rice), or alternate brackish-freshwater ecology.

- It is reasonable to consider the alternative freshwater resources in coastal areas by storing, pumping, and transferring freshwater from inland to the coast.

- The Mekong River flows through the territory of China, Myanmar, Laos, Thailand, Cambodia and Vietnam. Therefore, the collaboration among these countries to find a strategy for sustainable management of the river basin is critical. In particular, sharing data and installing more automatic measuring stations for water level, sand, and water quality data along the main river are needed. Furthermore, encouraging reservoir owners to share the reservoir operation rules to downstream countries allows all parties to be proactive in their plans to exploit and distribute water sources.

-

8.4 Outlook for future works

To follow up on the results and limitations of this research, some research directions should be addressed in future works:

1. It is highly recommended to use 3D modeling to answer how the spatial and temporal salinity distribution occurs in seven MR estuaries in different timescales while accounting for the daily, weekly, monthly and seasonal tidal cycles.
2. More accuracy in determining the boundaries of the three salinity ecological zones (Freshwater - Brackish water - Saltwater) is crucial to effective water use and planning land use.

3. Future studies can investigate the impact of water use on salinity processes and propose plans for land use that have less effect on salinity intrusion (SI) which is necessary to make effective use of agricultural land in the VMD.
4. Early forecast of flow changes and their impacts on SI when all upstream dams should be constructed in the near future.
5. Studying the impacts of three factors of flow, geomorphology and SLR according to long-term forecasting scenarios according to climate change scenarios for the middle and late 21st century. The purpose is to evaluate the impact of salinity intrusion on VMD in the long future.

References

Allison, M.A., Dallon Weathers, H., Meselhe, E.A., 2017a. Bottom morphology in the Song Hau distributary channel, Mekong River Delta, Vietnam. Cont. Shelf Res. 147, 51–61. doi:10.1016/j.csr.2017.05.010.

Allison, M.A., Nittrouer, C.A., Ogston, A.S., Mullarney, J.C., Nguyen, T.T., 2017b. Sedimentation and survival of the Mekong Delta: A case study of decreased sediment supply and accelerating rates of relative sea level rise. Oceanography 30, 98–109. doi:10.5670/oceanog.2017.318.

Annandale, G.., 2012. A Climate Resilient Mekong: Sediment Pass-Through at Sambor Dam, in: Golder Assoc. Inc., Lakewood, CO, Nat. Heritage Inst., San Francisco, Calif.

Anthony, E.J., Brunier, G., Besset, M., Goichot, M., Dussouillez, P., Nguyen, V.L., 2015. Linking rapid erosion of the Mekong River delta to human activities. Sci. Rep. 5, 1–12. doi:10.1038/srep14745.

Arias, M.E., Cochrane, T.A., Kummu, M., Lauri, H., Holtgrieve, G.W., Koponen, J., Piman, T., 2014. Impacts of hydropower and climate change on drivers of ecological productivity of Southeast Asia's most important wetland. Ecol. Modell. 272, 252–263. doi:10.1016/j.ecolmodel.2013.10.015.

Binh, D.V., Kantoush, S., Mai, N.P., Sumi, T., 2018a. Water level changes under increased regulated flows and degraded river in Vietnamese Mekong Delta. J. Japan Soc. Civ. Eng. Ser. B1 Hydraulic Eng. 74, 871–876.

Binh, D.V., Kantoush, S., Sumi, T., Mai, N.P., 2018b. Impact of Lancang cascade dams on flow regimes of Vietnamese Mekong Delta. Annu. J. Hydraul. Eng. JSCE 62.

Bravard, J.P., Goichot, M., Gaillot, S., 2013. Geography of Sand and Gravel Mining in the Lower Mekong River: First Survey and Impact Assessment. EchoGéo 26, 1–18.

Brunier, G., Anthony, E.J., Goichot, M., Provansal, M., Dussouillez, P., 2014. Recent morphological changes in the Mekong and Bassac river channels, Mekong delta: The marked impact of river-bed mining and implications for delta destabilisation. Geomorphology 224, 177–191. doi:10.1016/j.geomorph.2014.07.009.

Chapman, A., Darby, S., 2016. Evaluating sustainable adaptation strategies for vulnerable mega-deltas using system dynamics modelling: Rice agriculture in the Mekong Delta's An Giang Province, Vietnam. Sci. Total Environ. 559, 326–338. doi:10.1016/j.scitotenv.2016.02.162.

Chapman, E. C., He, D., (1996 Downstream implications of Chinas dams on the Lancang Jiang (Upper Mekong) and their potential significance for greater regional cooperation. Australian National Mekong Resource Centre, Sydney

CGIAR, 2016. Assessment Report: The drought and salinity intrusion in the Mekong River Delta of Vietnam. In: Research Program on Climate Change, Agriculture and Food Security 1.1, pp. 1–54.

Cameron, W. M., and Pritchard, D. W., 1963. Estuaries. In: M. N. Hill (editor), The Sea vol. 2. John Wiley and Sons, New York, pp. 306 - 324.

Dang, D.T., Cochrane, T.A., Arias, M.E., Tri, V.P.., 2018. Future hydrological alterations in the Mekong Delta under the impact of water resources development, land subsidence and sea level rise. J. Hydrol. Reg. Stud. 15, 119–133. doi:10.1016/j.ejrh.2017.12.002.

Dang, T.D., Cochrane, T.A., Arias, M.E., Van, P.D.T., Vries, T.T.D., 2016. Hydrological alterations from water infrastructure development in the Mekong floodplains. Hydrol. Process. 30, 3824–3838. doi:10.1002/hyp.10894.

DHI-HDR, 2015. Study on the Impacts of Mainstream Hydropower on the Mekong River. Impact Assessment Report. Volume 1-Models, Model Setup and Simulation, Ministry of Natural Resources and Environment.

DHI, 2009. Mike 11: A Modelling System for Rivers and Channels: Reference Manual.

Dyer, K.R., and New, A.L., 1986. Intermittency in Estuarine Mixing. Estuarine Variability, New York: Acad. Press.

Dyer, K.R., 1995. Sediment transport processes in estuaries. In: G.M.E. Perillo (ed.), Geomorphology and sedimentology of estuaries. Elsevier, Amsterdam, pp. 423 – 447.

Dyer, K.R., 1997. Estuaries, a physical introduction, second edition. John Wiley, London, 195 pp.

Doyle, T.W., Day, R.H., Michot, T.C., 2010. Development of sea level rise scenarios for climate change assessments of the Mekong Delta, Vietnam. U.S. Geol. Surv. Open-File Rep. 2010-1165 110 pp.

Duong, T.A., Hoang, L. P., Minh, B.D., Peter, R., 2017. Simulating Future Flows and Salinity Intrusion Using Combined One- and Two-Dimensional Hydrodynamic Modelling—The Case of Hau River, Vietnamese Mekong Delta. MDPI Water Journal, doi:10.3390/w10070897.

Eslami, S., Hoekstra, P., Kernkamp, H., Trung, N. N., Do Duc, D., Quang, T. T., Februarianto, M.,

Van Dam, A. and Van Der Vegt, M., 2019a. Flow Division Dynamics in the Mekong Delta: Application of a 1D-2D Coupled Model, Water, 11, https://doi.org/10.3390/w11040837, 2019a.

Eslami, S., Hoekstra, P., Trung, N. N., Kantoush, S. A., Binh, D. V., Dung, D. D., Quang, T. T., & Vegt, M. V. D. ,2019. Tidal amplification and salt intrusion in the Mekong Delta driven by anthropogenic sediment starvation. Scientific Reports, 9, 18746.

Fan, H., He, D., 2015. Temperature and Precipitation Variability and Its Effects on Streamflow in the Upstream Regions of the Lancang – Mekong and Nu – Salween Rivers. J. Hydrometeorol. 2248–2263. doi:10.1175/JHM-D-14-0238.1.

Fan, H., He, D., Wang, H., 2015. Environmental consequences of damming the mainstream Lancang-Mekong river: A review. Earth-Science Rev. 146, 77–91. doi:10.1016/j.earscirev.2015.03.007.

Fischer, H.B., Imberger, J., John List, E., Koh, R. C.Y., 1979. Brooks, N.H.: The book of Mixing in the Inland and Coastal Waters, Academic Press, INC, pp1- 483.

Gugliotta, M., Saito, Y., Nguyen, V.L., Ta, T.K.O., Nakashima, R., Tamura, T., Uehara, K., Katsuki, K., Yamamoto, S., 2017. Process regime, salinity, morphological, and sedimentary trends along the fluvial to marine transition zone of the mixed-energy Mekong River delta, Vietnam. Cont. Shelf Res. 147, 7–26. doi:10.1016/j.csr.2017.03.001.

Gong, W., Wang, Y., and Jia, J., 2012. The effect of interacting downstream branches on saltwater intrusion in the Modaomen Estuary, China. Journal of Asian Earth Sciences 45, 223-238.

Gong, W., Shen, J., 2011. Response of salt intrusion to changing river flow and tidal amplitude during winter season in the Modaomen Estuary, Pearl River Delta area, China. Continental Shelf Research 31, 769–788.

Gong, W., Lin, Z., Chen, Y., Chen, Z., Zhang, H., 2018. Effect of winds and waves on salt intrusion in the Pearl River estuary. Ocean Science, Vol. 14, 139-159.

Ha, D.T., Ouillon, S., Vinh, G.V., 2018. Water and Suspended Sediment Budgets in the Lower Mekong from High-Frequency Measurements (2009–2016). Water 10, 1–24. doi:10.3390/w10070846.

Hoang, P.L., Lauri, H., Kummu, M., Koponen, J., Vliet, M.T.H.V., Supit, I., Leemans, R., Kabat, P., Ludwig, F., 2016. Mekong River flow and hydrological extremes under climate change. Hydrol. Earth Syst. Sci. 20, 3027–3041. doi:10.5194/hess-20-3027-2016.

Hoanh, C.T., Jirayoot, K., Lacomne, G., Srunetr, V., 2010. Impacts of climate change and development on Mekong flow regimes First assessment – 2009, MRC Management Information Booklet Series No.4. doi: Mekong River Commission, Vientiane, Lao PDR.

Hong,B., Liu, Z., Shen, J., Wu, H., Gong, W., 2020. Potential physical impacts of sea-level rise on the Pearl River. Journal of Marine Systems. 201, 103245. doi.org/10.1016/j.jmarsys.2019.103245.

Hwang, J. H., Jang, D., Kim, Y. H., 2017. Stratification and Salt-wedge in the Seomjin River Estuary under the Idealized Tidal Influence. Ocean Science Journal. . doi.org/10.1007/s12601-017-0050-3.

IPPC report, 2016. Scenarios of Climate change and sea level rise for Vietnam, Ministry of Natural Resources and Environment. Vietnam Publishing House of Natural Resources, Environment and Cartography, pp. 1-188.

Khang, N.D., Kotera, A., Sakamoto, T., Yokozawa, M., 2008. Sensitivity of salinity intrusion to sea level rise and river flow change in Vietnamese Mekong Delta impacts on availability of irrigation water for rice cropping. Agriculture Meteorology Journal, 64(3):167-176.

Kantoush, S., Binh, D.V., Sumi, T., Trung, L.V., 2017. Impact of Upstream Hydropower Dams and Climate Change on Hydrodynamics of Vietnamese Mekong Delta. J. Japan Soc. Civ. Eng. Ser. B1 (Hydraulic Eng. 73, I_109-I_114.

Kondolf, G.M., Gao, Y., Annandale, G.W., Morris, G.L., Jiang, E., Zhang, J., Cao, Y., Carling, P., Fu, K., Guo, Q., Hotchkiss, R., Peteuil, C., Sumi, T., Wang, H.W., Wang, Z., Wei, Z., Wu, B., Wu, C., Yang, C.T., 2014. Sustainable sediment management in reservoirs and regulated rivers: Experiences from five continents. Earth's Futur. 2, 256–280. doi:10.1002/2013EF000184.

Kondolf, G.M., Rubin, Z.K., Minear, J.T., 2014. Dams on the Mekong: Cumulative sediment starvation. Water Resour. Res. 50, 5158–5169. doi:10.1002/2013WR014651.

Kondolf, G.M., Schmitt, R.J.P., Carling, P., Darby, S., Arias, M., Bizzi, S., Castelletti, A., Cochrane, T.A., Gibson, S., Kummu, M., Oeurng, C., Rubin, Z., Wild, T., 2018. Changing sediment budget of the Mekong: Cumulative threats and management strategies for a large river basin. Sci. Total Environ. 625, 114–134. doi:10.1016/j.scitotenv.2017.11.361.

Kuenze, C., Campbell, I., Roch, M., Leinenkugel, P., Tuan, V.Q., Dech, S., 2012. Understanding the impact of hydropower developments in the context of upstream-downstream relations in

the Mekong river basin. Sustainability Science, Vol.8, pp.565-584.

Lauri, H., De Moel, H., Ward, P.J., Räsänen, T.A., Keskinen, M., Kummu, M., 2012. Future changes in Mekong River hydrology: Impact of climate change and reservoir operation on discharge. Hydrol. Earth Syst. Sci. 16, 4603–4619. doi:10.5194/hess-16-4603-2012.

Nhan N. H., 2016. Tidal regime deformation by sea level rise along the coast of the Mekong Delta. Estuanire, Coastal and Shelf Science xxx, 1-10.

Nhan, N. H., and Nguyen B., C., 2019. Damming the Mekong: Impacts in the Vietnam and Solutions in Chapter 19, Book of Coastal and Estuaries: The Future., Amsterdam: Elsevier.

Nguyen, A.D., Savenije, H.H.G., Pham, D.N., Tang, T.D., 2008. Using salt intrusion measurements to determine the freshwater discharge distribution over the branches of a multi-channel estuary: the Mekong Delta case. Estuarine, Coastal and Shelf Science 77 (3), 433–445.

Nguyen, A.D. Savenije, H.H., 2006. Salt intrusion in multi-channel estuaries: a case study in the Mekong Delta, Vietnam. Hydrology and Earth System Sciences Discussions 10.5, pp. 743–754.

Nguyen, H.T., Gupta, A.S., 2001. Assessment of Water resources and salinity intrusion in the Mekong Delta. Water international 26.1, pp. 86–95.

M. v. Mikhailova, 2013. Processes of Seawater Intrusion into River Mouth. Water Resources, Vol. 40, No. 5, pp. 483–498.

Mai, N. P., Kantoush, S., Sumi, T., Thang, T. D., Trung, L. V., & Binh, D. V.,2018. Assessing and adapting the impacts of dams operation and sea level rising on saltwater intrusion into the Vietnamese Mekong Delta. Journal of Japan Society of Civil Engineers, Series B1 Hydraulic Engineering, 74, 373–378.

Mai, N.P., Trung, L.V., 2017. The evolution of salinity intrusion at Mekong River Mounths under the impact of Dams Upstream, Journal of Water Resource and Enviroinment Technology, Vol. 58 , pp. 157-163.

Mekong River Commission, 2016. Joint observation and evaluation of the emergency water supplement from China to the Mekong River. MRC technical report, pp. 1-74.

Manh, N.V., Dung, N.V., Hung, N.N., Kummu, M., Merz, B., Apel, H., 2015. Future sediment dynamics in the Mekong Delta floodplains: Impacts of hydropower development, climate change and sea level rise. Glob. Planet. Change 127, 22–33.

doi:10.1016/j.gloplacha.2015.01.001.

MRC, 2016. Annual Flood Report 2016, Mekong River Commission, Vientiane.

J.D. Milliman, K.L. Farnsworth, P.D. Jones, K.H. Xu, L.C., 2008. Smith Climate and anthropogenic factors affecting river discharge to the global ocean, 1951-2000 Glob. Planet. Change, 62, pp. 187-194

Nowacki, D.J., Ogston, A.S., Nittrouer, C.A., Fricke, A.T., Van, P.D.T., 2015. Sediment dynamics in the lowerMekong River: Transition from tidal river to estuary. J. Geophys. Res. Ocean. 120, 6363–6383. doi:10.1002/2015JC010754.

Orr, S., Pittock, J., Chapagain, A., Dumaresq, D., 2012. Dams on the Mekong River: Lost fish protein and the implications for land and water resources. Glob. Environ. Chang. 22, 925–932. doi:10.1016/j.gloenvcha.2012.06.002.

Pritchard, D.W., 1955. Estuarine circulation patterns. Proc. Am. Soc. Civ. Eng., vol. 81, no. 717, pp. 1–11.

Räsänen, T.A., Koponen, J., Lauri, H., Kummu, M., 2012. Downstream Hydrological Impacts of Hydropower Development in the Upper Mekong Basin. Water Resour. Manag. 26, 3495–3513. doi:10.1007/s11269-012-0087-0.

Räsänen, T.A., Someth, P., Lauri, H., Koponen, J., Sarkkula, J., Kummu, M., 2017. Observed river discharge changes due to hydropower operations in the Upper Mekong Basin. J. Hydrol. 545, 28–41. doi:10.1016/j.jhydrol.2016.12.023.

Smajgl, A., Toan, T.Q., Nhan, D.K., Ward, J., Trung, N.H., Tri, L.Q., Tri, V.P.D., Vu, P.T., 2015. Responding to rising sea levels in the Mekong Delta. Nat. Clim. Chang. 5, 167–174. doi:10.1038/nclimate2469.

Sumi, T., Kobayashi, K., Yamaguchi, K., Tanaka, Y., 2009. Study on the applicability of the assest management for reservoir sediment management, in: International Congress on Large Dams, Q.89-R.4, Brasilia, Brazil.

Sumi, T., Okano, M., Tanaka, Y., 2004. Reservoir sedimentation management with bypass tunnels in Japan, in: Proceedings of the Ninth International Symposium on River Sedimentation, Yichang, China. pp. 1036–1043.

Savenije, H.H.G., 2012. Salinity and Tides in Alluvial Estuaries, Amsterdam: Elsevier, Second Edition.

Toan, T.Q., 2014. Climate Change and Sea Level Rise in the Mekong Delta: Flood, Tidal

Inundation, Salinity Intrusion, and Irrigation Adaptation Methods. In: Coastal Disasters and Climate Change in Vietnam, Elsevier. Elsevier Inc. doi:10.1016/B978-0-12-800007-6.00009-5.

Trieu, T.T.N., Nguyen, T.P., 2015. The impact of climate change on salinity intrusion and Pangasius (Pangasianodon Hypophthalmus) farming in the Mekong Delta, Vietnam. Aquaculture International 23.2, pp. 523–534.

UNESCO, 1991. Guidelines on the study of seawater intrusion into rivers. Studies and Reports in Hydrology, Paris. No. 50.

Uncles, R.J., 2002. Estuarine physical processes research: some recent studies and progress. Estuarine, Coastal and Shelf Science 55 (6), 829-856.

Viet, N. T., Tanaka, H., 2007. Study on the Effect of Morphology Change on Salinity Distribution in the Dinh An Estuary, Lower Mekong River of Vietnam. Journal of Coastal Research, SI 50, 268-272.

Wolanski, E., Huan, N.N., Dao, L.T., Nhan, N.H., Thuy, N.N., 1996. Fine-sediment dynamics in the Mekong River Estuary, Viet Nam. Estuar. Coast. Shelf Sci. 43, 565–582. doi:10.1006/ecss.1996.0088.

Wolanski, E., Nhan, N.H., Spagnol, S., 1998. Sediment dynamics during low flow conditions in the Mekong River Estuary, Vietnam. J. Coast. Res. 14, 472–482.

Wu, X., Xiang, X., Chen, X., Zhang, X., Hua, W., 2018. Effects of cascade reservoir dams on the streamflow and sediment transport in the Wujiang River basin of the Yangtze River , China. Inl. Waters 8, 216–228. doi:10.1080/20442041.2018.1457850.

WUP-JICA, 2004. Vol. II: Supporting report, Paper VII: Maintenance of flows on the Mekong Mainstream. In: The study on Hydro-meteorological monitoring for water quantity rules in Mekong River Basin, Mekong River Commission.

Xing, F., Meselhe, E.A., Allison, M.A., Weathers III, H.D., 2017. Analysis and numerical modeling of the flow and sand dynamics in the lower Song Hau channel, Mekong Delta. Cont. Shelf Res. 147, 62–77. doi:10.1016/j.csr.2017.08.003.

Xue, Z., Liu, J.P., Ge, Q., 2011. Changes in hydrology and sediment delivery of the Mekong River in the last 50 years: Connection to damming, monsoon, and ENSO. Earth Surf. Process. Landforms 36, 296–308. doi:10.1002/esp.2036.

List of publications

Journal papers:

Mai, N.T.P,, Trung, L.V. (2017). The impact of Upstream Dams on the mechanism of salinity intrusion of estuaries of Mekong River, *Journal of Water Resources and Environment*, No. 58, pp. 157-163.

Mai, N.P., Kantoush, S., Sumi, T., Thang, T.D., Trung, L.V., and Binh, D.V. (2018). Assessing and adapting the impacts of dams operation and sea level rising on saltwater intrusion into the Vietnamese Mekong Delta. *Journal of Japan Society of Civil Engineering, Ser. B1 (Hydraulic Engineering)*, Vol. 74, No. 5, pp. I_373-I_378.

Binh, D.V., Kantoush, S., Sumi, T., and Mai, N.P. (2018). Impact of Lancang cascade dams on flow regimes of Vietnamese Mekong Delta. *Journal of Japan Society of Civil Engineering, Ser. B1 (Hydraulic Engineering)*, Vol. 74, No. 4, pp. I_487-I_492.

Binh, D.V., Kantoush, S., Mai, N.P., and Sumi, T. (2018). Water level changes under increased regulated flows and degraded river in Vietnamese Mekong Delta. *Journal of Japan Society of Civil Engineering, Ser. B1 (Hydraulic Engineering)*, Vol. 74, No. 5, pp. I_871-I_876.

Mai, N.P., Kantoush, S., Sumi, T., Thang, T.D., Trung, L.V., and Binh, D.V. (2019). Study on salinity intrusion processes into Hau river of Vietnamese Mekong Delta. *Journal of Japan Society of Civil Engineering, Ser. B1 (Hydraulic Engineering)*, Vol. 75, No. 5, pp. I_751-I_756.

Binh, D.V., Kantoush, S., Saber, M., Mai, N.P., Maskey, S., Phong, D.T., Sumi, T. (2020) "Long-term alterations of flow regimes of the Mekong River and adaptation strategies for the Vietnamese Mekong Delta. *Journal of Hydrology*, *Regional Studies*. 32, 100742. https://doi.org/10.1016/j.ejrh.2020.100742.

Loc, H.H., Binh, D.V., Park, E., Shrestha, S., Dung, T.D., Son, V.H., Truc, N.H.T., Mai, N.P., Seijger, C. (2021). Intensifying saline water intrusion and drought in the Mekong Delta: from physical evidence to policy outlooks. *Science of the Total Environment*, 757, 143919. DOI: 10.1016/j.scitotenv.2020.143919.

Binh, D.V., Kantoush, S.A., Sumi, T., Mai, N.P., Ngoc, T.A., Trung, L.V., An, T.D (2021). Effects of riverbed incision on the hydrology of the Vietnamese Mekong Delta. *Hydrological Processes,* 35, e14030, 2021 https://doi.org/10.1002/hyp.14030.

Mai, N.P., Kantoush, S.A., Sumi, T., Thang, T.D., (2021). Influence of river discharge and morphology on saltwater intrusion into the Vietnamese Mekong Delta, *Journal of Water*

Resources and Environment, *Journal of Water Resources and Environment*, No. 77, pp. 10-18.

Conference papers

Binh, D.V., Kantoush, S., Sumi, T., Mai, N.T.P., Ata, R., Kadi Abderrezzak, K.El., and Trung, L.V. (2017). Flow regime changes in Vietnamese Mekong Delta due to river-damming. In *Proceeding of 10th Symposium on River, Coastal and Estuarine Morphodynamics*, Padova, Italia, pp. 25.

La, T., Nguyen, M., Kantoush, S., Sumi, T., and Doan, B. (2017). Evaluation on the impacts of hydropower development on salinity intrusion into Vietnamese Mekong Delta. *The 3rd Symposium on JASTIP Disaster Prevention International Cooperation Research (JASTIP-WP4 Symposium)*.

Nguyen, T.P.M., La, V.T., Doan,V.B., Do, T.M.L. (2018). The evolution of salinity intrusion at Mekong River mouths under the impacts of dams upstream", *International Symposium on Lowland Technology (ISLT 2018).* Hanoi, Vietnam.

Mai, N.P., Kantoush, S., Sumi, T., Thang, T.D., Trung, L.V., and Binh, D.V. (2018). Impacts of cascade hydropower development on salinity intrusion into Vietnamese Mekong Delta. In *Proceeding of the 21st IAHR-APD Congress,* Yogyakarta, Indonesia, pp. 503-511.

Binh, D.V., Kantoush, S., Sumi, T., Mai, N.P., and Trung, L.V. (2018). Changes in the sediment budget and morphodynamics of Vietnamese Mekong Delta. In *E-Proceedings of the 12th ISE 2018*, Tokyo, Japan.

Binh, D.V., Sumi, T., Kantoush, S., Mai, N.P., and Trung, L.V. (2018). Historical changes of flow and sediment budget in Vietnamese Mekong Delta due to upstream dam development. In *Proceeding of the 21st IAHR-APD Congress 2018*, Yogyakarta, Indonesia, pp. 123-131.

Mai, N.P., Thang, T.D., Kantoush, S., Sumi, T., Trung, L.V., Binh, D.V. (2019). The processes of saltwater intrusion into Hau River. *Proceeding of the 10th International Conference on Asian and Pacific Coasts (APAC),* HaNoi, VietNam, pp.1477-1483.

Mai, N.P., Kantoush, S., Sumi, Thang, T.D., T., Binh, D.V., Trung, L.V. (2019). The influences of tidal regime and morphology change on salinity intrusion in Hau River. E-*Proceedings of the 38th IAHR World Congress,* Panama City. Doi:10.3850/38WC092019-1351, pp.2413-2420.

Binh, D.V., Kantoush, S., Sumi, T., Mai, N.P., and Trung, L.V. (2020). Dam-induced riverbed incision and saltwater intrusion in the Mekong Delta", *Proceedings of River Flow.* Taylor and

Francis group, London, ISBN 978-0-367-62773-7.

Binh, D.V., Kantoush, S., Sumi, T., Mai, N.P., and Trung, L.V. (2020). Riverbed incision in the Vietnamese Mekong Delta due to altered flow regime and sediment load. In *Proceeding of the 22st IAHR-APD Congress 2020*, Sapporo, Japan, pp. 123-131.